SYNTHESIS, CHARACTERIZATION, AND APPLICATIONS OF FUNCTIONALIZED POLYGLYCOLIDES

By

Erin B. Vogel

A DISSERTATION

Submitted to
Michigan State University
in partial fulfillment of the requirements
for the degree of

DOCTOR OF PHILOSOPHY

Chemistry

2008

ABSTRACT

SYNTHESIS, CHARACTERIZATION, AND APPLICATIONS OF FUNCTIONALIZED POLYGLYCOLIDES

By

Erin B. Vogel

Poly(*L*-lactide) has been widely used as a degradable material in environmental and biomedical fields; however, for many applications polylactide is not ideal due to its high crystallinity, hydrophobicity, and lack of functionalization. Strategies that provide routes to functionalized polyesters are necessary to produce materials with desired physical and chemical properties. We exploited two methods for polyester functionalization: the functional monomer approach and the post-polymerization modification approach.

Copolymers of lactide and functionalized glycolides can provide a range of polymer properties that can be tailored based on copolymer composition. However, if the two comonomers have unequal reactivity towards polymerization, "blocky" polymers can form with unpredictable properties. We copolymerized *rac*-lactide with five disubstituted lactide monomers and determined their relative reactivity ratios, which can be used to predict copolymer architecture. Our results indicated that the size of the substituent on the lactide framework directly influences monomer reactivity ratios and homopolymerization rates.

Adding functional groups, such as alcohols, increases the versatility of conventional polylactide, and permits further elaboration to enhance polymer hydrophilicity, provide attachment sites for biologically relevant molecules, and

serve as branching sites in the synthesis of complex polymer architectures. We synthesized 3-benzyloxyoctyl glycolide, an AB glycolide monomer derived from oleic acid that places a benzyl-protected primary alcohol eight methylene units from the polymer backbone. Copolymerization of 3-benzyloxyoctyl glycolide with *L*-lactide yielded high molecular weight copolymers. Quantitative hydrogenolysis of the benzyl groups provided functional polylactides with pendent primary alcohols distributed along the polymer backbone. Initiation of *L*-lactide polymerization from a copolymer with 5 mol% alcohol sites generated amorphous PLA comb polymers that crystallized upon capping the hydroxy groups at the termini of the teeth.

Post-polymerization modification via "click" chemistry provides a convenient route to functionalized polyesters. Using poly(propargylglycolide), an acetylene-functionalized polyglycolide, we prepared and characterized a family of degradable comb polymers that individually self-aggregate in aqueous solutions. The polymers encapsulate and release hydrophobic and hydrophilic molecules and display thermoresponsive behavior from room temperature to > 60 °C. Furthermore, we described the synthesis, characterization, and applications of chemically cross-linked comb polymers that retain chemical functionality. The organic nanoparticles exhibit prolonged controlled release and are biocompatible.

Be exalted, O God, above the heavens;
Let your glory be over all the earth.

ACKNOWLEDGEMENTS

I would like to thank my advisor, Dr. Gregory Baker, who not only taught me the basics of research and polymer chemistry, but also how to "be a scientist." Thanks to Drs. Christina Chan and S. Patrick Walton for meaningful conversations and an intriguing collaboration. Thanks to my guidance committee, Dr. Babak Borhan, Dr. Kevin Walker, Dr. Merlin Bruening, and Dr. Mitch Smith, for helpful discussions and suggestions.

Thanks to Dan Holmes, Kermit Johnson, Riu Huang, Kathy Severin, Dan Jones, Alicia Pastor, and Ewa Danielewicz for teaching me various characterization techniques. I would also like to thank past and current graduate students and group members: Xuwei, Feng, Leslie, DJ, Bao, Ying, Ping, Jon, Qin, Sampa, Tom, Tiffany, Joe, Amanda, Aman and Nicki for their assistance and friendship. They have taught me many things and made life at MSU enjoyable.

Finally I would like to thank my family for their endless encouragement and prayers and my husband, Mark, for his patience, support, and love. This would have not been possible without you.

TABLE OF CONTENTS

LIST OF TABLES

LIST OF FIGURES

Images in this dissertation are presented in color.

LIST OF SCHEMES

LIST OF ABBREVIATIONS

3-BMG	3-benzyloxymethyl glycolide
3-BMMG	3-benzyloxymethyl methyl glycolide
3-MG	3-methylglycolide
AFM	atomic force microscopy
BBA	4-*tert*-butylbenzyl alcohol
BOG	3-benzyloxyoctyl glycolide
br	broad
cHG	cyclohexylglycolide
CL	cross-linked
cmc	critical micelle concentration
d	doublet
δ	chemical shift
Da	Dalton
DCC	N,N'-dicyclohexylcarbodiimide
dd	doublet of doublets
DLS	dynamic light scattering
DMAP	4-dimethylaminopyridine
DMF	N,N-dimethyl formamide
DMSO-d_6	deuterated dimethyl sulfoxide
DSC	differential scanning calorimetry

dt	doublet of triplets
EG	ethylglycolide
ε-CL	epsilon-caprolactone
FG	functional group
FM	functional monomer
F-R	Fineman-Ross
g	graph
GC	gas chromatography
GPC	gel permeation chromatography
HOG	3-hydroxyoxyoctyl glycolide
Hz	Hertz
iPG	isopropylglycolide
IR	infrared spectroscopy
J	coupling constant
kD	kiloDalton
K-T	Kelen-Tudös
LC	liquid chromatography
LCS	*L*-cycloserine
LCST	lower critical solution temperature
LHS	*L*-homoserine lactone
LLA	*L*-lactide
LS	light scattering

m	multiplet
M	moles per liter
M_1 or M_2	monomer 1 or monomer 2
m/z	mass of ion (atomic units)/its charge number
MALLS	multi angle laser light scattering
MD	mandelide
mg	milligram
MHz	megaHertz
mL	milliliter
M_n	number average molecular weight
mp	melting point
mPEG	poly(ethylene glycol) monomethyl ether
MS	mass spectrometry
M_w	weight average molecular weight
MWCO	molecular weight cutoff
ν	wavenumber
nDG	*n*-decylglycolide
nHG	*n*-hexylglycolide
NLS	nonlinear least squares
NMR	nuclear magnetic resonance
NOE	nuclear Overhauser effect

NP	nanoparticle
p	pentet
p	para
PBS	phosphate buffered saline
PDI	polydispersity index
PEG	poly(ethylene glycol)
PEI	poly(ethylene imine)
PEO	poly(ethylene oxide)
PGL	propargylglycolide
PL	phenyllactide
PLA	polylactide
PLL	poly(*L*-lysine)
PLLA	poly(*L*-lactide)
PMMA	poly(methyl methacrylate)
POM	polarized optical microscopy
ppb	part per billion
PPGL	poly(propargylglycolide)
ppm	parts per million
PPM	post-polymerization modification
psi	pound per square inch
PTFE	poly(tetrafluoroethylene)
q	quartet

r	reactivity ratio
rac	racemic
ROP	ring opening polymerization
RT	room temperature
s	singlet
sec	secondary
$SnOct_2$	tin(II)-2-ethylhexanoate
t	triplet
TEM	transmission electron microscopy
tert	tertiary
T_g	glass transition temperature
THF	tetrahydrofuran
T_m	melting temperature
TsOH	*p*-toluenesulfonic acid
UV-vis	ultraviolet-visible

Chapter 1 Introduction

Structure and Properties of Functionalized Polyglycolides

Functionalized polylactides address two critical issues in polymer science: degradability and utility. An important physical characteristic of polymers is the glass transition temperature (T_g) since it defines the use temperature range for many applications.[1,2] Heating polymers through their T_g affects many physical properties and causes increased permeability, loss of dimensional stability, and increased resilience. Since the T_g of polylactide (PLA) is fairly low (50 – 60 °C), crystalline poly(L-lactide) (PLLA) is used in structural applications such as fibers and packaging,[3] orthopedic fixations,[4,5] sutures,[6] and scaffolds for tissue engineering.[7] Low T_g polylactides are rubbery at room temperature, degrade faster, and are preferred for applications such as controlled drug delivery. Although racemic polylactide (*rac*-PLA) has a fairly low T_g, its hydrophobicity and lack of functional group diversity prevents its widespread use as a degradable drug delivery vehicle. Two strategies have been developed to introduce functionality to the polylactide scaffold: the functional monomer (FM) approach and the post-polymerization modification (PPM) approach (**Scheme 1**). Both routes incorporate functional groups onto the polymer backbone to enhance properties or act as access points for further modification.

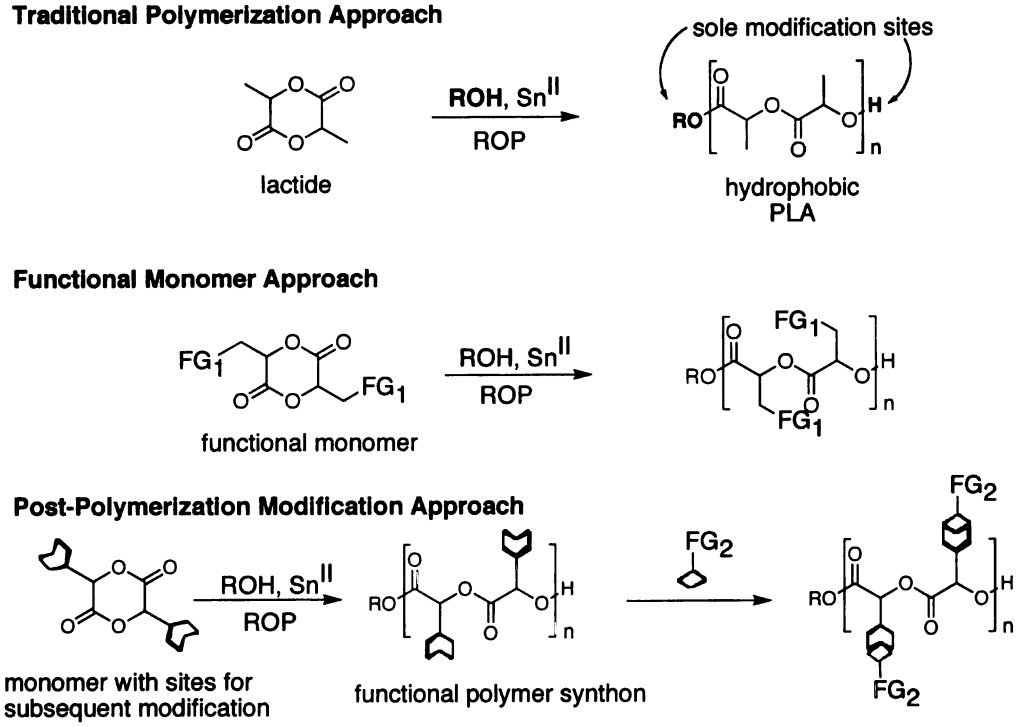

Scheme 1. Routes to functionalized lactide-based polymers. Lactide monomers are polymerized via catalytic ring opening polymerization. FG_1 and FG_2 represent functional groups (alcohols, amines, alkyl chains, acids, etc.) that can be appended to the polymer.

Functional Monomer Approach

Synthesis and Polymerization of Functionalized Glycolide Monomers

Prior to the commercialization of poly(lactide) by NatureWorks®, large-scale production of polylactide was too costly for all but medical applications. However, development of the low-cost "from corn to plastic" process has allowed for continuous processing of PLA and significant cost reduction. The process begins when field corn is harvested and the corn sugar, or dextrose, is isolated. The dextrose is fermented and distilled into lactic acid, which can undergo acid-

catalyzed oligomerization forming low molecular weight polylactide. The oligomers are then thermally cracked to the dimer, *L*-lactide, which is polymerized via ring opening polymerization (ROP) (**Scheme 2**). Since only a few other α-hydroxy acids such as 2-hydroxyisocaproic acid[8] and β-phenyllactic acid[9] can be isolated via fermentation most functionalized α-hydroxy acids rely on the synthesis of unique materials. As shown in **Scheme 3**, functionalized glycolide monomers are prepared by synthesizing functionalized α-hydroxy acids, which are dimerized in dilute organic solvents.

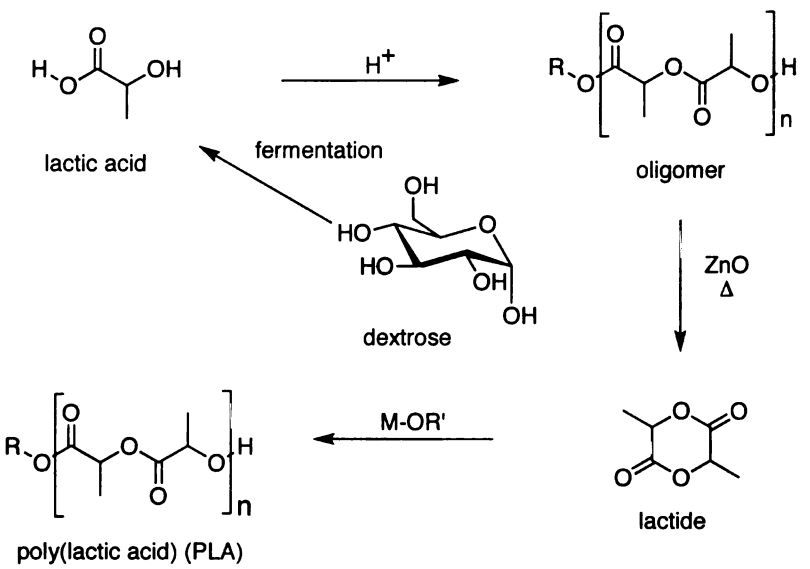

Scheme 2. NatureWork's® route to high molecular weight poly(lactide).

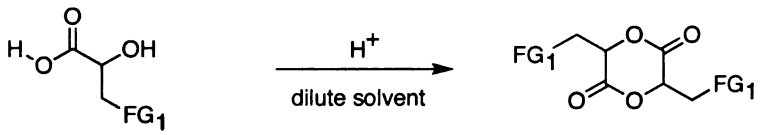

functional α-hydroxy acid | functional monomer

Scheme 3. Synthesis of functionalized glycolide monomer. FG_1 represents functional groups (alcohols, amines, alkyl chains, acids, etc.) that can be appended to the functional monomer.

Alkyl-Substituted Polyglycolides

Alkyl-substituted polyglycolides have been synthesized by polymerizing cyclic dimers derived from the corresponding α-hydroxy acids, which are obtained by enzymatic α-hydroxylation of fatty acids or by standard synthetic methods. Most standard syntheses follow one of two routes: reaction of Grignard reagents with diethyl oxalate, followed by reduction and hydrolysis of the α-ketoester, or hydrolysis of the cyanohydrin formed upon reaction of potassium cyanide with the corresponding aldehyde (**Scheme 4**). Using these methods, polyglycolides with *n*-alkyl chains up to 16 carbon atoms have been prepared. Usually, increasing the steric bulk of the substituents attached to the polymer backbone increases T_g, as seen in polyolefins, but the T_gs measured by differential scanning calorimetry (DSC) for polyglycolides show the opposite trend, longer alkyl chains decrease the T_g (**Figure 1**).[10] Apparently, the linear alkyl chains decrease the dipole-dipole interactions between the ester groups in the polymer backbone.

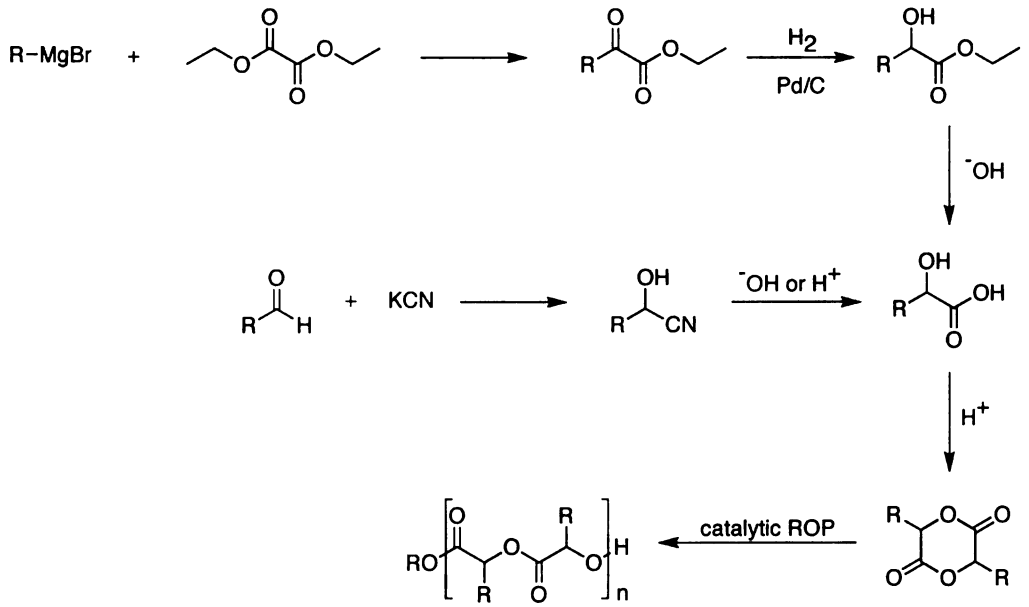

Scheme 4. Synthetic routes to alkyl substituted polyglycolides.

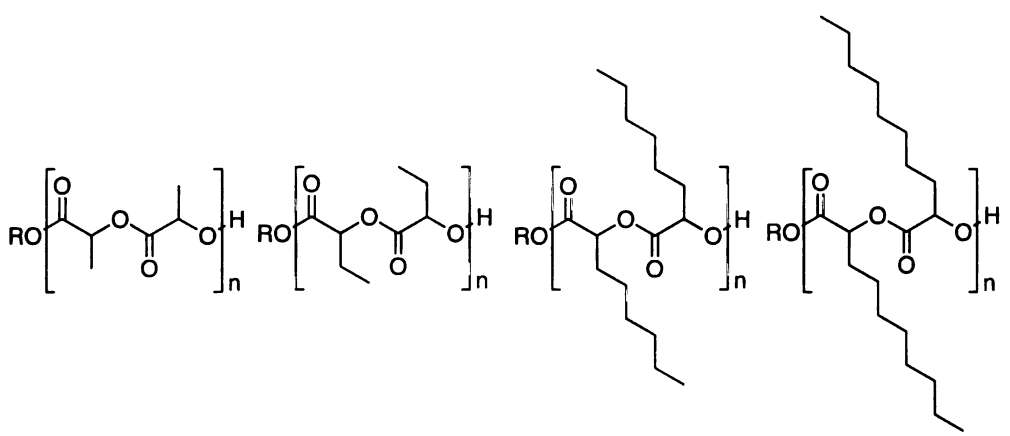

Figure 1. Linear alkyl-substituted polyglycolides and their glass transition temperatures.

If linear chains decrease the T_g, then branched alkyl chains would more effectively increase the T_g. Although several polyglycolides with branched chains have been synthesized, the structural diversity of polyglycolides is still modest. For example, poly(isopropylglycolide), a lactide analogue of polyvaline, and poly(isobutylglycolide) have been prepared. In poly(isopropylglycolide) the isopropyl group is directly attached to the polymer backbone, whereas in poly(isobutylglycolide) the isopropyl group is placed one carbon from the polymer backbone (**Figure 2**).[10] The T_g of poly(isopropylglycolide) and poly(isobutyl glycolide) are 50 and 23 °C, respectively, illustrating the importance of placing the bulky group adjacent to the polymer backbone. Clearly, the isopropyl group is more sterically demanding than the methyl group of lactide, but its failure to significantly increase T_g again points to the importance of dipole-dipole screening in determining T_g. A significant increase in the T_g was seen in poly(cyclohexylglycolide),[11] with a T_g of 98 °C. Apparently, the cyclohexyl group was sufficiently bulky to hinder rotation of the polymer backbone and increase the T_g.

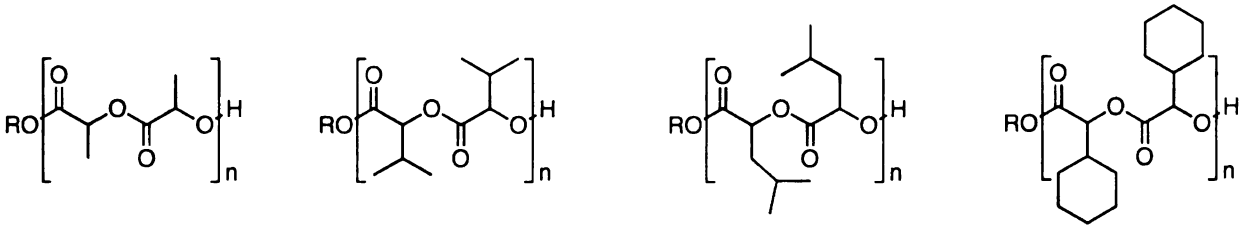

poly(lactide) T_g = 55 °C

poly(isopropylglycolide) T_g = 50 °C

poly(isobutylglycolide) T_g = 15 °C

poly(cyclohexylglycolide) T_g = 98 °C

Figure 2. Branched alkyl-substituted polyglycolides and their glass transition temperatures.

Non-symmetrical monomers provide another route to structural diversity in polylactide-related polymers. Polymerization of AB monomers, where two different glycolic acid derivatives are incorporated into one glycolide ring, is analogous to copolymerization. However, the growing chain end in an AB system discriminates between two different sites on the same glycolide monomer rather than between two comonomers (**Scheme 5**). For glycolides with simple alkyl and aryl substituents, steric effects largely define the rate of ring opening polymerization and increasing the difference in the relative size of the two ring substituents favors alternation. Shown in **Figure 3** are six examples of simple AB monomers and their polymers prepared by Baker and coworkers[10,12] The *n*-hexyl derivative was also reported by Trimaille *et al.*[13]

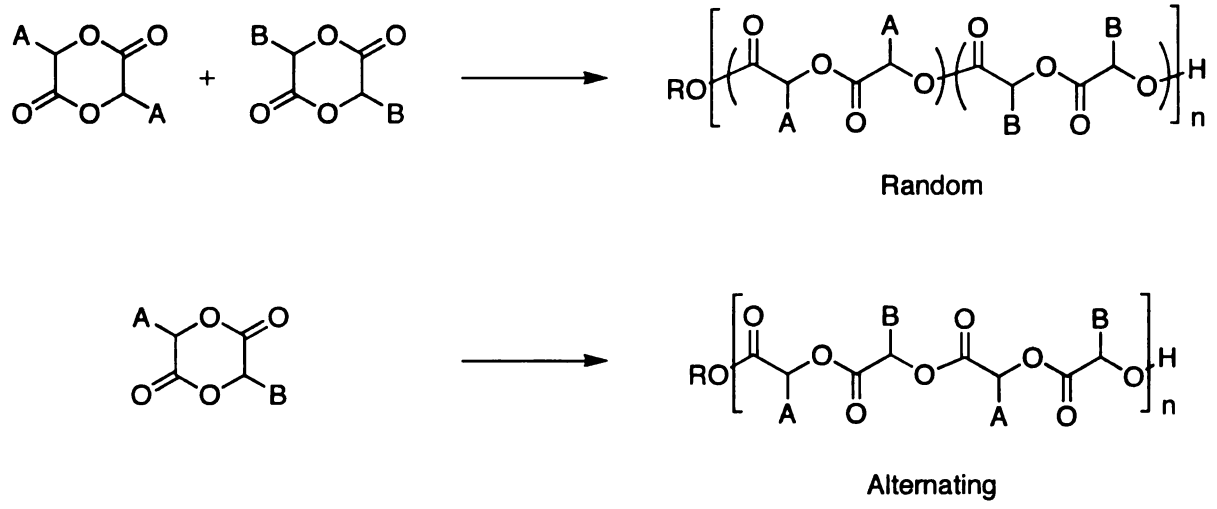

Scheme 5. Comparison between copolymerization of two symmetrical monomers and homopolymerization of AB monomer.

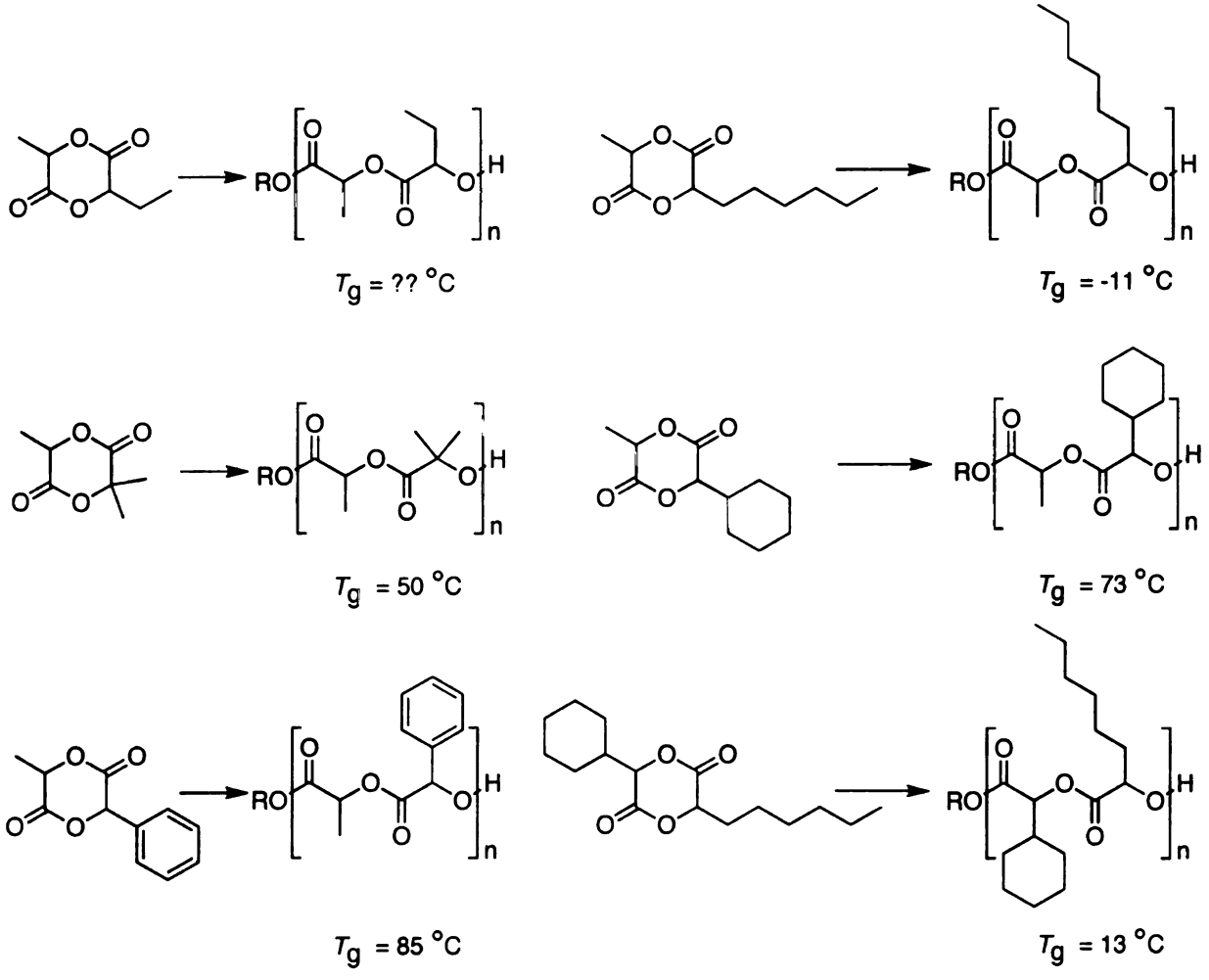

Figure 3. AB-substituted polyglycolides and their glass transition temperatures.

Aryl-Substituted Polyglycolides

By analogy to simple polyolefins, aryl-substituted polyglycolides are promising candidates for high T_g polymers. For example, while atactic polypropylene has a T_g of ~ -11 °C, polystyrene's T_g is 109 °C. Inspired by the high T_g of polystyrene and the availability of phenyllactic acid via various biosynthetic pathways,[14] polymers based on phenyllactide and its derivatives were synthesized and studied (**Figure 4**).[15,16] Despite the addition of a bulky aromatic ring and the potential for π-π interactions in the polymer, the T_g for high molecular weight polymer was only 50 °C. Although the T_g was comparable to that of poly(isopropylglycolide), it is significantly higher than poly(isobutylglycolide), which also contains a methylene group between the bulky group and the polymer backbone. As expected, the steric effects of alkyl groups or aromatic rings decrease as they are moved farther from the polymer backbone. To further increase the steric bulk, methyl groups were added to the aromatic rings. 4-Methylphenyllactide was synthesized and polymerized to high molecular weight, increasing the T_g to 59 °C, an improvement over poly(phenyllactide), but still far too low to be considered a high T_g material. The *meta* and *ortho* derivatives were also investigated and are suspected to have greater effects on increasing the T_g due to higher steric demands, however, their syntheses were problematic, and no reliable T_g data was reported.

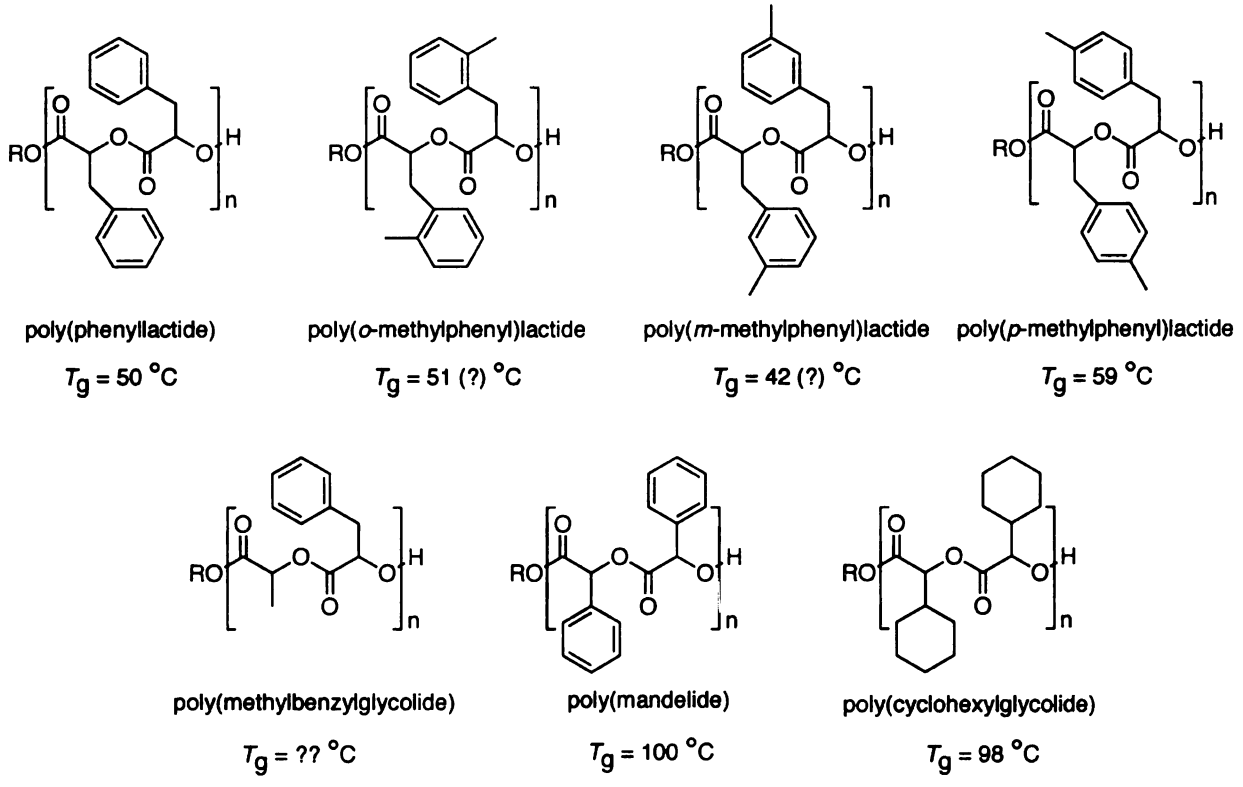

Figure 4. Aryl-substituted polyglycolides and their glass transition temperatures.

Comparing the T_gs of polystyrene and poly(allylbenzene), a structural analogue of poly(phenyllactide), suggests that using methylene groups to link the aromatic ring to the polymer backbone causes an ~30° drop in T_g. Using this logic, direct attachment of the aromatic ring to the polyglycolide backbone should significantly increase T_g. Thus, polymandelide, the cyclic dimer of mandelic acid should provide the appropriate structure. Like lactic acid, mandelic acid is a naturally occurring metabolite and in principle, poly(mandelide) synthesis could be a bio-based process. Early attempts to synthesize poly(mandelide) were hindered by impurities in the monomer synthesis that served as initiators in its polymerization and limited its molecular weight. The synthesis of poly(mandelide)

presented several challenges, most notably racemization of stereochemistry and poor monomer solubility, however, Baker *et al.* was able to generate high molecular weight polymers with T_gs of ~100°.[12] The materials were colorless, glassy amorphous solids, similar to polystyrene. However, poly(mandelide) may not be a perfect substitute for polystyrene due to yellowing that develops during melt processing of the polymer most likely a result of the highly reactive methine protons which are α to both a carbonyl and a benzene ring.

One way to alleviate the problems associated with poly(mandelide) would be to use the analogous structure without the reactive aromatic ring, which would minimize the reactivity of the methine protons. Jing *et al.* showed that both mandelic acid and mandelide could be hydrogenated directly to the corresponding cyclohexyl derivatives. Polymerization of cyclohexylglycolide yielded high molecular weight polymer with a T_g of 98 °C, comparable to both polystyrene and poly(mandelide), but with the decreased reactivity of the methine protons, no degradation was observed.[11]

Hydroxy-Functionalized Glycolides

One of the synthetic challenges of hydroxy-functionalized glycolides is the presence of the alcohol group itself. Water and alcohols are known initiators in the polymerization of lactide, and therefore the alcohol groups must either be introduced post-polymerization or via a protection/deprotection scheme. Feng and co-workers introduced the first hydroxy-functionalized glycolide, 3-

benzyloxymethyl-1,4-dioxane-2,5-dione (3-BMG), starting from 3-chloro-propanediol (**Scheme 6**).[17] Ring-opening polymerization catalyzed by tin(II)-2-ethylhexanoate ($SnOct_2$) generated an amorphous polymer with a T_g of 34 °C. Deprotection via catalytic hydrogenation removed the pendant benzyl groups, resulting in a water-soluble polymer, poly(3-hydroxymethyl-1,4-dioxane-2,5-dione) (poly(3-HMG)). The contact angle and the T_g of the polymer both decreased upon deprotection.

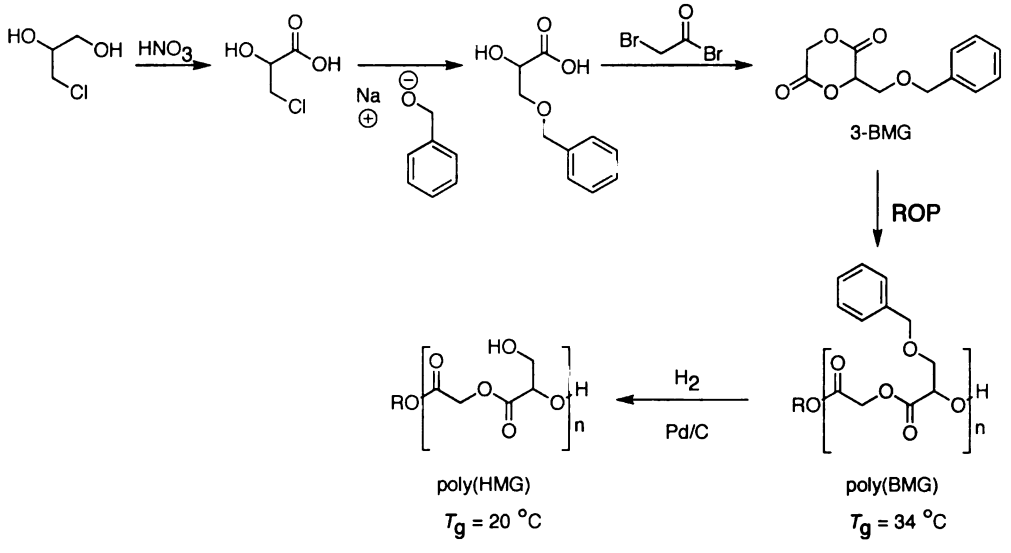

Scheme 6. Synthesis, polymerization, and deprotection of 3-benzyloxymethyl-1,4-dioxane-2,5-dione (3-BMG).

Hennink *et al.* and Weck *et al.* concurrently reported a more versatile route to substituted lactide monomers bearing hydroxy groups (**Scheme 7**).[18,19] Starting from optically pure O-Bn-*L*-serine, they obtained optically pure glycolides. In the synthesis of lactide derivatives however, *rac*-2-bromopropionyl bromide was used

in the intramolecular ring closing reaction and two diastereomers were formed. Hennink and co-workers separated the two diastereomers via flash column chromatography and used the (S,S) isomer for polymerizations.

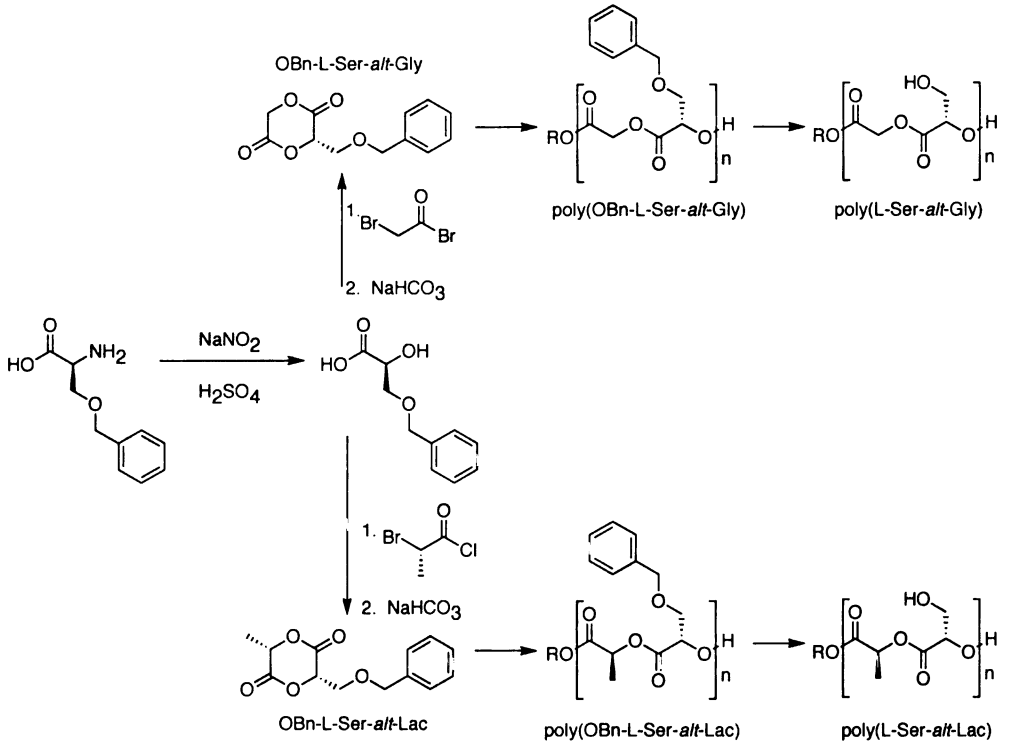

Scheme 7. Synthesis, polymerization, and deprotection of 3(*S*)-benzyloxylmethyl-1,4-dioxane-2,5-dione (OBn-*L*-Ser-*alt*-Gly) and 3(*S*)-(benzyloxymethyl)-6(*S*)-methyl-1,4-dioxane-2,5-dione (OBn-*L*-Ser-*alt*-Lac).

Hennink also compared the polymerization rates of the lactide- and glycolide-substituted benzyloxymethyl monomers, using ethylzinc phenolate and 2-propanol as the catalyst and initiator, respectively. Crystal structure analysis revealed minor differences in the placement of the OBn and methyl substituent in OBn-*L*-Ser-*alt*-Lac monomer, with both substituents in equatorial positions of the

dilactone ring. Since the groups presented almost identical steric demands, both carbonyls were nearly equally accessible and polymerization yielded a random polymer. However in OBn-*L*-Ser-*alt*-Gly, replacement of the methyl group with hydrogen results in a clear structural difference and preferential opening at the less hindered carbonyl, creating an alternating polymer. DSC analysis showed that both polymers were completely amorphous with T_gs of 30 °C and 25 °C for poly(OBn-*L*-Ser-*alt*-Lac) and poly(OBn-*L*-Ser-*alt*-Gly), respectively.

The protecting groups were removed from the two polymers via catalytic hydrogenation using Pd/C (10 %) and THF as a solvent. The homopolymers were completely deprotected after 24 hours and GPC showed no chain scission. Deprotected poly(*L*-Ser-*alt*-Lac) was completely amorphous with a T_g of 30 °C; whereas poly(*L*-Ser-*alt*-Gly) was semi-crystalline with a T_g of –4 °C and a T_m of 135 °C. Neither polymer was soluble in aqueous solution.[19]

Weck and co-workers obtained 21 kD poly(OBn-*L*-Ser-*alt*-Gly) via ring-opening polymerization using $SnOct_2$ as the catalyst. The amorphous polymer had a T_g of 18 °C and was deprotected by hydrogenolysis using $Pd(OH)_2$; however no molecular weight or T_g data was presented for the deprotected polymers.[18]

A second approach to hydroxy-modified glycolides was described by Vert and co-workers in their syntheses of 3-(1,2,3,4-tetraoxobutyl-diisopropylidene)-dioxane-2,5-dione (DiPAGYL) and 3-methyl-6-(1,2,3,4-tetraoxobutyl-

diisopropylidene)-dioxane-2,5-dione (DiPALAC), a monomer composed of a glycolyl and a *D*-gluconyl unit derived from gluconic acid (**Scheme 8**).[20] After selective protection of the four pendant alcohol groups with 2,2-dimethoxy propane and intramolecular ring closure with bromoacetyl chloride or 2-bromopropionyl chloride, the monomers were isolated as white crystals. Ring opening polymerization of DiPAGYL led to a 20 kD brittle amorphous polymer with a T_g of 95 °C. All attempts to polymerize DiPALAC led to oligomers with molecular weights of ~2 kD. Several methods to remove the isopropylidine groups were investigated, all under acidic conditions, but most degraded the polyester backbone.[21] The best results were accomplished using iodine in methanol or aqueous acetic acid; however even these methods showed modest degradation. The maximum deprotection obtained was 60 %, as determined by NMR. At 60 % percent deprotection, a fully protected 32 kD polymer degraded to 5 kD (versus 27 kD theoretical value). The partially deprotected polymers were soluble in hydrophilic solvents such as methanol and ethanol and were partially soluble in water.

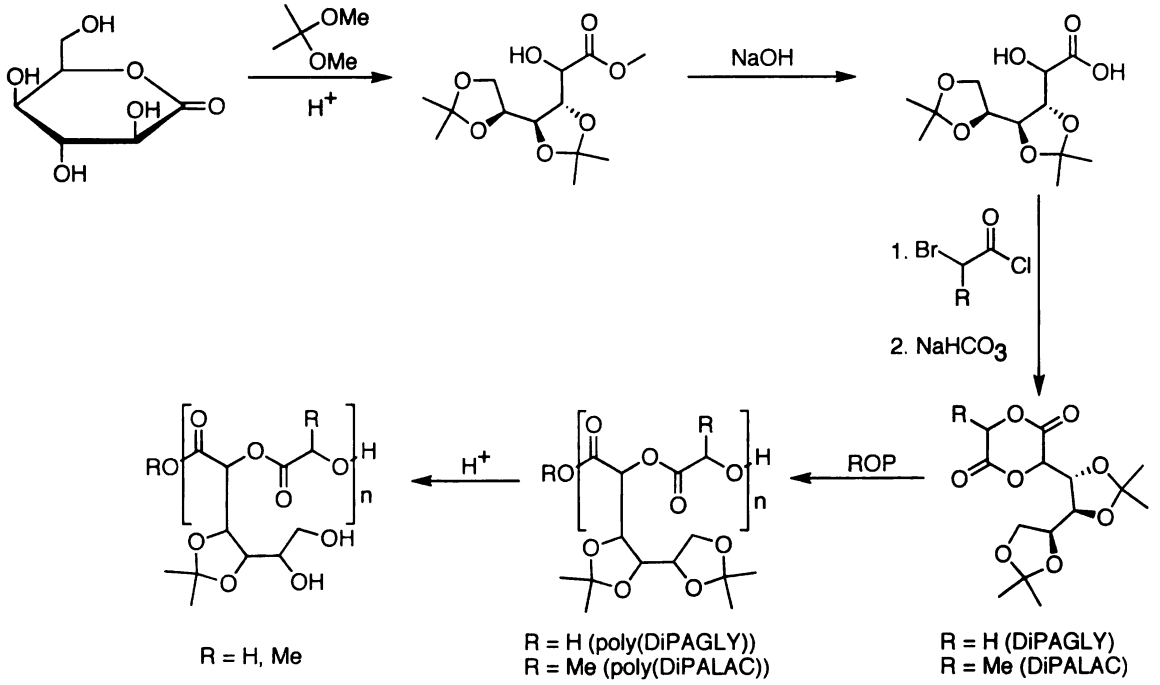

Scheme 8. Synthesis, polymerization, and partial deprotection of 3-(1,2,3,4-tetraoxobutyl-diisopropylidene)-dioxane-2,5-dione (DiPAGYL) and 3-methyl-6-(1,2,3,4-tetraoxobutyl-diisopropylidene)-dioxane-2,5-dione (DiPALAC).

Carboxylic Acid-Functionalized Polyglycolides

Biomedical and pharmaceutical applications often require water-soluble biodegradable polymers. Since the hydrolysis rates of widely used poly(α-hydroxy acids) are often slow and limited by crystallinity, methods to decrease crystallinity and hydrophobicity are important for *in vivo* applications. One method for imparting hydrophilic character to polymers is to functionalize them with hydrophilic groups, such as carboxylic acids.

Taguchi and co-workers described the synthesis of 3(*S*)-[(benzyloxycarbonyl)methyl]-1,4-dioxane-2,5-dione which was polymerized to an alternating copolymer consisting of glycolic acid and benzyl α-(*S*)-malate units

(**Scheme 9**).[22] Ring-opening polymerizations were run in solution and bulk utilizing $SnOct_2$ or Et_2Zn (diethyl zinc) as the catalyst. Molecular weights ranged from 2 kD to 21 kD. The polymers were deprotected via catalytic hydrogenolysis using platinum oxide or palladium carbon yielding crystalline, water-soluble polymers. No molecular weight data were reported for the deprotected polymers.

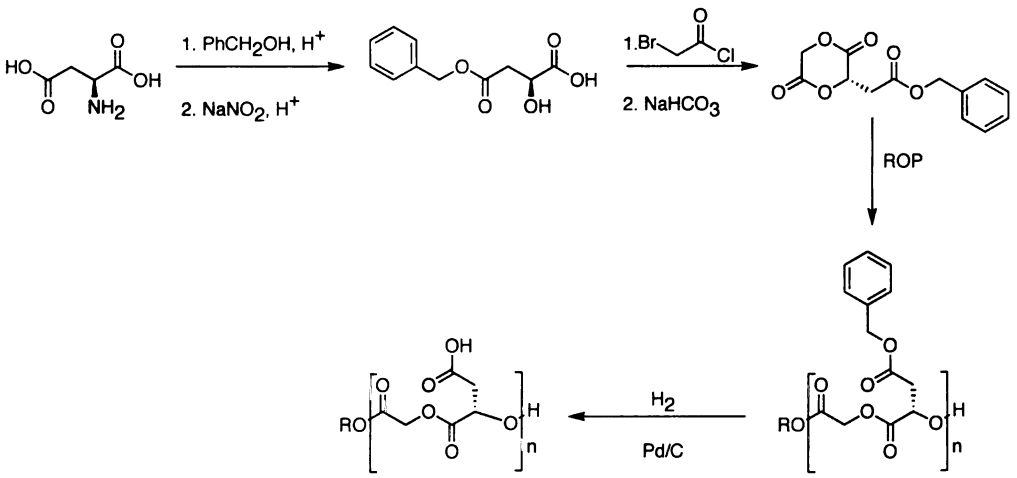

Scheme 9. Synthesis, polymerization, and deprotection of 3(S)-[(benzyloxycarbonyl)methyl]-1,4-dioxane-2,5-dione.

Malide dibenzyl ester, the cyclic dimer of β-benzyl malate, was prepared by Ouchi and co-workers[23] using either *L*-malic acid (L-MA) or *L*-aspartic acid (L-AA); however higher yields were obtained using L-MA (**Scheme 10**). Ring-opening polymerization was carried out at 220 °C using organotin compounds as catalysts. The protecting groups were removed by hydrogenation using palladium-carbon in ethyl acetate.

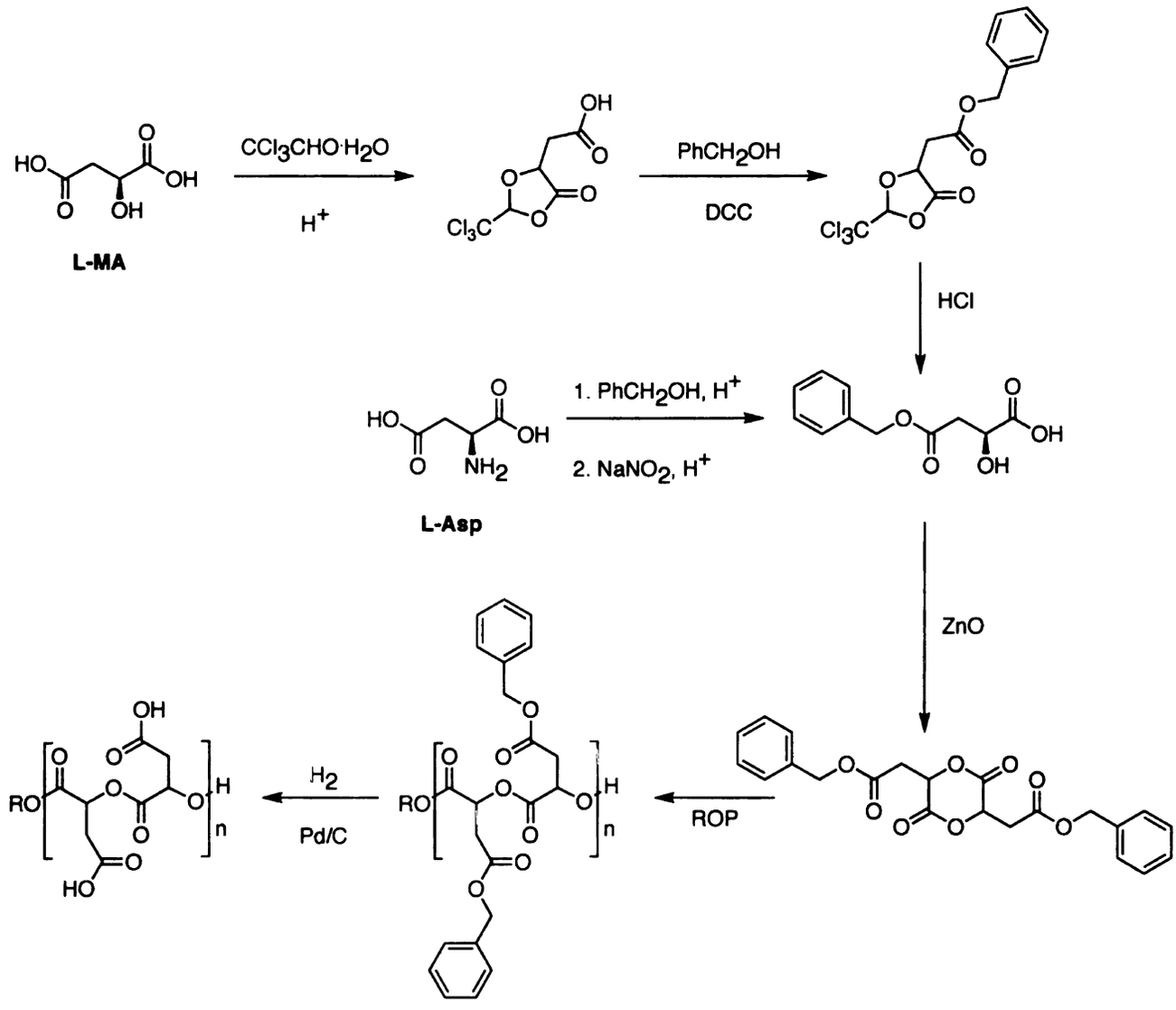

Scheme 10. Synthesis, polymerization, and deprotection of malide dibenzyl ester prepared from either *L*-malic acid (L-MA) or *L*-aspartic acid (L-Asp).

More recently Weck and co-workers prepared a glutamic acid polylactide derivative, OBn-L-Glu-*alt*-Lac. Diazotization of glutamic acid to its corresponding α-hydroxy acid and reaction with (*S*)-2-bromopropionic acid in the presence of N-N'-dicyclohexylcarbodiimide (DCC) and 1-hydroxybenzotriazole followed by intramolecular ring closure led to the functionalized monomer. Ring-opening polymerizations were carried out in the presence of $SnOct_2$ at 140 °C (**Scheme 11**).[18] The highest molecular weight obtained was 3 kD, reportedly due to

interaction between the monomer's side chain and the catalyst. A T_g of 10 °C was reported; however this value may change significantly with higher molecular weight polymers. Deprotection of the polymers via hydrogenolysis using $Pd(OH)_2$ resulted in quantitative removal of the protecting groups as seen from the ^1H NMR.

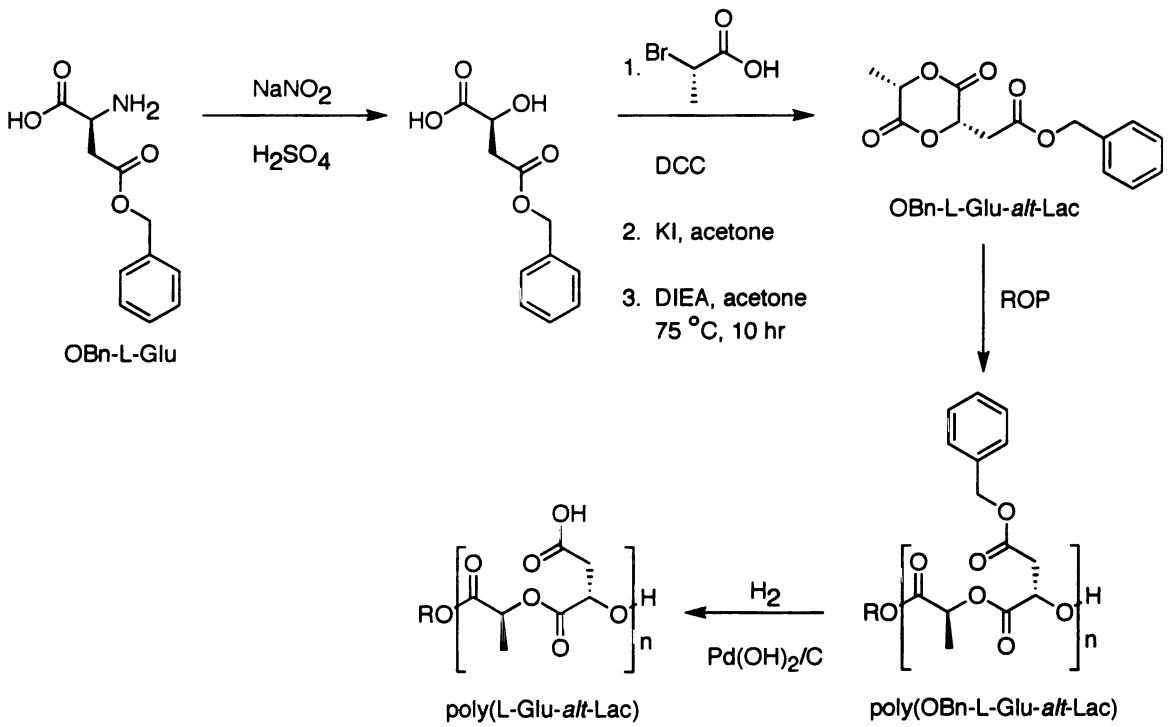

Scheme 11. Synthesis, polymerization, and deprotection of OBn-L-Glu-*alt*-Lac.

Amine-Substituted Glycolides

Although many morpholine-2,5-diones have been described,[24-27] very few amine functionalized lactide derivatives exist.[18] Gerhard *et al.* synthesized a lactide analog of polylysine, Cbz-L-Lys-*alt*-Lac (**Scheme 12**). Ring-opening polymerization provided an 8 kD amine protected polymer with a T_g of 20 °C, and

complete deprotection of the benzyl carbamate using HBr (33 %)/AcOH caused little backbone degradation. Molecular weight data for the polymer were not obtained due to poor solubility in CH_2Cl_2; however, the GPC trace of a 30 kD polylactide had the same M_n and peak shape before and after exposure to the deprotection conditions.

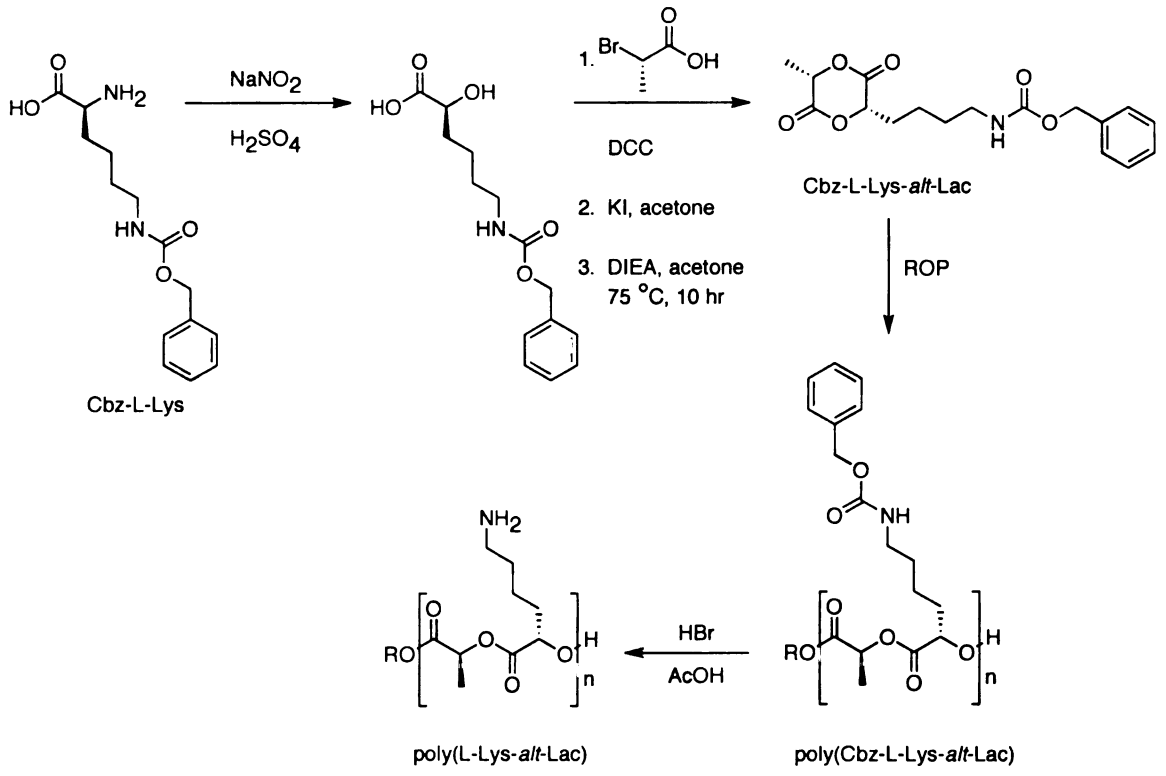

Scheme 12. Synthesis, polymerization, and deprotection of Cbz-*L*-Lys-*alt*-Lac.

Peg-Grafted Glycolides

Recent reports have shown that introducing oligo(ethylene glycol) groups to hydrophobic polymers render them hydrophilic.[28-32] In addition, these polymers often exhibit lower critical solution temperature (LCST) behavior, making them ideal targets in applications such as drug delivery systems, smart surfaces, and

bioseparations. At the LCST, these materials undergo a solution-gel transition that corresponds to the entropically driven expulsion of solvating water molecules from the polymer. Recent research on responsive LCST materials, especially those that contain mPEG segments, suggests that tuning the hydrophobic/hydrophilic balance in materials can shift the LCST over a broad temperature range. Lactide derivatives with 1-4 oligo(ethylene glycol) segments have been synthesized and polymerized using $SnOct_2$ (**Scheme 13**).[33] The synthetic approach to the monomers entails reaction of an oligo(ethylene glycol) monomethyl ether with 1,6-dibromohexane to generate the corresponding bromine capped oligo(ethylene glycol) monomethyl ether. Reaction with magnesium followed by the addition of diethyl glyoxalate provides the corresponding α-keto ester. Catalytic hydrogenation of the α-keto-ester, followed by hydrolysis, gave the corresponding α-hydroxy acid, which was dimerized to the PEG-substituted glycolide. Since high molecular weight polymers require complete removal of trace water and alcohol impurities prior to polymerization, the PEG-functionalized monomers were dried under vacuum at 100 °C. High molecular weight polymers catalyzed by $SnOct_2$ were obtained: M_n = 149,500, 56,400, 59,800 and 10,600 g/mol for polymers containing 1, 2, 3, or 4 ethylene glycol units per repeat unit, respectively.

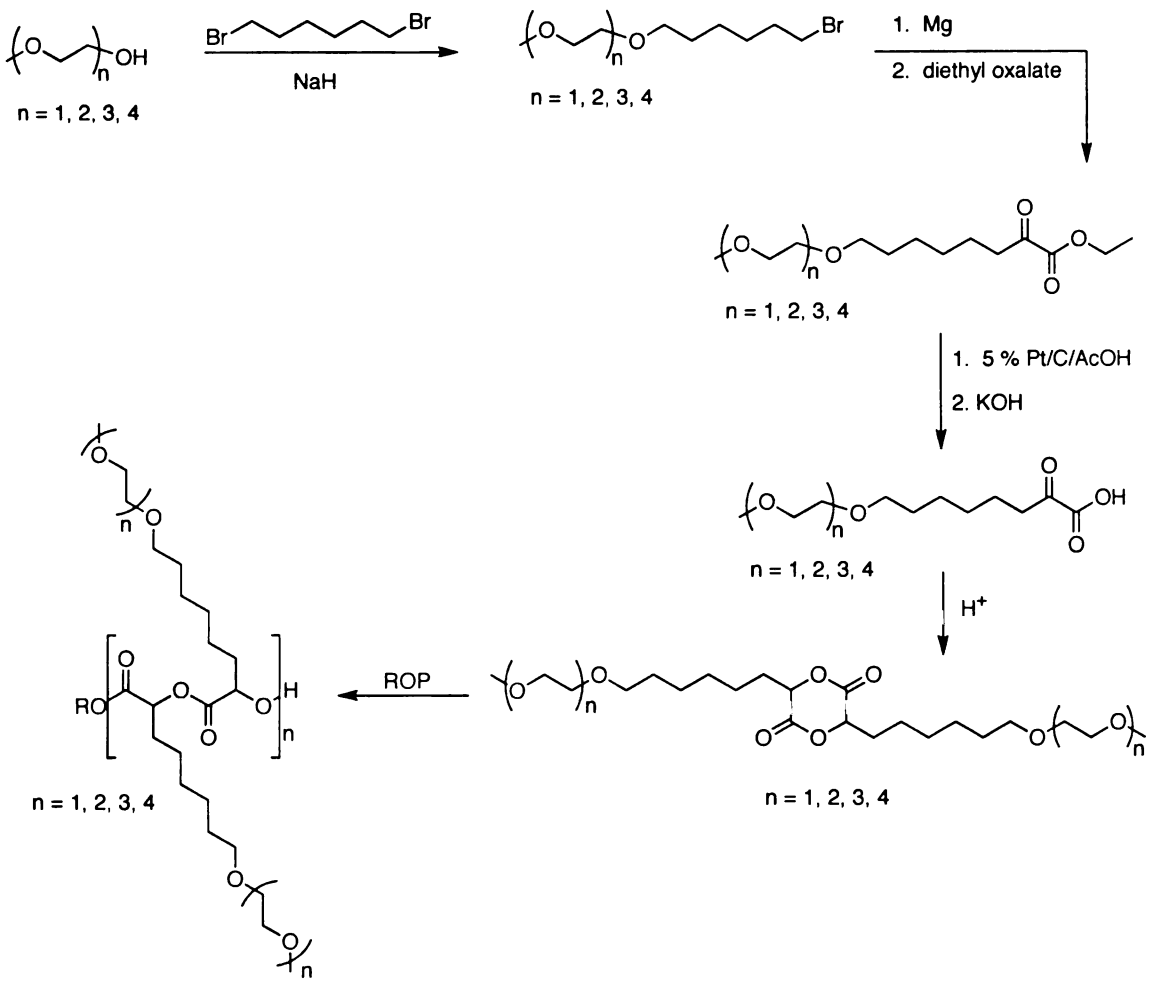

Scheme 13. Synthesis and polymerization of oligo(ethylene glycol) monomethyl ether-modified polyglycolides.

Alkenyl- and Alkynyl-Substituted Polyglycolides

The versatility of post-polymerization reactions has driven the synthesis of monomers that incorporate functional groups tolerant of polymerization conditions, but available for future modification. For example, pendant alkene groups could be used in cross metathesis reactions, which inspired the synthesis of diallylglycolide (DAG), shown in **Scheme 14**.[34] Diallylglycolide was polymerized in toluene at 80 °C for 3 days using $SnOct_2$ to give a tacky solid with a T_g of –10 °C. Melt

polymerization was not as effective as it lead to poor control over molecular weight and polydispersity index (PDI) due to the higher reaction temperature. Copolymerization of lactide with DAG spaced the reactive sites along the polymer backbone.

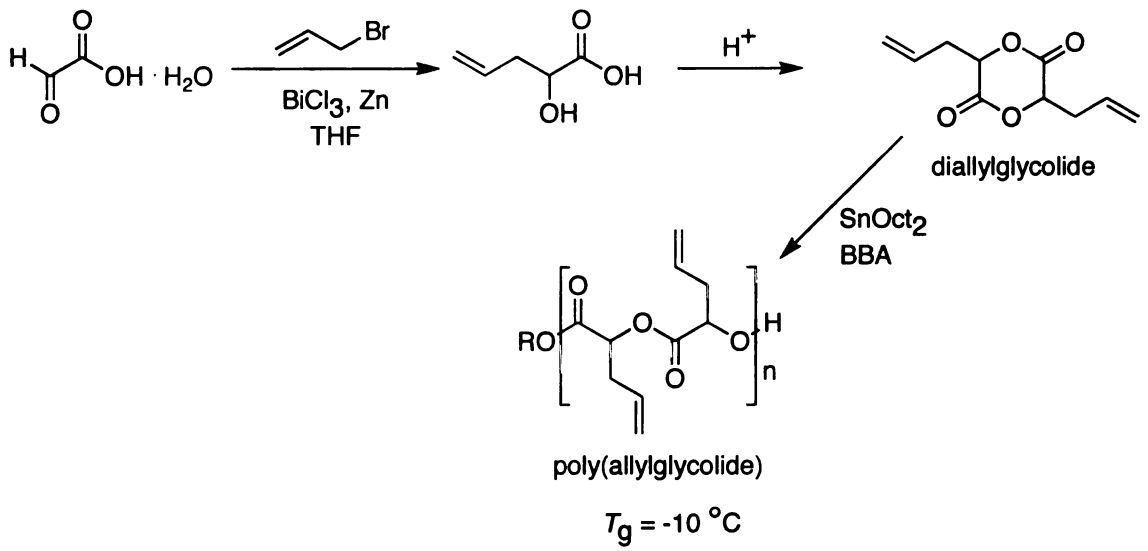

Scheme 14. Synthesis of and polymerization of diallylglycolide.

A second example is the synthesis of alkyne functionalized monomers that can be used in "click" chemistry reactions, specifically 1,3-dipolar cycloaddition reactions between an alkyne and azide. Propargylglycolide (PGL), an alkyne functionalized lactide derivative, was synthesized in three steps beginning with a Reformansky-type reaction between propargyl bromide and ethyl glyoxalate in the presence of activated zinc (**Scheme 15**).[33] Bulk polymerization of the monomer in the presence of $SnOct_2$ shows a linear relationship between the number average molecular weight (M_n) and conversion, indicating a reasonably controlled

homopolymerization; the polymer was amorphous with a T_g of 30 °C.

Incorporation of propargylglycolide in a copolymer with lactide was consistent with the feed ratios and ^{13}C NMR is consistent with propargylglycolide being evenly distributed throughout the copolymer (**Figure 5**).

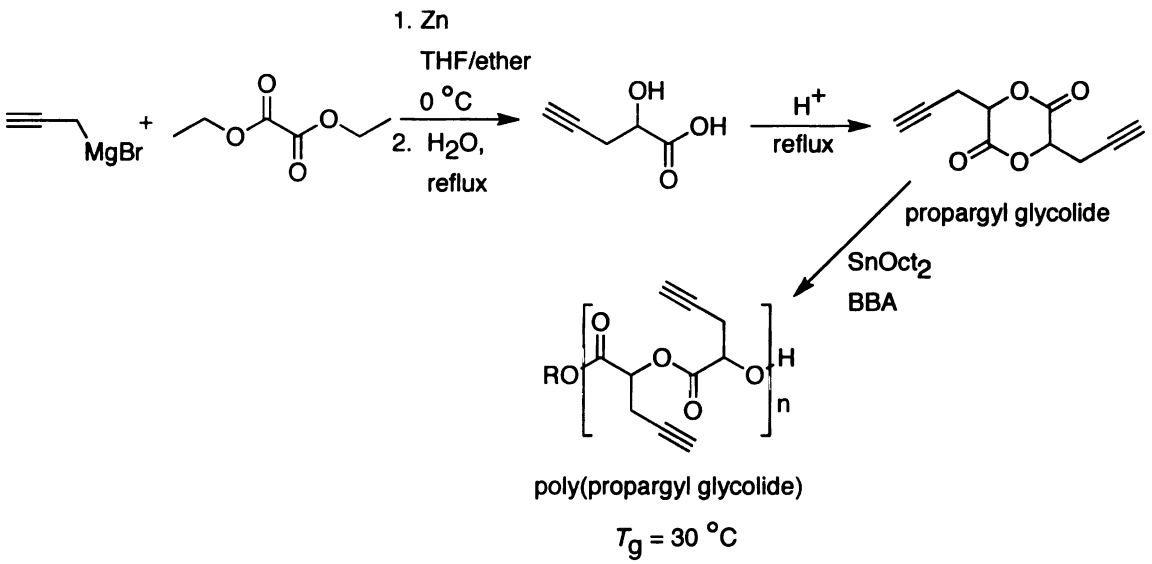

Scheme 15. Synthesis and polymerization of propargylglycolide.

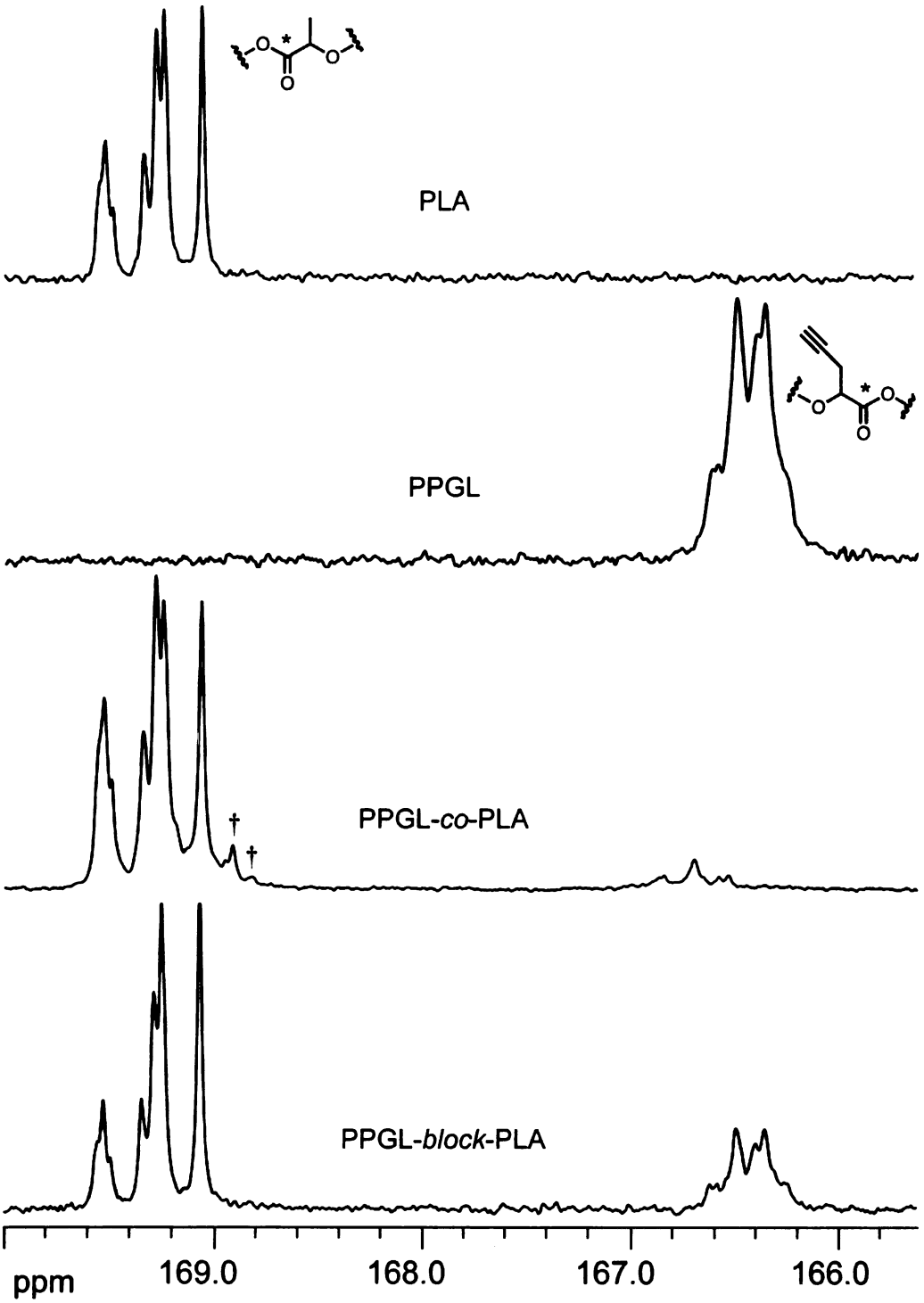

Figure 5. 75 MHz ^{13}C NMR carbonyl regions of propargylglycolide homopolymer (PPGL), copolymers, and polylactide (run in $CDCl_3$). †Unique lactide carbonyl resonances in poly(lactide-*co*-propargylglycolide) (PLA-*co*-PPGL).[33]

Post-Polymerization Modification

As shown in **Scheme 1**, the functional monomer approach involves multi-step synthetic procedures each time modification is desired. Moreover, the functionality that is initially introduced must be compatible with polymerization conditions. Similarly, post-polymerization modification requires careful control of reaction conditions to avoid backbone degradation, but in contrast to the functional monomer approach, it offers the distinct advantage that an array of polymers can in principle be accessed from a single monomer. Having a single, simple procedure for placing a broad spectrum of pendant functional groups onto polyester substrates is highly desirable. The ideal post-polymerization modification approach should utilize a chemical process that does not degrade the polyester backbone and be compatible with a wide range of functional groups, solvents, and conditions.

Although this document primarily focuses on glycolide and polyglycolide derivatives, most examples of post-polymerization modification on polyesters use various poly(ε–caprolactone) derivatives and thus these examples will be used as background in this area.

Direct Grafting of Functional Groups

Directly grafting functional groups to a polymer backbone is appealing because of the vast number of groups that can potentially be attached to a single polymer scaffold. For example, Vert reported the derivatization of ε-caprolactone (ε-CL) using lithium diisopropylamide (LDA) and electrophiles such as methyl

iodide, benzylaldehyde, carbon dioxide, naphthoyl chloride, bromoacetylated α-hydroxy-ω-methoxy-poly(ethylene glycol) and polylysine (**Scheme 16**).[35-38] Successful implementation of this method however, is limited due to polymer degradation by main chain cleavage and low grafting densities, typically 10 %.

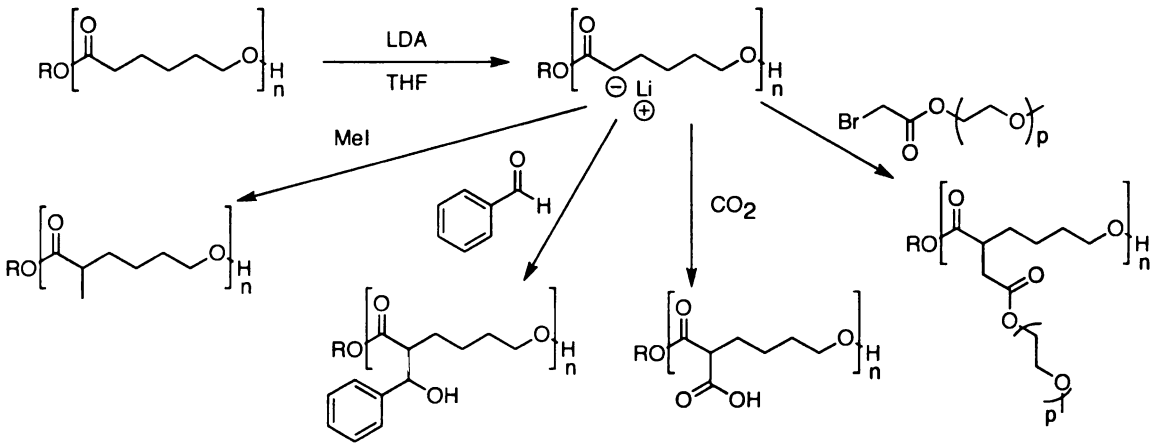

Scheme 16. Functionalized poly(ε-caprolactone) via anionic derivatization.

Luo and co-workers described a similar approach, using free radical reactions.[39] Radical reactions initiated by benzoyl peroxide, a radical initiator, covalently grafted maleic anhydride to PLA (**Scheme 17**). Amidation of maleic anhydride with hexanediamine resulted in the formation of carboxylic acid and amine side chains. The use of free radicals is also limited by significant backbone degradation, losing up to 20 % of the original M_n, and very low grafting densities, a maximum of 3 %.

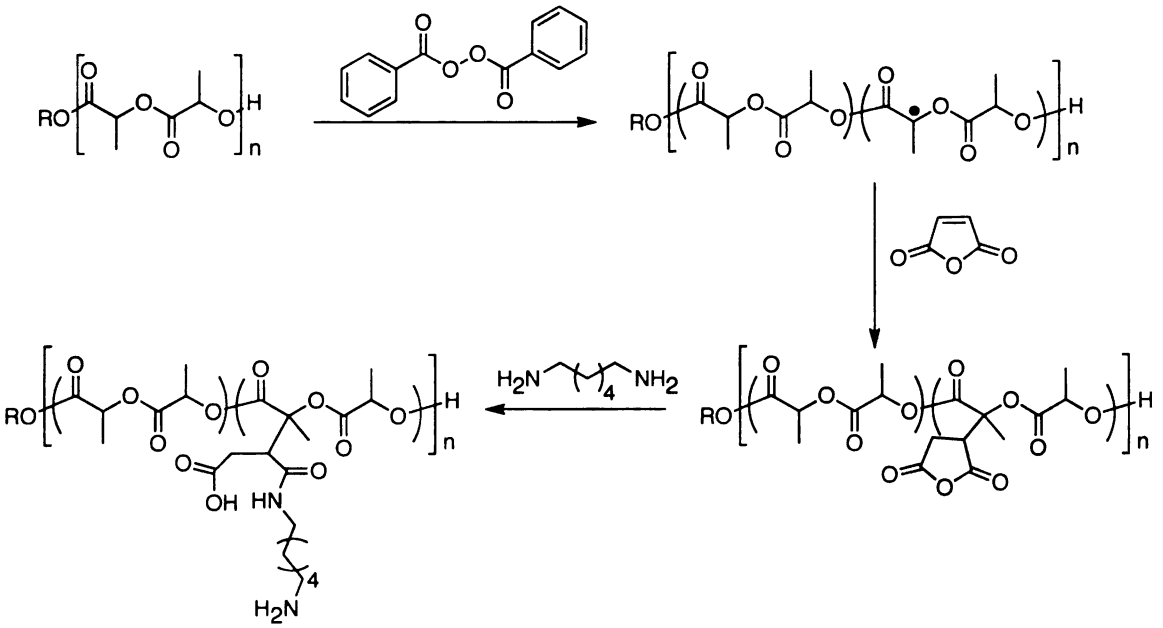

Scheme 17. Synthesis of functionalized polylactide via free radical addition of maleic anhydride and functionalization of maleic anhydride with hexanediamine.

Lactide Initiation from Pendant Alcohol Groups

One way to control PLA's poor compatibility with soft tissue is to modify its crystallinity and degradation rate by introducing branching into the polymer structure. Branching affects physiochemical properties such as crystallinity, T_g, and T_m. Recently a number of examples of branched polymer structures have been reported including hyperbranched,[40-42] star-shaped,[43-45] and dendritic[46-48] polymers, all showing interesting rheological and mechanical properties. For example, Ouchi *et al.* synthesized poly(cyclo[Gly-Ser(OBzl)]-*co*-LA), a copolymer of a protected cyclodepsipeptide consisting of glycolic acid (Gly) and *O*-benzyl-*L*-serine (OBzl) and lactide (**Scheme 18**).[49,50] The functionalized monomer was copolymerized with lactide, spacing the alcohol groups along the polymer

backbone. Comb polymers were synthesized by polymerizing lactide "teeth" from pendant alcohol groups. *In vitro* degradation suggests that comb-type PLA degrades significantly faster than linear PLA due to increased number of hydroxy end groups.

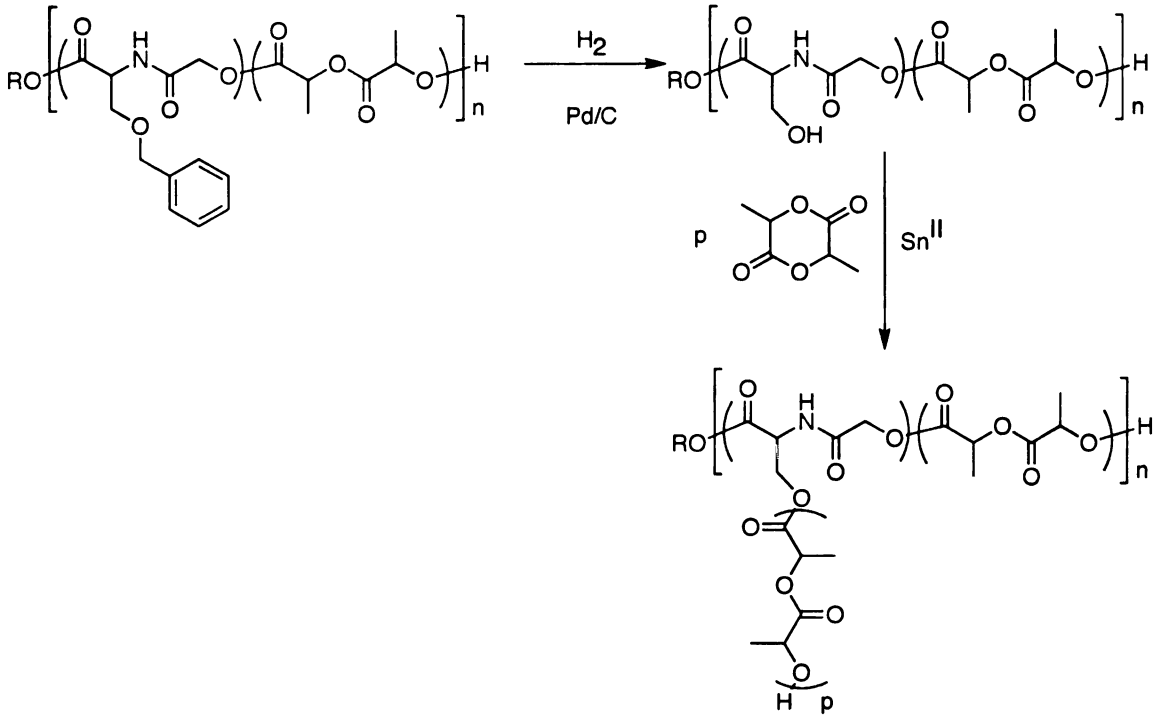

Scheme 18. Synthesis of comb PLA via macroinitiation of lactide from pendant alcohol groups.

Polymers such as poly(vinyl alcohol) PVA can also act as a scaffold for the polymerization of lactide.[51-56] Kissel and co-workers used a hydrophilic polymer backbone, poly(vinyl alcohol) (PVA), and polymerized hydrophobic poly(lactide-*co*-glycolide) (PLGA) branches to be used in parenteral protein delivery systems (**Scheme 19**).[56] The addition of short hydrophobic polylactide chains to a hydrophilic backbone promotes rapid water uptake and faster biodegradation rates.

Polymers were synthesized with molecular weights up to 773 kD and intrinsic viscosity measurements ranged from 0.26-0.53 supporting a branched polyester. DSC analysis revealed only one transition suggesting that the components are entirely miscible. Noticeably, both the T_g and T_m decreased with increasing PVA/PLGA ratio due to higher chain mobility; this allowed the synthesis of polymers with specific thermomechanical properties.

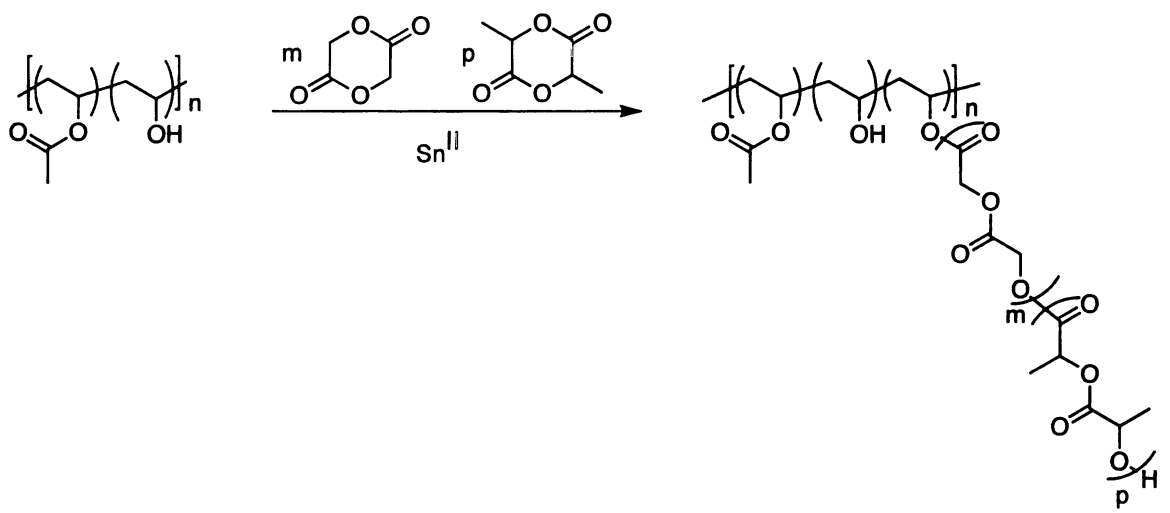

Scheme 19. Synthesis of poly(vinyl alcohol-*graft*-poly(lactide-*co*-glycolide)) via macroinitiation of lactide and glycolide from poly(vinyl alcohol).

DCC Coupling Reactions

Polyesters that contain pendant alcohol groups can also be used to graft small molecules. Emrick *et al.* has shown DCC-coupling of aliphatic polyesters and succinic acid ester derivatives of various PEG monomethyl ethers.[57] The synthesis of the necessary α-cyclopentene-δ-valerolactone was accomplished in three steps and is shown in **Scheme 20**. The coupling reaction was performed in

refluxing dicholoromethane and grafting efficiencies of 70-80 % were achieved with little to no backbone degradation.

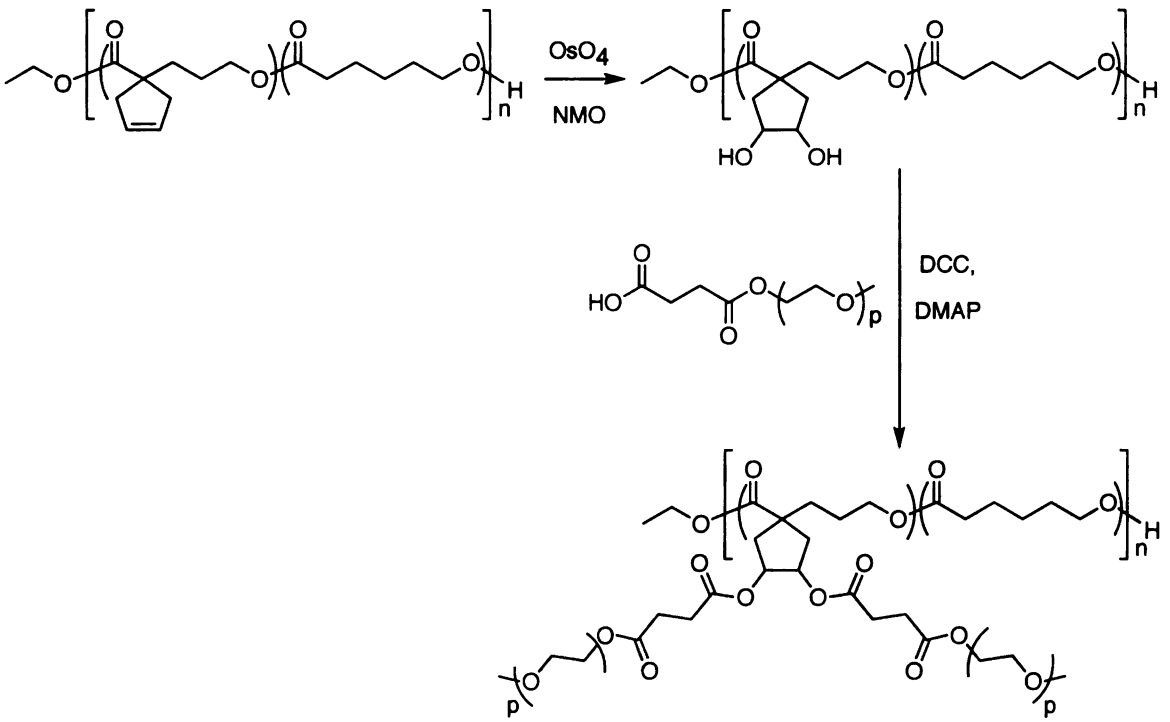

Scheme 20. Synthesis of polyester-*g*-poly(ethylene glycol) copolymers via DCC coupling of terminal alcohol groups and succinic anhydride derivatives.

Linear polylactides with pendant alcohol groups have also been prepared by the hydroboration-oxidation of poly(lactide-*co*-diallylglycolide) (**Scheme 21**).[34,58] Stirring the alkene-functionalized polymer with 9-borabicyclo[3.3.1]nonane (9-BBN), and oxidation by hydrogen peroxide and sodium acetate provided terminal alcohol groups. GPC analysis showed that the polymer did not degrade under these conditions and the disappearance of all allyl resonances in the ^{1}H NMR spectrum confirmed complete oxidation of the allyl groups. In order to investigate the influence of fatty acids on osteoblast phenotypes, Radano used DCC coupling to attach a variety of long-chain fatty acids without backbone degradation.[58]

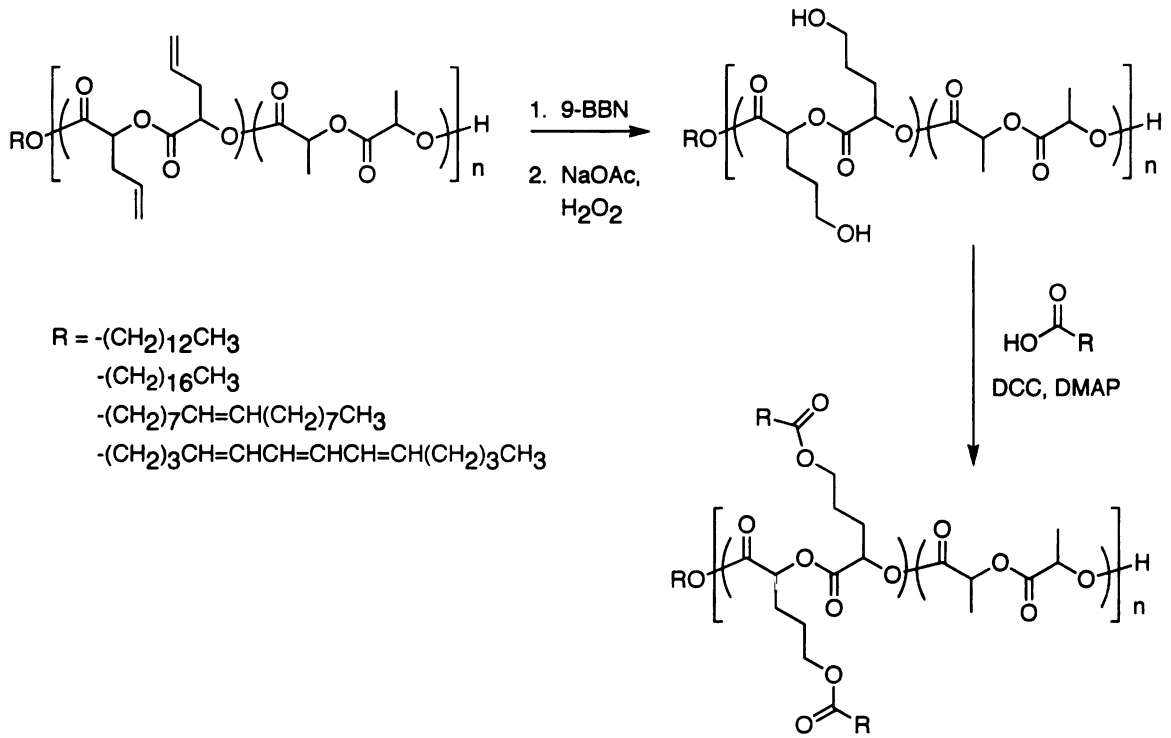

Scheme 21. Hydroxylation and functionalization of poly(*L*-lactide-*co*-diallylglycolide).

Ketoximine Coupling Reactions

Another approach to post polymerization modification is the selective reaction between a ketone-bearing polyester and an aminooxy-terminated functional group. Using Jérôme's 1,4,8-trioxaspiro[4.6]-9-undecanone[59-61] ketone-functionalized polyester, Griffith and co-workers showed selective coupling of aminooxy-terminated poly(ethylene oxide)s (PEO) ranging from 3-45 ethylene glycol units (**Scheme 22**).[62] Griffith *et al.* varied the amount of the functionalized ε-caprolactone in the copolymer from 7 to 31 mol percent. Chemoselective coupling was performed by mixing the aminooxy-terminated PEOs and the ketone-bearing ε-caprolactone in chloroform at various stoichiometries and temperatures.

No backbone degradation occurred during the coupling reaction and when the PEO content exceeded 50 wt%, the polymer became water-soluble. In addition, the grafted polymers had higher thermal stability than the pre-grafted polymers. Nevertheless, copolymers with high ketone content were insoluble in organic solvents, which restricts the use of these functional polymers.[63]

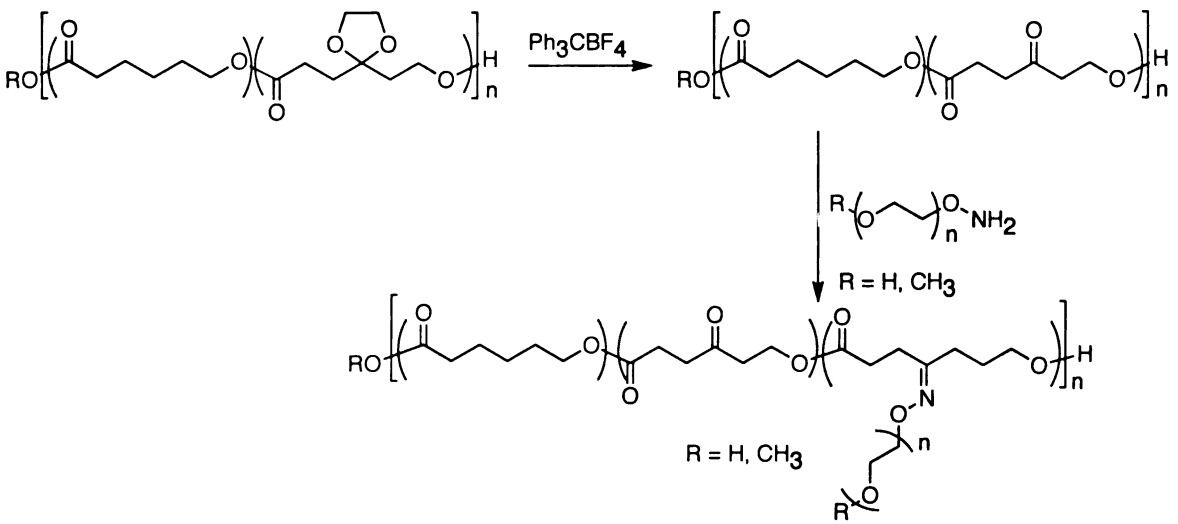

Scheme 22. Synthesis of poly(ε-caprolactone-*graft*-poly(ethylene oxide)) via ketoximine ether functionalization.

Wooley used similar chemistry for the post-polymerization modification and cross-linking of poly(ε-caprolactone-*co*-2-oxepane-1,5-dione) (poly(CL-*co*-OPD)) (**Scheme 23**).[64] The aminooxy molecules were synthesized in two steps from the corresponding alkyl bromides. Using *p*-toluenesulfonic acid as a catalyst, complete conversion to the ketoxime was observed in 2 hours with up to 80 % grafting efficiency. In addition to functionalization with alkyl ligands, a difunctional oxyamine was used to cross-link poly(ε-CL) and enhance the polymer's

robustness. Reaction times of 10 days produced an insoluble cross-linked gel material, which was characterized by IR spectroscopy.

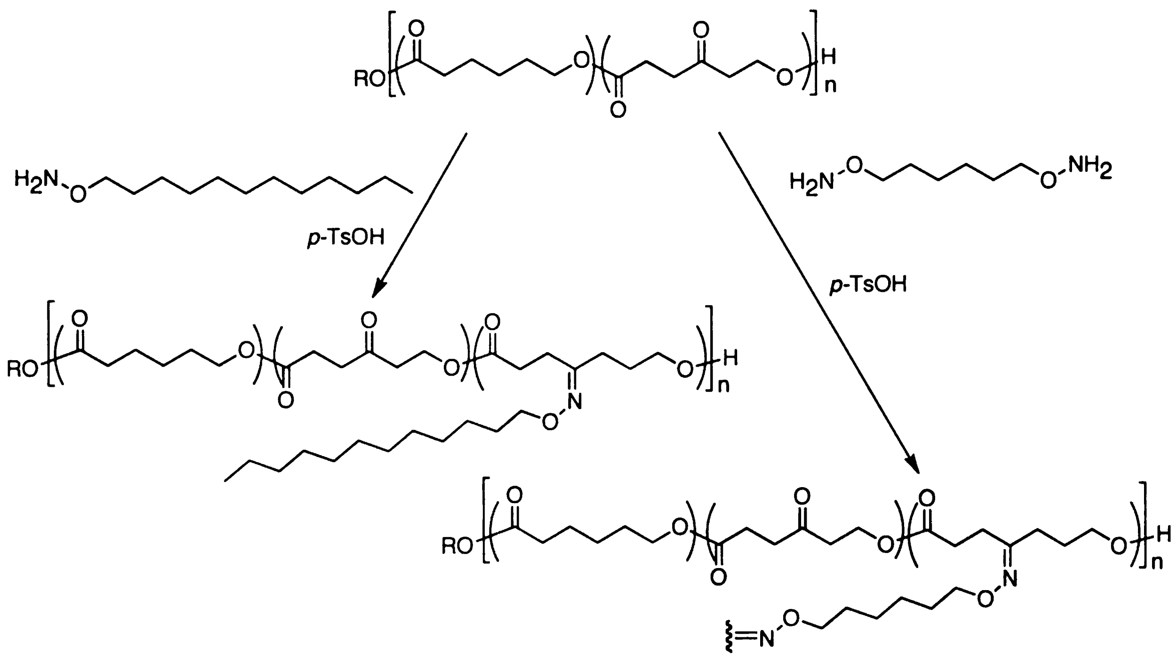

Scheme 23. Functionalization and cross-linking of poly(ε-caprolactone-*co*-2-oxepane-1,5-dione) with 1-aminooxydecane or 1,6-bis(aminooxy)hexane.

Michael Addition Reactions

Recently, the addition of sulfur to pendant acrylate groups has been investigated as a modification strategy. The γ-acrylic-ε-caprolactone was synthesized in three steps starting from 1,4-cyclohexane-diol (**Scheme 24**) and polymerized into homo- and co-polymers with ε-caprolactone and lactide.[65] Thiol end-capped PEO was added to the pendant acrylic groups via Michael addition in the presence of pyridine, resulting in 65 % conversion of the acrylic groups. Other Michael reactions included the attachment of triphenylmethanethiol and mercaptoacetic acid.[66] Although no degradation was observed under the reaction

conditions, the Michael reaction was not quantitative and cross-linking between the residual acrylic groups occurred.

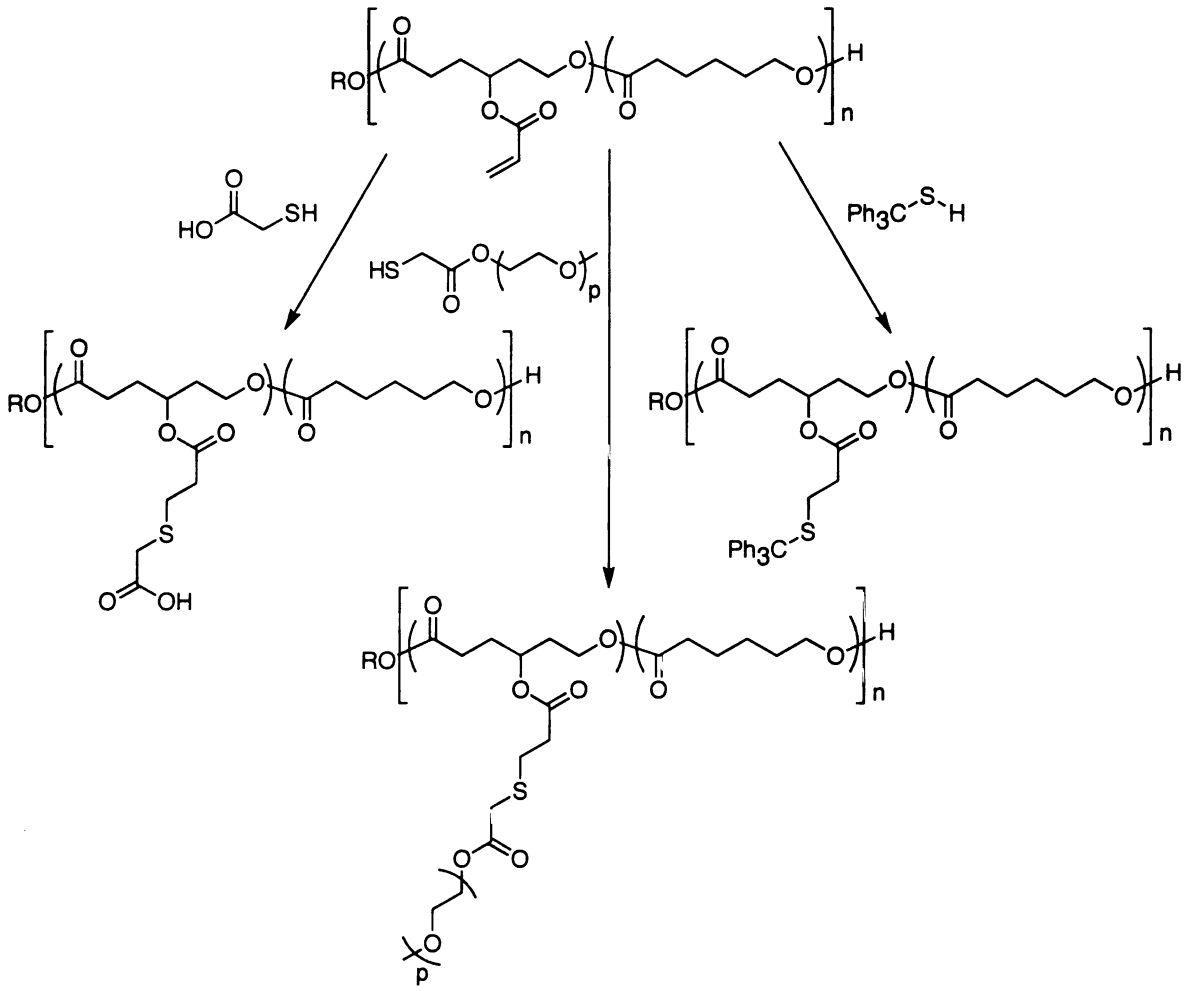

Scheme 24. Functionalization and grafting of poly(ε-caprolactone) by Michael-type addition.

Atom Transfer Radical Addition Reactions

Atom transfer radical addition (ATRA) is the radical substitution of a radical initiator with a "grafting group," frequently containing a double bond. One of the most commonly used monomers is α-chloro-ε-caprolactone because its activated chloride is well suited for ATRA. α-Chloro-ε-caprolactone can be easily

synthesized by Baeyer—Villiger oxidation of 2-chlorohexanone.[67] Various olefins have been grafted to polymers via ATRA such as 3-buten-1-ol, 1,2-epoxyhex-5-ene, and α-methoxy-ω-acrylate-PEO using CuBr/Me_6TREN (copper(I) bromide/ tris[2-(dimethylamino)ethyl]amine) in DMF (**Scheme 25**). Unfortunately, many chlorinated units were lost by reduction during ATRA, which decreased the grafting efficiency.[68,69]

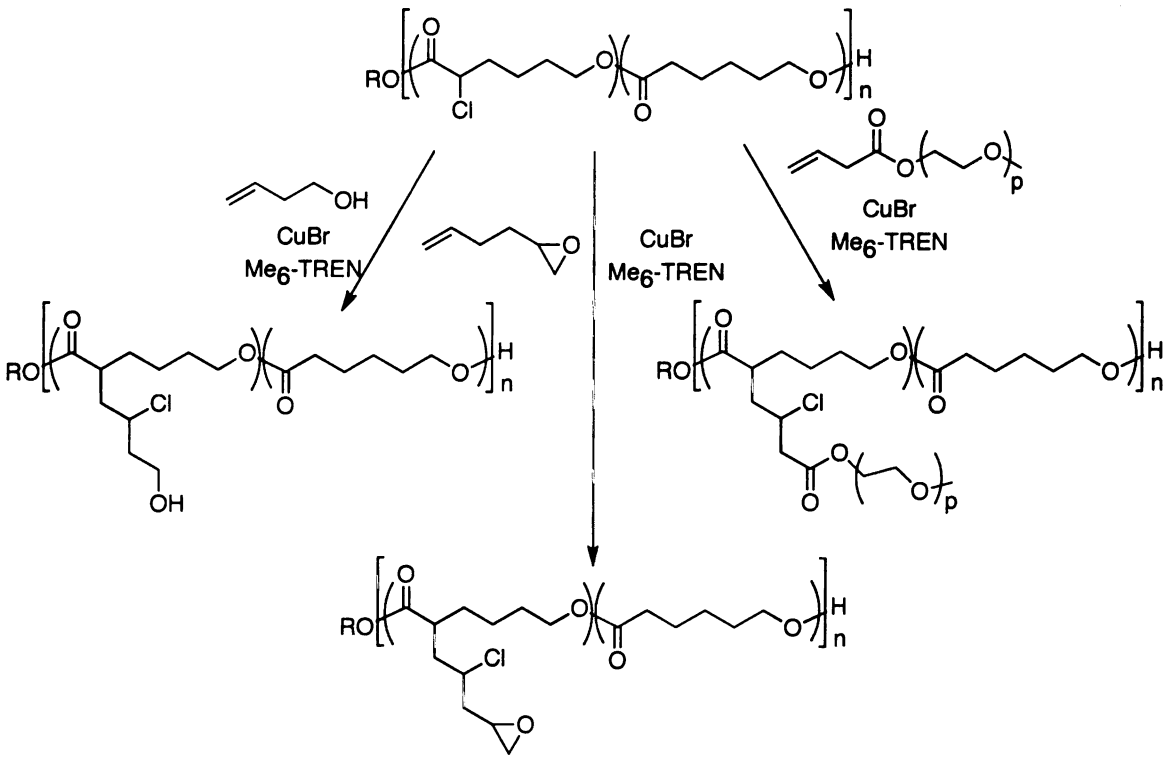

Scheme 25. Functionalization of poly(ε-caprolactone) by atom transfer radical addition.

Olefin Cross Metathesis

Olefin cross-metathesis and ring-opening olefin metathesis have become standard procedures in polymer chemistry; however they have only been applied to PLA in one example. Radano *et al.* performed olefin cross-metathesis using

Grubbs' 1st generation ruthenium carbene catalyst on an allyl-functionalized copolymer, poly(lactide-*co*-diallylglycolide), using 9-decenyl-1-oxy-(4-nitrobenzene), allylbenzene, 2-(2-propenyloxy)benzaldehyde, 9-decane-1-oxy-(*tert*-butyldimethylsilane), or 9-decen-1-al. (**Scheme 26**).[34] Although the polymer showed no signs of degradation, the polymer was discolored indicating possible ruthenium contamination. Using a nitrobenzene UV tag, the conversion of olefins undergoing metathesis could be calculated, typically 26-29 %. In addition, a viscous gel formed in the absence of an olefin substrate, presumably the result of cross-linking the pendant allyl groups. To prevent cross-linking, five equivalents of the olefin substrate were required.

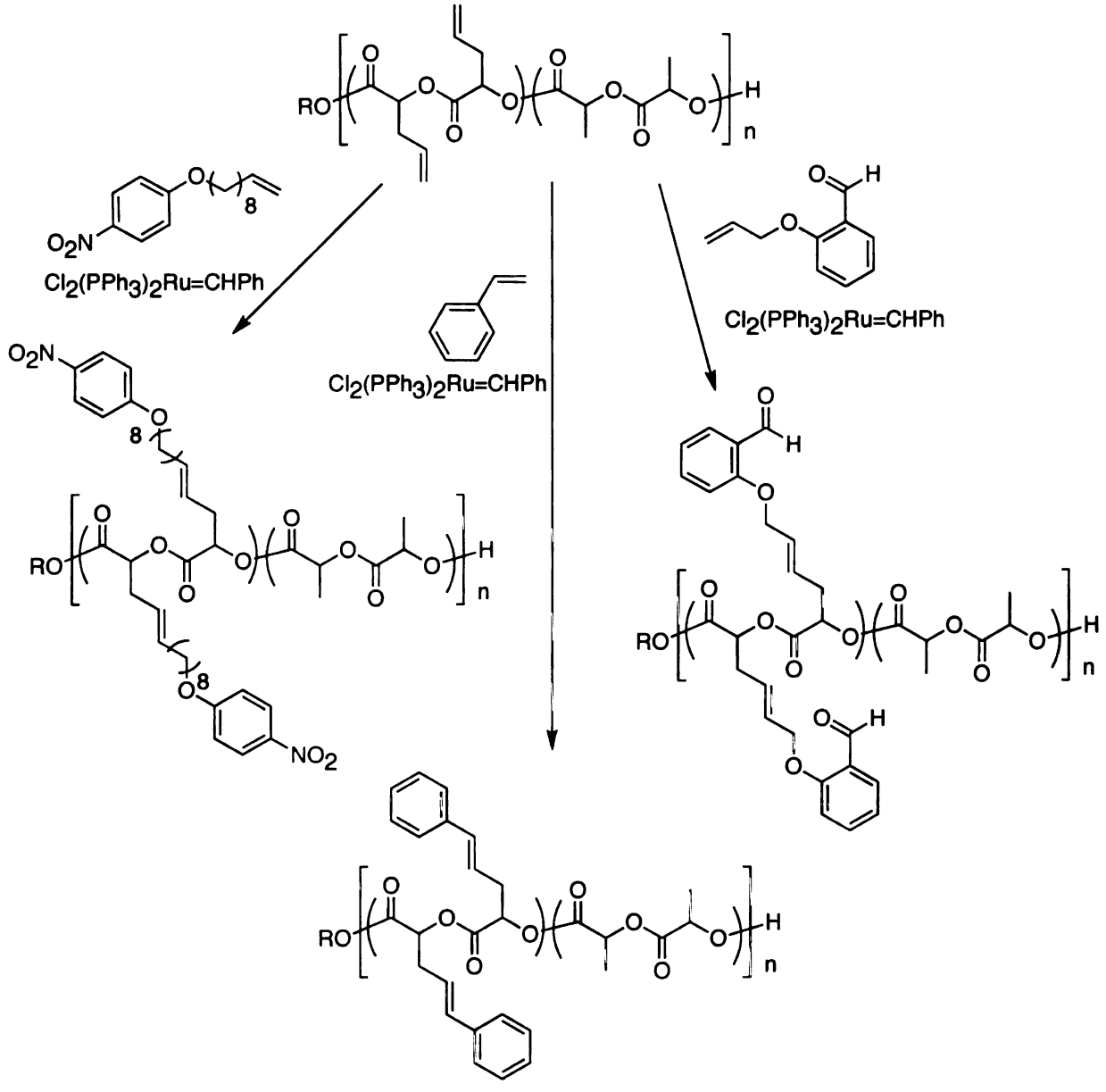

Scheme 26. Functionalization of poly(*L*-lactide-*co*-diallylglycolide) using olefin cross metathesis.

"Click" Chemistry

Because of its high selectivity, reliability, and tolerance to a broad range of functional groups and reaction conditions, "click" chemistry, specifically the copper(I)-mediated 1,3-dipolar cycloaddition of azides and alkynes, is a powerful strategy for elaborating polymer architectures. The Emrick group first described the

use of aqueous "click" chemistry to graft azide-terminated PEO and peptides onto polyesters containing pendant acetylene groups (**Scheme 27**).[70] Later, Jérôme and co-workers found Emrick's conditions caused significant backbone degradation during functionalization.[71,72] Using less severe conditions (THF as the solvent), they were able to introduce PEO, tertiary amines and ammonium salts onto caprolactone-based polyesters having pendant azides (**Scheme 28**).

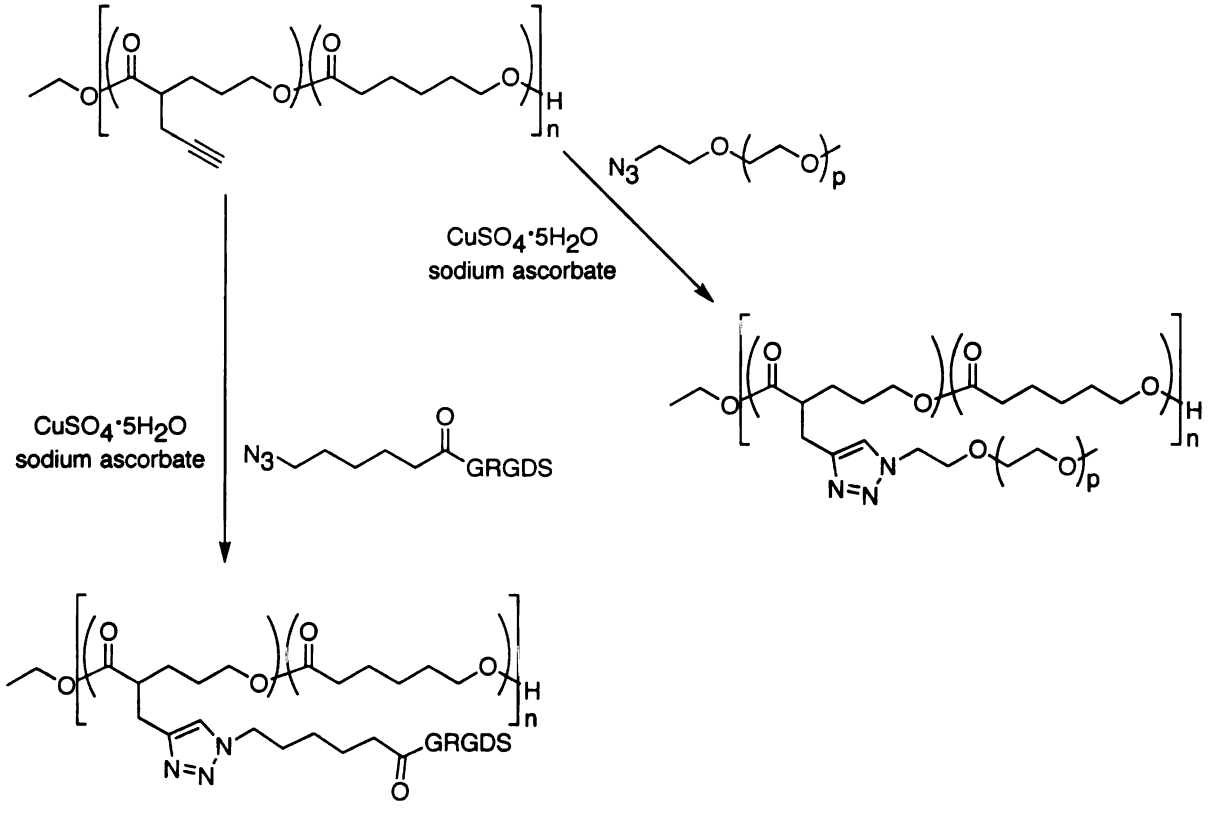

Scheme 27. Emrick's synthesis of PEG-functionalized polyesters by click chemistry.

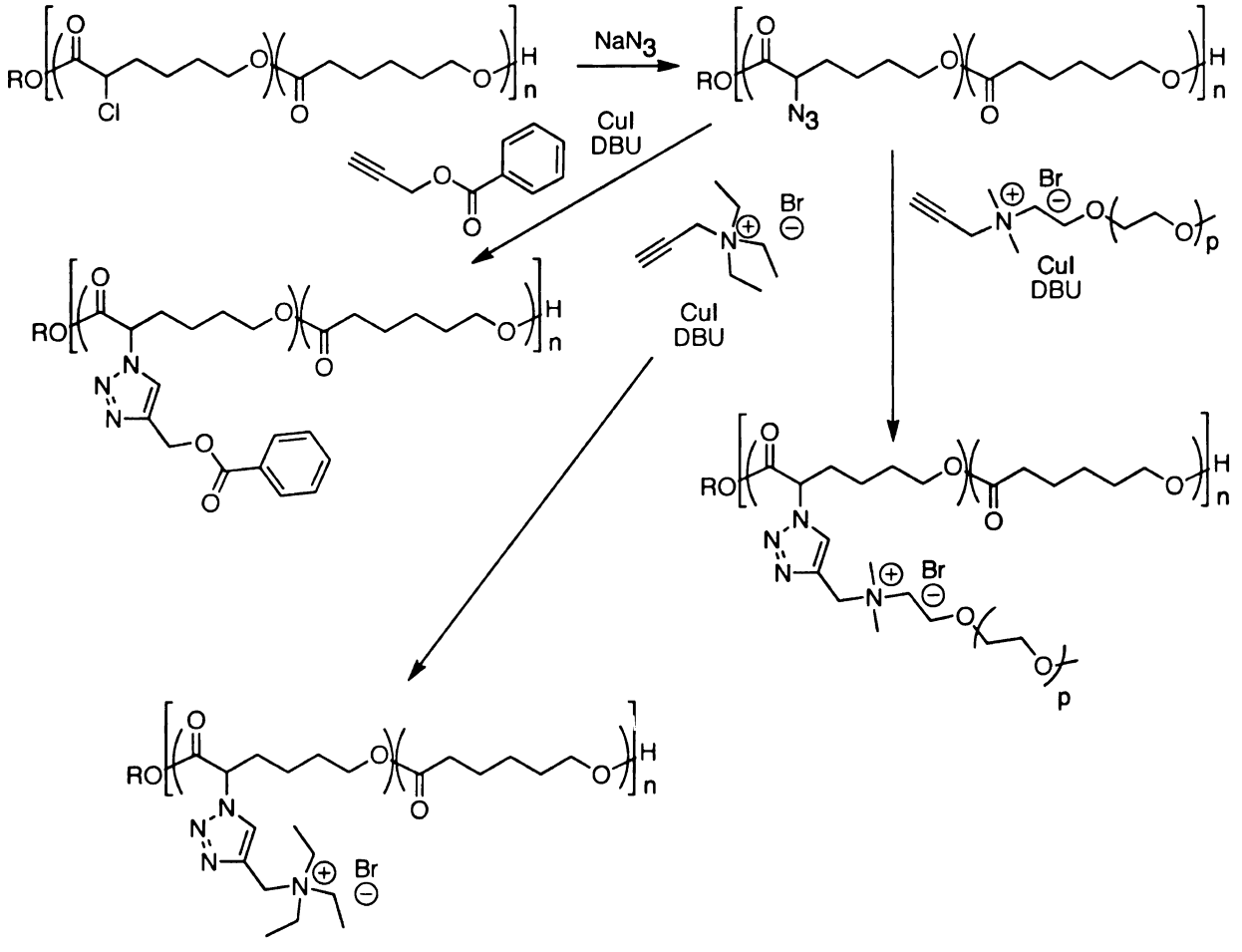

Scheme 28. Jérôme's synthesis of functionalized polyesters by Cu(I) catalyzed click chemistry.

Recently we introduced an acetylene modified lactide derivative capable of post-polymerization modification by click chemistry (**Scheme 29**). Using milder conditions, DMF and room temperature, we were able to functionalize the polyester with alkyl and poly(ethylene glycol) branches. We showed good control over the degree of functionalization and no backbone degradation under the new click conditions.[73]

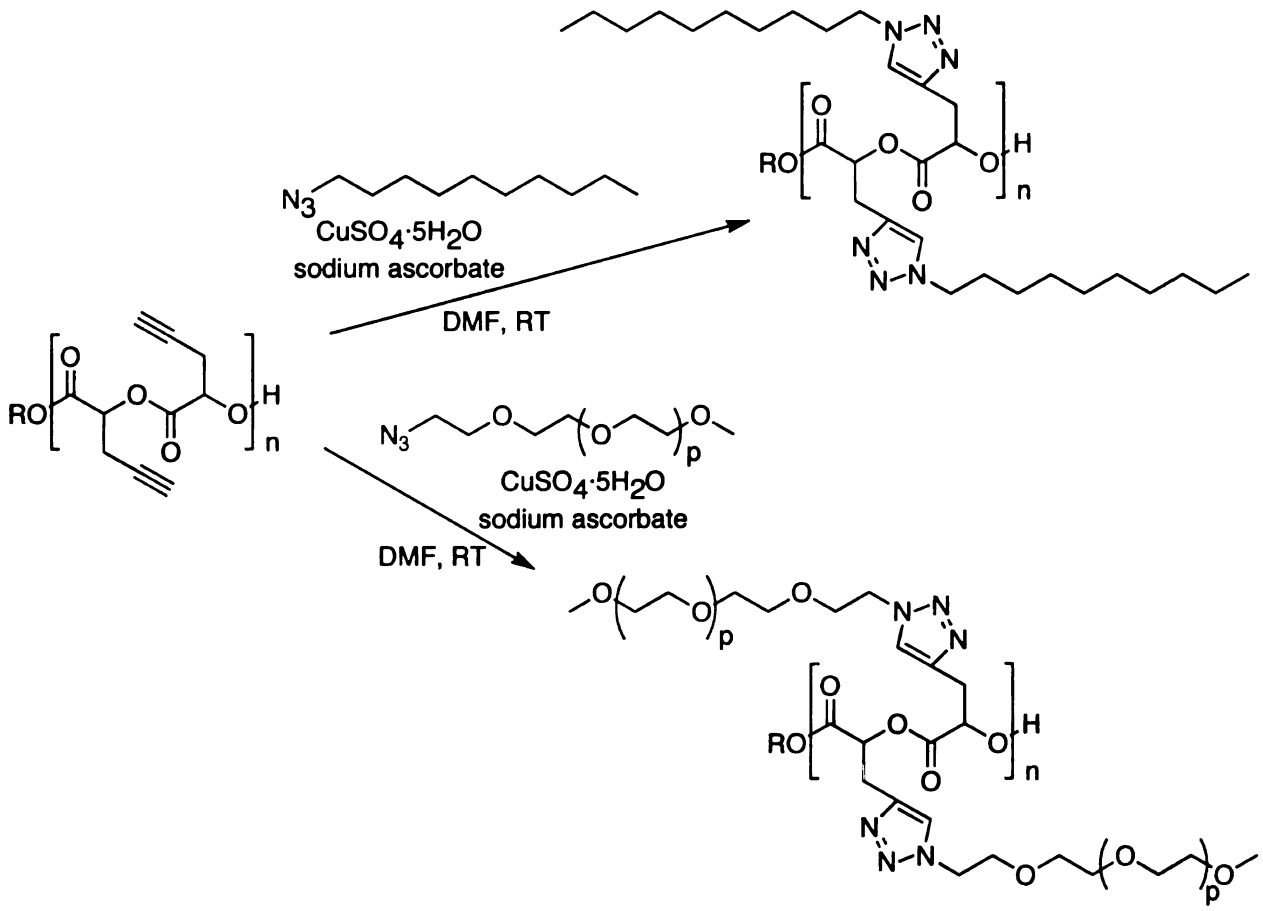

Scheme 29. Synthesis of alkyl- and poly(ethylene glycol)-functionalized poly(propargylglycolide).

Conclusion

Functionalized polyglycolides greatly enhance PLA's role in biomedical and structural applications. Modification via either the functional monomer approach or the post-polymerization modification approach provides opportunities to modify the polymers' T_g, T_m, and mechanical properties. Large bulky substituents increase the T_g relative to PLA and long flexible chains degrease the T_g of the homopolymer. The addition of functional groups provides access to many polymer architectures via post-polymerization.

Chapter 2 Reactivity Ratios of Substituted Lactide Monomers

Introduction

Biodegradable polyesters are used widely in pharmaceutical, biomedical, and environmental applications.[17,24,26,74-76] Many of these applications require specific material properties such as a high T_g, controlled crystallinity, a specific degradation rate, and high mechanical strength that cannot be obtained from the homopolymers alone. Typical approaches used to control these properties include manipulation of stereochemistry,[77-79] preparation of block copolymers,[80-83] and the synthesis of specialized monomers.[10,13,16] Perhaps the simplest method, however, is the copolymerization of two or more monomers which can provide multiple materials from a few starting monomers.[84-86] For example, copolymers of lactide and glycolide or ε-caprolactone are now commercially available and have been used use as sutures, implants, drug carriers, and cell scaffolds for tissue engineering.[86-88]

Although copolymerizations are often assumed to be completely "random", few are actually random from a statistical point of view due to the higher reactivity of one monomer towards polymerization. The products of such copolymerizations are often "blocky" and exhibit multi-phasic properties. Access to homogeneous polymers is particularly important in drug delivery and other applications because the polymer degradation rate and drug release profile are affected by the polymer crystallinity. Drugs diffuse more rapidly through amorphous domains than through

the crystalline regions,[89] and in poly(lactide-*co*-glycolide) and poly(lactide-*co*-ε-caprolactone) crystalline regions degrade far slower than amorphous regions.[90] In both systems, crystallization is the outcome of different monomer reactivities and the nonrandom placement of the monomers in the copolymers. In the copolymerization of lactide and ε-caprolactone[86] lactide is approximately 30 times more reactive, whereas in the copolymerization of lactide and glycolide,[91] glycolide is 11 times more reactive than lactide.

In a copolymerization of two monomers, M_1 and M_2, four rate equations describe the rates of homo- and cross-propagation when the addition of monomer to a growing chain is only dependant on the chain end. In each expression, the rate of monomer addition is described by the rate constant, k. For example, when M_1 adds to a propagating chain ending in M_2, the rate constant is defined as k_{21}.

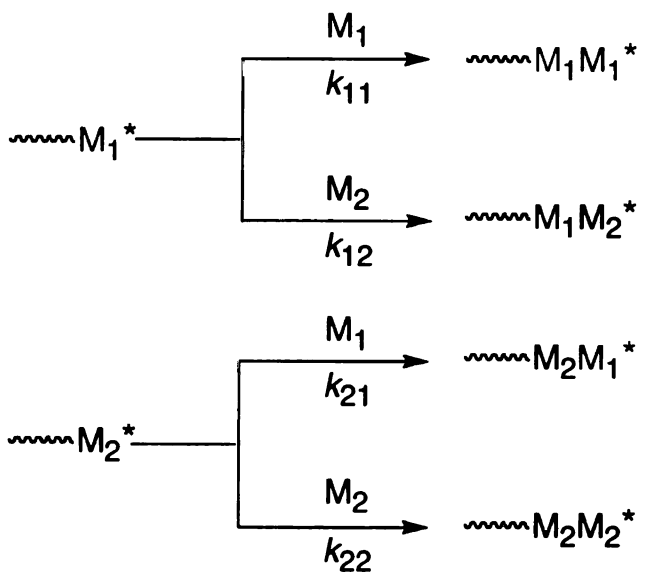

(1)

(2)

(3)

(4)

$$r_1 = \frac{k_{11}}{k_{12}} \quad \text{and} \quad r_2 = \frac{k_{22}}{k_{21}} \tag{5}$$

Unfortunately, absolute rate constants are often inaccessible. Therefore the reactivity ratios, r_1 and r_2 (equation 5), are extracted from competitive reactions in lieu of the rate constants to describe the reactivity of the monomers in the copolymerization. The instantaneous polymer composition of the copolymer is described by the relative incorporation of M_1 and M_2 expressed in terms of the monomer reactivity ratios, r_1 and r_2 (equation 6). Reactivity ratios are usually extracted from polymerization data using the Fineman-Ross (F-R)[92] or Kelen-Tudös (K-T)[93] methods however more statistically sound methods such as non-linear least squares[94] are generally preferred.

$$\frac{d[M_1]}{d[M_2]} = \frac{[M_1](r_1[M_1]+[M_2])}{[M_2]([M_1]+r_2[M_2])} \qquad (6)$$

Monomer reactivity ratios provide a straightforward method for predicting copolymer architectures and ultimately copolymer properties such as T_g and degradation profiles. Once determined, monomer reactivity ratios can be used to predict copolymer architectures. Random copolymers are formed when $r_1 = r_2$, and "blocky" copolymers containing long homopolymer segments form when $r_1 > r_2$ or $r_2 > r_1$. Although the reactivity ratios for many nondegradable polymers have been determined,[94-98] the reactivity ratios of most substituted lactide derivatives are unknown.[99,100] The few examples include the copolymerization of lactide with glycolide (GA) ($r_{LA} = 0.22$ and $r_{GA} = 3.4$),[91] 3-methylglycolide (3-MG) ($r_{LA} = 0.92$

and $r_{3\text{-MG}}$ = 1.71),[95] ε-caprolactone (r_{LA} = 26.5 and $r_{\varepsilon CL}$ = 0.92),[86] 3-(1,2-3,4-tetraoxobutyl-diisopropylidene)-1,4-dioxane-2,5-dione (DIPAGYL) (r_{LA} = 1.24 and $r_{DIPAGYL}$ = 0.4)[96] and 3-benzylmethylglycolide (3-BMG) (r_{LA} = 0.37 and $r_{3\text{-BMG}}$ = 1.96).[97] Since these monomers are based on the same glycolide structure, the differences in reactivity are primarily based on steric hindrance around the ring carbonyls.

Functionalized lactide derivatives have been shown to have wide success in medical applications[17,25,26,73-75] and as effective initiators in the synthesis of comb or brush polymers.[49,50,83,102] Understanding the placement of the functionalized monomer in the polymer backbone is especially important when it contains a functional group that can undergo post-polymerization modification or serve as an initiator for the synthesis of comb polymers. Leemhuis and co-workers[19] evaluated the thermal properties of *L*-lactide copolymers comprised of ≥ 75 % *L*-lactide and 2 functional monomers with benzyl-protected hydroxy groups, 3-benzyloxymethyl glycolide (3-BMG) or 3-benzyloxymethyl methyl glycolide (3-BMMG); copolymers of *L*-lactide and 3-BMG contained highly crystalline regions, but copolymers with 3-BMMG were amorphous, indicating that the reactivity of 3-BMMG was similar to lactide. The difference between the two monomers is that 3-BMG lacks a methyl group at the 6-position, which increases its reactivity and leads to blocky polymers.

As part of our interest in designing, synthesizing, and characterizing functionalized lactide monomers,[10,12,16,73,98-100] we copolymerized *rac*-lactide with

five disubstituted lactide monomers and determined their reactivity ratios. We compared the reactivity ratio data with the thermal properties of *rac*-lactide copolymers and homopolymerization rate data to develop simple structure-reactivity relationships that will guide the design of future functionalized lactide monomers.

Results and Discussion

Monomer Syntheses

The syntheses of the substituted lactide derivatives—ethylglycolide (EG), isopropylglycolide (iPG), *n*-hexylglycolide (nHG), cyclohexylglycolide (cHG) and phenyllactide (PL) are shown in **Scheme 30**. The α-hydroxy acids used to prepare the disubstituted monomers were commercial products, as in the case of *DL*-phenyllactic acid, or synthesized.

2-Hydroxybutanoic acid (**2**) was prepared from reaction of propanal (**1**) with potassium cyanide followed by acidic hydrolysis of the cyanohydrin. Diazotization of *DL*-valine followed by alcohol displacement of the diazonium salt provided 2-hydroxy-3-methyl butyric acid (**5**).[101] 2-Hydroxyoctanoic acid (**8**) was prepared from reaction of *n*-hexyl Grignard with diethyl glyoxalate, followed by hydrogenation over Pd/C to give the α-hydroxy ester, which was hydrolyzed to **8**. Catalytic hydrogenation of mandelic acid provided 2-cyclohexyl-2-hydroxyacetic acid (**11**).[100] The α-hydroxy acids were dimerized to the symmetrical monomers using a previously reported protocol.[10] The *meso*-isomer was separated from the *racemic*-

isomers via recrystallization or column chromatography to eliminate potential isomer effects in determining the reactivity ratios (**Scheme 31**).

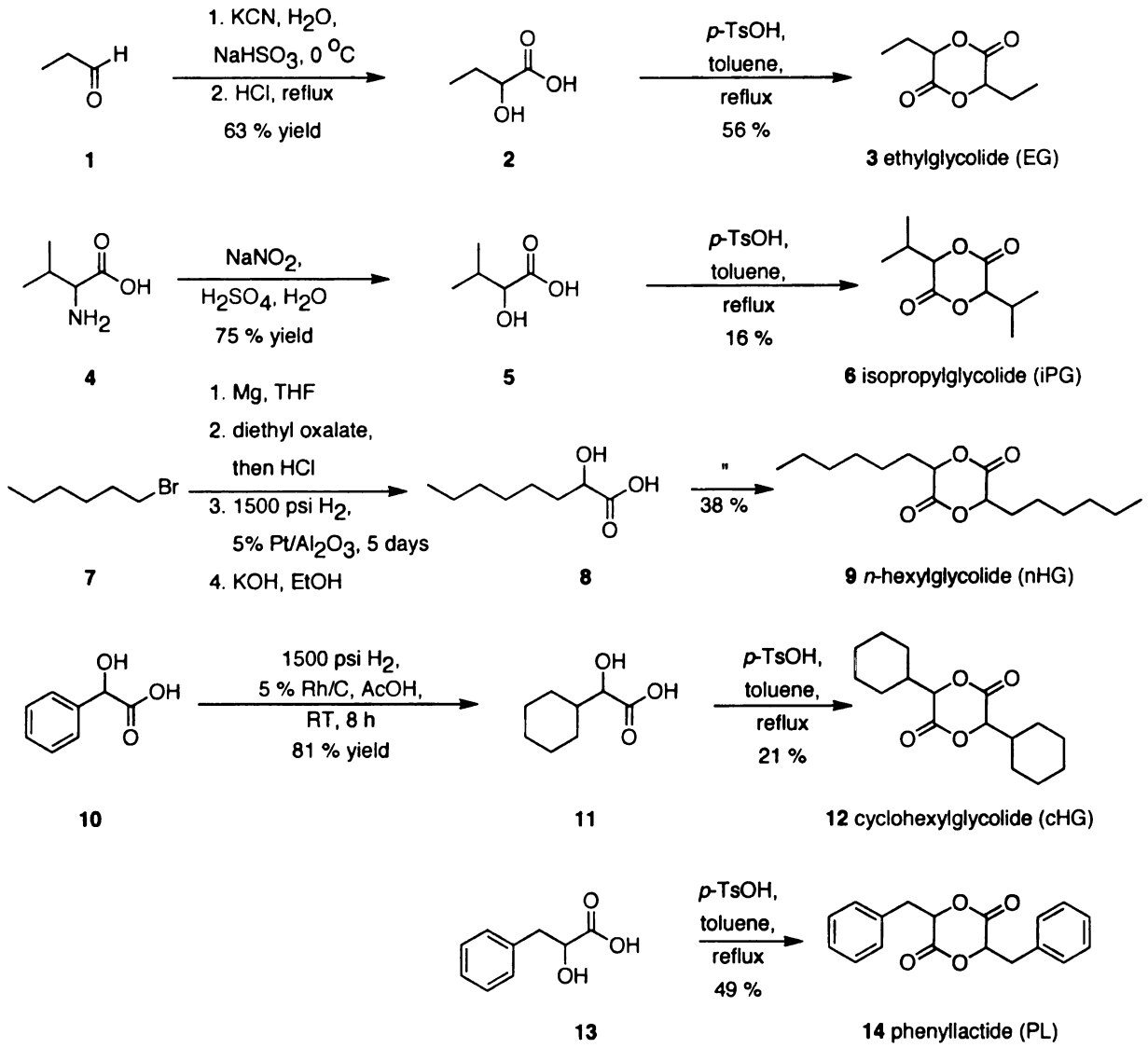

Scheme 30. Synthesis of disubstituted lactide monomers, ethylglycolide (EG), isopropylglycolide (iPG), *n*-hexylglycolide (nHG), cyclohexylglycolide (cHG) and phenyllactide (PL).

Copolymerization and Copolymer Isolation

The racemic glycolides were polymerized with *rac*-lactide at various mole fractions under solvent free conditions using $SnOct_2$ and *t*-butylbenzyl alcohol

(BBA) as the catalyst and initiator, respectively ([monomer]:[catalyst]:[initiator] = [400:1:1]) (**Scheme 31**). Since the monomer pool changes with conversion, the monomers were immersed in a preheated oil bath for 45 seconds and then quenched in ice to ensure low conversion (< 10 %). The monomer/polymer mixture was dissolved in CH_2Cl_2 and passed through a short silica column to separate the polymer from the monomers. After the separation was complete, the copolymer adsorbed onto the silica was transferred into a 25 mL round bottom flask containing MeOH. The mixture was stirred for 4 hours and then centrifuged. The colorless polymer solution was decanted from the silica gel, evaporated to dryness, and analyzed by ^1H NMR.

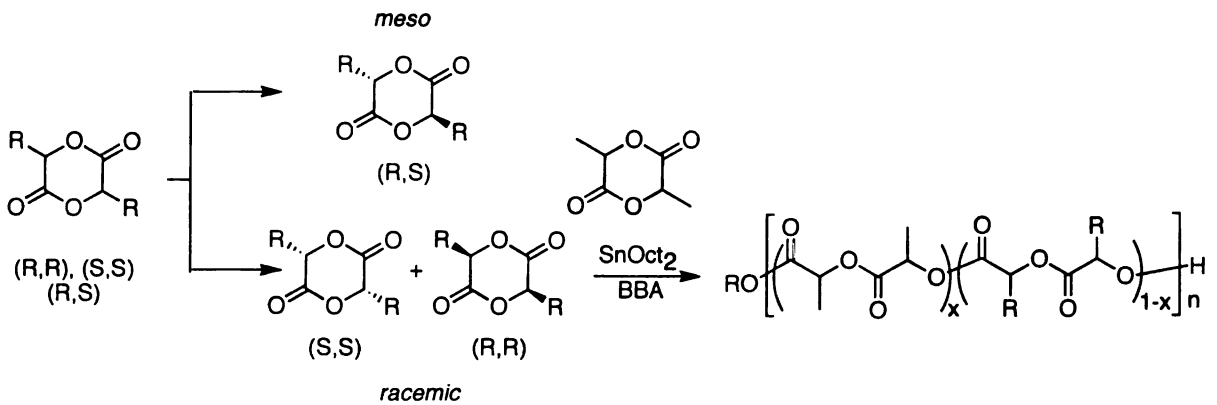

Scheme 31. Separation of *meso*- and *rac*- monomers, and copolymerization with *rac*-lactide. R denotes the substituent on the disubstituted glycolide.

Monomer Reactivity Ratios and Copolymer Architectures

We determined the relative incorporation of each monomer in the copolymers by comparing the integration of the methine peaks of each monomer in the copolymer ^1H NMR spectra. The molar fraction of lactide in the copolymer was

determined by equation 7, where F_1 is the molar ratio of lactide in the copolymer and I_{LA} and I_{M2} are the total integration of the methine protons of *rac*-lactide and the comonomer, respectively.

$$F_1 = \frac{I_{LA}}{I_{LA} + I_{M2}} \quad (7)$$

For example, in the copolymerization of lactide and *n*-hexylglycolide (molar lactide feed ratio (f_{LA}) = 0.81) (**Figure 6**), the signals from the methine protons of nHG and LA overlap, and the composition of the copolymer was calculated using the 3:2:1 ratio between the methyl protons (CH_3, 1.9-1.8 ppm), methylene protons (CH_2, 2.0-1.7 ppm), and methine protons of nHG (CH 5.2-2.0 ppm). We arbitrarily set the integration of the methylene protons ($I_{nHG\ CH_2}$) to be 2.00, which is consistent with the integration of the methyl protons ($I_{nHG\ CH_3}$ = 3.05). Subtracting the expected integration due to the nHG methine protons ($I_{nHG\ CH}$ = 1.00) from the total methine integration ($I_{nHG\ and\ LA\ CH}$ = 6.32) gave the relative integration of the lactide methine protons ($I_{LA\ CH}$ = 5.32). These values were used in equation 7 to calculate F_1 (f_1 = 0.81, F_1 = 0.84).

Figure 6. 500 MHz ^{1}H NMR of poly(LA-*co*-nHG) at 8 % conversion. The molar fraction of lactide in the copolymer (F_1) was determined using the relative integrations of the two comonomers (see text, f_1 = 0.81, F_1 = 0.84).

Reactivity Ratio Determination

We copolymerized *rac*-lactide and *rac*-ethylglycolide at eight different mole fractions of lactide (f_1). The final compositions of the copolymers at low conversion in terms of the mole fraction of lactide (F_1) are given in **Table 1**. Using Origin (OriginLab, Massachusetts, USA), we plotted the instantaneous copolymer composition (F_1) versus the comonomer feed composition (f_1) for the various lactide feeds. The reactivity ratios were extracted from the data via a nonlinear least squares (NLS) fit of the data to equation 8 using an iterative process for the selection of r_1 and r_2 values,[102]

$$F_1 = \frac{r_1 f_1^2 + f_1 f_2}{r_1 f_1^2 + 2 f_1 f_2 + r_2 f_2^2} \quad (8)$$

where F_1 and f_1 are the mole fractions of lactide in the copolymer and in the feed, respectively, and f_2 is the mole fraction of the disubstituted lactide derivative in the feed. The reactivity ratios calculated for the copolymerization of *rac*-LA and *rac*-EG were r_{LA} =1.29 and r_{EG} = 0.71 (**Figure 7**).

Table 1. Mole fractions of lactide in the feed (f_1) and copolymer (F_1) for the copolymerization of lactide and ethylglycolide.

f_1	F_1
0.95	0.97
0.89	0.92
0.86	0.89
0.75	0.80
0.71	0.77
0.55	0.60
0.36	0.45
0.16	0.20

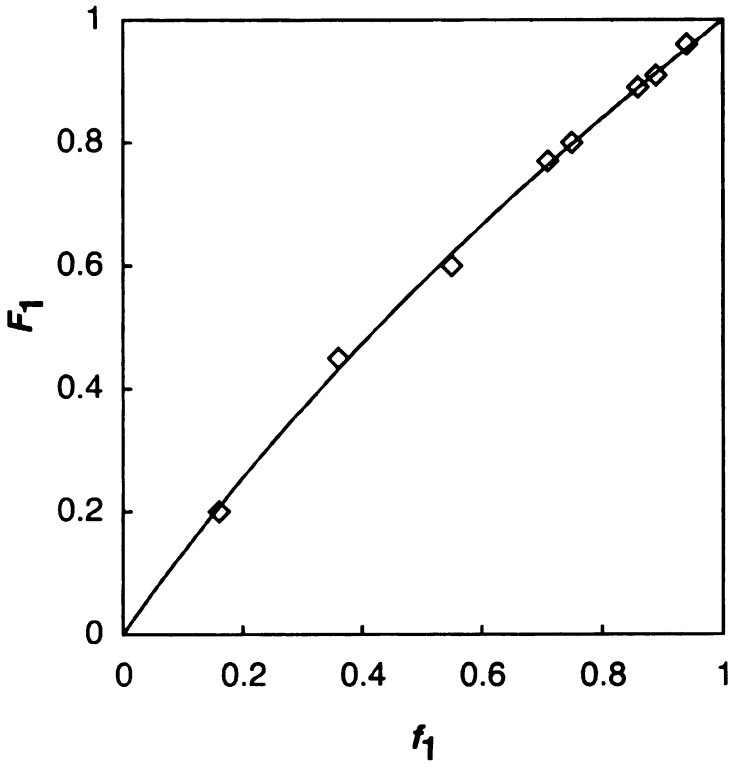

Figure 7. Nonlinear least squares fit of the copolymerization data of *rac*-lactide and *rac*-ethylglycolide to equation 7. The reactivity ratios were determined to be r_{LA} =1.29 and r_{EG} = 0.71.

The traditional methods for determining reactivity ratios were procedures that linearized the copolymerization data. For example, the Fineman-Ross method for analyzing copolymerization data expresses the copolymerization equation in terms of the mole fractions of the monomers, M_1 and M_2 in the feed (f) and the mole fraction of monomers, M_1 and M_2, in the copolymer (F_1):

$$\frac{F_1}{f_1}(f_1 - 1) = r_1\frac{F_1^2}{f_1} - r_2 \qquad (9)$$

where r_1 and r_2 are the reactivity ratios of the two monomers.[92] A plot of $\frac{f_1(1-2F_1)}{F_1(1-f_1)}$ versus $\frac{f_1^2(F_1-1)}{F_1(1-f_1)^2}$ should yield a straight line with a slope of r_1 and a y-intercept of r_2.

An analysis of the copolymerization using the Fineman-Ross method is shown in **Figure 8**. A linear least squares fit to the data provides y = 1.4x + 0.82 (r_{LA} = 1.4 and r_{EG} = 0.82).

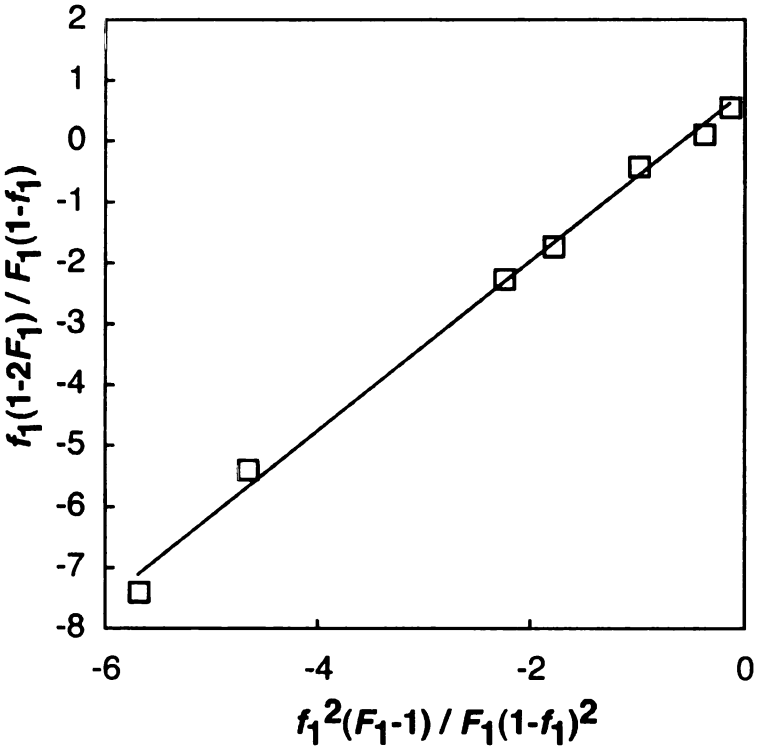

Figure 8. Fineman-Ross plot of the *rac*-lactide and *rac*-ethylglycolide copolymerization data. A least squares linear fit to the data gave y = 1.4x + 0.82 (r_{LA} = 1.4 and r_{EG} = 0.82).

Like the Fineman-Ross method, the Kelen-Tudös method also determines the reactivity ratios by linearization of the experimental data; however, it introduces an arbitrary constant α that distributes the experimental data symmetrically on the plot. The results are expressed in the following form:

$$\eta = (r_1 + \frac{r_2}{\alpha})\xi - \frac{r_2}{\alpha} \tag{10}$$

where η and ξ are functions of the parameters G and H:

$$\eta = \frac{G}{\alpha + H} \text{ and } \xi = \frac{H}{\alpha + H} \tag{11}$$

where $G = \frac{F_1(f_1 - 1)}{f_1}$, $H = \frac{F_1^2}{f_1}$, and α is a constant that is equal to $(H_{max} \times H_{min})^{1/2}$ with H_{max} and H_{min} being the highest and lowest H values, respectively.[93] Plotting η versus ξ generates a straight line that gives $-r_2/\alpha$ and r_1 on extrapolation to $\xi = 0$ and $\xi = 1$, respectively. A Kelen-Tudös analysis for the copolymerization of *rac*-lactide and *rac*-ethylglycolide is shown in **Figure 9**. A linear least squares fit of the data and extrapolation to $\xi = 0$ and $\xi = 1$ gave reactivity ratio values of $r_{LA} = 1.3$ and $r_{EG} = 0.72$. Notably, the results from the three analyses gave similar values and are summarized in **Table 2**. Although the F-R and K-T methods give a good first approximation of the reactivity ratios, they have two disadvantages. First, both methods use the initial feed composition instead of the instantaneous feed composition. If the reactivity's of the two monomers are not identical, the more reactive monomer enters the copolymerization more rapidly than the less reactive

monomer, and thus the residual monomer mixture progressively changes its composition. The second disadvantage is the arbitrariness contained in the visual best-fit line that is drawn upon linearizing the experimental data.

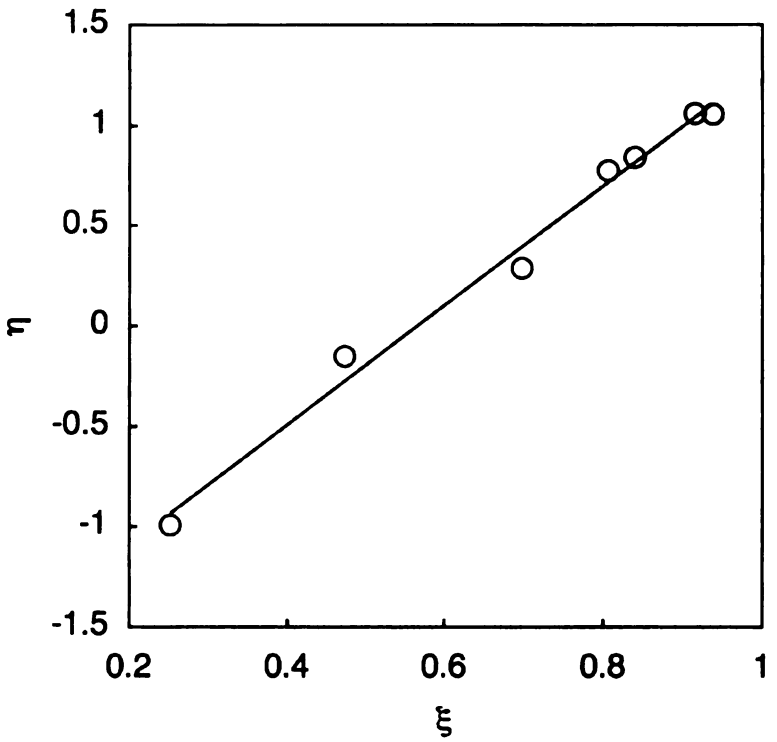

Figure 9. Kelen-Tudös plot for the copolymerization of *rac*-lactide and *rac*-ethylglycolide. Extrapolation to $\xi = 0$ and $\xi = 1$ gave reactivity ratio values of $r_{LA} = 1.3$ and $r_{EG} = 0.72$.

Table 2. Reactivity ratios calculated for *rac*-lactide (r_1) and disubstituted glycolides (r_2).

entry	Monomers	Method [a]	r_1 [b]	r_2 [b]	$r_1 r_2$
1	EG/LA	F-R	1.4	0.82	1.1
		K-T	1.3	0.72	0.93
		NLS	1.29 (± 0.07)	0.71 (± 0.05)	0.92
2	nHG/LA	F-R	1.4	0.24	0.33
		K-T	1.3	0.16	0.22
		NLS	1.30 (± 0.03)	0.15 (± 0.01)	0.20
3	iPG/LA	F-R	2.7	0.081	0.22
		K-T	2.8	0.10	0.29
		NLS	2.5 (± 0.2)	0.08 (± 0.01)	0.21
4	cHG/LA	F-R	3.1	0.015	0.046
		K-T	3.0	0.011	0.034
		NLS	3.3 (± 0.1)	0.015 (± 0.006)	0.049
5	PL/LA	F-R	1.0	1.2	1.2
		K-T	1.0	1.2	1.2
		NLS	1.05 (± 0.02)	1.22 (± 0.03)	1.2

(a) Fineman-Ross (F-R), Kelen-Tudös (K-T) and nonlinear least squares (NLS) methods. (b) Errors reported are standard deviations.

The product of the two reactivity ratios gives information regarding the copolymer microstructure. For example, when the product of $r_1 r_2$ is close to unity, the copolymerization is termed "ideal" or "random." Using the NLS method of analysis, the $r_1 r_2$ value for the copolymerization of lactide and ethylglycolide was 0.92, suggesting that both lactide and ethylglycolide should be randomly distributed along the polymer backbone. If this is correct, DSC analysis of these copolymers should show only one glass transition temperature that increases with increasing lactide content (T_g (LA) = 66 °C, T_g (EG) = 15 °C). We synthesized a

series of copolymers (monomer ratios LA/EG: 5/1, 3/1, 1/3, 1/5) via ring opening polymerization catalyzed $SnOct_2$ (**Table 3**).[103] Thermal analysis of these copolymers revealed homogeneous materials with a single, well-defined T_g that systematically increased as lactide composition increased (**Figure 10**).

Table 3. T_gs of poly(lactide-*co*-ethylglycolide) copolymers.

Polymer	M_n (kD)[a]	PDI	T_g (°C)[b]
poly(LA)	35.2	1.89	66
poly(LA/EG) (5/1)	41.5	1.85	42
poly(LA/EG) (3/1)	47.8	1.76	38
poly(LA/EG) (1/1)	41.7	1.88	30
poly(LA/EG) (1/3)	50.8	1.92	23
poly(LA/EG) (1/5)	43.6	1.85	19
poly(EG)	45.6	1.78	15

(a) determined by GPC using polystyrene standards. (b) determined by DSC, heating rate 10 °C/min.

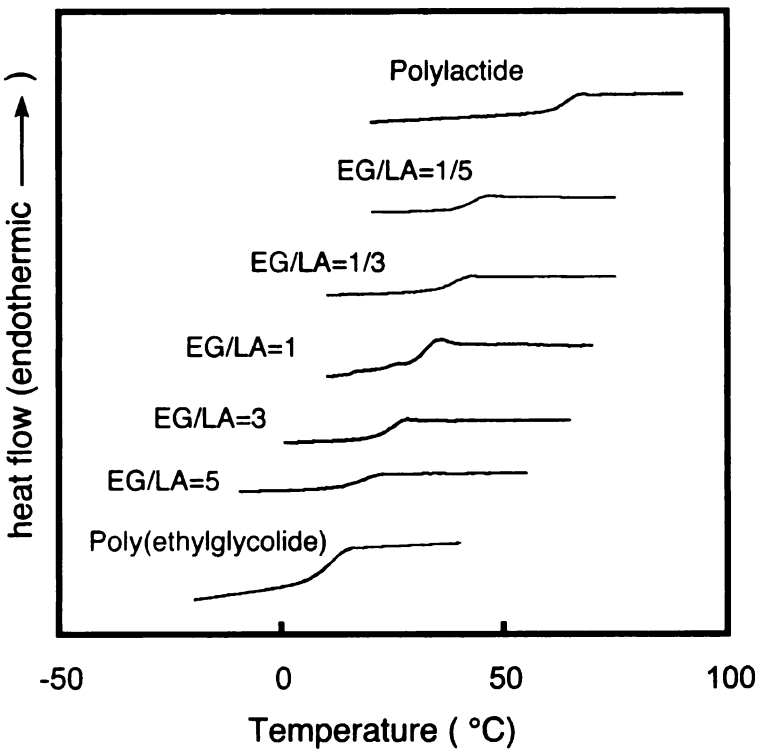

Figure 10. Glass transition temperatures of ethylglycolide (EG) and lactide (LA) copolymers as a function of polymer composition. DSC samples were run under a nitrogen atmosphere at a heating rate of 10 °C/min.

Lactide and ethylglycolide are structurally similar, favoring the formation of random copolymers, however, the reactivity ratio for lactide was higher than ethylglycolide, presumably due to the steric difference between the two monomers. This trend should be more prominent as the alkyl chain is lengthened. We copolymerized lactide and *n*-hexylglycolide at 6 feed ratios (**Table 4**) and analyzed the data using to nonlinear least squares (**Figure 11**), Fineman-Ross (**Figure 12**), and Kelen-Tudös (**Figure 13**) methods. A summary of the kinetic data for the copolymerization of lactide and *n*-hexylglycolide is listed in **Table 2**. Again, the three methods are in good agreement, and as expected, the r_{LA} and r_{nHG} values differ considerably, r_{LA} = 1.30 and r_{nHG} = 0.15.

Table 4. Mole fraction of lactide in the feed (f_1) and copolymer (F_1) for the copolymerization of lactide and *n*-hexylglycolide.

f_1	F_1
0.90	0.93
0.81	0.86
0.70	0.79
0.61	0.74
0.32	0.54
0.15	0.49

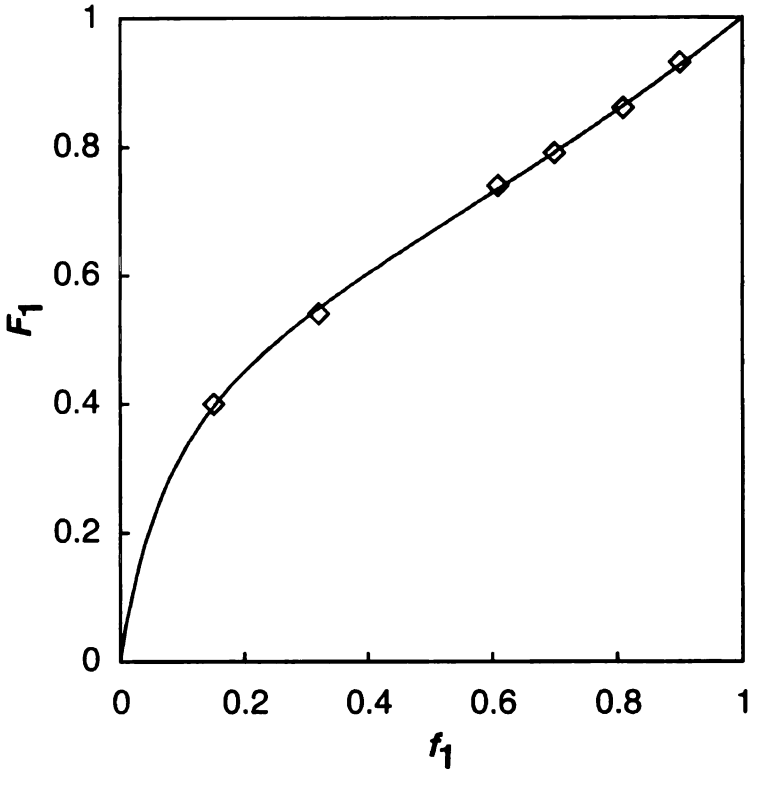

Figure 11. Nonlinear least squares fit of the copolymerization data of *rac*-lactide and *rac-n*-hexylglycolide to equation 7. The reactivity ratios were determined to be r_{LA} =1.30 and r_{nHG} = 0.15.

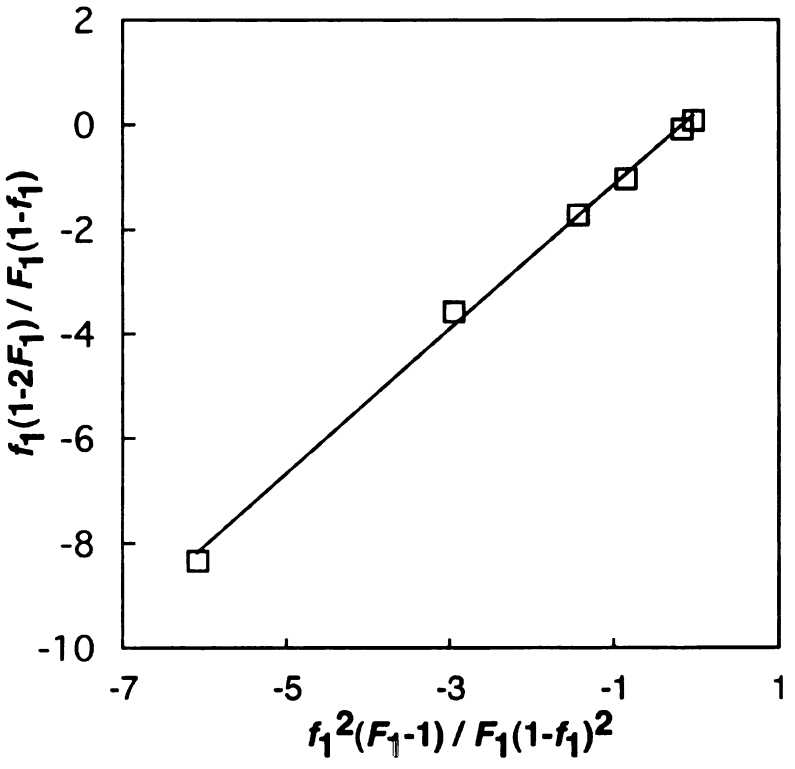

Figure 12. Fineman-Ross plot of the *rac*-lactide and *rac-n*-hexylglycolide copolymerization data. A least squares linear fit to the data gave y = 1.4x + 0.24 (r_{LA} = 1.4 and r_{nHG} = 0.24).

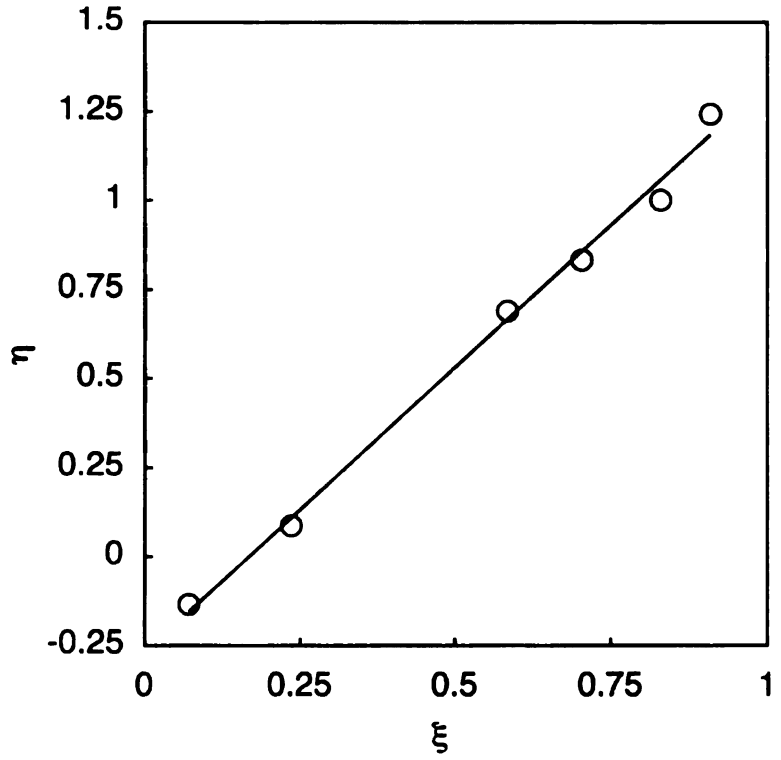

Figure 13. Kelen-Tudös plot for the copolymerization of *rac*-lactide and *rac-n*-hexylglycolide. Extrapolation to $\xi = 0$ and $\xi = 1$ gave reactivity ratio values of r_{LA} = 1.3 and r_{nHG} = 0.16.

If *n*-alkyl chains decrease the reactivity of the disubstituted lactide monomers towards copolymerization, then branched chains should further decrease the reactivity, especially when the branch is close to the ring carbonyl. We copolymerized lactide and isopropylglycolide at seven feed ratios (**Table 5**) and analyzed the data according to nonlinear least squares (**Figure 14**), Fineman-Ross (**Figure 15**), and Kelen-Tudös (**Figure 16**) analyses. A summary of the copolymerization data for lactide and isopropylglycolide is listed in **Table 2**. Again, the difference between the reactivity ratios of LA and iPG increased (r_{LA} = 2.5, r_{iPG} = 0.08), suggesting a blocky or tapered architecture ($r_1 r_2$ =0.21).

Table 5. Mole fractions of lactide in the feed (f_1) and copolymer (F_1) for the copolymerization of lactide and isopropylglycolide.

f_1	F_1
0.78	0.91
0.67	0.87
0.59	0.83
0.35	0.65
0.31	0.63
0.19	0.55
0.10	0.43

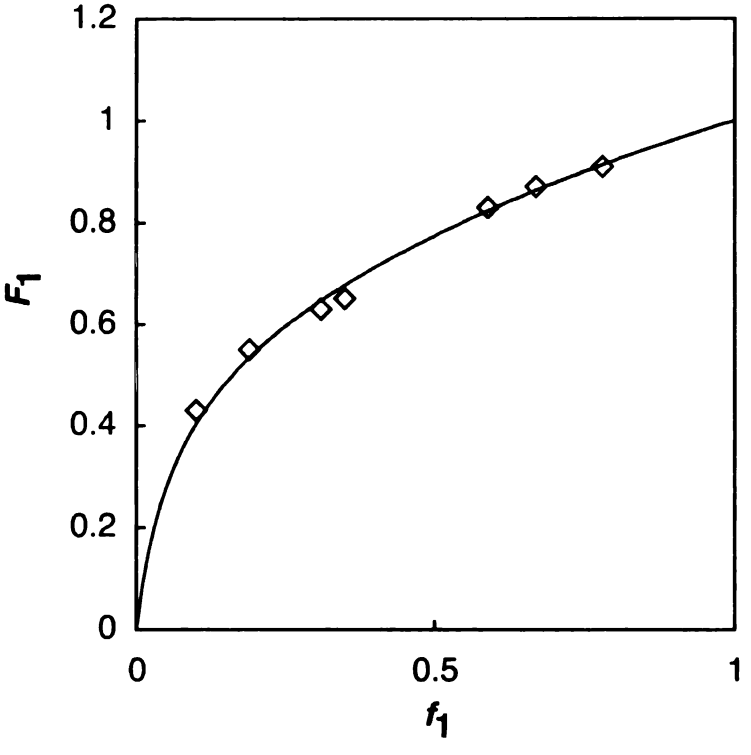

Figure 14. Nonlinear least squares fit to the copolymerization data of *rac*-lactide and *rac*-isopropylglycolide to equation 7. The reactivity ratios were determined to be $r_{LA} = 2.5$ and $r_{IPG} = 0.080$.

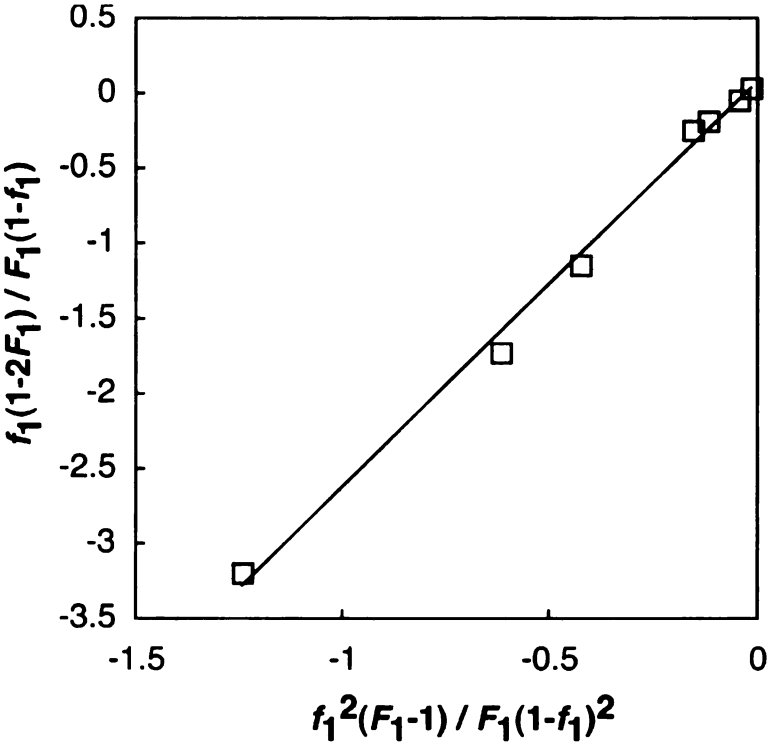

Figure 15. Fineman-Ross plot of the *rac*-lactide and *rac*-isopropylglycolide copolymerization data. A least squares linear fit to the data gave y = 2.7x + 0.081 (r_{LA} = 2.7 and r_{iPG} = 0.081).

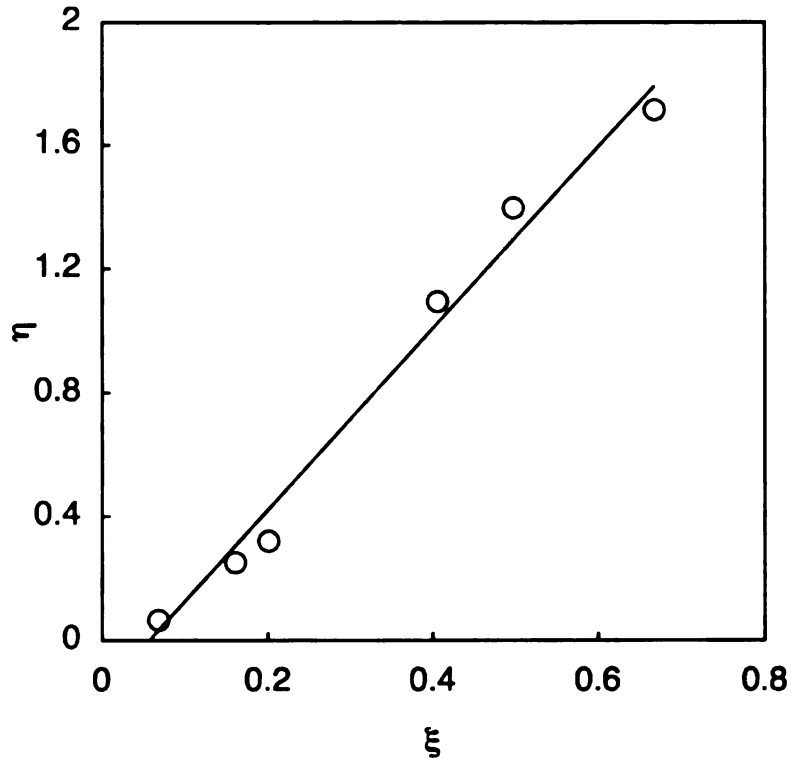

Figure 16. Kelen-Tudös plot for the copolymerization of *rac*-lactide and *rac*-isopropylglycolide. Extrapolation to $\xi = 0$ and $\xi = 1$ gave reactivity ratio values of $r_{LA} = 2.8$ and $r_{iPG} = 0.10$.

To determine whether this difference would manifest itself in the thermal properties of the copolymer, we prepared a series of lactide-*co*-isopropylglycolide copolymers (monomer ratios LA/iPG: 3/1, 1/1, 1/3).[104] Again the copolymers only showed a single T_g and behaved as single-phase materials (**Table 6**). Despite the presence of only one T_g, the value of $r_1 r_2$ (0.21) suggests that the polymer should be slightly blocky, although the blocks may not be sufficiently long to cause phase separation.

Table 6. T_gs of poly(lactide-*co*-isopropylglycolide) copolymers.

Polymer	M_n (kD)[a]	PDI	T_g (°C)[b]
poly(LA)	35.4	1.78	56
poly(LA/iPG) (3/1)	27.8	1.82	48
poly(LA/iPG) (1/1)	25.7	1.76	48
poly(LA/iPG) (3/3)	28.2	1.90	43
poly(iPG)	32.6	1.74	42

(a) determined by GPC using polystyrene standards. (b) determined by DSC, heating rate 10 °C/min.

A bulky substituent situated close to the ring carbonyls should have the greatest effect on relative reactivity data. We copolymerized lactide and cyclohexylglycolide at six feed ratios (**Table 7**) and plotted the data according to nonlinear least squares (**Figure 17**), Fineman-Ross (**Figure 18**), and Kelen-Tudös (**Figure 19**) analyses. A summary of the copolymerization data for lactide and cyclohexylglycolide is listed in **Table 2**. All three methods confirmed the sluggish reactivity of cHG in the copolymerization with lactide (r_{LA} = 3.3 and r_{cHG} = 0.015, $r_1 r_2$ =0.049).

Table 7. Mole fraction of lactide in the feed (f_1) and copolymer (F_1) for the copolymerization of lactide and cyclohexylglycolide.

f_1	F_1
0.91	0.97
0.86	0.95
0.70	0.89
0.55	0.83
0.32	0.72
0.15	0.59

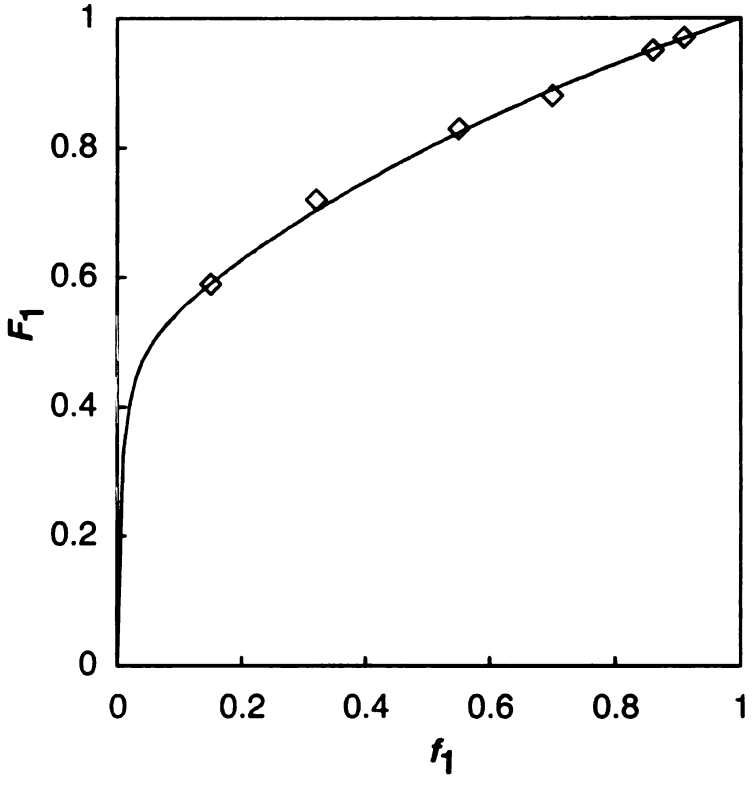

Figure 17. Nonlinear least squares fit of the copolymerization data for *rac*-lactide and *rac*-cyclohexylglycolide to equation 7. The reactivity ratios were determined to be of $r_{LA} = 3.3$ and $r_{cHG} = 0.015$.

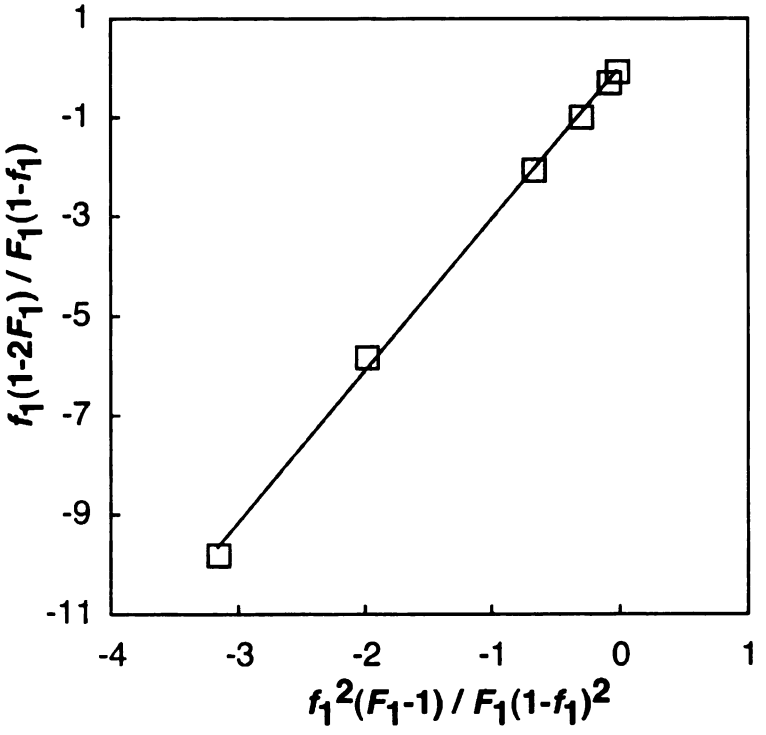

Figure 18. Fineman-Ross plot of the *rac*-lactide and *rac*-cyclohexylglycolide copolymerization data. A least squares linear fit to the data gave y = 3.3x + 0.015 (r_{LA} = 3.1 and r_{CHG} = 0.015).

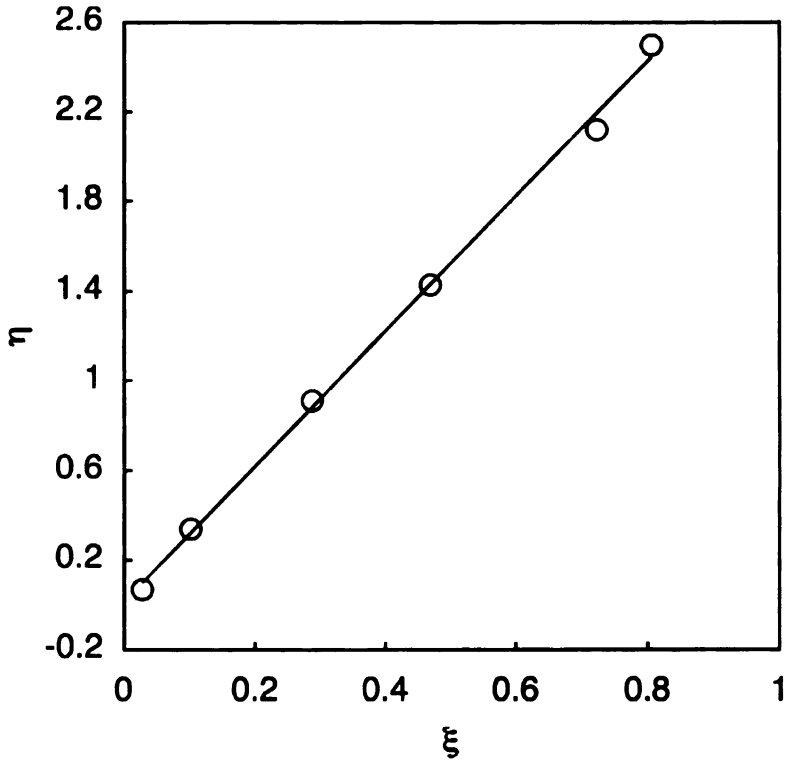

Figure 19. Kelen-Tudös plot for the copolymerization of *rac*-lactide and *rac*-cyclohexylglycolide. Extrapolation to $\xi = 0$ and $\xi = 1$ gave reactivity ratio values of $r_{LA} = 3.0$ and $r_{CHG} = 0.011$.

Since the electronic structures of alkyl glycolides are similar, we expect that reactivity should primarily depend on the steric constraints of the monomer. If true, there should be a relationship between the reactivity ratio and rate of homopolymerization. We compared the homopolymerization rates for a series of structurally similar monomers and found that the reactivity ratios reflected their polymerization rates. For example, the homopolymerization rates for lactide, ethylglycolide, *n*-hexylglycolide, and *n*-decylglycolide were 0.051, 0.048, 0.015, and 0.0062 $L \cdot s^{-1} \cdot mol^{-1}$, respectively (**Table 8**). Notably, as the length of the *n*-alkyl chain increased, both the homopolymerization rate and reactivity ratio for the copolymerization with lactide decreased. The trend suggests that comparison of

homopolymerization rates can be used as a rough estimate of reactivity ratios for electronically similar monomers. Furthermore, a comparison between isopropylglycolide, cyclohexylglycolide, and methylcyclohexylglycolide, a non-symmetrical AB monomer where a methyl group replaces one cyclohexyl groups, suggests that the rates of homopolymerization scale with the size of the ring substituents. The homopolymerization rate of lactide was approximately 10x faster than isopropylglycolide and 360x faster than cyclohexylglycolide. Yet when compared with cHG, the polymerization rate of methylcyclohexylglycolide was ~100x faster, implying preferential ring opening at the carbonyl adjacent to the methyl group. Such differences in reactivity leads an alternating sequence of methyl and cyclohexyl groups situated along the polymer backbone.[105]

Although the polymerization rates scale with the reactivity ratios, the homopolymer T_gs do not (**Table 8**). The lack of correlation indicates that the interaction between polymer chains is significantly different than the ring-opening step during polymerization.

Table 8. Solution polymerization rates for the homopolymerization of substituted glycolides.[a]

Monomer	k_p (L•s^{-1}•mol^{-1}) x 10^3	r_{LA}[b]	r_{M2}[b]	T_g (°C)[c]
rac-lactide	0.051	--	--	55
rac-ethylglycolide	0.048	1.3	0.71	15
rac-*n*-hexylglycolide	0.015	1.3	0.20	-37
rac-*n*-decylglycolide	0.0062	--	--	nd
rac-isopropylglycolide	0.0053	2.5	0.08	56
rac-cyclohexylglycolide	0.00014	3.3	0.02	98
rac-methylcyclohexylglycolide	0.014	--	--	73

(a) solution polymerization catalyzed by $SnOct_2$ at 90 °C. (b) reactivity ratio for the copolymerization of *rac*-lactide (r_{LA}) and comonomer (r_{M2}) as determined by nonlinear least squares analysis. (c) determined by DSC, heating rate 10 °C/min. nd indicates that the T_g was not detected (T_m of nDG = -18 °C).

The most surprising monomer in this study was *rac*-phenyllactide, a benzyl substituted glycolide. Although the benzyl groups should increase the steric bulk around the ring carbonyls, they had little effect on reactivity. We copolymerized lactide and phenyllactide at seven feed ratios (**Table 9**) and plotted the data according to nonlinear least squares (**Figure 20**), Fineman-Ross (**Figure 21**), and Kelen-Tudös (**Figure 22**) analyses. A summary of the kinetic data for the copolymerization of lactide and phenyllactide is listed in **Table 2**. Nonlinear least squares analysis gave reactivity ratios of r_{LA} = 1.05 and r_{PL} = 1.22 and an $r_1 r_2$ value of 1.2. The results suggest that lactide and phenyllactide form random copolymers and phenyllactide may be slightly more reactive than lactide.

Table 9. Mole fractions of lactide in the feed (f_1) and copolymer (F_1) for the copolymerization of lactide and phenyllactide.

f_1	F_1
0.90	0.87
0.85	0.82
0.70	0.67
0.56	0.51
0.33	0.30
0.16	0.14

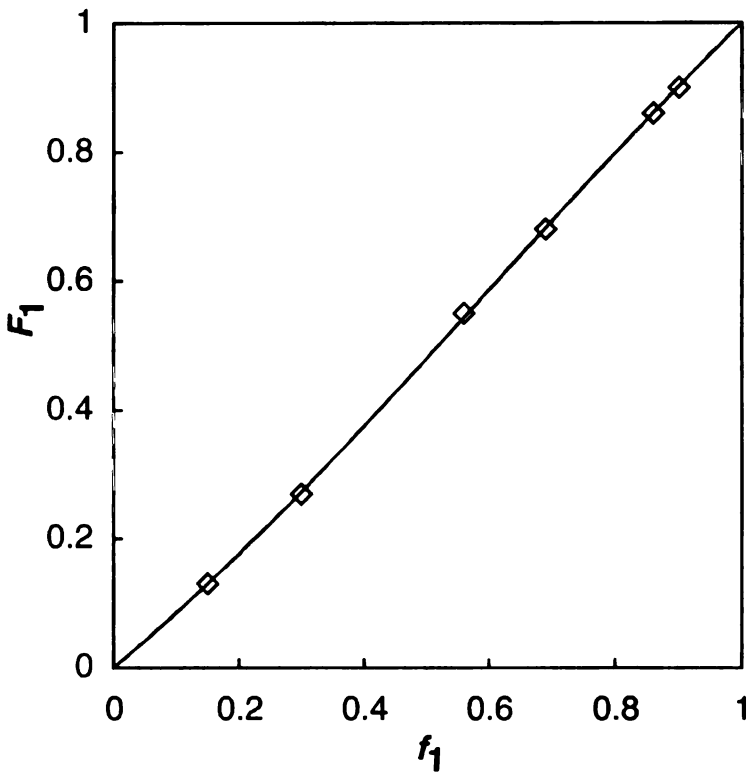

Figure 20. Nonlinear least squares fit of the copolymerization data of *rac*-lactide and *rac*-phenyllactide to equation 7. The reactivity ratios were determined to be r_{LA} = 1.05 and r_{PL} = 1.22.

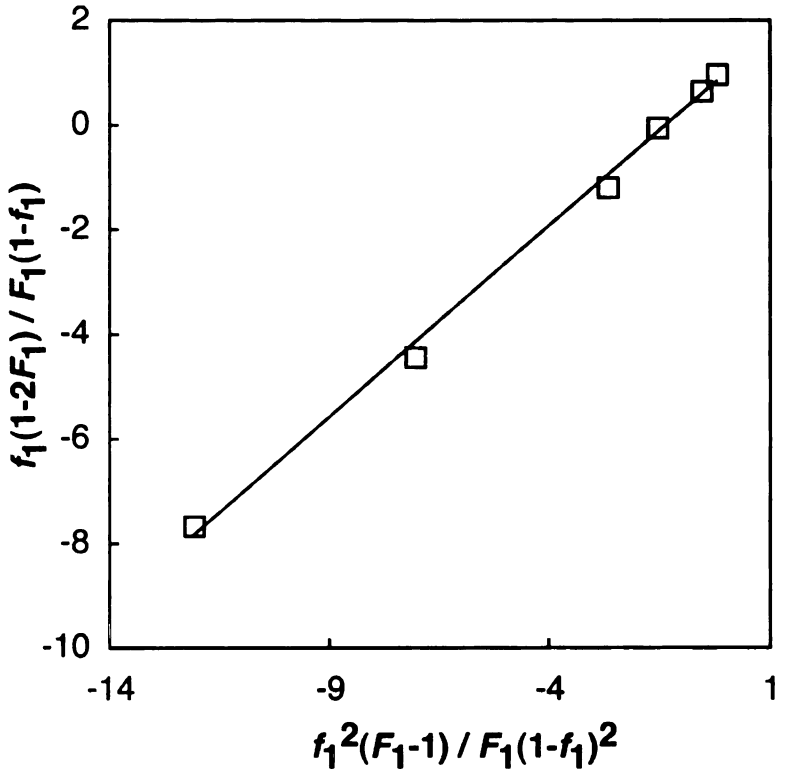

Figure 21. Fineman-Ross plot of the *rac*-lactide and *rac*-phenyllactide copolymerization data. A least squares linear fit to the data gave y = 1.0x + 0.12 (r_{LA} = 1.0 and r_{PL} = 1.2).

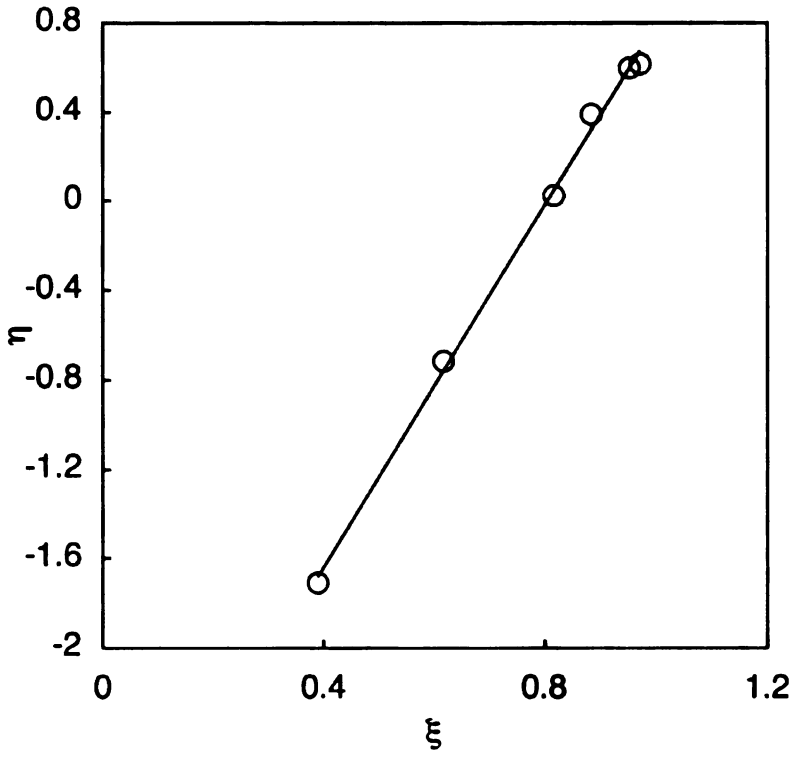

Figure 22. Kelen-Tudös plot for the copolymerization of *rac*-lactide and *rac*-phenyllactide. Extrapolation to $\xi = 0$ and $\xi = 1$ gave reactivity ratio values $r_{LA} = 1.0$ and $r_{PL} = 1.2$.

In addition, copolymers of lactide and mandelide, a phenyl-substituted glycolide, also form random copolymers. Mandelide should be even more sterically congested as the phenyl ring is closer to the carbonyls. However, copolymers of lactide and mandelide were homogeneous materials and DSC scans showed single T_gs for each copolymer (**Figure 23**). The T_gs ranged from 48 °C to 100 °C, the T_gs of polylactide and polymandelide, respectively (**Table 10**).[106] Furthermore, copolymerizations with *L*-lactide did not show any crystallinity, even up to 90 % *L*-lactide content, suggesting random placement of the mandelide within the polymer backbone.

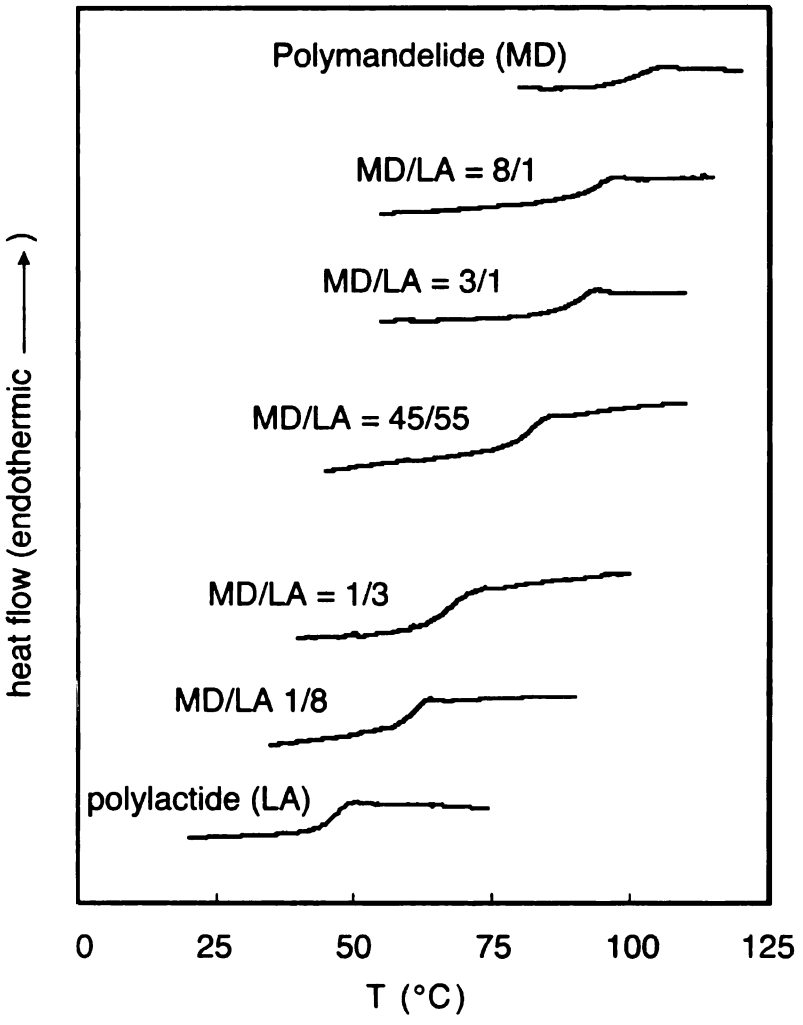

Figure 23. Glass transition temperatures of mandelide (MD) and lactide (LA) copolymers as a function of polymer composition. DSC samples were run under a nitrogen atmosphere at a heating rate of 10 °C/min.

Table 10. T_gs of poly(lactide-*co*-mandelide) copolymers.

Polymer	M_n (kD)[a]	PDI	T_g (°C)[b]
poly(LA)	35.4	1.78	56
poly(LA/MD) (9/1)	98	1.65	61
poly(LA/MD) (75/25)	80	1.65	67
poly(LA/MD) (55/45)	58	1.47	82
poly(LA/MD) (25/75)	42	1.60	90
poly(LA/MD) (1/9)	37	1.45	95
poly(MD)	68	1.63	100

(a) determined by GPC using polystyrene standards. (b) determined by DSC, heating rate 10 °C/min.

The synthesis of functionalized lactide derivatives generated both racemic and *meso* isomers, and their separation is often challenging. To determine whether different isomers affect the copolymerization, we calculated the reactivity ratios for the copolymerization of a mixture of *meso* and *rac*-ethylglycolide with *rac*-lactide. From the analysis of the copolymerization data, we concluded that the *meso* isomer may be slightly less reactive (*rac*-EG and *rac*-LA: $r_{LA} = 1.29$, $r_{EG} = 0.72$, $r_1 r_2 = 0.92$; *rac*- and *meso*-EG with *rac*-LA: $r_{LA} = 1.48$, $r_{EG} = 0.65$, $r_1 r_2 = 0.96$), however, the difference was not significant (**Figure 24**).[106] Therefore our design rules can be applied to any mixture of isomers within a homologous series and will be valuable when designing functionalized lactide monomers.

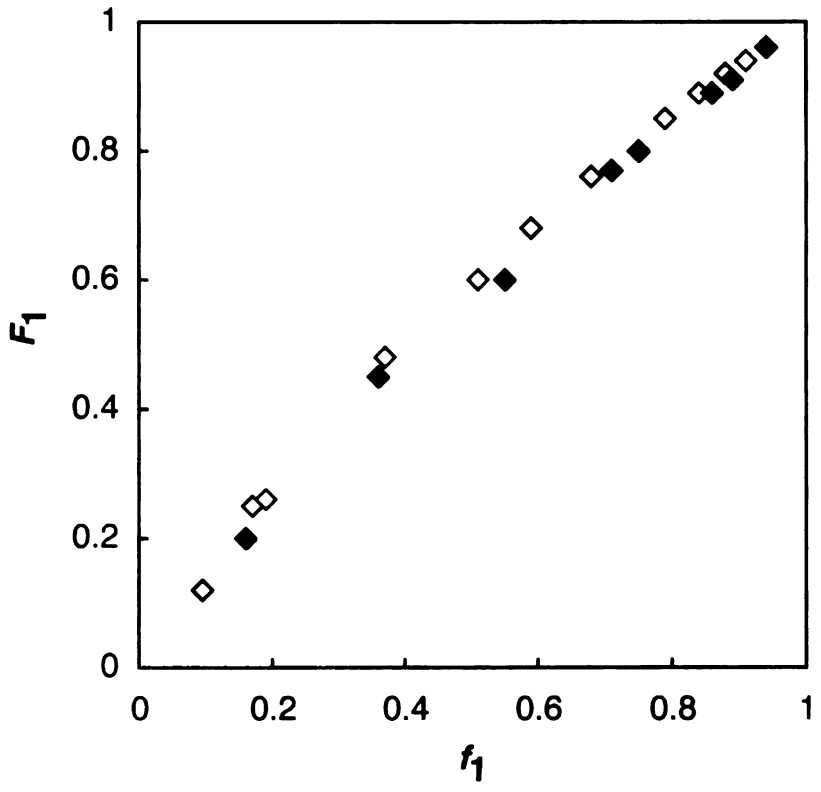

Figure 24. Instantaneous copolymer composition (F_1) as a function of monomer feed ratio (f_1) for the copolymerization of *rac*-ethylglycolide and *rac*-lactide (r_{EG} = 0.72, r_{LA} = 1.29, $r_1 r_2$ = 0.92) (◆) and copolymerization of *rac*- and *meso*-ethylglycolide with *rac*-lactide (r_{EG} = 0.65, r_{LA} = 1.48, $r_1 r_2$ = 0.96) (◇).

Conclusion

In conclusion, the reactivity ratios of five disubstituted lactide derivatives were analyzed with respect to *rac*-lactide using three methods of analysis: the nonlinear least squares, Fineman-Ross, and Kelen-Tudös methods. The reactivity ratios provided information regarding the microstructure of the copolymers and related well to homopolymerization rates. The information allowed elucidation of structure-reactivity relationships that can be applied to the synthesis of future lactide derivatives.

Experimental Section

Unless otherwise specified, ACS reagent grade starting materials and solvents were used as received from commercial suppliers without further purification. *Rac*-lactide was purchased from Aldrich and sublimed prior to use. ^{1}H NMR (300 or 500 MHz) and ^{13}C NMR (75 or 125 MHz) spectra were acquired using either a Varian Gemini 300 spectrometer or a Varian UnityPlus 500 spectrometer with the residual proton signal from the $CDCl_3$ solvent used as chemical shift standard. Mass spectral analyses were carried out on a VG Trio-1 Benchtop GC-MS. IR spectra were taken with Mattson Galaxy 3000 FT-IR. Elemental Analyses were determined using a Perkin-Elmer 2400 CHNS/O Analyzer. Melting points were taken on an Electrothermal capillary melting point apparatus and are uncorrected. Differential Scanning Calorimetry (DSC) analyses of the polymers were obtained using a TA DSC Q100. Samples were run under a nitrogen atmosphere at a heating rate of 10 °C/min, with the temperature calibrated with an indium standard. Copolymerization data for the NLS method were fit to the copolymer equation (equation 8) using Origin (OriginLab Massachusetts, USA).

Substituted Lactide Derivatives

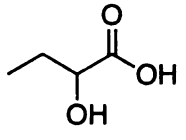

2-Hydroxybutanoic acid (2). To a cooled (0 °C) solution of propanal (20.0 g, 340 mmol) dissolved in 20 mL THF and 400 mL saturated aqueous $NaHSO_3/H_2O$ (3:5)

was added a solution of potassium cyanide (45.2 g, 690 mmol) in H_2O (250 mL) dropwise over 1 hour. The reaction was stirred for 5.5 hours at 0 °C and then extracted with ether (4 × 200 mL). The combined organic layers were washed with saturated aqueous NaCl (2 x 50 mL), dried over $MgSO_4$ and concentrated to give 2-hydroxybutanenitrile (19.1 g, 225 mmol, 65 %) as a colorless liquid, which was used without further purification. ^{1}H NMR (300 MHz) δ 4.42, (t, 1H, *J* = 7.32 Hz), 1.87 (m, 2H), 1.08 (dd, 3H, *J* = 7.42, 7.69 Hz).

Concentrated HCl (45 mL) was added to the cyanohydrin (19.1 g, 221 mmol) and the solution was stirred at room temperature for 18 hours and at reflux for 2.5 hours. Once cooled, the reaction was quenched with H_2O (100 mL) and extracted with EtOAc (3 x 100 mL). The combined organic layers were washed with saturated aqueous NaCl (1 x 100 mL), dried over $MgSO_4$, and concentrated. Purification by recrystallization (toluene at –30 °C) provided 2-hydroxybutanoic acid (16.7 g, 161 mmol, 63 %) as colorless crystals. ^{1}H NMR (300 MHz) δ 4.24 (m, 1H), 2.0-1.8 (m, 1H), 1.8-1.6 (m, 1H), 0.99 (t, 3H, *J* = 7.32 Hz). ^{13}C NMR (75 MHz) δ179.84, 71.19, 27.24, 8.89. mp = 40-41 °C.

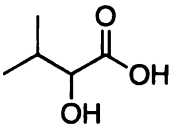

2-Hydroxy-3-methyl butyric acid (5). A solution of $NaNO_2$ (72 g, 1.0 mol) in water (50 mL) was added dropwise to a cooled (0 °C) solution of *DL*-valine (30 g,

250 mmol) in 1 M H_2SO_4 (530 mL). The solution was stirred at 0 °C overnight and then extracted with ether (4 × 300 mL). The organic layers were dried over $MgSO_4$ and the ether evaporated. Recrystallization from toluene yielded white crystals that were collected by filtration and dried under vacuum to give 2-hydroxy-3-methyl butyric acid (23 g, 195 mmol, 75 %) as a white solid. ^{1}H NMR (300 MHz) δ 4.13 (d, 1H, J = 3.42 Hz), 1.8-2.0 (m, 1H), 1.06-1.04 (d, 3H, J = 6.84), 0.92-0.90 (d, 3H, J = 6.84 Hz). ^{13}C NMR (75 MHz) δ 178.94, 74.78, 32.01, 18.76, 15.82. mp 169-170 °C.

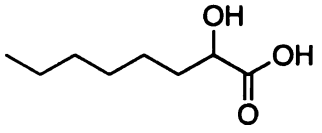

2-Hydroxyoctanoic acid (8). A solution of 1-bromohexane (43 g, 260 mmol) in anhydrous THF (250 mL) was stirred with magnesium turnings (9.4 g, 390 mmol) at 0 °C. The resulting Grignard reagent was transferred to an addition funnel and the solution was added dropwise under nitrogen to a mechanically stirred solution of diethyl oxalate (29.5 g, 200 mmol) in anhydrous THF (100 mL) at -80 °C.[107] After stirring for 30 minutes at -80 °C, the reaction was quenched with 2 M HCl (200 mL). The aqueous layer was extracted with ether (3 × 300 mL) and the combined organic layers were washed with saturated aqueous NaCl (1 x 200 mL), dried over $MgSO_4$, and the ether evaporated to give a light brown oil. The oil was poured into chilled methanol (300 mL, 0 °C), filtered, and the methanol was removed by rotary evaporation. Without further purification, a solution of the crude ketoester in acetic acid (250 mL) and 0.5 g of 5 % Pt/Al_2O_3 (Aldrich) was hydrogenated at 1500 psi

for 5 days at room temperature. The solution was filtered, poured into 500 mL ether and the acetic acid was removed by washing with water (3 x 200 mL). The ether was removed under reduced pressure and the colorless oil was hydrolyzed in a refluxing mixture of KOH in 70 % aqueous ethanol (15 wt/wt %, 500 mL). After 2 days, the reaction was quenched with 2 M HCl and extracted with CH_2Cl_2 (3 × 400 mL). The combined organic layers were dried over $MgSO_4$ and the methylene chloride was evaporated. The crude α-hydroxy acid was recrystallized from hexanes to give 2-hydroxyoctanoic acid, isolated as white crystals (25.6 g,160 mmol, 60 %). ^{1}H NMR (500 MHz) δ 4.27-4.23 (dd, 1H), 1.87-1.77 (m, 1H), 1.72-1.62 (m, 1H), 1.49-1.36 (br, 2H), 1.35-1.21 (br, 6H), 0.94-0.77 (t, 3H, J = 6.84 Hz). ^{13}C NMR (125 MHz) δ 180.04, 70.28, 34.09, 31.58, 28.88, 24.66, 22.52, 14.00. MS (EI, *m/z*): 161.4 (M^+). mp 67-69 °C (lit. 70 °C).[108]

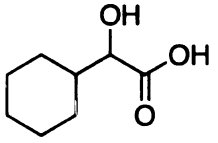

2-Cyclohexyl-2-hydroxyacetic acid (11). The synthesis of 2-cyclohexyl-2-hydroxyacetic acid was carried out according to Jing and Baker.[100] Mandelic acid (38.0 g, 250 mmol) was added to a mixture of MeOH (200 mL), acetic acid (2.5 mL), and 5 % Rh/C. The mixture was sealed in a Parr bomb, purged with nitrogen, and then pressurized to 1400 psi. After 8 hours, the reaction mixture was filtered, and evaporated to dryness. The resulting product was recrystallized from toluene to yield 2-cyclohexyl-2-hydroxyacetic acid (31.8 g, 203 mmol, 81 %) as colorless

crystals which were collected via vacuum filtration. ^{1}H NMR (500 MHz, DMSO-d_6) δ 3.71 (d, 1H, J = 4.4 Hz), 1.66-1.55 (m, 6H), 1.16-1.09 (m, 5H). ^{13}C NMR (125 MHz, DMSO-d_6) δ 175.27, 74.19, 41.15, 28.86, 26.74, 25.84, 25.76, 25.57. *Anal.* Calcd. for $C_8H_{14}O_3$: C, 60.74; H, 8.92. Found: C, 61.12; H, 9.28. mp 135-136 °C.

General Procedure for the Synthesis of Symmetrical Substituted Lactides. A solution of 160 mmol of the appropriate α-hydroxy acid and *p*-toluenesulfonic acid (1.0 g) in toluene (1600 mL) was refluxed 3-6 days, removing the water azeotropically via a Dean-Stark trap. The toluene was evaporated and the solid was dissolved in ethyl acetate, washed with a saturated aqueous $NaHCO_3$ (3 x 100 mL), dried over $MgSO_4$. The ethyl acetate was evaporated and the crude product was purified via recrystallization. Exceptions are noted below.

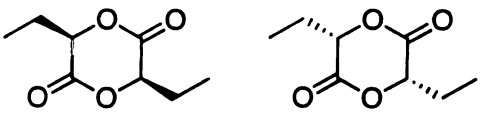

***Rac*-3,6-Diethyl-1,4-dioxane-2,5-dione (3, EG).**[10] A solution of 2-hydroxybutanoic acid (10 g, 100 mmol) and *p*-toluenesulfonic acid (0.2 g) in toluene (700 mL) was refluxed 3 days. After concentrating the solution, 0.1 g ZnO was added and the residue was distilled under reduced pressure using a Kugelrohr distillation apparatus. Ethylglycolide was collected at 140 °C (3 mtorr) as a mixture of diastereomers (4.3 g, 25 mmol, 56 %). *Rac*-ethylglycolide was separated from *meso*-ethylglycolide by flash chromatography on silica gel (1:2 ether/hexanes eluent) to provide 1.2 g of *rac*-3,6-diethyl-1,4-dioxane-2,5-dione (7 mmol, 56 %).

^{1}H NMR (300 MHz) δ 4.8 (dd, 1H, *J* = 7.32, 5.37 Hz), 4.8 (dd, 1H, *J* = 7.32, 4.88 Hz), 2.2-2.0 (m, 2H), 2.0-1.9 (m, 2H), 1.2-1.0 (dt, 3H, *J* = 7.32, 4.88 Hz). ^{13}C NMR (125 MHz) δ 166.7, 76.5, 23.5, 8.83. *Anal.* Calcd. for $C_8H_{12}O_4$: C, 55.81; H, 6.98. Found: C, 55.99; H, 6.98. MS (EI, *m/z*): 173.1 (M^+). mp 51.5-52.5 °C.

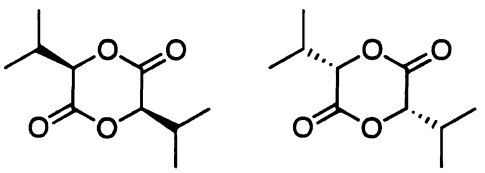

***Rac*-3,6-Diisopropyl-1,4-dioxane-2,5-dione (6, iPG).**[10] *Rac*-isopropylglycolide was recrystallized from toluene three times removing the *meso* isomer to provide *rac*-3,6-diisopropyl-1,4-dioxane-2,5-dione (1.5 g, 7.5 mmol, 16 % yield from 10.7 g *rac*-2-hydroxy-3-methylbutyric acid). ^{1}H NMR (500 MHz) δ 4.68 (2, 2H, *J* = 3.17 Hz), 2.46-2.57 (m, 2H), 1.15-1.13 (d, 6H, *J* = 6.96 Hz), 1.05-1.04 (d, 6H, *J* = 6.96 Hz). ^{13}C NMR (125 MHz) δ 166.3, 79.6, 29.4, 18.6. *Anal.* Calcd. for $C_{10}H_{16}O_4$: C, 59.98; H, 8.05. Found: C, 59.22 ; H, 7.60. MS (EI, *m/z*): 200.1 (M^+). mp 137.5-138.0 °C.

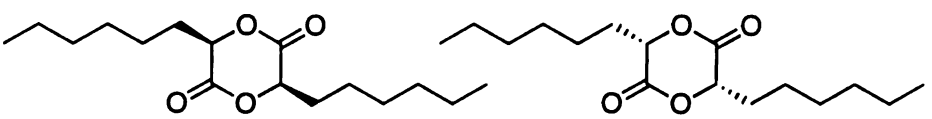

***Rac*-3,6-Dihexyl-1,4-dioxane-2,5-dione (9, nHG).**[10] *n*-Hexylglycolide was recrystallized from hexanes and isolated as white crystals to provide 3,6-dihexyl-1,4-dioxane-2,5-dione (5.9 g, 22.3 mmol, 38 %). ^{1}H NMR (500 MHz) δ 4.88 (dd, *J* = 8.05 Hz and *J* = 4.88 Hz) and 4.83 (dd, *J* = 7.81 Hz and *J* = 4.39 Hz) (2H total for the signals at 4.88 and 4.83), 2.10-1.97 (m, 2H), 1.97-1.88 (m, 2H), 1.56-1.40 (br

m, 4H), 1.36-1.22 (br m, 12H), 0.91-0.75 (t, 6H J = 6.84 Hz). ^{13}C NMR (125 MHz) δ 166.99, 165.84, 76.36, 75.56, 31.89, 31.41, 30.36, 30.06, 28.69, 28.52, 24.45, 24.28, 22.44, 22.41, 13.96, 13.93. MS (EI, *m/z*): 285.2 (M^+). mp 77-80 °C (lit. 78-80 °C).[10]

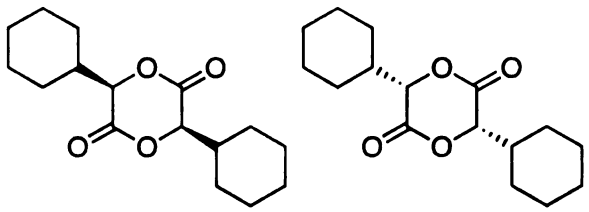

***Rac*-3,6-Dicyclohexyl-1,4-dioxane-2,5-dione (12, cHG).**[100] *Rac*-cyclohexylglycolide was recrystallized from toluene and then cyclohexane. The white crystals were collected by filtration and dried under vacuum to give *rac*-3,6-dicyclohexyl-1,4-dioxane-2,5-dione (4.8 g, 17.1 mmol, 21 %). ^{1}H NMR (500 MHz, DMSO-d_6) δ 4.66 (d, 2H, J = 2.9 Hz), 2.20-2.12 (m, 2H), 1.86-1.64 (m, 10 H), 1.54-1.43 (dq, 2H, J = 3.5, 12.8 Hz), 1.37-1.24 (m, 6H), 1.22-1.11 (m, 2H). ^{13}C NMR (125 MHz, DMSO-d_6) δ 166.24, 79.33, 38.82, 28.94, 26.11, 25.75, 25.73 (peaks at 25.75 and 25.73 ppm were resolved to three separate peaks by adding NMR shift reagent europium(III) tris(3-trifluoromethylhydroxymethylene)-*d*-camphorate)). MS (EI, *m/z*) 198.1,(M^+). mp 183-185 °C.

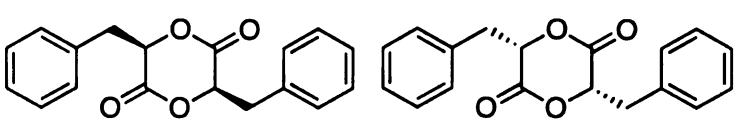

3,6-Diphenyl-1,4-dioxane-2.5-dione (14, PL).[16] Phenyllactide was synthesized according to Simmons and Baker; except, *DL*-phenyllactic acid was used instead of *L*-phenyllactic acid to generate *rac*-phenyllactide. After recrystallization from

ethyl acetate and hexanes the colorless crystals were collected by vacuum filtration to provide phenyllactide (2.48 g from 10 g phenyllactic acid, 8.5 mmol, 31 %) as a mixture of diastereomers. *Rac*-phenyllactide was isolated from *meso*-phenyllactide by recrystallization from ethyl acetate and hexanes to provide *rac*-3,6-diphenyl-1,4-dioxane-2,5-dione (700 mg, 2.4 mmol, 49 % from 1.42 g *rac*- and *meso- mixture*): ^{1}H NMR (500 MHz) δ 7.31-7.23 (m, 10H), 5.03-4.99 (dd, 2H, *J* = 3.85, 7.97 Hz), 3.37-3.31 (dd, 2H, *J* = 3.85, 14.83 Hz), 3.01-2.93 (dd, 2H, *J* = 8.24, 14.83 Hz). ^{13}C NMR (125 MHz) δ 165.4, 134.6, 129.7, 128.7, 127.5, 36,7. *Meso*-3,6-diphenyl-1,4-dioxane-2,5-dione: ^{1}H NMR (500 MHz) δ 7.2-7.1 (m, 10H), 4.2 (t, 2H, *J* = 4.95 Hz), 3.2 (d, 4H, *J* = 4.95 Hz), ^{13}C NMR (125 MHz) δ 164.8, 133.7, 129.9, 129.0, 127.9, 38.4. MS (EI, *m/z*) 296, (M^{+}) mp 165 °C.

General Procedure for the Copolymerization of *rac*-Disubstituted Lactides with *rac*-Lactide. Monomers and a small magnetic stir bar were added to ampoules prepared from 3/8 in. diameter glass tubing. The ampoule was connected via a Cajon® fitting to a T-shaped vacuum adapter fitted with a stopcock and an air-free Teflon valve. The apparatus was attached to a vacuum line and evacuated through the Teflon valve. The ampoule was backfilled with argon, and a syringe was used to add predetermined amounts of the Sn(2-ethylhexanoate)$_2$ and 4-*tert*-butylbenzyl alcohol solutions (both 38.1 mM in toluene) ([monomer]:[catalyst]:[initiator] = 400:1:1) to the ampoule through the stopcock. After removing solvent *in vacuo*, the ampoule was flame-sealed and immersed in a preheated oil bath for 45 seconds (timing started once the monomers were

melted). The polymerization was quenched in ice at low conversion (<10 %), opened, and the monomer/copolymer mixture dissolved in CH_2Cl_2.

General Procedure for the Determination of Copolymer Composition.

The monomer/copolymer CH_2Cl_2 solution was passed through a short column of silica gel prepared from a 9-inch long Pasteur pipette to separate the polymer from the monomers. The eluent was collected in 20 mL vials, evaporated to dryness, and analyzed to confirm that the recovered material was free from polymer. After the separation was complete, the copolymer absorbed onto the silica was transferred into a 25 mL round bottom flask containing 20 mL MeOH. The mixture was stirred for 4 hours and then centrifuged 30 minutes. The colorless solution was decanted, evaporated to dryness, and the composition of the resulting copolymers was analyzed by ^1H NMR using a VarianUnity Plus-500 Spectrometer at 500 MHz. The molar fraction of *rac*-LA in the copolymer (F_1) was calculated according to equation 7 (see text):

$$F_1 = \frac{I_{LA}}{I_{LA} + I_{M2}} \qquad (7)$$

where I_{LA} and I_{M2} are the total integration of the methine protons of LA and the comonomer, respectively. Representative 500 MHz ^1H NMR spectra are available in the appendix.

Determination of F_1 via 500 MHz ^{1}H NMR

Copolymerization of ethylglycolide and lactide: Ethylglycolide and lactide were polymerized at 130 °C. The integration of the overlapping methine protons of EG and LA (5.1-4.9 ppm and 5.3-5.1 ppm, respectively) was resolved by deconvolution using Varian software.

Copolymerization of isopropylglycolide and lactide: Isoproplyglycolide and lactide were polymerized at 165 °C. The methine protons of iPG (5.0 ppm and 2.4-2.3 ppm) and the methine protons of LA (5.3-5.1 ppm) were used to determine F_1.

Copolymerization of *n*-hexylglycolide and lactide: *n*-Hexylglycolide and lactide were polymerized at 130 °C. The integration of the overlapping methine protons of nHG and LA were resolved using the 3:2:1 ratio between the methyl protons (CH_3, 1.9-1.8 ppm), methylene protons (CH_2, 2.0-1.7 ppm), and methine protons of nHG (see text). Once the number of methine protons of nHG was determined using the integration ratio of the methyl and methylene protons, the value was subtracted from the total methine proton integration (5.0-5.3 ppm), giving the integration of the methine protons of LA.

Copolymerization of cyclohexylglycolide and lactide: Cyclohexylglycolide and lactide were polymerized at 185 °C. The methine protons of cHG (5.0-4.9 ppm and 2.0-1.9 ppm) and the methine protons of LA (5.3-5.1 ppm) were used to determine F_1.

Copolymerization of phenyllactide and lactide: Phenyllactide and lactide were polymerized at 185 °C. The integration of the overlapping methine protons of PL and LA were resolved using the 2:1 ratio between the methylene protons (CH_2, 2.7-3.4 ppm) and methine protons of PL. Once the number of methine protons of PL was determined using the integration of methylene protons the value was subtracted from the total methine proton integration (5.4-5.0 ppm), giving the integration of the methine protons of LA.

Chapter 3 Branched Poly(lactide)s

Introduction

Linear poly(lactide) has many pharmaceutical and biomedical applications including orthopedic fixtures,[4,5] sutures,[6] tissue engineering,[7] and drug delivery.[109] However, PLA's hydrophobicity and lack of functional groups limit its utility. Functional polylactides, i.e. polylactides that contain pendant functional groups that permit further chemical elaboration, increase the versatility of conventional polylactide.[110,111] Several examples of functional polylactides have been reported where functional groups were used to enhance hydrophilicity,[18,23,112] provide attachment sites for biologically relevant molecules,[58,113] and serve as branching sites in the synthesis of complex polymer architectures.[49,50] Since functional groups such as pendent amines, carboxylic acids, and alcohols often interfere with lactide polymerizations, they are usually introduced in a protected form. For example, groups have reported the synthesis and polymerization of side-chain protected *L*-amino acid morpholine-2,5-dione monomers[25-27,114,115] and polyester derivatives[17-19,75,112,115] to provide functionalized biomaterials. Most of these examples use serine, lysine, and other amino groups to introduce the functional groups, placing the group in close proximity to the polymer backbone, which may complicate deprotection and limit post-polymerization modifications.

Complex polylactide architectures can be accessed using pendent functional groups to add branches, either by coupling reactions or initiation of lactide polymerization. Hyperbranched,[40-42] star-shaped,[43-45] and dendritic[46-48]

polymers are more compact than linear polymers and have useful rheological and mechanical properties. In general, long-chain branches decrease viscosity and increase elasticity, whereas short-chain branches affect crystallinity. These properties provide control over degradation rates and drug release kinetics.[49,52] Branched architectures also provide multiple functional groups on polymer surfaces.

With a goal of simplifying deprotection and chemical elaboration of functional groups in polylactides, we synthesized 3-benzyloxyoctyl glycolide, BOG (**1**), an AB glycolide monomer derived from oleic acid, an inexpensive and renewable resource found in soybean oil. Moving the functional group farther from the polymer backbone allowed facile deprotection of benzyl-protected primary alcohols, as exemplified by the initiation of *L*-lactide polymerization from the sites to generate PLA comb polymers. This chapter describes the preparation, characterization, and derivatization of alcohol-functionalized polylactides.

Results and Discussion

Monomer Synthesis

The synthesis of 3-(8-(benzyloxy)octyl)-1,4-dioxane-2,5-dione (BOG) from oleic acid is shown in **Scheme 32**. This approach places a benzyl-protected primary alcohol eight methylene units from the polymer backbone, which should minimize any steric effects associated with the polymer backbone during chemical transformations at the pendent hydroxy group. Ironically, in this synthesis the carboxylic acid of the α-hydroxy acid is derived from the oleic acid double bond,

while the primary alcohol is generated by reduction of the oleic acid carboxylic acid.

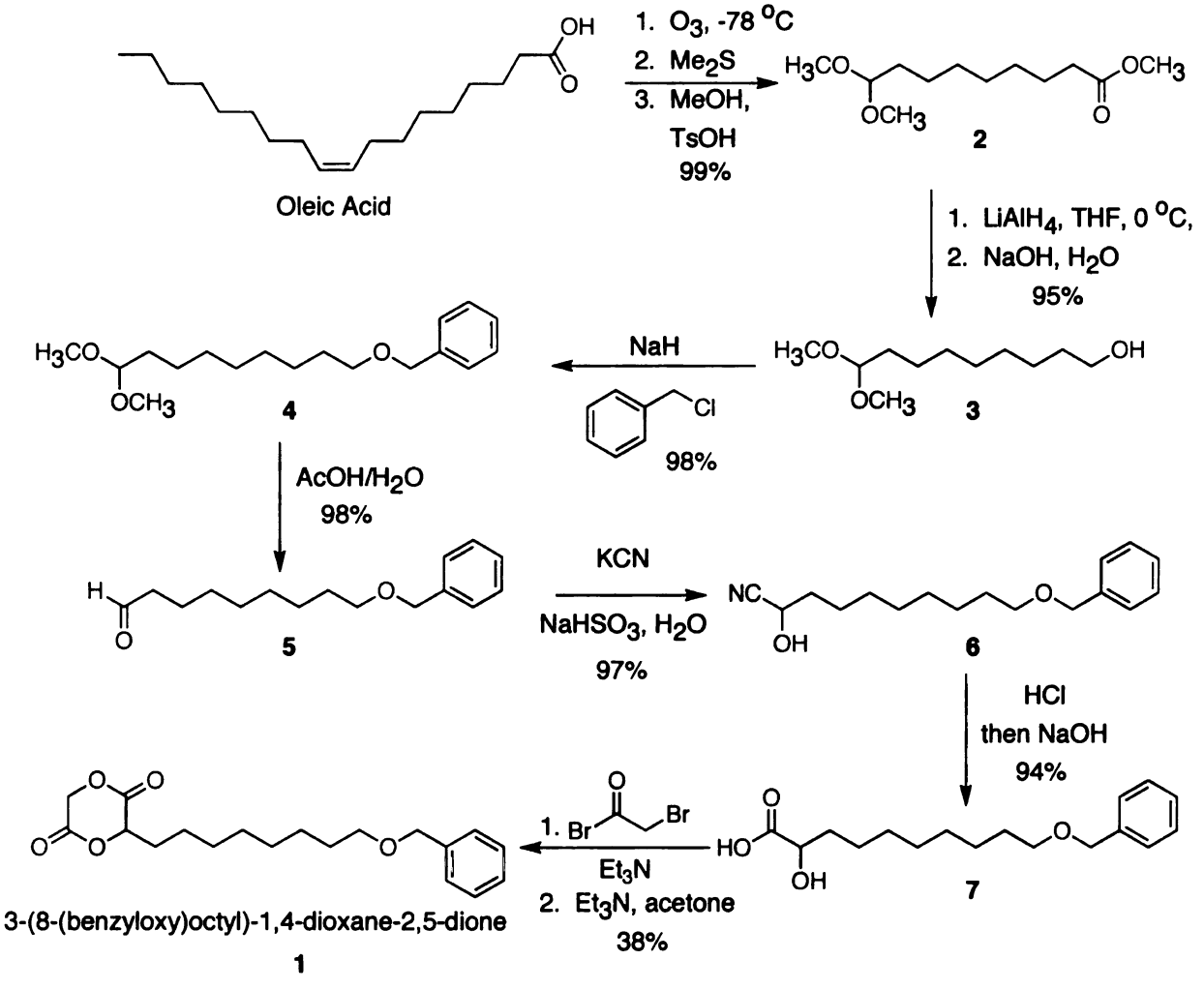

Scheme 32. Synthesis of the AB glycolide 3-(8-(benzyloxy)octyl)-1,4-dioxane-2,5-dione.

Ozonolysis of oleic acid in a 1:4 mixture of $MeOH/CH_2Cl_2$ at –78 °C followed by a reductive workup with dimethyl sulfide and aldehyde protection provided 1,1-dimethoxynonane and methyl 9,9-dimethoxynonanoate (**2**), which were separated via vacuum distillation. $LiAlH_4$ reduction of ester **2** provided 9,9-dimethoxynonanol (**3**) as a colorless liquid; Soxhlet extraction of 9,9-

dimethoxynonanol from the aluminum salts increased the yield to 95 %. The primary alcohol was benzyl-protected to prevent it from acting as a competing polymerization initiator.[83,116] Treating acetal **4** with acetic acid deprotected the aldehyde, and reaction with KCN gave 10-(benzyloxy)-2-hydroxydecanenitrile (**6**). Acidic hydrolysis of the cyanohydrin gave an amide intermediate that was converted to α-hydroxy acid **7** by basic hydrolysis. Finally, we used a previously reported protocol[17] to condense the α-hydroxy acid with bromoacetyl bromide to form the unsymmetrical glycolide. The monomer was purified via flash chromatography using ethyl acetate as the eluent and crystallized from ether at 0 °C to give BOG in 38 % yield. The ^{1}H NMR spectrum of BOG is shown in **Figure 25.** The methine and methylene protons of the substituted glycolide appear at 4.7 ppm and 4.8 ppm, respectively.

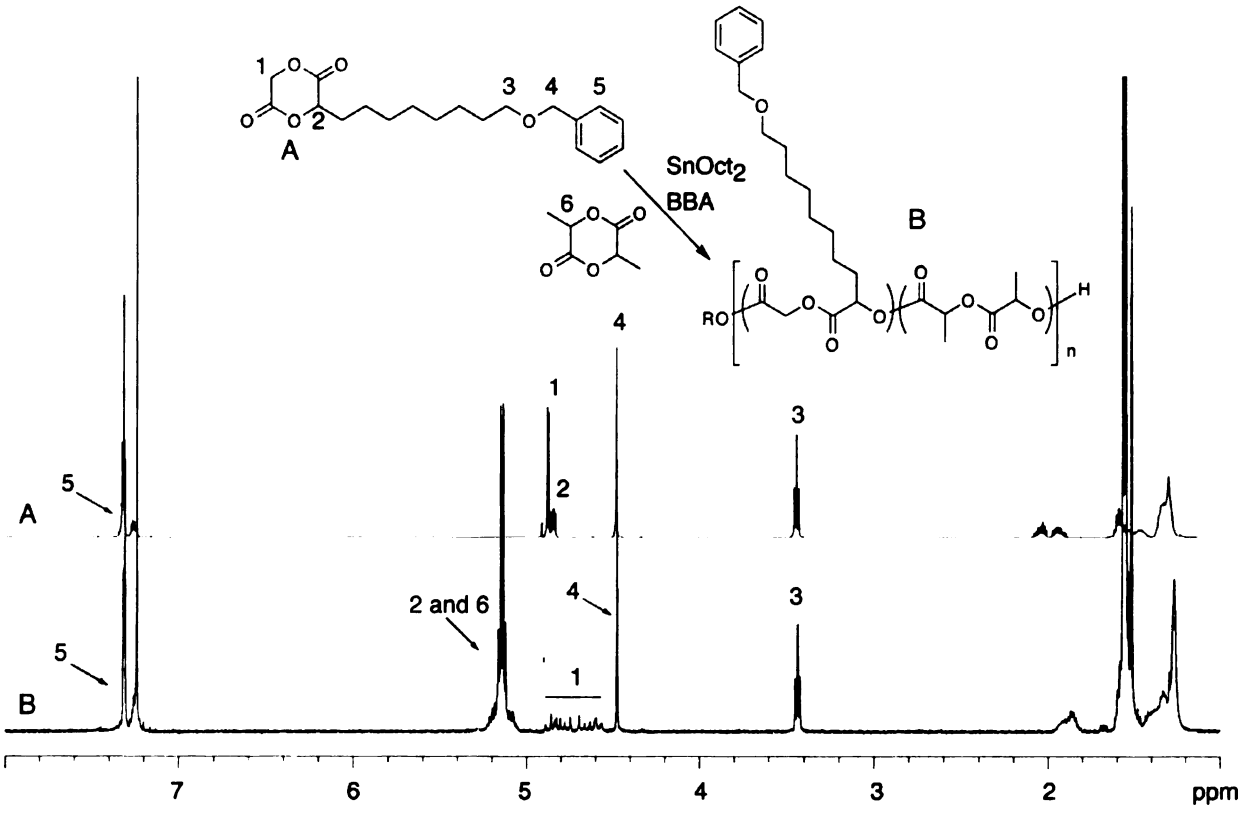

Figure 25. 500 MHz ^{1}H NMR of BOG (A) and poly(BOG-*co*-LLA) (B).

Bulk Polymerization

Glycolide and lactide derivatives can be polymerized via ring opening polymerization in bulk or solution polymerization. Bulk polymerizations, or solvent-free polymerizations, are usually run at a temperature slightly higher than the melting point of the monomer whereas solution polymerizations are run at lower temperatures with the monomer dissolved in an organic solvent. We initially investigated bulk polymerization since solution polymerization rates for substituted glycolides are often slow. Melt polymerizations were run in sealed ampoules at 130 °C using $SnOct_2$ as the catalyst and BBA as the initiator. High molecular weight polymers were obtained in ~45-60 minutes. The polymers were purified by

precipitation from cold methanol and analyzed by ^{1}H NMR, ^{13}C NMR, GPC, and DSC. It is interesting to note the effect of the pendant carbon chains on the T_g of poly(BOG) and poly(BOG-*co*-LLA). Long pendent groups decrease the dipole-dipole interactions between the ester groups in the polymer backbone and degrease the glass transition temperature.[10] Accordingly, the T_g of BOG-*L*-lactide copolymers decreased as the mole fraction of BOG in copolymers increased, reaching a limiting T_g of -32 °C for the BOG homopolymer. In addition, all copolymers were amorphous, suggesting that BOG is distributed along the polymer backbone. The T_g of poly(BOG) (-32 °C) is relatively low when compared to poly(3-benzyloxymethyl-1,4-dioxane-2,5-dione), which has only a two carbon tether (34 °C, **Chapter 1, Scheme 6**).[17]

Table 11. GPC and DSC characterization of BOG homo- and co-polymers before and after benzyl ether deprotection.[a]

	poly(BOG-*co*-LLA)					poly(HOG-*co*-LLA)			
entry	mol%[b]	conv.	M_n x 10^{-3} (g/mol)[c]	PDI	T_g (°C)[d]	M_n x 10^{-3} (g/mol)[c] theor.	M_n x 10^{-3} (g/mol)[c] actual	PDI	T_g (°C)[d]
1	100	45 %	22.9	1.2	-32	16.6	14.2	1.3	-5
2	50	95 %	20.6	1.1	-15	17.3	17.4	1.1	-3
3	20	93 %	51.0	1.3	26	45.8	42.2	1.4	39
4	10	96 %	36.0	1.2	35	34.0	33.7	1.3	45
5	5	97 %	32.6	1.2	46	31.6	31.5	1.2	54

(a) Polymerization Conditions: 130 °C, [$SnOct_2$]:[BBA] = 1:1, 45 minutes. (b) mol % BOG in BOG-*co*-LLA copolymer; determined by NMR (c) measured by GPC using poly(styrene) standards. (d) Determined by DSC, second heating scan; heating rate of 10 °C/min.

Solution Polymerization

Solution polymerizations are more controlled than bulk polymerization due to lower polymerization temperatures and more efficient mixing during polymerization. The ring-opening polymerization of lactides and lactones follow first order kinetics, which are expressed by equation 12

$$R = -\frac{d[M]}{dt} = k_p[M][I] \tag{12}$$

where [M] and [I] are the concentration of the monomer and initiator and k_p is the rate constant for propagation. In living polymerizations, [I] is constant and integration of equation 12 gives equation 13

$$-\ln\left(\frac{[M]_t}{[M]_o}\right) = k_p[I]_o t \tag{13}$$

where $[M]_t$ is the concentration of the monomer at time t; $[M]_o$ is the initial monomer concentration at t = 0, and $[I]_o$ is the concentration of the initiator. According to equation 13, a plot of $-\ln([M]_t/[M]_o)$ versus time is linear for a polymerization with first order kinetics.

We briefly examined the solution polymerization kinetics of BOG in toluene at 90 °C using $SnOct_2$ and BBA as the catalyst and initiator, respectively. The polymerizations were relatively slow because of the 8-carbon tether, reaching 90 % conversion in 48 h. **Figure 26** shows the evolution of molecular weight with conversion for the polymerization of BOG. The data show a linear relationship between M_n and conversion, although the data do not extrapolate to zero as expected. The polymerization of BOG is 1^{st} order in monomer concentration and initiator at low conversion; however, the polymerization rate drops at high conversion, never reaching 100 percent conversion (**Figure 27**).

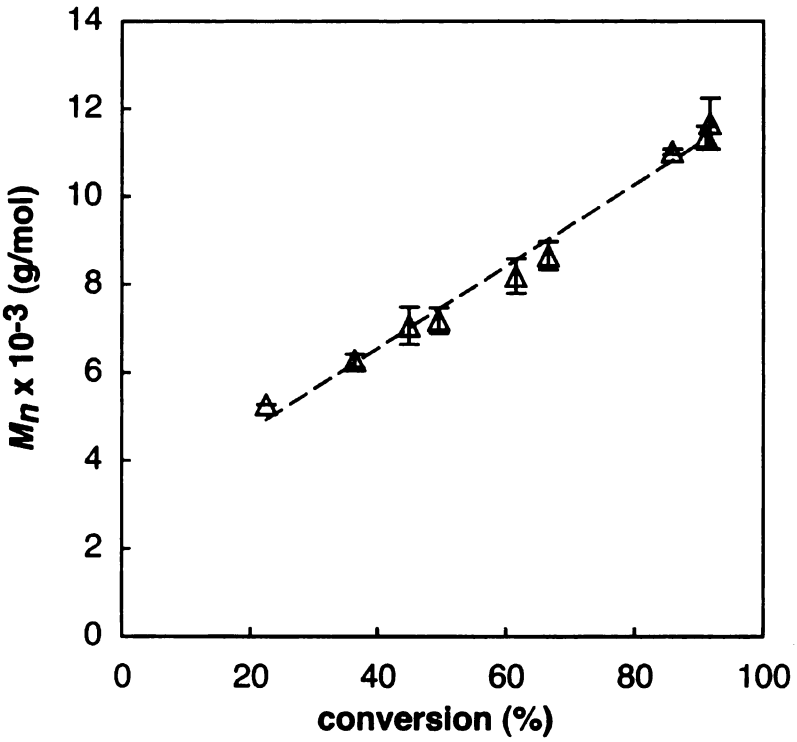

Figure 26. Molecular weight versus conversion for the polymerization of BOG. Solution polymerization conditions: 90 °C, [$SnOct_2$]:[BBA]:[monomer] = 1:1:100. M_n determined via GPC using poly(styrene) standards. Each point corresponds to an average of three samples and the error bars represent the standard deviation.

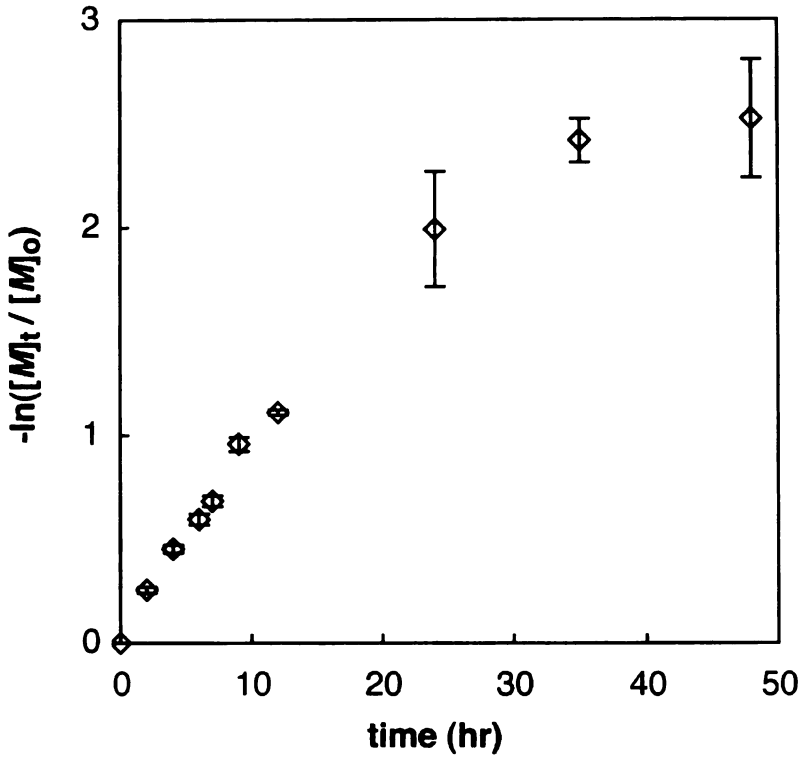

Figure 27. Solution polymerization of BOG with $SnOct_2$ at 90 °C. All reactions were carried out in a 0.2 M BOG solution in toluene with a [$SnOct_2$]:[BBA]:[monomer] ratio of 1:1:100. Each point corresponds to an average of three samples and the error bars represent the standard deviation.

Failure to reach full conversion in lactide polymerizations is often due to an equilibrium between polymerization and depolymerization. In these cases, lactide polymerization kinetics must be analyzed as a series of equilibrium reactions and account for the equilibrium monomer concentration ($[M_{eq}]$).[10,116-118] Incorporating $[M_{eq}]$ into equation 13 gives equation 14, which describes the effect of the equilibrium between polymerization and depolymerization on the observed first order kinetics.

$$-\ln\left(\frac{[M]_t - [M]_{eq}}{[M]_o - [M]_{eq}}\right) = k_{obs}[I] \qquad (14)$$

In equation 14 $[M]_{eq}$ is the monomer concentration at equilibrium, $[M]_o$ is the initial monomer concentration, k_{obs} is the observed propagation rate, and [I] is the initiator concentration. The data of **Figure 27** were plotted according to equation 14 and **Figure 28** shows that a 0.2 M polymerization of BOG followed first order kinetics, assuming an equilibrium monomer concentration ($[M]_{eq}$) 0.02 M, comparible with the $[M_{eq}]$ seen in other substituted glycolides.[10,16] Also, the polydispersity remained narrow throughout the polymerization, ~1.2-1.3, consistent with minimal transesterification during the entire 50 hour polymerization.

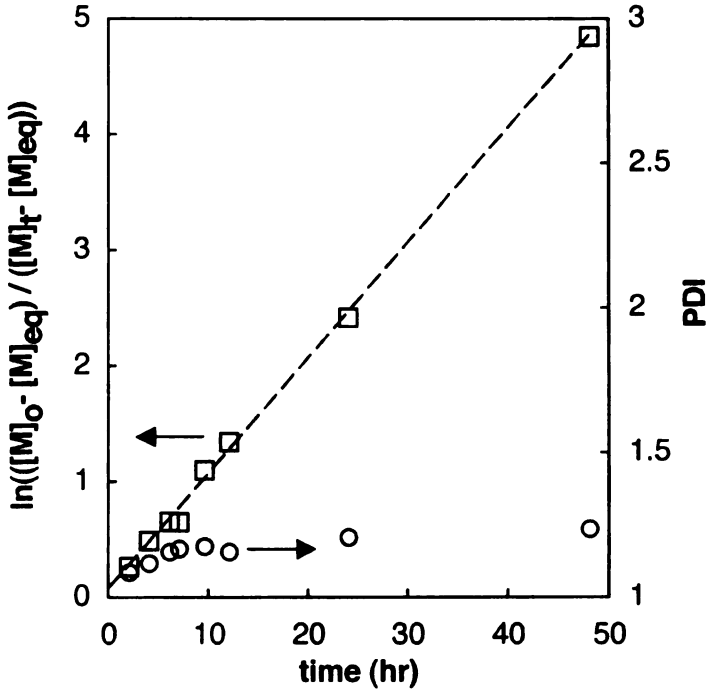

Figure 28. Solution polymerization kinetics of BOG with $SnOct_2$ at 90 °C. All reactions were carried out at 0.2 M BOG solution in toluene with a [$SnOct_2$]:[BBA]:[monomer] ratio of 1:1:100. The equilibrium monomer concentration, $[M]_{eq}$, is assumed to be 0.020 M. The line is a least squares fit to the data.

Copolymerization

One advantage of copolymerizations is the large number of materials that can be generated from few starting monomers. As mentioned in chapter 2, monomer structure affects the relative reactivity of the two monomers, which in turn determines the copolymer architecture, ranging from random or alternate to blocky structures. In a random copolymerization, the growing chain shows no preference between monomers and a homogeneous material is formed. In contrast, block copolymers are formed when one monomer preferentially polymerizes over the

other, generating multi-phase materials where each block has the properties of its corresponding homopolymer.[102]

When *n*-hexylglycolide is copolymerized with lactide, the polymer tends to be blocky (r_1 = 1.30, r_2 = 0.15). Since the polymerization of a symmetrical disubstituted 3-benzyloxyoctyl glycolide monomer should result in a more highly blocky architecture, we synthesized an AB glycolide to increase the reactivity of BOG relative to lactide and provide access to random copolymers. Copolymers of BOG and *L*-lactide were synthesized in bulk using $SnOct_2$ and BBA as the catalyst and initiator, respectively (**Scheme 33**). The results are summarized in **Table 11** (entries 2-4). The crude polymers were purified by precipitation into cold methanol to remove residual monomer, washed with dilute hydrochloric acid to remove catalyst impurities, and dried under vacuum. The copolymers were colorless solids with molecular weights ranging from 15 to 60 kD.

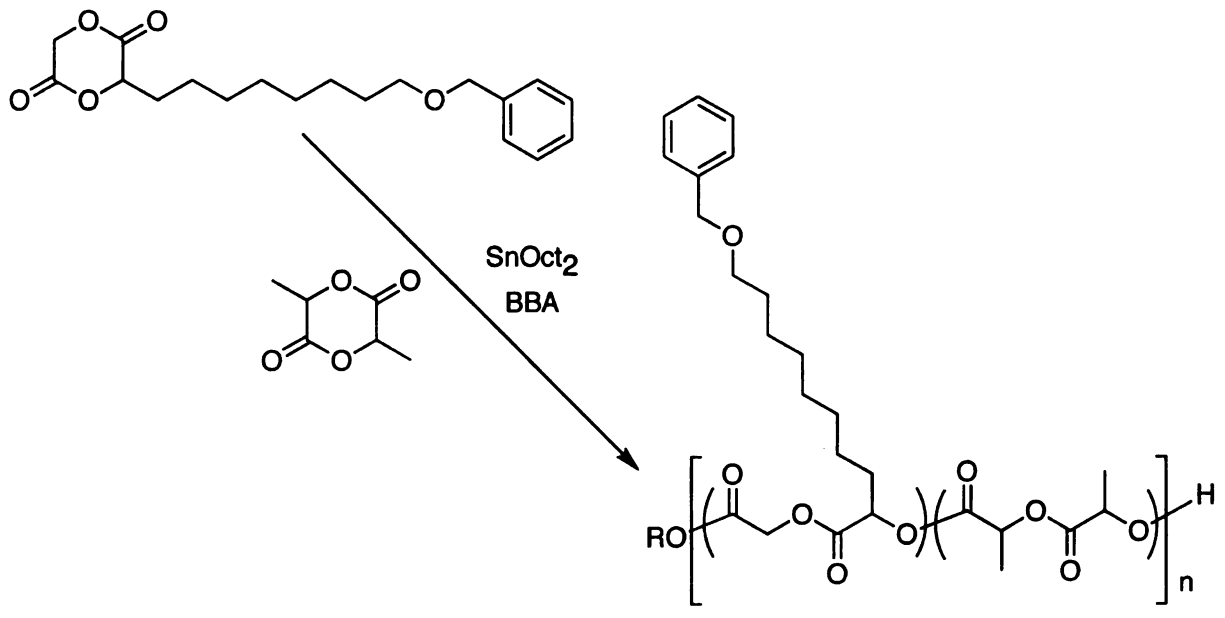

Scheme 33. Synthesis of BOG-*co*-LLA copolymers. Polymerizations were run at 130 °C (bulk) or 90 °C (toluene solution) using $SnOct_2$ and BBA as catalyst and initiator, respectively.

Physical Properties of poly(BOG-*co*-LLA)

We measured the thermal properties of various poly(BOG-*co*-LLA) copolymers using differential scanning calorimetry. DSC analysis showed that increasing the mol % of BOG in the copolymer decreased the T_g (**Table 11**). Furthermore, the lack of crystallinity suggested random incorporation of the comonomers. A nonrandom distribution would result in crystalline poly(LLA) segments, whose melting temperature would be detectable by DSC.[19]

Benzyl Deprotection

Post-polymerization modification strategies require complete and efficient deprotection of pendant functional groups. We examined a variety of solvents and conditions for removal of the benzyl groups from poly(BOG) and poly(BOG-*co*-LLA)

copolymers and found that hydrogenolysis using 10 % Pd/C in MeOH/THF effected quantitative debenzylation with no detectable polymer degradation to give poly(3-hydroxyoxyoctyl glycolide) (poly(HOG)) and poly(HOG-*co*-LLA). In a typical deprotection reaction, we dissolved the polymer in CH_2Cl_2 (~ 0.5 mL) and added it to a solution of MeOH/THF (1:1 vol %) containing 10 % Pd/C. The polymer was subjected to 1000-1500 psi hydrogen gas for 2-3 days. After filtration to remove the catalyst, the deprotected polymers were dissolved in CH_2Cl_2 and precipitated from cold MeOH (copolymers) or dissolved in EtOH and precipitated from cold hexanes (homopolymer). Polymer samples were analyzed by ^1H NMR, ^{13}C NMR, GPC, and DSC. The absence of peaks at 7.2-7.4 and 4.5 ppm in the ^1H NMR spectrum shows quantitative removal of the benzyl ether protecting groups (**Figure 29**). This was confirmed by ^{13}C NMR. The success of this strategy was previously demonstrated by the quantitative removal of the benzyl groups from the amphiphilic PEG/alkyl-grafted polymers synthesized in our lab.[98]

GPC analysis of the deprotected polymers showed minimal molecular weight degradation and changes in the PDI (**Table 11**). For example, the measured molecular weight of a deprotected poly(HOG-*co*-LLA) (5 % HOG) was 31.5 kg/mol, closely matching the theoretical molecular weight of 31.6 kg/mol (**Table 11**, entry 5). Branched polymers are more compact than linear polymers the same molecular weight and therefore have different sizes. When measured against linear polystyrene standards, the more branched copolymers (high BOG content) showed an apparent decrease in molecular weight upon deprotection;

degradation of the polylactide backbone was ruled out by control experiment that was run using linear polylactide. Thermal analysis showed an increased T_g of the material upon benzyl deprotection, as expected for hydrogen bonding between alcohol groups of the deprotected polymer. Poly(HOG) was completely soluble in methanol and swelled in aqueous solution.

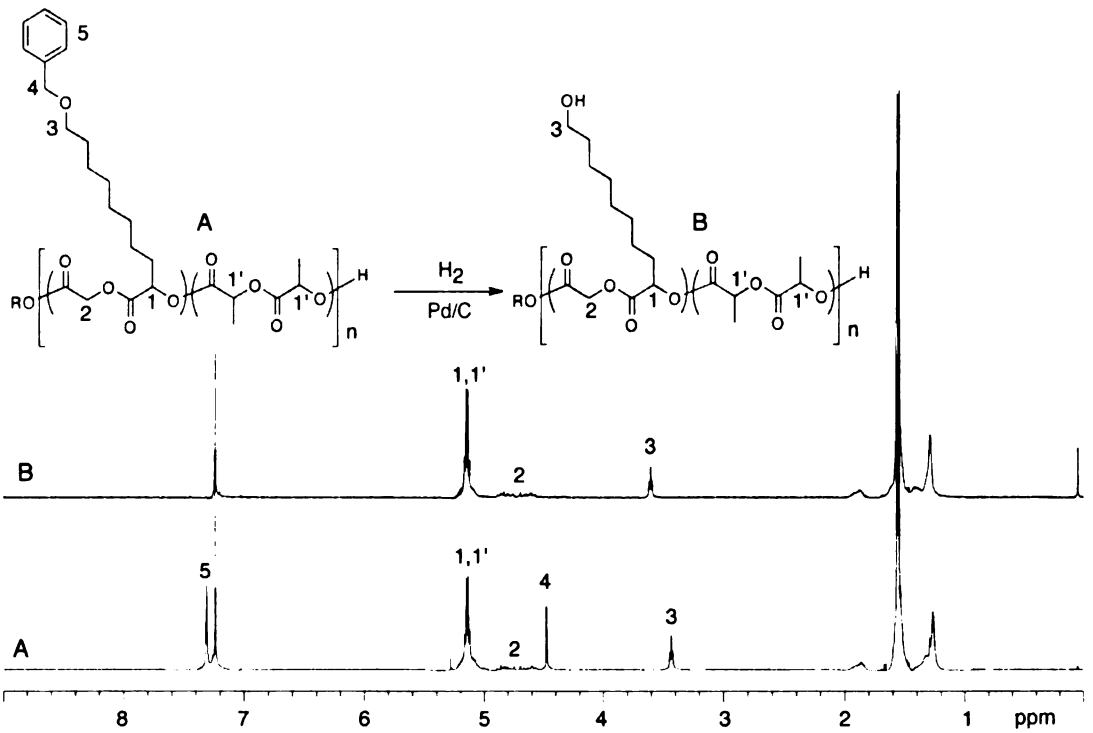

Figure 29. ^{1}H NMR spectrum for poly(BOG-*co*-LLA) (5 mol% BOG) (top) and poly(HOG-*co*-LLA) (bottom) taken in $CDCl_3$ at 500 MHz. Absence of peaks at 7.2-7.4 ppm in the spectra indicates complete removal of the benzyl ether protecting groups.

Degradation of poly(HOG-*co*-LLA)

Crystalline poly(L-lactide) may take years to degrade by hydrolysis at body temperatures, however, drug delivery and other *in vivo* applications require a more rapid and controlled degradation. Introducing pendent alcohol groups to PLLA by

using BOG as a comonomer should lower the polymer T_g, suppress crystallization, and increase the polymer's hydrophilicity, all of which should accelerate the hydrolytic degradation rate. However, the hydrophobic 8-carbon tether should slow degradation. We compared the accelerated degradation rates of poly(*rac*-lactide), PLLA and poly(HOG-*co*-LLA) at 55 °C in pH 7.4 phosphate buffered saline (PBS) solution. Although the temperature of the experiment was above the T_g for all three samples, PLLA showed no appreciable degradation, while both poly(*rac*-lactide) and poly(HOG-*co*-LLA) degraded within 25 days (**Figure 30**). The degradation rate of poly(HOG-*co*-LLA) was similar to poly(*rac*-lactide) suggesting that the alcohol groups compensate for the hydrophobicity of the pendent alkyl chains.

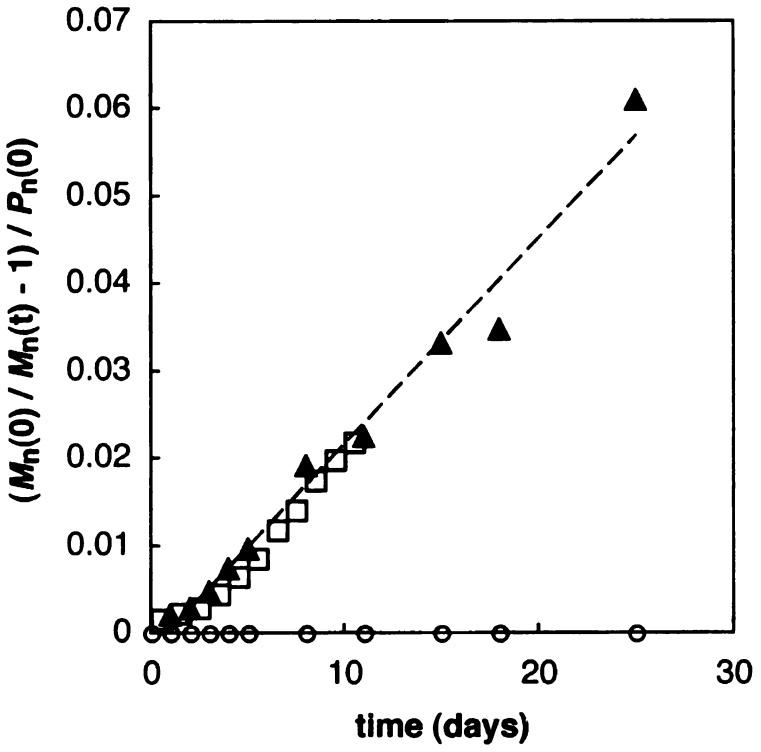

Figure 30. Normalized molecular weight decrease for poly(HOG-*co*-LLA) (50 mol % HOG) (▲), poly(*rac*-LA) (□) and PLLA (○) during hydrolytic degradation at 55 °C in pH = 7.4 phosphate buffer saline solution. Each point corresponds to the average of 3 samples and the line is a least squares fit to the poly(HOG-*co*-LLA) data.

Graft Polymerizations

Branched polyesters are popular drug delivery vehicles because the crystallinity, T_g, and degradability can be controlled by varying the number and length of polymer branches.[49] To demonstrate the accessibility of the pendant alcohol groups, we polymerized *L*-lactide branches from poly(HOG-*co*-LLA) using $SnOct_2$ as the catalyst. The branch lengths ranged from 5-60 lactide units, and representative polymerization and characterization data are shown in **Table 12**. ^1H NMR confirmed initiation from all alcohol groups; the ^1H NMR signal at 3.6 ppm

from the protons adjacent to the alcohol in poly(HOG-*co*-LLA) shifted completely to 4.1 ppm (**Figure 31**). Since GPC analysis using poly(styrene) standards underestimates the molecular weight of branched polymers due to their smaller hydrodynamic volume, we used GPC with multiangle laser light scattering (GPC-MALLS) to determine absolute molecular weights. Representative polymerization data is given in **Table 12**.

Table 12. Macroinitiation of *L*-lactide from poly(HOG-*co*-LLA) containing 5 mol % HOG.[a]

polymer	DP[b]	M_n (10^{-3})[c]	M_w (10^{-3})[c]	PDI	[η] (mL/g)[d]	*a*[e]	T_g (°C)[f]
5	0	31.6	36.0	1.19	___	0.74	46
5a	4.9	39.3	78.3	1.99	22.4	0.45	45
5b	15	55.2	113	2.05	25.5	0.42	47
5c	30	79.8	174	2.18	36.3	0.45	51
5d	41	96.4	226	2.34	37.8	0.39	49
5e	63	131	255	1.95	40.6	0.38	51

(a). Bulk polymerization of *L*-lactide from poly(HOG-*co*-LLA (5 mol% HOG) at 130 °C catalyzed by $SnOct_2$, [$SnOct_2$]:[alcohol initiator] = 1:1. (b) Degree of polymerization of lactide side chains determined by GPC-MALLS. (c) Determined by GPC-MALLS. (d) Determined by viscometry. (e) Mark-Houwink a value determined by viscosity measurements. (f) Determined by DSC second heating scans, at a heating rate of 10 °C/min.

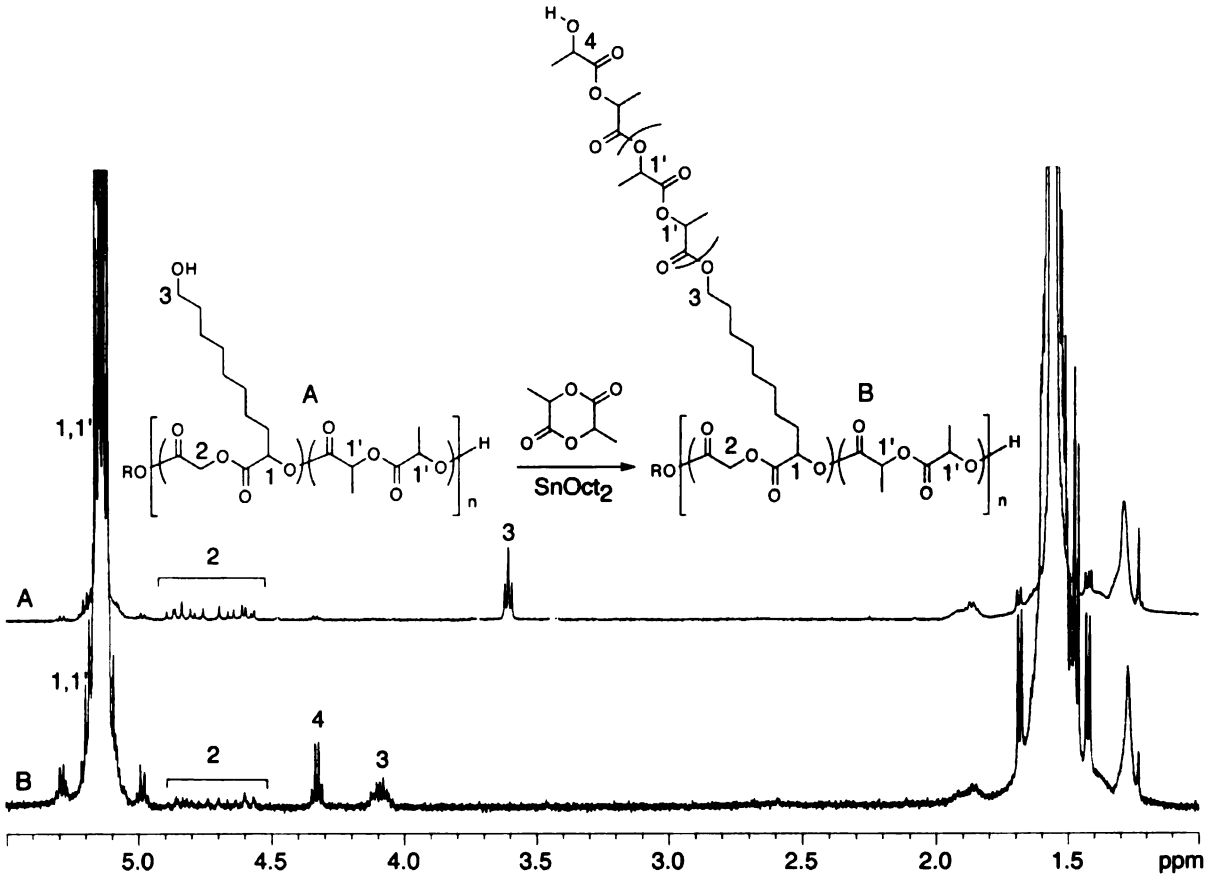

Figure 31. 500 MHz ^{1}H NMR spectrum of poly(HOG-*co*-LLA) (5 mol% HOG) (top) and poly((HOG-*co*-LLA)-*g*-LLA) (bottom) taken in $CDCl_3$.

Branching in poly((HOG-*co*-LLA)-*g*-LLA) also was confirmed by analyzing the light scattering and viscosity data from GPC-MALLS. Linear and branched polymers of the same molecular weight can be discriminated by their size; branched polymers are more compact than linear polymers and their different size/molecular weight relationships can be probed by intrinsic viscosity measurements and by evaluating the relationship between the root-mean squared radius of gyration and polymer molecular weight. According to equation 15, a log-log plot of the radius of gyration and polymer molecular weight (M_i) allows

evaluation of the slope *a*, which contains information concerning the molecular architecture of the polymer. [51]

$$\log r_i = k + a \log M_i \qquad (15)$$

Branched polymers have smaller *a* values than random coils due to their compact structure. **Figure 32** shows the rms radius of gyration extracted from the light scattering data of two GPC runs, linear PLA and poly((HOG-*co*-LLA)-*g*-LLA) (HOG = 5 %, LLA = 95 %; branch DP = 60). The data for PLA yielded $a = 0.81$, a typical value for extended random coil, and $a = 0.24$ for poly((HOG-*co*-LLA)-g-LLA) consistent with a compact, branched structure.

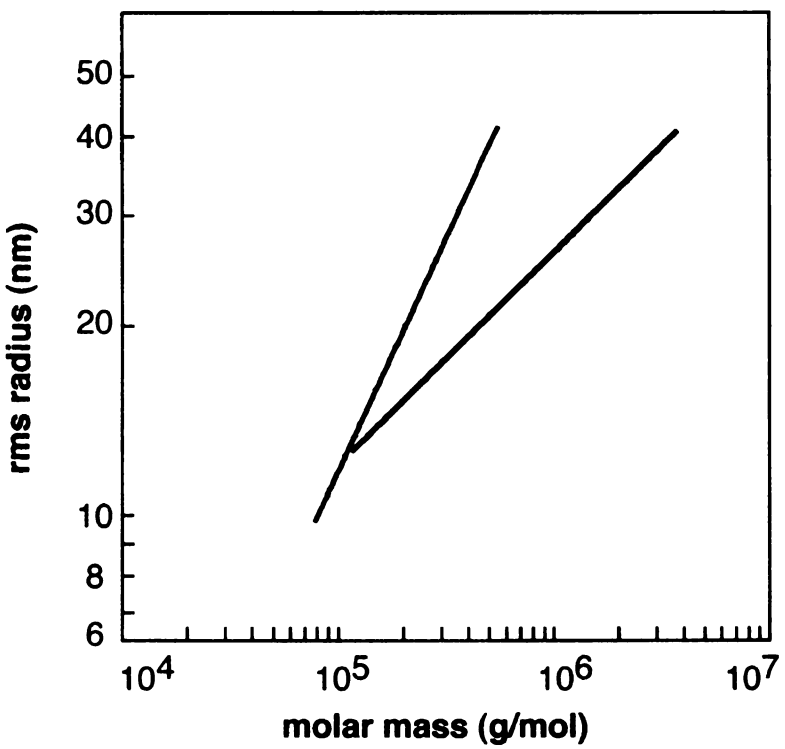

Figure 32. Double logarithmic plot of rms radius of gyration versus molecular mass of linear PLA (broken red line) and poly((HOG-*co*-LLA)-*g*-LLA) (solid blue line) in THF at 35 °C. The smaller slope for poly((HOG-*co*-LLA)-*g*-LLA), $a = 0.24$, compared to linear PLA, $a = 0.81$, is consistent with the branched architecture of poly((HOG-*co*-LLA)-*g*-LLA). The HOG content in poly((HOG-*co*-LLA)-*g*-LLA) sample was 5 mol %, and the degree of polymerization of the LLA branches was 60.

We also confirmed the molecular architecture using the Mark-Houwink relationship,

$$[\eta] = KM_V^a \quad (16)$$

where $[\eta]$ is the intrinsic viscosity, M_V is the viscosity average molecular weight, and K and *a* are constants for a particular polymer-solvent pair at a defined temperature. Branched polymers are more compact and have smaller *a* values than linear polymers of comparable molecular weight.[119] **Figure 33** shows intrinsic viscosity data obtained for the two polymers of **Figure 32**. The log-log plot of the data shows a lower *a* value (slope of log-log plot) expected for a branched polymer. Data for the series of poly((HOG-*co*-LLA)-*g*-LLA) polymers are shown in **Table 12**, which show a steady decrease in *a* as the polymers transform from linear polymers to a comb architecture with long branches.

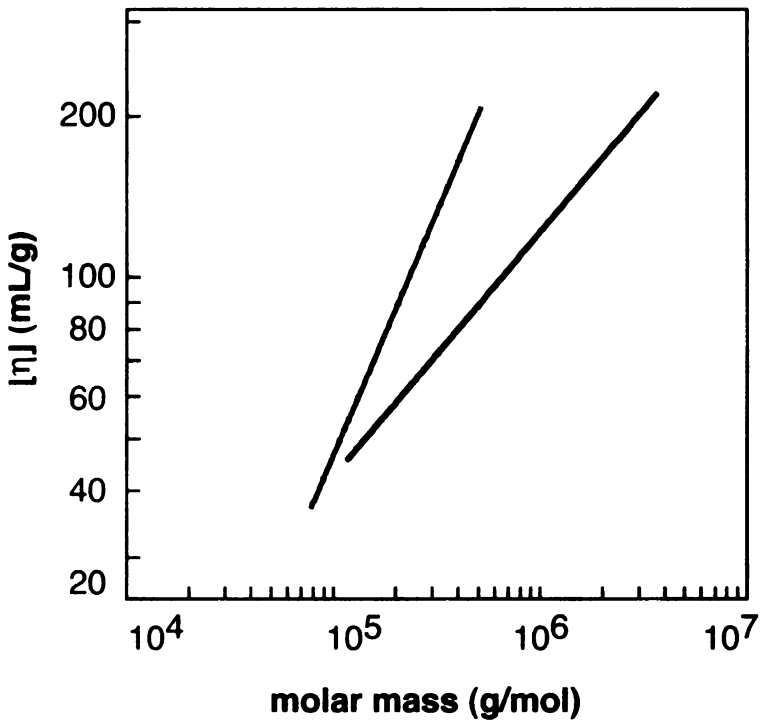

Figure 33. Mark-Houwink plots for linear (broken red line) and branched (solid blue line) PLA in THF at 35 °C using light scattering and dilute-solution viscometry data, extracted from GPC-MALLS. The smaller slope for poly((HOG-*co*-LLA)-*g*-LLA) is consistent with the branched architecture of poly((HOG-*co*-LLA)-*g*-LLA). The HOG content in poly((HOG-*co*-LLA)-*g*-LLA) was 5 mol%, and the degree of polymerization of the LLA branches was 60. Linear PLA, $a = 0.74$; branched PLA, $a = 0.34$.

Side Chain Crystallinity of poly((HOG-*co*-LLA)-*g*-LLA)

DSC scans of the branched polymers did not detect crystallization of the branches despite degrees of polymerization of 60. We surmised that the lack of crystallization of the PLLA branches was related to the hydroxy groups at the termini of the branches, which could inhibit chain mobility by forming hydrogen bonds with adjacent branches. To test this hypothesis, we converted each terminal alcohol to an ester derived from either acetic or stearic acid using DCC coupling (**Figure 34**). Consistent with our hypothesis, esterification immediately led to

crystallization of the branches, as confirmed by DSC (**Figure 35**) and polarized optical microscopy (not shown). Interestingly, the stearic acid derivative also showed a weak melting transition at 40 °C, which is consistent with melting of the C_{18} alkyl chains. Furthermore, the ΔH_{fus} associated with melting was linearly related to the branch length, confirming the notion that the crystallinity was limited to the PLLA branches (**Figure 36**). The near-zero intercept also suggests that the branches were highly crystalline, and only a few lactide repeat units, presumably adjacent to the alkyl chains, were in the amorphous phase.

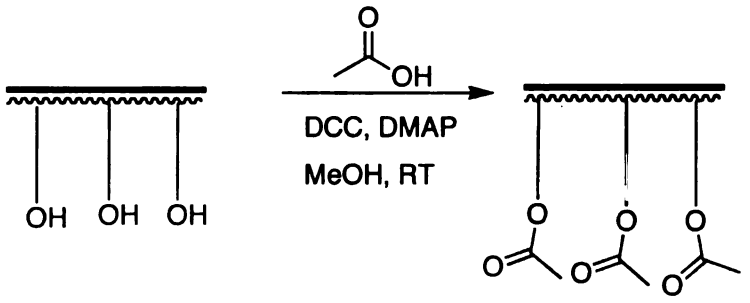

Figure 34. Acylation of poly((HOG-*co*-LLA)-*g*-LLA) using DCC coupling.

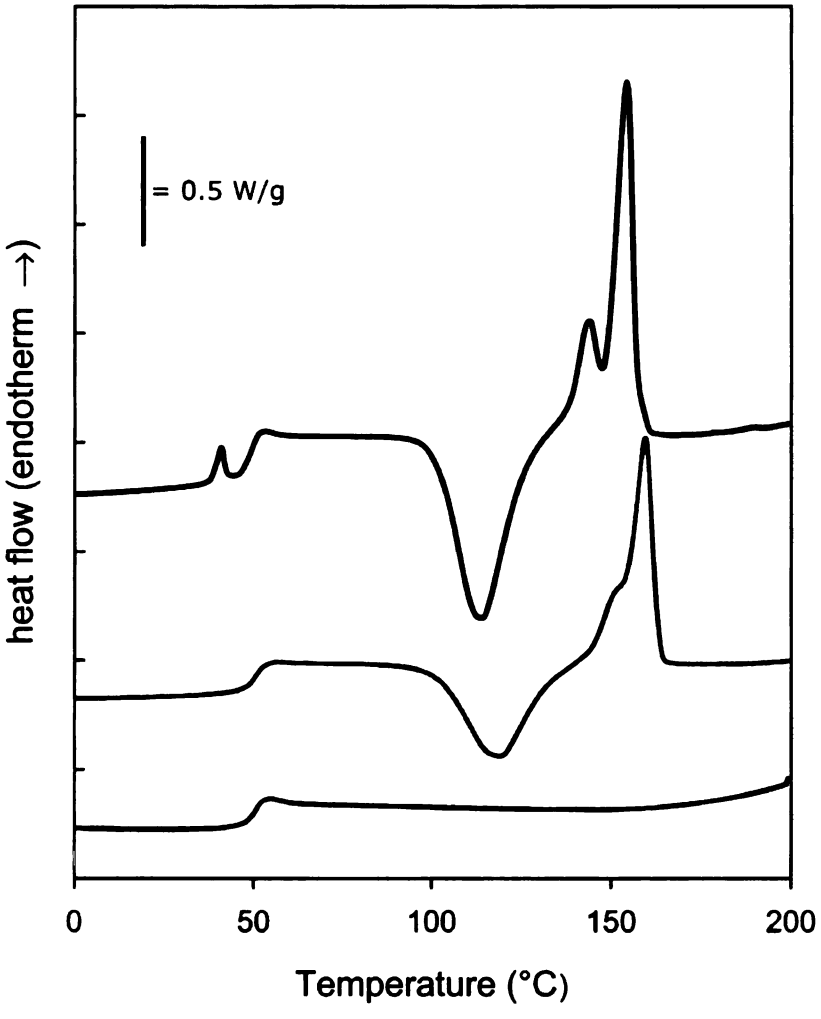

Figure 35. DSC second heating scans of poly((HOG-*co*-LLA)-*g*-LLA) at a heating rate of 10 °C/min. The degree of polymerization of the PLLA branches is 40; (OH terminated (— bottom), acetate terminated (— middle), and stearate terminated (— top)).

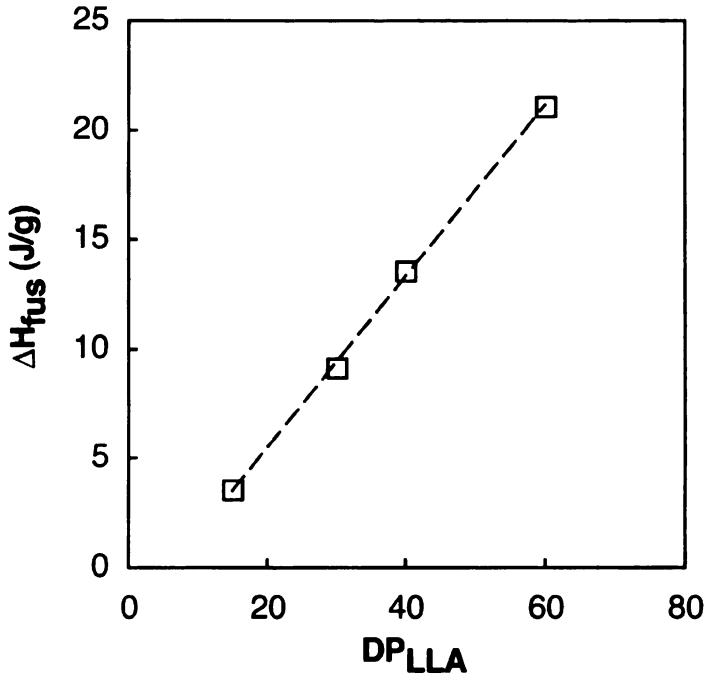

Figure 36. Relationship between ΔH_{fus} and the branch length for poly((HOG-*co*-LLA)-*g*-LLA). The terminal $-CH_2OH$ groups of the branches were acetylated.

Conclusion

We designed and synthesized a functionalized lactide derivative that places a benzyl protected alcohol eight methylene units away from the polyester backbone. Copolymerization with *L*-lactide yielded high molecular weight polymers with low PDIs. Quantitative hydrogenolysis of the benzyl ether groups provided functionalized lactides with pendant primary alcohols distributed along the polymer backbone. Initiation of *L*-lactide from the alcohol groups provided high molecular weight polylactide comb polymers, confirmed by viscosity and light scattering data. Capping the hydroxy groups at the end of the PLLA branches provided crystalline comb polymers with melting points of 150-160 °C.

Experimental Section

General. Unless otherwise specified, ACS reagent grade starting materials and solvents were used as received from commercial suppliers without further purification. *L*-lactide was purchased from Aldrich and sublimed prior to use. ^{1}H NMR (300 or 500 MHz) and ^{13}C NMR (75 or 125 MHz) spectra were acquired using either a Varian Gemini 300 spectrometer or a Varian UnityPlus 500 spectrometer with the residual proton signal from the $CDCl_3$ solvent used as chemical shift standard. Mass spectral analyses were carried out on a VG Trio-1 Benchtop GC-MS. IR spectra were taken with Mattson Galaxy 3000 FT-IR. Elemental Analyses were determined using a Perkin-Elmer 2400 CHNS/O Analyzer. Melting points were taken on an Electrothermal capillary melting point apparatus and are uncorrected.

Polymer Characterization. Polymer molecular weights were determined by GPC-MALLS at 35 °C using two PLgel 10μ mixed-B columns in series (manufacturer-stated linear molecular weight range of 500-10×10^6 g/mol). The eluting solvent was THF at a flow rate of 1 mL/min, and the concentration of polymer solutions used for GPC was 1 mg/mL. An Optilab rEX (Wyatt Technology Co.) and a DAWN EOS 18-angle light scattering detector (Wyatt Technology Co.) with a laser wavelength of 684 nm were used to calculate absolute molecular weights. Differential scanning calorimetry analyses of the polymers were obtained using a TA DSC Q100. Samples were run under a nitrogen atmosphere at a heating rate of 10 °C/min, with the temperature calibrated with an indium standard. Polarized optical micrographs

were taken on a Nikon Optiphot2-POL polarizing optical microscope equipped with a Mettler FP82 hot stage and a CCD camera.

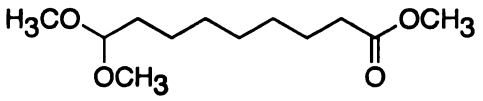

Methyl 9,9-dimethyoxynonanoate. Oleic acid (90 %, 25.71 g, 82 mmol) was dissolved in 450 mL of dichloromethane/methanol (4:1) and the solution was cooled to –78 °C in a dry ice/acetone bath. Ozone was bubbled through the solution until a blue color remained. The resulting ozonide solution was purged with nitrogen, quenched with dimethyl sulfide (365 mmol, 27 mL) and stirred for 5 hours at room temperature. After the solvent was evaporated *in vacuo*, the residue was dissolved in ether (250 mL), washed with saturated aqueous NaCl (2 x 100 mL), dried over $MgSO_4$ and the ether evaporated. The residue was dissolved in methanol (400 mL), *p*-toluenesulfonic acid (3.0 g) was added, and the solution was stirred overnight at room temperature. Sodium bicarbonate was added until the pH reached 10 and then the methanol was removed *in vacuo*. The residue was redissolved in ether (200 mL), washed with saturated aqueous $NaHCO_3$ (2 x 100 mL) and saturated aqueous NaCl (1 x 100 mL), dried over $MgSO_4$, and the ether evaporated. Vacuum distillation (90 °C, 10 mTorr) yielded methyl 9,9-dimethoxynonanoate (18.3 g, 79 mmol, 96 %) as a colorless liquid. ^{1}H NMR (300 MHz) δ 4.29 (t, 1H, J = 5.62 Hz), 3.60 (s, 3H), 3.25 (s, 6H), 2.24 (t, 2H, J = 7.57 Hz), 1.45-1.62 (m, 4H), 1.20-1.40 (m, 8H). ^{13}C NMR (75 MHz) δ 174.2, 104.4, 52.5, 51.3, 34.0, 32.3, 29.2, 29.1, 28.9, 24.8, 24.4.

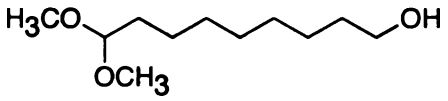

9,9-Dimethoxynonanol. Under a nitrogen atmosphere, a solution of methyl 9,9-dimethoxynonanoate (17.0 g, 73.2 mmol) in anhydrous THF (250 mL) was added dropwise to a cooled (0 °C) suspension of $LiAlH_4$ (54.9 mmol, 2.1 g) in 150 mL of anhydrous THF. After the addition was complete, the solution was stirred for 4.5 h at 0 °C, and then carefully quenched by the sequential addition of H_2O (2.5 mL), 1 M NaOH (2.5 mL), and H_2O (5 mL). After stirring for 30 minutes, the product was isolated from the salts via Soxhlet extraction (THF, 36 h). The THF was evaporated and the residue was dissolved in ether, washed with saturated NaCl solution (1 × 100 mL), and dried over $MgSO_4$ to yield 9,9-dimethyoxynonanol (14.2 g, 69.6 mmol, 95 %) as a colorless liquid. ^1H NMR (300 MHz) δ 4.32 (dd, 1H, J = 5.86 and 5.62), 3.58 (t, 2H, J = 6.59 Hz), 3.23 (s, 6H), 1.45-1.50 (m, 4H), 1.2-1.4 (m, 10H). ^{13}C NMR (75 MHz) δ 104.5, 62.9, 52.5, 32.7, 32.4, 29.4, 29.33, 29.26, 25.7, 24.5.

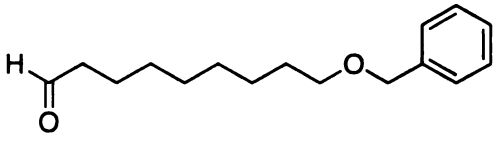

(9-benzyloxy)nonanal. Under a nitrogen atmosphere, a solution of 9,9-dimethoxynonanol (14.2 g, 69.5 mmol) dissolved in anhydrous THF (100 mL) was added to a suspension of sodium hydride (60 % in mineral oil, washed with hexanes, 3.2 g, 139 mmol) in anhydrous THF (300 mL). The mixture was stirred at room temperature for 5 minutes and a solution of benzyl chloride (90.4 mmol, 10.4

mL) in 10 mL of anhydrous THF was added. The reaction was heated to reflux for 24 h under nitrogen, cooled to room temperature and poured into 100 mL saturated aqueous NaCl. The THF was removed *in vacuo*, and the aqueous phase extracted with EtOAc (3 × 100 mL). The combined organic layers were washed with a saturated NaCl solution (1 × 100 mL), dried over $MgSO_4$, and the ethyl acetate was evaporated to give 1,1-dimethoxy-9-benzyloxynonane (20.0 g, 68.0 mmol, 98 %) as a pale yellow liquid, which was used without further purification. ^{1}H NMR (300 MHz) δ 7.20-7.33 (m, 5H), 4.50 (s, 2H), 4.38 (t, 1H, *J* = 5.77 Hz), 3.46 (dd, 2H, *J* = 6.59, 6.87), 3.31 (s, 9H), 1.55-1.65 (m, 4H), 1.20-1.41 (m, 10H). ^{13}C NMR (75 MHz) δ 138.7, 128.3, 127.6, 127.4, 104.5, 72.8, 70.4, 52.5, 32.4, 29.7, 29.5, 29.4, 29.3, 26.1, 24.5.

1,1-Dimethoxy-9-benzyloxynonane (20.0 g, 68 mmol) was dissolved in a solution of THF (30 mL) and 50 % acetic acid (200 mL) and stirred at room temperature overnight. The reaction was quenched at 0 °C by the addition of sodium bicarbonate until the pH = 12. The combined organic layers were extracted with ether (3 × 100 mL), washed with saturated $NaHCO_3$ (2 × 75 mL) and saturated aqueous NaCl (1 × 75 mL), and then dried over $MgSO_4$. The ether was evaporated to give (9-benzyloxy)nonanal (16.5 g, 66.5 mmol, 98 %) as a pale yellow liquid. ^{1}H NMR (300 MHz) δ 9.7 (t, 1H, J = 1.95 Hz), 7.2-7.4 (m, 5H), 4.5 (s, 2H), 3.4-3.5 (t, 2H, *J* = 6.59 Hz), 2.3-2.5 (td, 2H, *J* = 7.32 and 1.95 Hz), 1.5-1.8 (m,

4H), 1.2-1.5 (m, 10H). ^{13}C NMR (75 MHz) δ 202.9, 138.6, 128.3, 127.6, 127.4, 72.8, 70.4, 43.8, 29.7, 29.2, 29.2, 29.0, 26.1, 22.0.

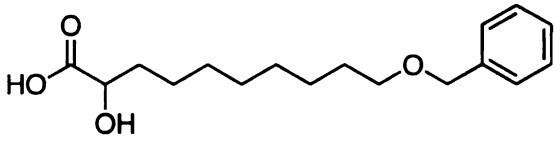

10-(Benzyloxy)-2-hydroxydecanoic acid. Saturated aqueous $NaHSO_3$ (30 mL) and H_2O (50 mL) were added to a solution of (9-benzyloxy)nonanal (16.5 g, 66.5 mmol) dissolved in THF (30 mL). The reaction was purged with nitrogen and stirred at room temperature until a white slurry formed. The mixture was cooled to 0 °C, and a solution of KCN (13 g, 200 mmol) in H_2O (70 mL) was added. After stirring for 6 hours at 0 °C, the aqueous phase was extracted with ether (4 × 100 mL) and the combined organic phases were washed with saturated aqueous NaCl (1 x 100 mL) and dried over $MgSO_4$. Evaporation of the ether yielded 10-(benzyloxy)-2-hydroxydecanenitrile (17.7 g, 64.4 mmol, 97 %) as a pale yellow liquid, which was used without further purification. ^1H NMR (300 MHz) δ 7.2-7.4 (m, 5H), 4.5 (s, 2H), 4.3 (dd, 1H, J = 6.59, 6.87 Hz), 3.4 (t, 2H, J = 6.59 Hz), 1.8 (m, 2H), 1.6 (m, 2H), 1.4 (m, 2H), 1.2-1.4 (m, 8H). ^{13}C NMR (75 MHz) δ 138.3, 128.3, 127.7, 127.6, 120.0, 72.8, 70.4, 61.1, 35.1, 29.6, 29.2, 28.7, 26.0, 24.4.

Concentrated HCl (30 mL) was added to the cyanohydrin (17.5 g, 64 mmol) and the solution was stirred at room temperature overnight. The solution pH was then adjusted to 12 with 6 M NaOH and the resulting amide was collected via vacuum filtration, washed with hexanes, and added to 250 mL 2.5 M NaOH. The

mixture was refluxed for 36 h and then acidified with 6 M HCl. The aqueous phase was extracted with ether (4 × 100 mL) and the combined organic layers were washed with saturated aqueous NaCl (1 × 100 mL), and then dried over $MgSO_4$. After filtration, evaporation of the ether gave 17.5 g (60.2 mmol, 94 %) of the crude α-hydroxy acid. Recrystallization from hexanes/EtOAc (1:9) provided 9.9 g (33.7 mmol, 56 %) of 10-(benzyloxy)-2-hydroxydecanoic acid as white crystals. ^1H NMR (500 MHz) δ 7.2-7.2 (m, 5H), 4.5 (s, 2H), 4.2 (dd, 1H, J = 7.32, 7.57 Hz), 3.5 (t, 2H, J = 6.59 Hz), 1.9 (m, 1H), 1.7 (m, 1H), 1.6 (m, 2H), 1.4 (m, 4H), 1.2-1.4 (m, 10H). ^{13}C NMR (125 MHz) δ 178.5, 138.5, 128.4, 127.7, 127.5, 72.8, 70.5, 70.2, 34.1, 29.6, 29.2, 29.2, 29.1, 26.0, 24.6. mp 51-52 °C.

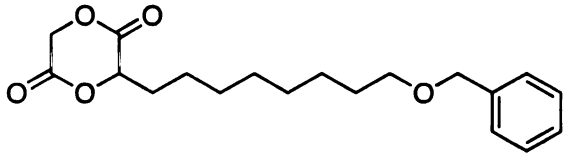

3-(8-(benzyloxy)octyl)-1,4-dioxane-2,5-dione (BOG). 10-(Benzyloxy)-2-hydroxydecanoic acid (9.5 g, 33 mmol), 2-bromoacetyl bromide (3.3 mL 39 mmol) and 300 mL of ether were added to a 500 mL 3-neck flask. The flask was purged with nitrogen, cooled to 0 °C, and then a solution of Et_3N (8.7 mL) in ether (50 mL) was added dropwise. After stirring for 6 hours at 0 °C, the mixture was filtered to remove a white precipitate and the filtrate was washed with 2 N HCl (2 × 50 mL) and saturated aqueous NaCl (1 × 100 mL), and then dried over $MgSO_4$. Filtration and removal of the solvent *in vacuo* gave the crude linear acid ester as a viscous liquid (11.5 g, 27.7 mmol). The ester was dissolved in a mixture of acetone (700

mL) and Et_3N (44.5 mmol, 6.3 mL), and refluxed for 2 hours. The solids were removed by filtration and the filtrate was concentrated *in vacuo*. The residue was dissolved in ethyl acetate (100 mL), washed with 2 M HCl (2 × 50 mL), saturated $NaHCO_3$ (2 × 50 mL) and saturated NaCl (1 × 50 mL), and then dried over $MgSO_4$. The product was purified by flash chromatography (EtOAc) and dried under vacuum. Recrystallization from ether (0 °C) provided 2.7 g (8.08 mmol, 38 %) of 3-(8-(benzyloxy)octyl)-1,4-dioxane-2,5-dione as colorless crystals. ^1H NMR (500 MHz) δ 7.3 (m, 5H), 4.9 (m, 2H), 4.9 (m, 1 H), 4.5 (s, 2H), 3.5 (t, 2H, J = 6.59 Hz), 2.1 (m, 1H), 1.9 (m, 1H), 1.6 (m, 2H), 1.5 (m, 1H), 1.5 (m, 1H), 1.2-1.4 (m, 8H). ^{13}C NMR (125 MHz,) δ 165.6, 164.3, 138.6, 128.3, 127.6, 127.4, 75.6, 72.8, 70.4, 65.2, 30.8, 29.7, 29.2, 29.1, 28.8, 26.0, 24.3. IR (KBr) ν (cm^{-1}) 2928, 2909, 2845, 1752, 1297, 1325, 1122, 1081. Anal. Calcd. For $C_{19}H_{26}O_5$: C, 68.24; H, 7.84. Found: C, 68.09; H, 7.99. MS (EI), *m/z* 334 (M^+), 316, 107, 91, 45, 40. mp 65.5-66.5 °C.

Solution Polymerization Kinetics of BOG. A Schlenk flask loaded with BOG (0.669 g, 2.0 mmol) and a magnetic stir bar was fitted with a rubber septum and evacuated under vacuum. Sn(2-ethylhexanoate)$_2$ (525 μL of a 38.1 mM solution in anhydrous toluene) and 4-*tert*-butylbenzyl alcohol (525 μL of a 38.1 mM solution in anhydrous toluene) were added to the flask through the septum ([BOG]:[I]:[catalyst] = 100:1:1). Anhydrous toluene (8.95 mL) was added (monomer concentration = 0.2 M) and the Schlenk flask was immersed in a preheated oil bath at 90 °C.

Aliquots of the reaction solution were removed via syringe at specific intervals and analyzed via NMR to determine the conversion of monomer to polymer.

Bulk Polymerization and Copolymerization of BOG. Monomer(s) and a small magnetic stir bar were added to ampoules prepared from 3/8 in. diameter glass tubing. The ampoule was connected via a Cajon® fitting to a T-shaped vacuum adapter fitted with a stopcock and an air-free Teflon valve. The apparatus was attached to a vacuum line and evacuated through the Teflon valve. The ampoule was backfilled with argon, and a syringe was used to add predetermined amounts of the $SnOct_2$ and BBA solutions (both 38.1 mM in toluene) to the ampoule through the stopcock. After removing solvent *in vacuo*, the ampoule was flame-sealed and immersed in an oil bath at 130 °C for the desired polymerization time. The polymerization was quenched in ice and a portion of the polymer was analyzed by ^1H NMR to evaluate conversion. The remaining polymer was dissolved in CH_2Cl_2, precipitated into cold methanol, and dried under vacuum (4 mTorr) at 40 °C for 24 h and analyzed by GPC to determine the molecular weight.

Poly(BOG). ^1H NMR (500 MHz) δ 7.2-7.4 (m, 5H), 5.1-5.2 (m, 1H), 4.6-4.9 (m, 2H), 4.5 (s, 2H), 3.4 (t, 2H, J = 6.59 Hz), 1.8-2.0 (m, 2H), 1.5 (m, 2H), 1.2-1.4 (m, 10H). ^{13}C NMR (125 MHz) δ (note: minor chemical shifts due to polymer tacticity not included) 168.9, 166.6, 138.7, 128.3, 127.6, 127.4, 75.6, 72.8, 70.4, 65.2, 60. 7, 30.9, 29.7, 29.3, 29.0, 28.8, 26.1, 24.9.

Poly(BOG-*co*-LLA). ^1H NMR (500 MHz) δ (assignments based on a 50:50 feed ratio of BOG and LLA) 7.2-7.4 (m, 5H), 5.1-5.3 (m, 3H), 4.6-4.9 (m, 2H), 4.5 (s,

2H), 3.4 (t, 2H, J = 6.34 Hz), 1.8-2.0 (m, 2H), 1.4-1.6 (m, 8H), 1.2-1.4 (m, 8H). ^{13}C NMR (125 MHz, $CDCl_3$) δ (note: minor chemical shifts due to polymer tacticity not included) 169.5, 166.5, 138.7, 128.3, 127.6, 127.4, 72.8, 75.6, 70.4, 69.0, 65.2, 60.7, 30.9, 29.7, 29.3, 29.0, 28.8, 26.1, 24.9, 16.6, 15.8.

Removal of Benzyl Ether Protecting Group from poly(BOG).[120] Benzyl ether protected poly(BOG) or poly(BOG-*co*-LLA) was dissolved in CH_2Cl_2 (1 mL) and added to a mixture of THF/MeOH (100 mL, 1:1 vol%) containing 20 mg of 10 % Pd/C. The heterogeneous solution was sealed in a Parr bomb, purged with hydrogen, and then pressurized with H_2 to 1000-1500 psi. After 2-3 days at room temperature, the reaction mixture was filtered through a borosilicate microfiber filter, and evaporated to dryness. The crude product was dissolved in CH_2Cl_2 and precipitated into cold MeOH (copolymers) or dissolved in EtOH and precipitated into cold hexanes (homopolymer). The product was isolated as a white solid (copolymers) or a viscous oil (homopolymer).

Poly(HOG). ^1H NMR (500 MHz, DMSO-d_6) δ 5.1-5.2 (m, 1H), 4.8-5.0 (m, 2H), 4.3 (s, OH), 3.3-3.4 (dd, 2H, J = 11.48, 6.10 Hz), 1.7-1.9 (m, 2H), 1.3-1.5 (m, 2H), 1.2-1.3 (m, 10H). ^{13}C NMR (125 MHz, DMSO-d_6) δ (note: minor chemical shifts due to polymer tacticity not included) 168.6, 166.8, 75.6, 72.2, 60.7, 32.5, 30.5, 28.8, 28.5, 25.5, 24.7, 24.1.

Poly(HOG-*co*-LLA). ^{1}H NMR (500 MHz) δ (assignments based on a 50:50 feed ratio of BOG:LLA in the original copolymer) 5.1-5.3 (m, 3H), 4.6-4.9 (m, 2H), 3.6 (t, 2H, J = 6.59 Hz), 1.8-2.0 (m, 2H), 1.4-1.6 (m, 8H), 1.2-1.4 (m, 8H). ^{13}C NMR (125 MHz) δ (note: minor chemical shifts due to tacticity not included) 169.6, 166.5, 72.8, 70.4, 69.0, 66.7, 60.7, 32.7, 30.8, 29.1, 28.8, 28.5, 25.6, 24.7, 16.6.

Degradation Studies. Polymer samples (10 mg) were placed in 20 mL culture tubes and 10 mL PBS solution (pH = 7.4) was added. The tubes were sealed and placed in a degradation chamber at 55 °C. At allotted times samples were removed and the solvent was decanted from the samples. Once the residue was dried the molecular weight was determined by GPC-MALLS.

Graft Polymerization of *L*-Lactide for Branched Polylactides. Solvent-free graft polymerizations were carried out in sealed ampoules as described above. Bulk polymerization of *L*-lactide from poly(HOG) and poly(HOG-*co*-LLA) was catalyzed by $SnOct_2$ ([OH groups]:[catalyst] = 1:1). Poly(HOG) or poly(HOG-*co*-LLA) (100 mg) was dissolved in anhydrous THF (500 μL) and introduced into the ampoule, followed by the predetermined amount of LLA. The contents were stirred for 30 minutes and the solvent removed *in vacuo.* $SnOct_2$ (38.1 mM solution in toluene) was added under nitrogen, the solvent evaporated, and the ampoule was sealed as described above. The sealed tubes were placed in an oil bath at 170 °C for 90 seconds and transferred to an oil bath at 130 °C for 45 minutes. Purification was carried out as described above.

Poly((HOG-*co*-LLA)-*g*-LLA): Poly(HOG-*co*-LLA) (50 mg, 5 mol % HOG, M_n = 31.6 kg/mol, PDI = 1.19) gave 51 mg of poly((HOG-*co*-LLA)-*g*-LLA) (96 %, M_n = 39.3 kg/mol, PDI = 1.99) after purification. ^{1}H NMR (500 MHz) δ 5.0-5.3 (m, COC**H**(CH_3)O), 4.8-4.9 (m, COC$\mathbf{H_2}$O), 4.3 (dd, J = 13.67 and 6.84 Hz, COC**H**(CH_3)OH), 4.1 (m, $(CH_2)_6C\mathbf{H_2}OCO$), 1.8-2.0 (m, $CHC\mathbf{H_2}(CH_2)_6O$), 1.4-1.8 (m, COCHC$\mathbf{H_3}$), 1.2-1.4 (m, $CHCH_2(C\mathbf{H_2})_6OCO$). ^{13}C NMR (125 MHz) δ (note: minor chemical shifts due to polymer tacticity not included) 175.1, 169.6, 72.4, 69.0, 66.7, 65.6, 30.8, 30.2, 29.7, 29.1, 29.0, 28.4, 25.6, 20.5, 16.6, 16.5.

Esterification of Poly((HOG-*co*-LLA)-*g*-LLA). The procedure for the acetate synthesis is described; the stearate derivative was prepared using the same procedure. A small round bottom flask containing poly((HOG-*co*-LLA)-*g*-LLA) (5 mol% HOG, 50 mg, 5.2×10^{-7} mol, 6.2 μmol OH groups, M_n = 96.4 kg/mol) and DMAP (1.3 μmol, 0.2 mg) were dried under vacuum for four hours. Anhydrous CH_2Cl_2 (10 mL) was added via syringe under nitrogen and the solution was stirred until completely dissolved. Acetic acid (19 μmol, 107 μL of a 1 mM solution) and DCC (13 μmol, 195 μL of 64 mM solution in CH_2Cl_2) were added via syringe and the reaction was stirred under nitrogen overnight. The reaction mixture was filtered to remove the insoluble dicyclohexyl urea byproduct, further concentrated, and filtered again to fully remove the urea. The CH_2Cl_2 polymer solution was further

concentrated to a 10 wt % solution and precipitated from cold methanol. The polymer was dried under vacuum to yield 40 mg (80 %) of the acetylated polymer (M_n = 97.0 kg/mol, PDI = 1.75).

Chapter 4 Post-Polymerization Modification of Polyglycolides via "Click" Chemistry

Introduction

The term "synthetic biopolymers" refers to a class of polymers that includes polymeric drugs,[121-123] polymer-drug conjugates,[124-127] encapsulated drugs within polymer micelles,[113,128] and multicomponent polyplexes that are being developed as non-viral vectors for delivery of siRNA and DNA.[129-131] All of these polymers are water-soluble and are intrinsically bioactive or are an inert carrier of the active drug, protein, or gene.

Functionalized polyesters are particularly suited for these applications because they are biodegradable and can contain a variety of functional groups, which impart a wide range of properties. Recent examples of polylactide derivatives with pendant alkyl,[10,33] aryl,[16,105] allyl,[34] and poly(ethylene glycol)[33] have been reported. In addition, polylactides with pendant functional groups such as alcohols, amines, and carboxylic acids have been described by others and us.[18,19,25,26,76] Incorporation of functional groups affects polymer physical properties such as hydrophilicity, degradability, and the glass transition temperature. Water-soluble polyesters containing hydrophilic poly(ethylene glycol) segments are especially interesting targets because they enhance a polymer's *in vivo* delivery capabilities by preventing uptake by the reticuloendothelial system (RES).[62,70,72,132] The RES eliminates old cells, debris, foreign substances and pathogens from the blood stream and can complicate controlled delivery.[133]

The synthesis of functionalized polyesters can be accomplished via two routes: the functional monomer approach or the post-polymerization modification approach. The functional monomer approach adds the desired functionality directly to the monomer (**Scheme 1, Chapter 1**). However, since many functional groups are incompatible with polymerization conditions they must be protected prior to polymerization and deprotected in a second step. The deprotection steps must be highly regulated to ensure complete removal of the protecting groups and to minimize backbone degradation. Although several groups have reported successful deprotection strategies,[17-20,22] simple methods for the introduction functional groups are still desired. In addition, any small polymer modification requires the synthesis and characterization of new monomers.

A second functionalization route is post-polymerization modification, which introduces functionality after polymerization. This approach minimizes the number of protection-deprotection steps, and perhaps more importantly, allows a wide range of polymers to be synthesized from a single monomer. Examples of strategies for post-polymerization modification of polyesters include direct grafting,[35-38] DCC-coupling,[34,57]ketoximine coupling,[59-61] Michael addition,[66,134] atomic transfer radical addition,[67,69,72] and click chemistry.[70-72] Probably the most successful of these approaches is "click" chemistry, specifically the copper(I)-mediated 1,3-dipolar cycloaddition of azides and alkynes (**Scheme 34**). Originally introduced in polymer science by Sharpless,[135,136] click chemistry has now been

used in the synthesis of dendrimers,[137-140] block copolymers,[141,142] dendronized linear polymers,[141,143-145] and branched polymers.[70-72,146]

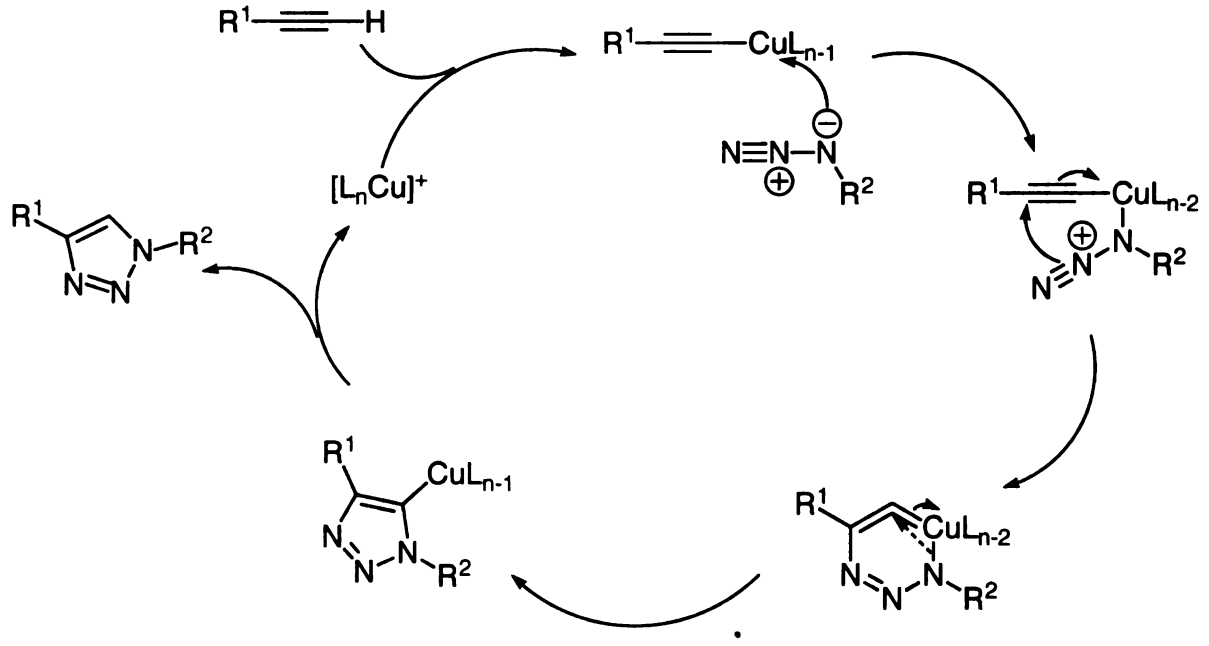

Scheme 34. Mechanism for the copper(I)-mediated 1,3-dipolar cycloaddition between alkynes and azides, also known as "click" chemistry.

Recently we reported the synthesis of an acetylene functionalized glycolide derivative, 3,6-dipropargyl-1,4-dioxane-2,5-dione (propargylglycolide, PGL), and its post-polymerization via click chemistry.[73] We demonstrated appropriate conditions to apply click chemistry to polyglycolides, which are more hydrolytically sensitive than other polyesters, such as ε-caprolactone.[70,72] Generating Cu(I) *in situ* via copper sulfate pentahydrate and sodium ascorbate in DMF at room temperature prevented degradation of the polyglycolide backbone.

We applied these techniques to the synthesis of water-soluble comb polyglycolides by the addition of short poly(ethylene glycol) segments to the poly(PGL) (PPGL) backbone. The polymers self-assemble in aqueous solution

into small, uniform unimolecular micelles (**Figure 37**) that are unaffected by a critical micelle concentration (cmc).[147] In contrast, traditional micelles are often formed from amphiphilic block copolymers and exist as single molecules below the cmc and as dynamic aggregates above the cmc.[148-152] Although there has been some progress towards unimolecular micelles, including dendrimers and a few aliphatic graft-copolymer systems, synthetic challenges have impeded their wide spread use.[153-158] Dendrimers are structurally well-defined molecules with high functional group densities; however many dendrimer syntheses are tedious and low yielding due to their iterative nature. Aliphatic graft-copolymers could be useful, however simple attachment of hydrophilic groups to hydrophobic polymer backbones currently remains a challenge. This chapter describes the synthesis, characterization, and applications of functionalized PPGL polymers.

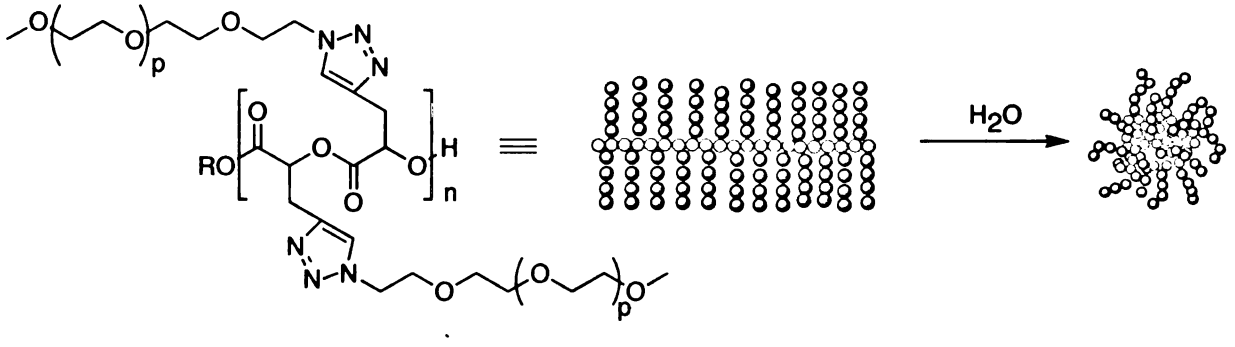

Figure 37. The comb architecture of poly(propargylglycolide)-*graft*-poly(ethylene glycol monomethyl ether) and formation of a unimolecular micelle in aqueous solution. The hydrophobic backbone and hydrophilic side chains are illustrated in red and blue, respectively.

Results and Discussion

Post-Polymerization Modification

Scheme 35 shows the synthesis and post-polymerization functionalization of poly(propargylglycolide) by click chemistry.[159] The synthesis of propargylglycolide began with a Reformansky-type reaction of propargyl bromide with ethyl glyoxalate, in the presence of activated zinc, to generate ethyl 2-hydroxy-3-butynoate. Hydrolysis of the ester in refluxing water yielded 2-hydroxy-3-butanoic acid, which was dimerized in refluxing toluene using *p*-toluenesulfonic acid as a catalyst, giving propargylglycolide in 34 % yield. The monomer was polymerized via ring opening polymerization using $SnOct_2$ and BBA as the catalyst and initiator, respectively.

An mPEG azide suitable for click chemistry was synthesized by tosylation of 2,5,8,11,14-pentaoxahexadecan-16-ol (tetraethylene glycol monomethyl ether, mPEG) followed by displacement of the tosyl group by sodium azide, giving 16-azido-2,5,8,11,14-pentaoxahexadecane (tetraethylene glycol monomethyl ether azide, mPEG-azide). The azide group is easily identified by its characteristic IR absorbance at 2105 cm^{-1} and the resonances from the methylene α to the azide at 3.38 ppm in its ^1H NMR spectrum and 50.5 ppm in its ^{13}C NMR spectrum. The click reaction was performed under the reported conditions, generating Cu(I) *in situ* (5 mol % copper(II) sulfate pentahydrate and 12 mol % sodium ascorbate) in DMF at room temperature.

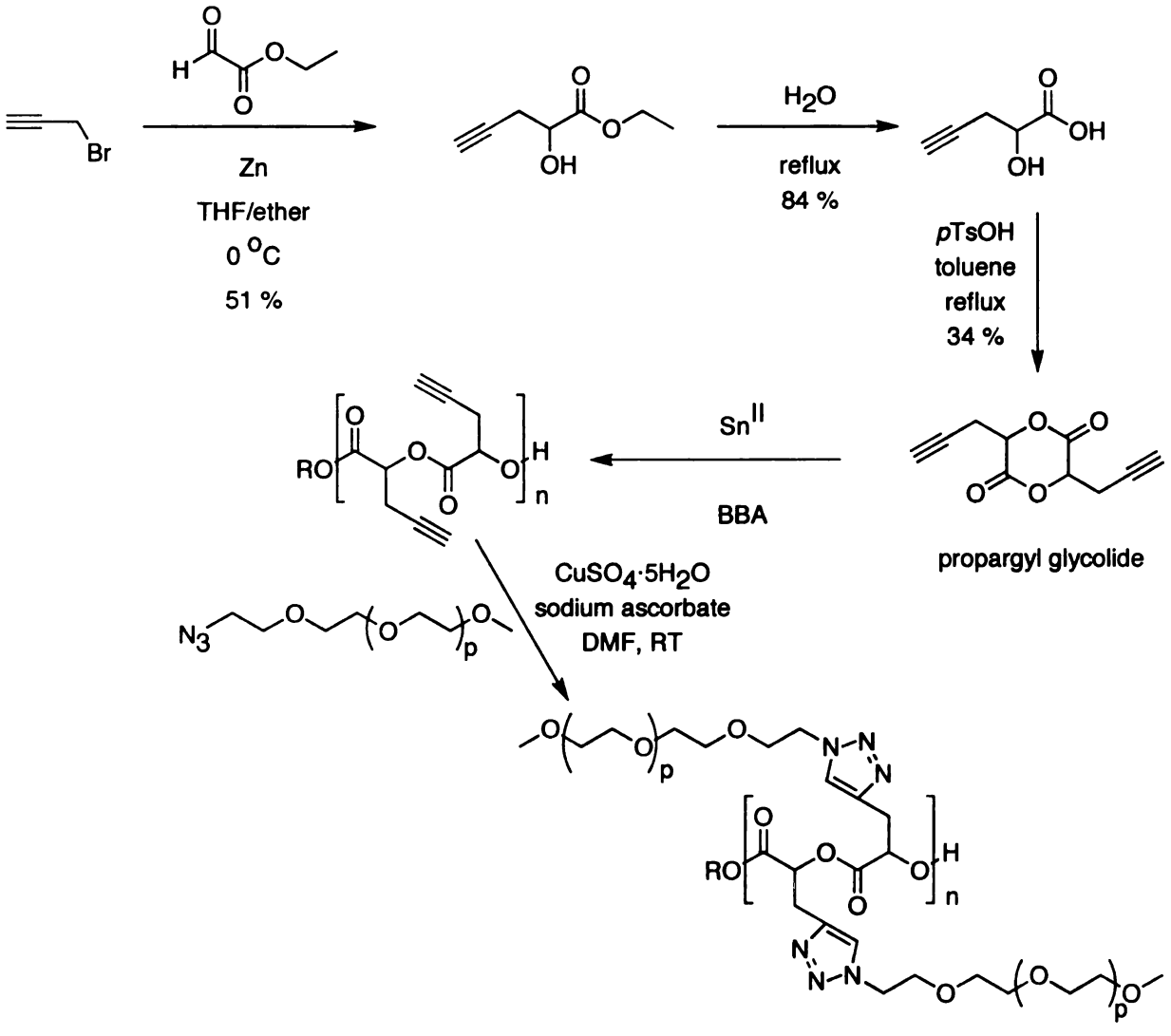

Scheme 35. Synthesis, polymerization, and functionalization of poly(propargylglycolide).

The ^{1}H NMR spectra of the polymer before and after click functionalization with mPEG-azide are shown in **Figure 38**. The reaction went to 100 % completion as indicated by the disappearance of the resonances at 2.85 ppm (-C$\underline{H_2}$-CCH) and 2.05 ppm (-$CH_2CC\underline{H}$) and the appearance of a new resonance at 7.6 ppm corresponding to the triazole proton.

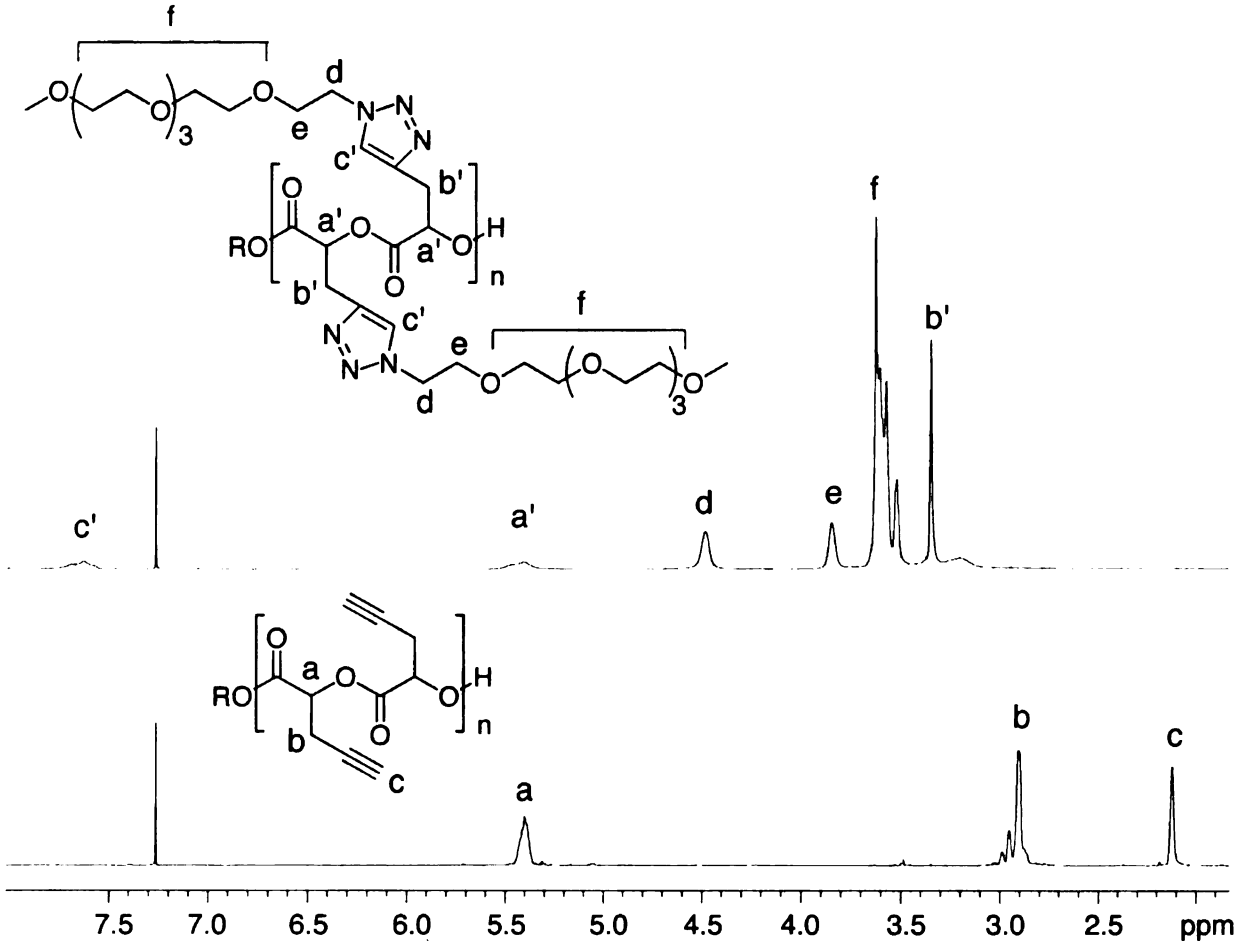

Figure 38. 500 MHz ^{1}H NMR spectra of poly(propargylglycolide) and its click functionalization with mPEG-azide. Integration of a = c = a' = c' = 1.

The click reaction can also be characterized via infrared (IR) spectroscopy. The spectra of unfunctionalized PPGL (bottom) and PPGL-*graft*-poly(ethylene glycol) monomethyl ether (PPGL-*g*-mPEG) (top), is shown in **Figure 39**. Notably, the alkyne-stretching mode at 3200 cm^{-1} completely disappears upon click functionalization and a new band appears at 3300-2500 cm^{-1} from the triazole N-H. CH_2 stretching at 3000 cm^{-1} also increased in accordance with the addition of PEG branches. The absence of a band at 2105 cm^{-1} suggests that the polymer is free of residual azides.

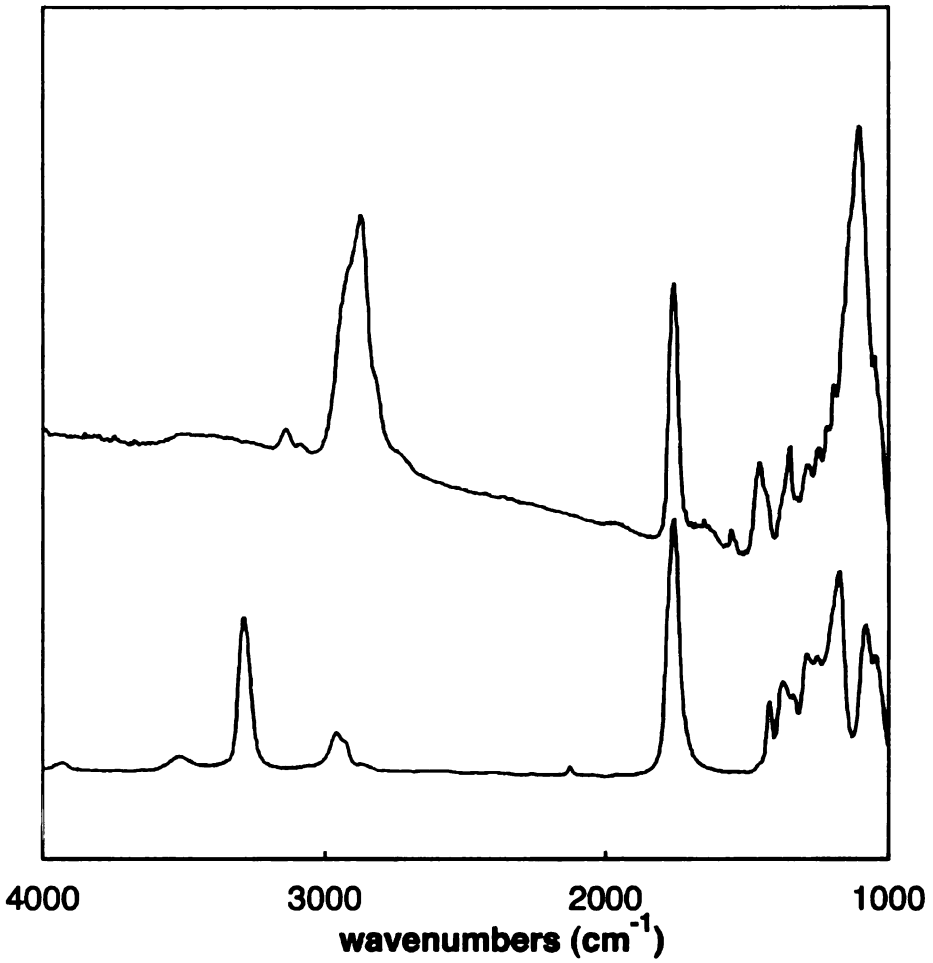

Figure 39. IR spectra of unfunctionalized PPGL (bottom) and PPGL-*g*-mPEG (top). Notably, the alkyne stretch at 3200 cm^{-1} completely disappears upon click functionalization and a new stretch at 3300-2500 cm^{-1} from the N-H triazole stretch appears.

Although the click reaction is highly selective and functional group tolerant, it suffers from residual copper contamination. Triazoles coordinate multivalent ions such as Cu^{2+}, which tainted the functionalized polymers light green and increased the polymer's toxicity in *in vivo* applications. While polymers are often extensively dialyzed against Milli-Q water to remove residual copper, polylactides degrade significantly under the same conditions. As an alternative, we used ion exchange resin beads (Amberlite® IRC-748 ion exchange resin) to remove residual copper

from the polymers. Since exposure to the slightly basic beads in Milli-Q water degraded the polymers, we added the beads directly to DMF polymer solutions after the "click" reaction was complete. When exposed to the beads in DMF for 24 hours the copper concentration was reduced to < 10 ppb (determined by flame atomic absorption) without appreciable degradation (initial polymer: M_n = 56,200, PDI = 1.07; after 24 hour exposure to ion exchange resin in DMF: M_n = 55,900, PDI = 1.12) **(Figure 40)**. Alternatively, polymer-supported Cu(I) catalysts could be used, which do not require additional steps to remove the copper from the final product.[160]

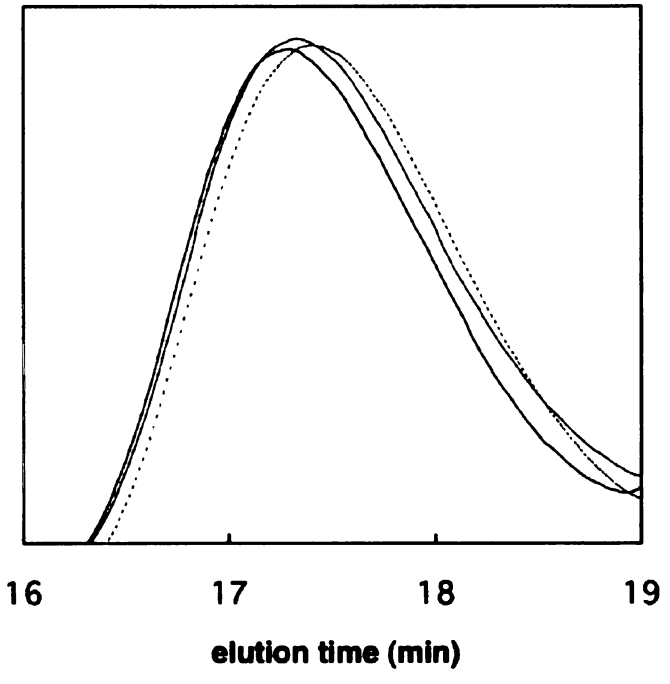

Figure 40. GPC traces of PPGL-*g*-mPEG polymers before and after exposure to ion exchange resin beads. The Cu(II) concentration was reduced to < 10 ppb. Original polymer (M_n = 56,200; PDI = 1.07; solid blue line); dialysis solution without ion exchange resin (M_n = 56,600; PDI = 1.11; dashed green line); polymer after 24 hours exposure to ion exchange resin in DMF (M_n = 55,900; PDI = 1.12; dotted red line).

Formation and Characterization of Unimolecular Micelles

Previous work on PEG-substituted polylactides suggested that grafting PEG chains onto PPGL should provide hydrophilic and perhaps water-soluble polylactides.[161] Using PPGL polymers with molecular weights ranging from 7-60 kD, we covalently linked oligo(ethylene glycol) segments as the hydrophilic branches. PEG is important for *in vivo* applications because it increases blood circulation time and decreases polymer-protein interactions.[162]

There have been many examples of PEG block copolymers that organize into micelles on the order of 20 to 60 nm in aqueous solution.[133,163-167] The micelles are dynamic aggregates above the cmc and single molecules below the cmc. Typically the micelles are formed using an oil-in-water process. We applied this technique to the PPGL-*g*-mPEG polymers. The polymer was dissolved in acetone (< 0.5 mL) and added dropwise to Milli-Q water. The acetone was removed by passing a stream of nitrogen through the solution or *in vacuo*, which caused micellization.

Micelle characterization often includes determination the critical micelle concentration (cmc) by pyrene encapsulation,[168,169] dynamic light scattering (DLS),[170] or surface tension measurements.[168] For example, when pyrene is added to a solution of polymer micelles, the pyrene is preferentially solubilized in the hydrophobic regions due to its low water solubility, and the pyrene 333 nm peak in the pyrene emission spectra shifts to 338.5 nm. The cmc for amphiphilic molecules can be determined by monitoring the pyrene emission spectra over a range of concentrations. Below the cmc the equilibrium shifts from micelles to

individual surfactant molecules and the pyrene emission band is at 333 nm.[171] To determine the cmc of PPGL-*g*-mPEG micelles we prepared polymer concentrations (0.05 – 100 μg/mL) containing 1 x 10^{-6} M pyrene. When excited, all solutions emitted at 338 nm suggesting that pyrene was sequestered within the polymers at all the polymer concentrations.

Dynamic light scattering (DLS) measures the hydrodynamic radius of a particle in solution by monitoring its time-dependent fluctuation in scattering intensity due to Brownian motion. At short time delays, the correlation is high because the particles cannot move very far away; as time increases, the correlation decays to zero. Since larger particles move more slowly than smaller particles, the decay is related to the size of the particles through the Stokes-Einstein equation, equation 17, which calculates the size of a particle based on its velocity due to Brownian motion, where D is the diffusion constant, k_B is the Boltzmann's constant, T is the temperature, η is the viscosity of the solution and r is the radius of a spherical particle.

$$D = \frac{\kappa_B T}{6\pi\eta r} \tag{17}$$

When traditional micelles reach their cmc, there is a dramatic shift in the hydrodynamic radius (R_h), indicating the formation of micelles. We analyzed the PPGL-*g*-mPEG micelles at various polymer concentrations using a Protein Solutions Dyna Pro-MS/X system at 25 °C. Prior to analysis, the polymer was dissolved in Milli-Q water and filtered through 0.2 μm Whatman PTFE

(poly(tetrafluoroethylene)) filter. Notably, the hydrodynamic radius the PPGL-*g*-mPEG polymers was unaffected by polymer concentration, suggesting the formation of unimolecular micelles. The DLS data are compiled in **Table 13** and a representative unimodal particle distribution can be seen in **Figure 41**.

Table 13. Properties and size of PPGL-*g*-mPEG unimolecular micelles.

Polymer	M_n (PPGL)[a]	PDI[a]	M_n (PPGL-*g*-mPEG)[a]	R_h (nm)[b]	H_{ave} (nm)[c]	D_{ave} (nm)[d]
1a	10,000	1.19	31,300	35 ± 2	3.2 ± 0.1	10 ± 1
2a	23,800	1.30	69,000	35 ± 2	3.0 ± 1.0	11 ± 1
3a	31,000	1.28	90,000	37 ± 2	3.0 ± 0.1	14 ± 1

(a) determined by GPC-MALLS using THF as the eluting solvent at 35 °C. (b) determined by DLS at 25 °C. (c) determined by AFM; 0.20 mg/mL solution spin coated in Si wafer. (d) determined by TEM; 0.20 mg/mL solution dropped on Formvar-coated nickel grid; stained with 2 % uranyl acetate solution.

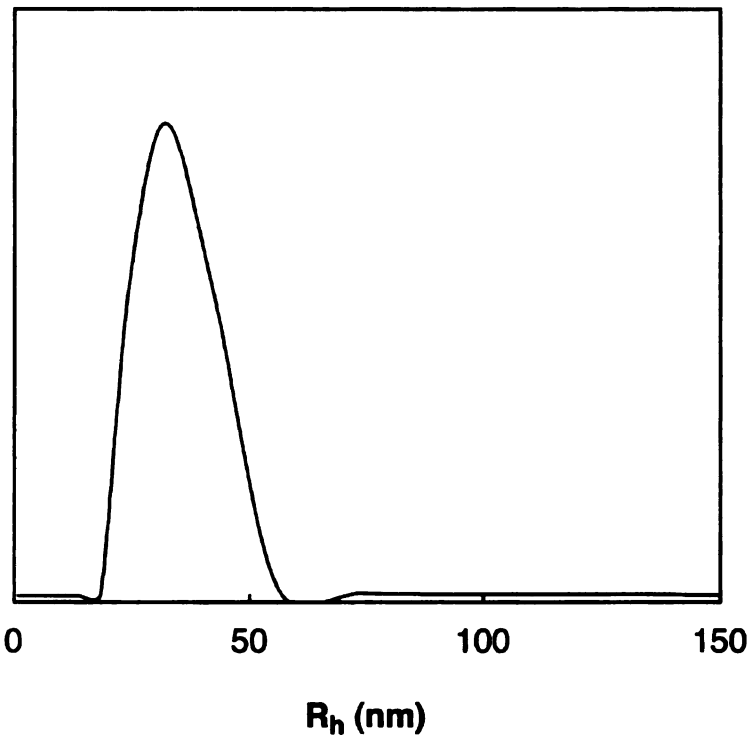

Figure 41. Hydrodynamic radius of PPGL-*g*-mPEG micelles as determined by dynamic light scattering (R_h = 31 nm; 2 mg/mL solution in Milli-Q water).

Analysis of the structural differences between block and comb copolymers sheds light on micelle formation. In dilute aqueous solution, a single diblock amphiphilic copolymer cannot assemble properly to shield the hydrophobic block from water so it aligns itself at the air-water interface. Once the interface becomes saturated with polymer, the addition of more polymer chains causes the spontaneous formation of micelles; the hydrophilic exterior surrounding the hydrophobic domain. In contrast, when short PEG segments were grafted to PPGL, a comb architecture was formed that naturally shields the hydrophobic backbone by the hydrophilic PEG shell (**Figure 42**).

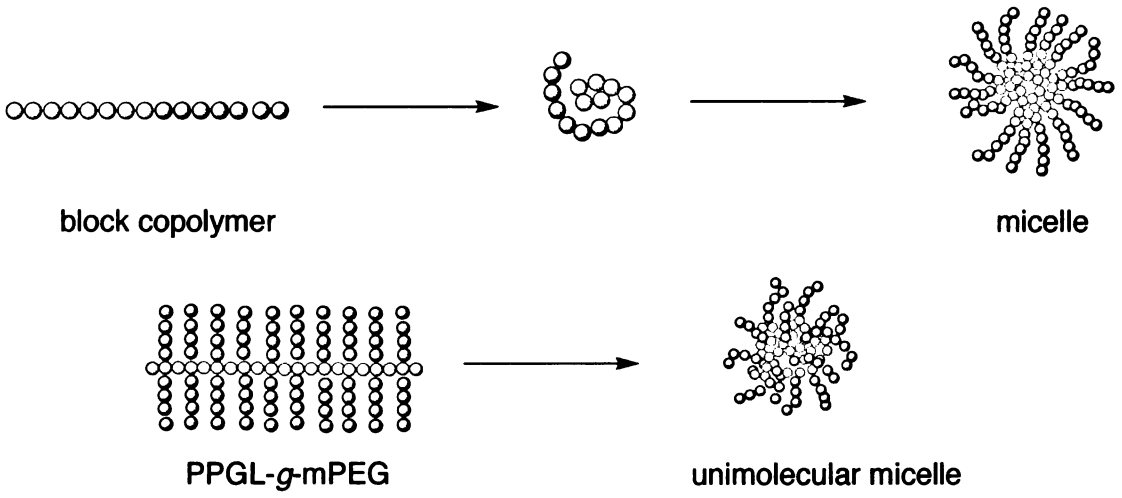

Figure 42. Organization of traditional micelles and unimolecular micelles from block copolymers and PPGL-*g*-mPEG, respectively. The red and blue spheres indicate hydrophobic and hydrophilic polymer segments, respectively.

We further characterized the unimolecular micelles via tapping mode atomic force microscopy (AFM) and transmission electron microscopy (TEM). AFM measures the height of particles mounted on a flat surface via an oscillating probe. AFM samples were prepared by spin coating a 200 μg/mL polymer solution on a freshly cut silicon wafer. **Figure 43** shows a representative AFM height image of PPGL-*g*-mPEG on a silicon surface. The image shows uniformly sized particles and the narrow height distribution provides evidence that only single polymer chains are present without particle agglomeration. AFM heights measurements are reported in **Table 13**. To rule out dust contamination, we analyzed a series of polymer solutions and determined that the number of particles scaled according to the polymer concentration.

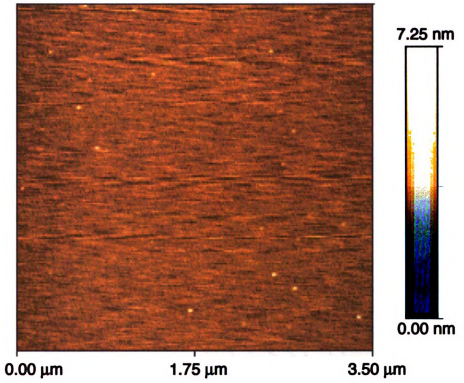

Figure 43. AFM height image of PPGL-*g*-mPEG on a silicon wafer substrate; height = 3.0 ± 0.1 nm.

Finally, we analyzed the particles via transmission electron microscopy. TEM samples are examined by passing a beam of electrons though an ultra thin specimen. The image generated by the transmitted electrons is focused by objective lens and projected onto a fluorescent screen. Staining allows the sample to be seen more clearly because high-Z metals such as osmium, lead, or uranium have high scattering cross-sections. In negative staining, the heavy atoms are deposited around the sample causing the background around the sample to appear dark in the images. Samples were prepared for TEM by dropping an aqueous polymer solution on a Formvar-coated nickel grid. After two minutes, the excess solution was removed and the sample was negatively stained

with a 2 % uranyl acetate solution. As seen in **Figure 44**, the particles are uniformly dispersed and have a uniform size distribution. TEM diameter measurements are reported in **Table 13**.

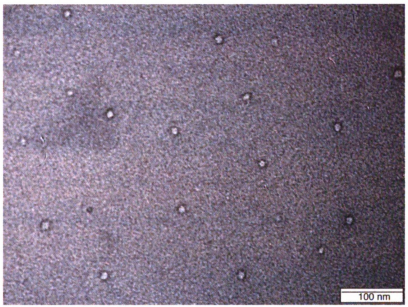

Figure 44. TEM image of PPGL-*g*-mPEG stained with uranyl acetate; diameter = 10 ± 2 nm. Image taken at 200,000x; scale bar represents 100 nm.

Hydrophobic Guest Encapsulation

Self-assembling block copolymer micelles have long been explored as drug carriers, delivering both encapsulated and conjugated drug molecules to appropriate cells. Hydrophobic drugs are sequestered within polymeric carriers using an oil-in-water emulsion approach.[172-174] The encapsulated material is released by permeation through the polymeric carrier or by *in vivo* degradation of a biodegradable polymeric carrier.

Unimolecular micelles from comb polymers seem particularly promising as drug carriers because they can be prepared by controlled polymerization methods,

the functional group density can be very high, and they are not subject to a cmc. We dissolved azobenzene, a UV-active surrogate for hydrophobic drugs, and PPGL-*g*-mPEG polymer (M_n = 116,500 g/mol) in acetone (<1 mL) and dispersed the solution in Milli-Q water. The acetone was removed and the solution was filtered to remove any unencapsulated azobenzene. The homogenous solution appeared yellow, an indication of azobenzene within the polymeric micelles. We confirmed its encapsulation by its characteristic absorbance at 320 nm (**Figure 45**). The UV absorbance in the polymer spectra can be attributed to the polyester backbone (260 nm) and pendant triazoles (< 250 nm).

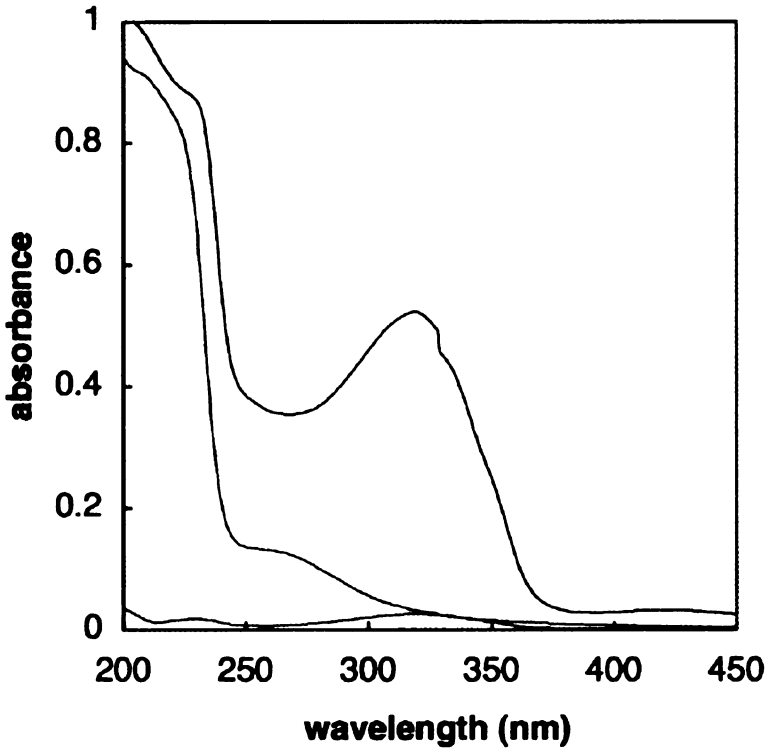

Figure 45. UV-vis spectra of azobenzene loaded polymeric micelles (top, blue), polymeric micelles (middle, green), and azobenzene (bottom, red) in Milli-Q water at room temperature (polymer concentration = 1 mg/mL).

To track the release of azobenzene from the unimolecular micelles, we placed the azobenzene-loaded micelles in dialysis tubing (molecular weight cutoff (MWCO) = 12-14 kD; concentration 1 mg/mL) and dialyzed with Milli-Q water. Removing aliquots of the micelle solution from the dialysis bag and measuring their UV-vis spectrum allowed us to monitor the continual release of azobenzene over 10 hours (**Figure 46**). After analysis, the micelle solution was returned to the dialysis bag and the surrounding Milli-Q water was replaced. The high molecular weight of the polymer and its relatively slow degradation prevented the polymer from escaping the dialysis membrane.

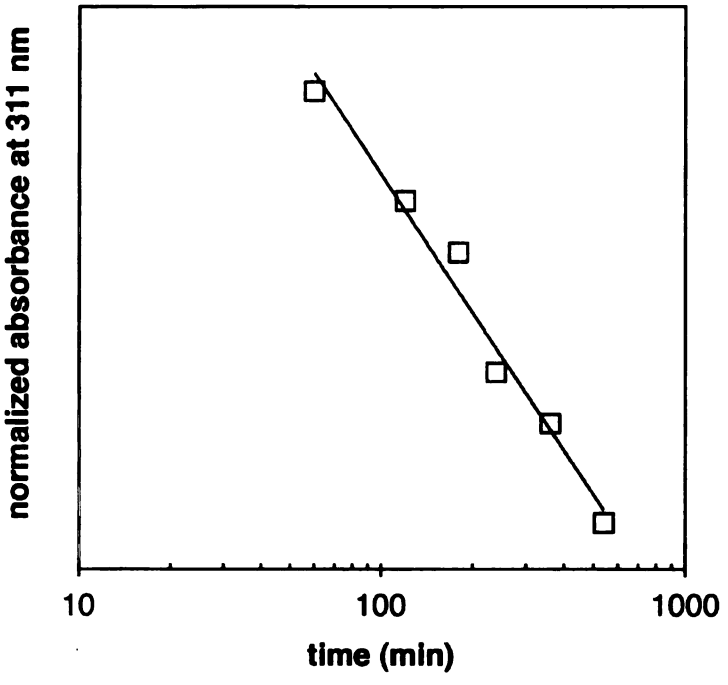

Figure 46. Continual release of azobenzene from loaded polymeric micelles suspended in Milli-Q water at room temperature over 10 hours. At each time point, the azobenzene remaining in the micelles was determined (at 311 nm) by UV-vis spectroscopy.

Although the nanoparticles effectively encapsulated azobenzene, many therapeutic molecules, such as proteins, are much larger. As a proof of principle, for encapsulating large molecules, we encapsulated poly(methyl methacrylate) (PMMA) in micelles. The PMMA was tagged with azobenzene by initiating polymerization of MMA from an azobenzene ATRP initiator as shown in **Scheme 36**. Following the same encapsulation procedure used for azobenzene, we encapsulated azobenzene-initiated PMMA (azobenzene-PMMA) in PPGL-*g*-mPEG micelles. PMMA polymers with molecular weights of up to 10 kD were successfully encapsulated (**Figure 47**). The lower azobenzene UV absorbance and higher ester UV absorbance is consistent with the azobenzene-PMMA structure.

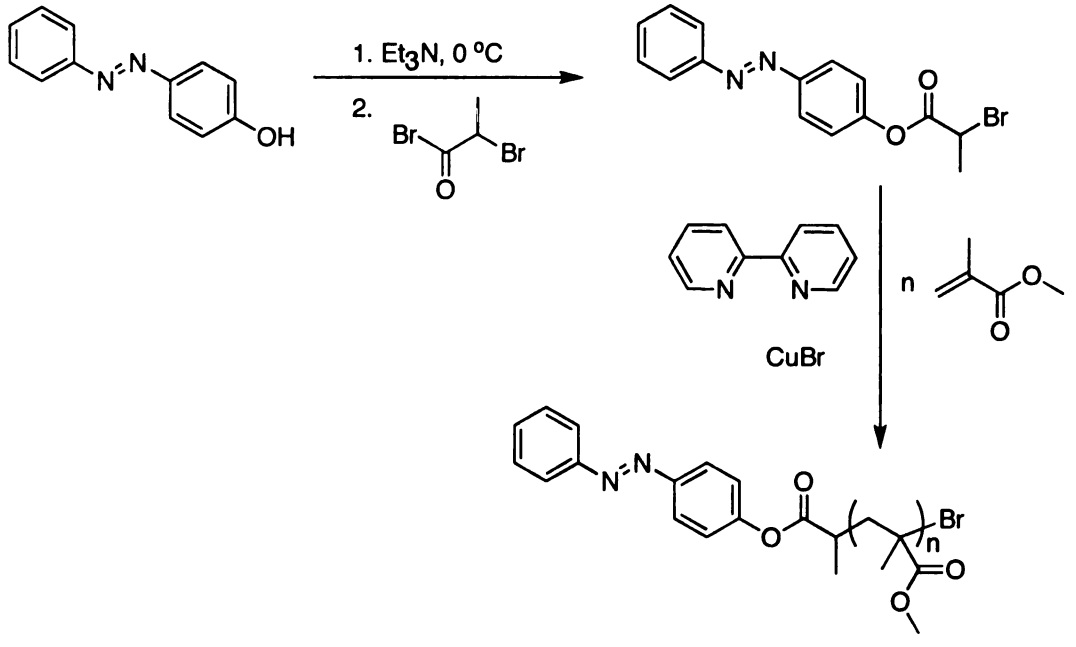

Scheme 36. Synthesis of azobenzene PMMA initiator and ATRP polymerization of poly(methyl methacrylate) using CuBr/2,2'-bipyridine in anisole at room temperature.

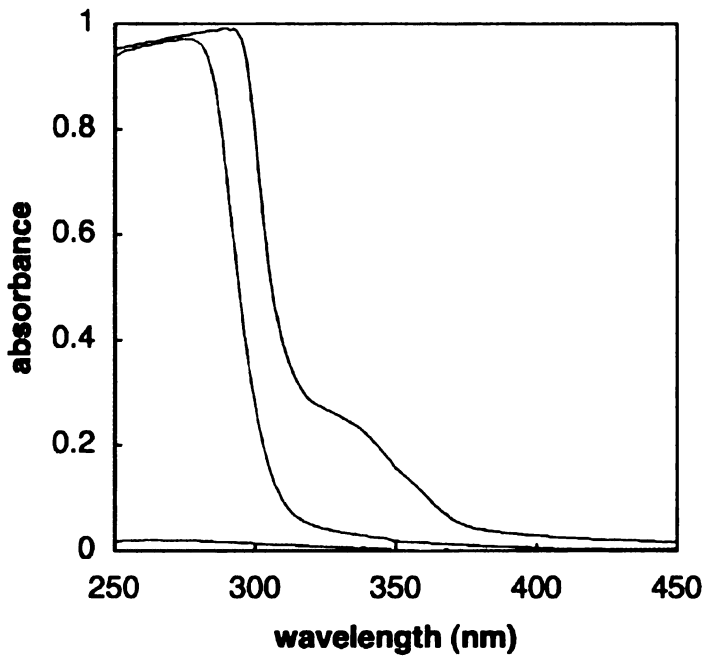

Figure 47. UV-Vis spectra of azobenzene-PMMA (M_n = 10 kD) loaded polymeric micelles (top, blue), polymeric micelles (middle, green), and azobenzene-PMMA (bottom, red) in Milli-Q water at room temperature.

Prodrug Conjugation

Conjugation of biologically relevant molecules is another important aspect of controlled drug delivery. Common water-soluble molecules that cannot be encapsulated are directly conjugated to the polymer or to a prodrug linker. Prodrugs are inactive until released from the polymer, minimizing potential toxic side effects. [126,175-177] Uhrich and co-workers[122,178-182] synthesized polymerizable prodrugs that released the active drug as the polymer degrades. For example, degradation of salicylic acid-derived poly(anhydride esters), released up to 62 wt% of active drug.

Active drugs can also be tethered to polymer through a site that does not compromise drug activity. Emrick and co-workers reported the synthesis of a polyester-*graft*-drug copolymer conjugate that attached camptothecin to a water-soluble polyester. The water solubility of the conjugate and the biodegradability of the polyester backbone allowed the polymer conjugate to be used in polymer therapies.[113]

In collaboration with Christina Chan in the Chemical Engineering Department at Michigan State University, we investigated the delivery and release of *L*-cycloserine (LCS), a small molecule inhibitor in the ceramide synthesis pathway relevant to Alzheimer's disease. Preliminary results suggested that inhibiting *de novo* ceramide synthesis in primary astrocytes with *L*-cycloserine prevented tau hyperphosphorylation and decreased the oxidative-stress effects seen in neurons.[183-186] However, achieving appropriate *in vivo* levels of LCS required impractical injection frequencies. Polymeric carriers that provide sustained controlled release can overcome this limitation.

To explore the possibility of LCS delivery, we appended the LCS to a hydrolysable methyl actetoacetate derived linker.[187] The linker and mPEG was then attached to PPGL via click chemistry (**Scheme 37**). The short oligo(ethylene glycol) segments impart water-solubility and increase *in vivo* circulation time.

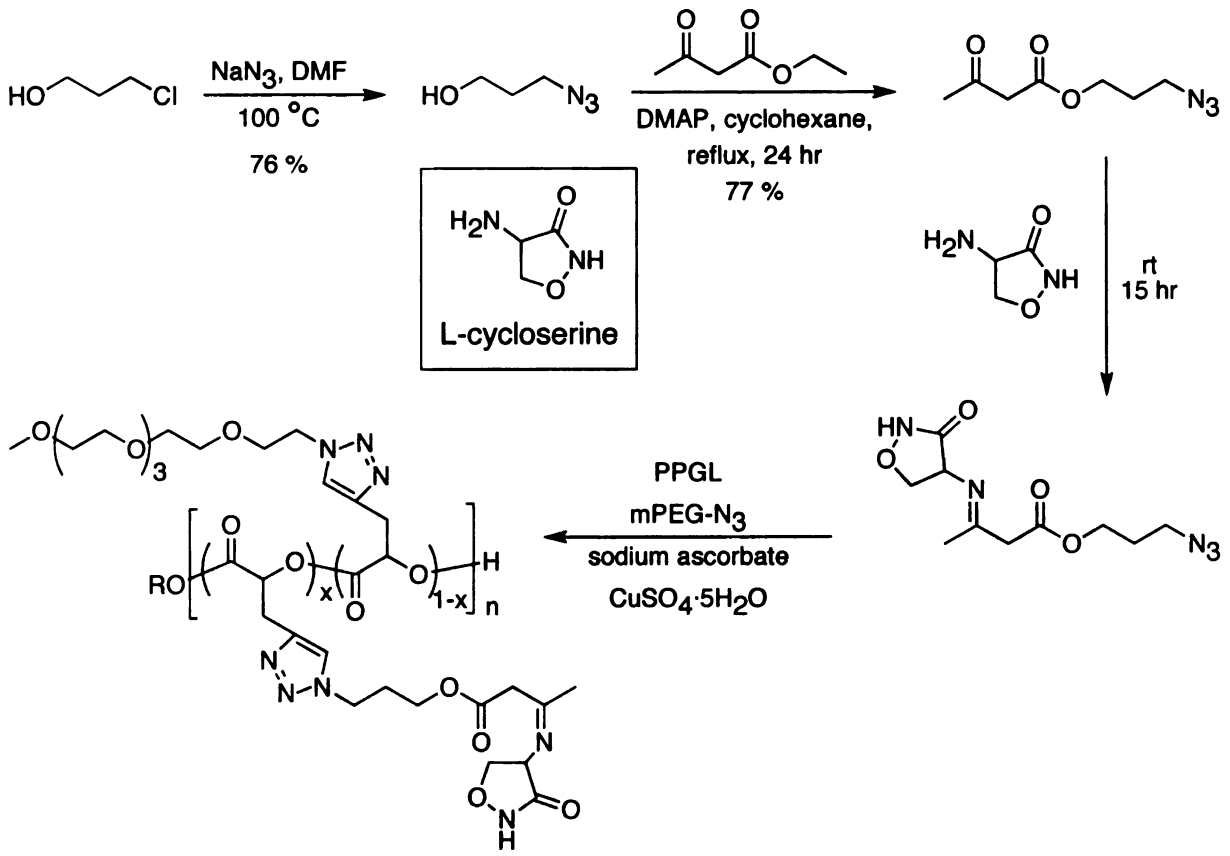

Scheme 37. Synthesis of *L*-cycloserine hydrolyzable linker and conjugation to PPGL-*g*-mPEG.

We monitored the release of LCS from the LCS functionalized polymer at pH 6.0 and pH 7.4. The functionalized polymer was dissolved in water (10 mg/mL), placed in dialysis membrane (MWCO = 1 kD) and dialyzed with Milli-Q water (pH = 6.0) or PBS solution (pH = 7.4). At allotted times, the exterior solution was removed, frozen, and replaced. Thawed samples were analyzed for released LCS using liquid chromatography-mass spectrometry (LC-MS).

Unfortunately, quantification of the LCS released was severely complicated by the dynamic equilibrium of LCS between its monomeric and multiple dimeric forms.[188] To avoid this problem, we synthesized *L*-homoserine lactone

hydrobromide (LHS), a structural mimic of LCS, in 97 % yield from *L*-methionine for kinetic studies. Its synthesis and conjugation to PPGL is shown in **Scheme 38.**[189]

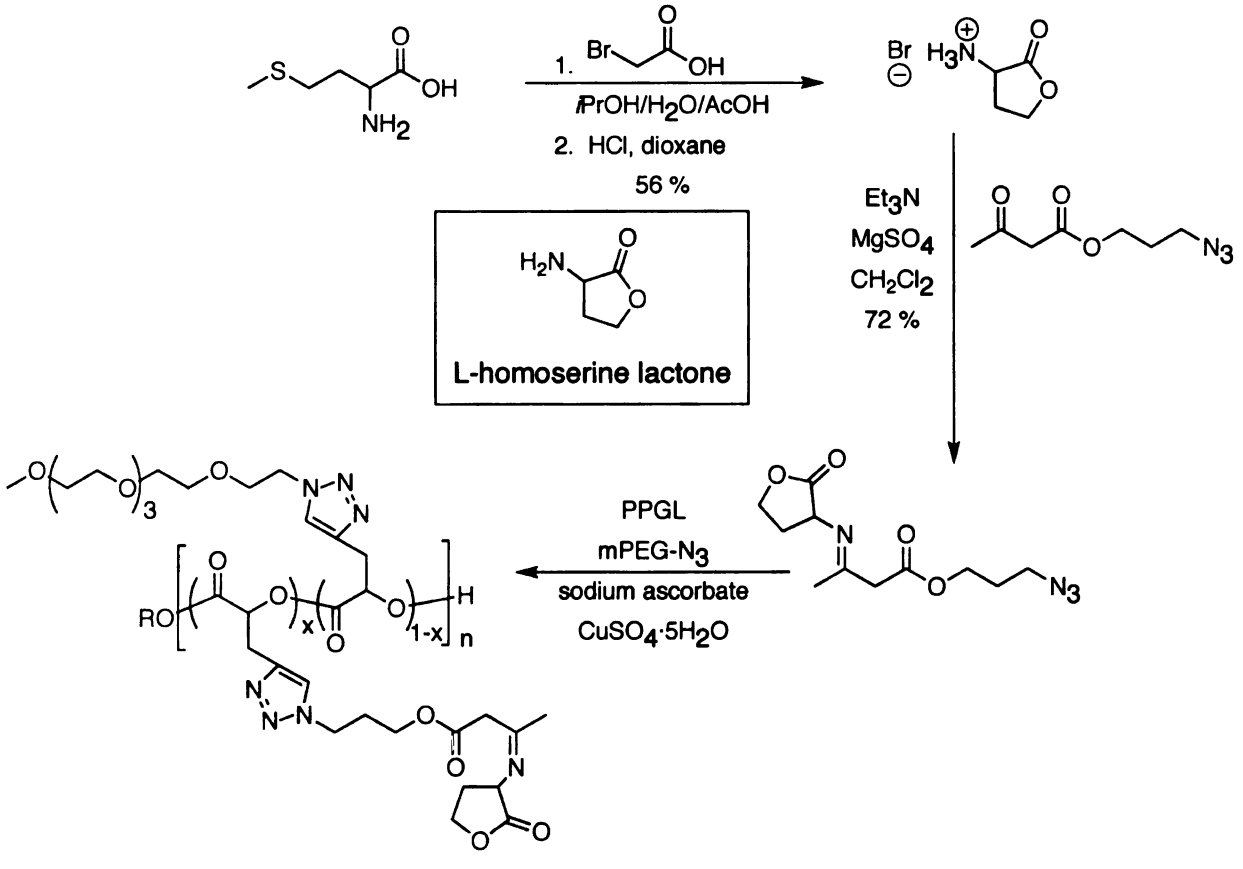

Scheme 38. Synthesis of *L*-homoserine lactone hydrobromide and conjugation to PPGL-*g*-mPEG.

We repeated the previous experiment using *L*-homoserine lactone at pH 6.0 (Milli-Q water) and 7.4 (PBS solution), quantifying the release of LHS using LC-MS based on external LHS standards. During the initial 11 hours of the experiment, we observed rapid LHS release at both pH conditions, most likely from the release of unbound, encapsulated LHS. However, analyses over two weeks showed controlled release of LHS as a function of pH (**Figure 48**).

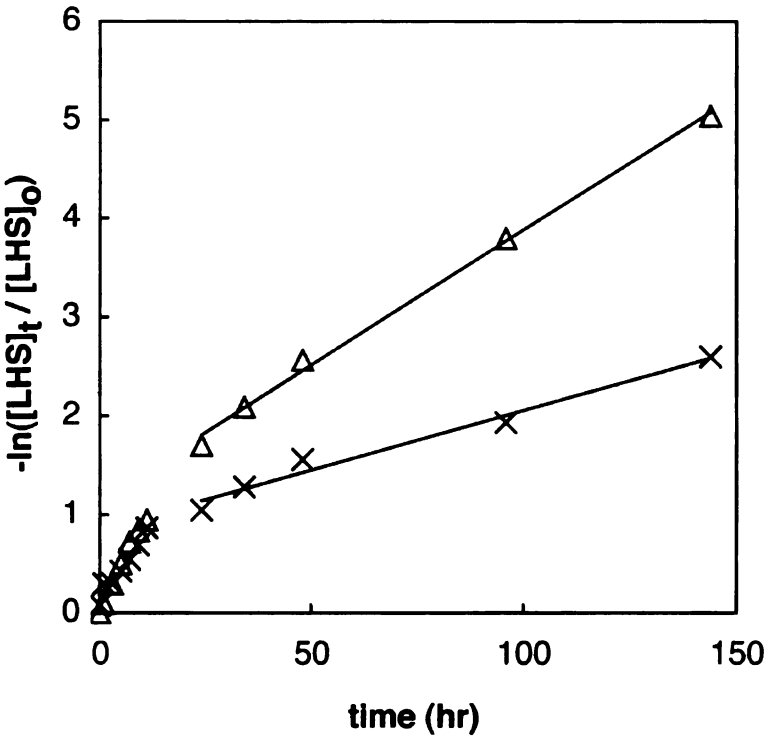

Figure 48. Release of *L*-homoserine lactone from PPGL-*g*-mPEG polymer in Milli-Q water (pH = 6.0; △) and PBS solution (pH = 7.4; ×).

Lower Critical Solution Temperature Materials

One of the most interesting applications for functionalized biopolymers is as a "smart" material that responds to various environmental stimuli such as pH or temperature. For example, poly(N-isopropyl acrylamide) (pNIPAAm) and poly(acrylic acid) (pAAc) respond to the cell's acidic endosome by releasing their cargo upon entry into the cell.[190-192] Thermoresponsive behavior has also been well documented.[193-195] For example, NIPAAm and PMMAs exhibit sharp transitions when the polymer is heated through its lower critical solution temperature. At the LCST, polymers undergo a solution-gel transition that corresponds to the entropically driven expulsion of solvating water molecules from the polymer. Such materials have a variety of interesting and potentially useful applications. For

example, a thermally responsive bioadhesive surface becomes resistant to protein adsorption below its LCST, enabling facile growth and harvesting of biomaterials from surfaces.[196-198]

Recently there has been increasing emphasis on responsive LCST materials that contain PEG segments[28-32,199-202] and current research is focusing on how chemical composition and structure influences the LCST. Recently, Lutz and co-workers synthesized a family of PEG-grafted methacrylate polymers that exhibit LCST behavior over a wide temperature range. Varying the hydrophilic/hydrophobic ratio of the two comonomers, poly(ethylene glycol) methyl ether methacrylate and 2-(2'-methoxyethoxy)ethyl methacrylate (less hydrophilic) provided accurate control over the LCST from 27 °C to 90 °C.[30,200] While Lutz's work is an excellent example of control over LCST behavior, the methacrylate system has limitations; each polymer must be individually synthesized and characterized, and the polymers are not biodegradable, limiting *in vivo* applications.

Following a similar approach, we synthesized biodegradable thermoresponsive polymers via click chemistry. However, instead of copolymerizing two monomers, we controlled the hydrophilic/hydrophobic ratio by attaching a mixture of diethylene glycol monomethyl ether-azide (mDEG-azide, hydrophilic) and decyl azide (hydrophobic) segments to PPGL (**Scheme 39**). Varying the ratio between the hydrophobic alkyl and hydrophilic PEG segments, we obtained LCST values ranging from 25-65 °C. To monitor the LCST, the

purified polymers were dissolved in Milli-Q water and their cloud point temperatures were determined by measuring the solution turbidity as a function of temperature. Choosing a wavelength where the polymers show ~95 % transmittance below their cloud point, 450 nm, we increased the temperature while monitoring the change in transmittance. At the LCST, the "apparent transmittance" decreased because gel formation caused a dramatic increase in scattering (**Figure 49**). A representative plot in **Figure 50** shows the transition to be relatively sharp, spanning a temperature range of ~ 3 °C.

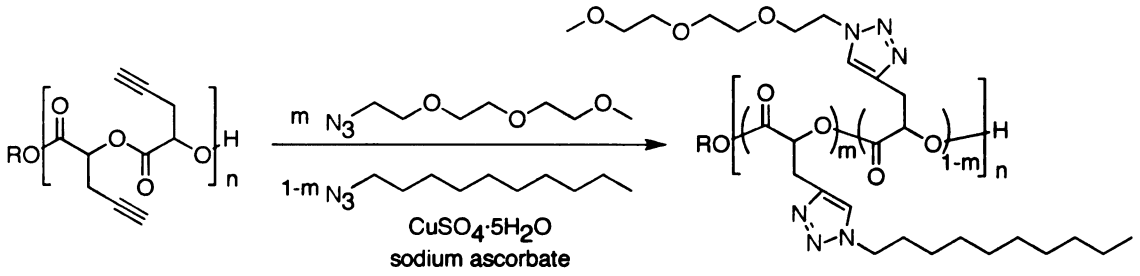

Scheme 39. Synthesis of thermoresponsive polyglycolides.

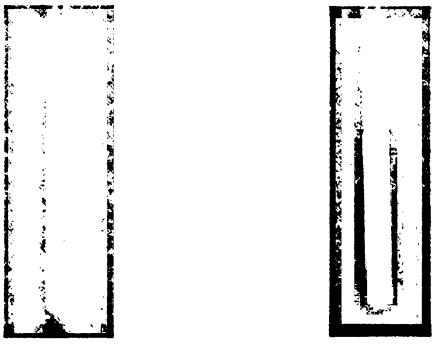

below LCST

above LCST

Figure 49. Visualization of thermoresponsive poly(glycolide) (59 % mDEG; 41 % decyl) below (left) and above (right) its LCST (26 °C).

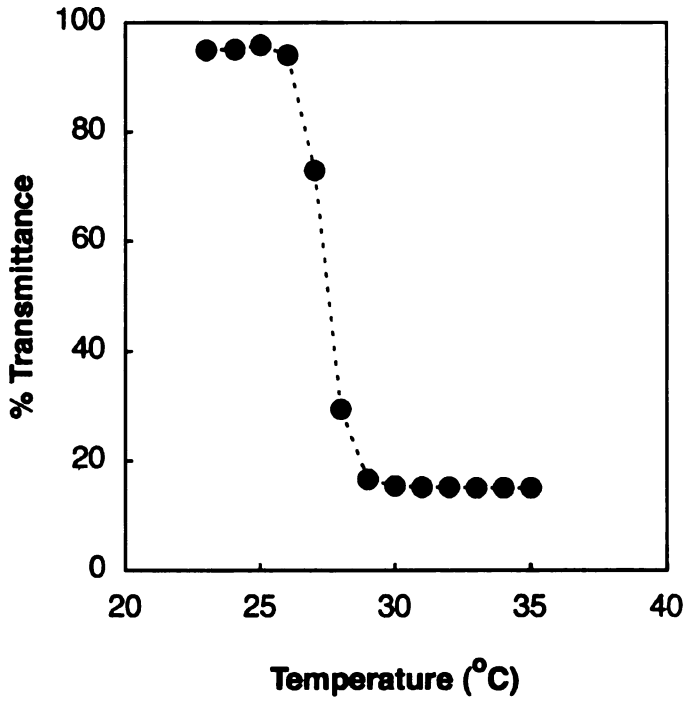

Figure 50. Cloud point determination at 450 nm for PPGL "clicked" with a mixture of hydrophobic alkyl and hydrophilic PEG chains. The composition of the "clicked" polymer, (59 % mDEG chains, 41 % decyl chains) was determined by ^{1}H NMR.

Significantly, the relationship between the cloud point temperature and the mole fraction of mPEG chains in the polymer is linear, as shown in **Figure 51**.

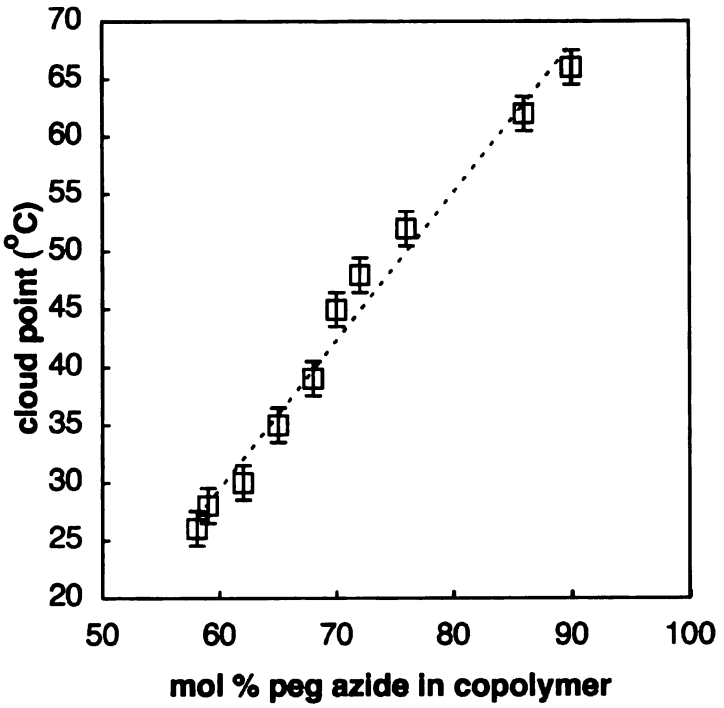

Figure 51. Relationship between the cloud point observed at 450 nm and the mole percentage of PEG chains "clicked" onto the PPGL homopolymer. The broken line is a least squares fit to the data.

We also observed polymer aggregation above the LCST via TEM (**Figure 52**). Two TEM samples were prepared by dropping an aqueous polymer solution onto Formvar-coated nickel grids below the LCST of the polymer. Before removing the excess water, we heated one sample above the LCST using a hot plate and kept the other sample at room temperature (below its LCST). After two minutes the excess water was removed and the samples were stained with a 2 % uranyl acetate solution. Images of the two samples were taken at 270,000x. Clearly the sample heated and dried above the LCST showed polymer agglomeration, confirming the LCST transition.

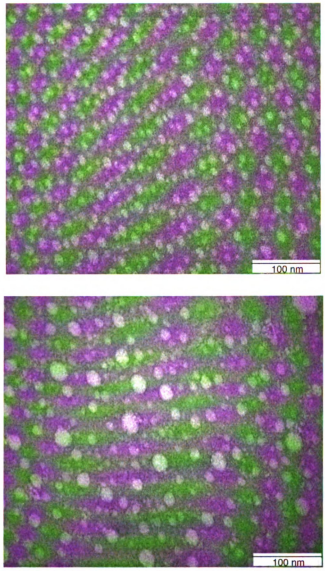

Figure 52. TEM images of thermoresponsive poly(glycolide) (59 % mDEG; 41 % decyl) below (top) and above (bottom) its LCST (26 °C).

Degradation of Poly(propargylglycolide)-*graph*-poly(ethylene glycol)

PLA and related polymers are susceptible to hydrolytic degradation, degrading into natural metabolites. We ran degradation experiments on PPGL-*g*-mPEG polymers at 36 °C in Milli-Q water to assess the polymer degradation rate. Shown in **Figure 53** is the evolution in molecular weight during degradation, where

$M_n(0)$ and $M_n(t)$ are the initial and partially degraded number average molecular weight at time t, respectively. Since the PPGL-*g*-mPEG polymer was completely water soluble, we collected and analyzed both the polymer and its degradation products at each time point.

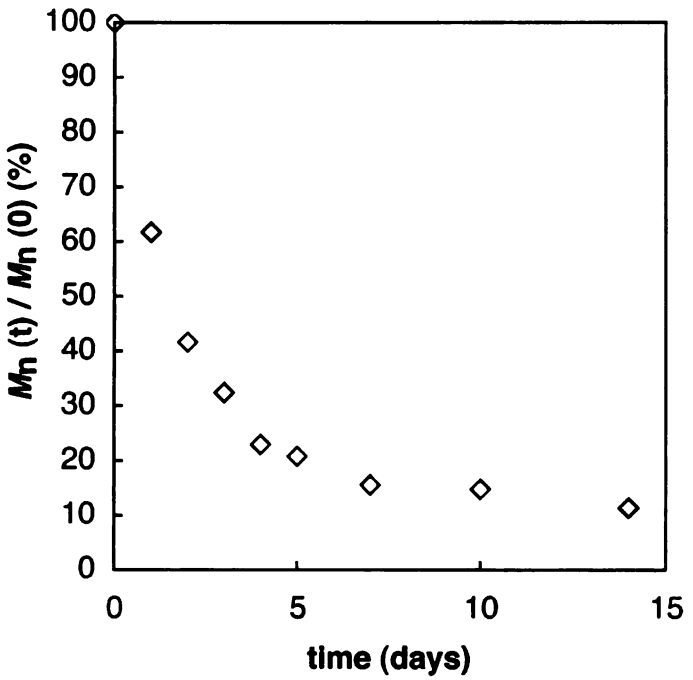

Figure 53. Molecular weight change of PPGL-*g*-mPEG during hydrolytic degradation in Milli-Q water at 36 °C. Each point represents an average of three samples.

To further evaluate the degradation of PPGL-*g*-mPEG, we analyzed the decrease in molecular weight according to the random chain scission model, $(M_n(0)/M_n(t)-1)/P_n(0)$, where $P_n(0)$ is the initial degree of polymerization.[203] Data plotted from polymers that undergo random chain scission are linear and the degradation rates (slopes) can be easily compared to other degradable polymers.

As shown in **Figure 54**, PPGL-*g*-mPEG degrades more rapidly than *rac*-lactide run under accelerated degradation conditions (55 °C), as expected.

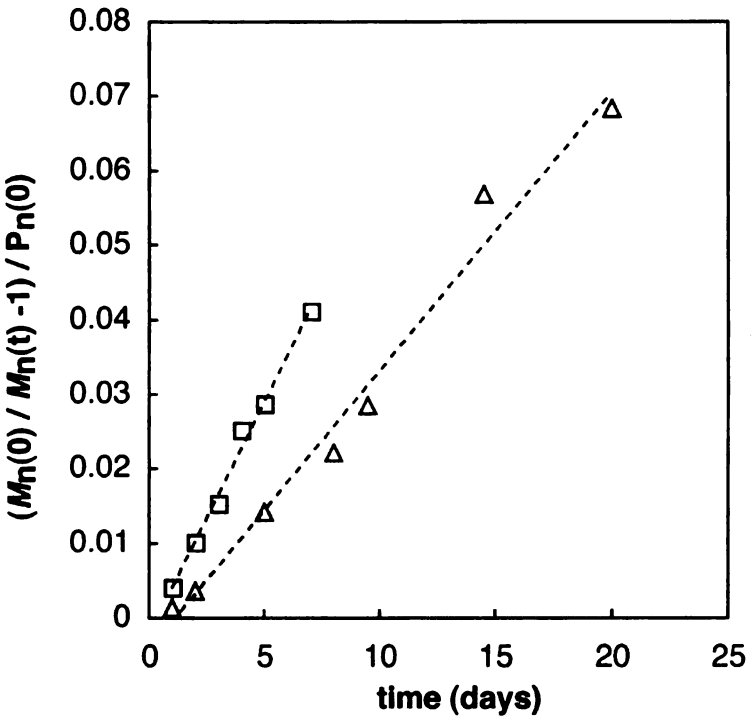

Figure 54. Molecular weight change of PPGL-*g*-mPEG (□) and *rac*-PLA (△) during hydrolytic degradation. Degradation experiments were run at 36 °C for PPGL-*g*-mPEG and 50 °C for *rac*-PLA. The lines are least squares fits to a random chain scission model. The data points represent an average of 3 samples.

Conclusion

Using "click" chemistry we prepared poly(ethylene glycol) grafted polyglycolides. In aqueous solution the polymers self-assembled into unimolecular micelles on the order of a few nanometers as demonstrated by DLS, AFM and TEM. We showed the encapsulation and release of hydrophobic molecules, conjugation and release of water-soluble, biologically active molecules, and the hydrolytic degradation of PPGL-*g*-mPEG polymers. In addition, we prepared

functionalized biodegradable polymeric materials that show lower critical solution temperature behavior over a wide and physiological temperature range.

Experimental Section

General. Unless otherwise specified, ACS reagent grade starting materials and solvents were used as received from commercial suppliers without further purification. Ethyl glyoxalate (Alfa Aesar, 50 wt % in toluene) was distilled prior to use. THF was dried over sodium and benzophenone, methylene chloride was dried over CaH_2, DMF was dried over activated 4Å molecular sieves and methyl methacrylate was purified by passage through activated basic alumina. Zinc (Spectrum, 20 mesh) was pretreated with 2M HCl, and then washed sequentially with distilled water and absolute ethanol and dried under vacuum at 60 °C. Propargyl bromide (Alfa Aesar, 80 wt % in toluene) was used as received. Ion exchange resin beads (Amberlite® IRC-748) were purchased from Aldrich and washed with DMF prior to use. ^{1}H NMR (300 or 500 MHz) and ^{13}C NMR (75 or 125 MHz) spectra were acquired using either a Varian Gemini 300 spectrometer or a Varian UnityPlus 500 spectrometer with the residual proton signal from the $CDCl_3$ solvent used as chemical shift standard. Mass spectral analyses were carried out on a VG Trio-1 Benchtop GC-MS. IR spectra were taken with Mattson Galaxy 3000 FT-IR. Elemental Analyses were determined using a Perkin-Elmer 2400 CHNS/O Analyzer. Melting points were taken on an Electrothermal capillary melting point apparatus and are uncorrected.

Polymer Characterization. Polymer molecular weights were determined by GPC-MALLS 35 °C using two PLgel 10μ mixed-B columns in series (manufacturer-stated linear molecular weight range of 500-10×10^6 g/mol). The eluting solvent was THF at a flow rate of 1 mL/min, and the concentration of polymer solutions used for GPC was 1 mg/mL. A Waters 2410 differential refractometer was used as the detector and an Optilab rEX (Wyatt Technology Co.) and a DAWN EOS 18-angle light scattering detector (Wyatt Technology Co.) with a laser wavelength of 684 nm were used to calculate absolute molecular weights. Flame atomic absorption analyses were carried out on a Hitachi Z-9000 Graphite Furnace Atomic Absorption Spectrophotometer. Liquid chromatography-mass spectrometry analyses were carried out on a Quattro micro API (Waters Corporation, Milford, MA). UV-Vis spectra were recorded with a Cary 300 Bio WinUV, Varian spectrophotometer. Fluorescence was recorded using a Fluorolog-3 (Instruments S.A., Inc.) fluorometer. All samples were diluted to 1×10^{-6} M using Milli-Q water, excited at λ_{ex} = 440 nm, and the fluorescence emission spectra were observed from 450-500 nm. Dynamic light scattering (DLS) data were obtained using a temperature-controlled Protein Solutions Dyna Pro-MS/X system. All samples were filtered through a 0.2 μm Whatman PTFE syringe filter and allowed to equilibrate in the instrument for 15 minutes at 25 °C before measurements were taken. The uniformity of the particle sizes were determined by a monomodal curve fit, which assumes a single particle size with a Gaussian distribution. Surface profile measurements were performed with a Pacific Nanotechnology Nano-R

atomic force microscope in close contact (oscillating) mode to generate height images that were not altered other than a simple leveling procedure. Silicon tips with a spring constant of 36 N/m, tip curvature of 10-20 nm, and a resonance frequency of 286-339 kHz were used for all experiments. The polymeric micelles were dispersed in Milli-Q water and the solutions (typical concentration, 20-300 μg/mL) were spin coated at 5000 rpm for 40 sec on freshly cut silicon substrates. Heights were determined using AFM by taking the average of 20 particle heights. The lateral size could not be determined due to convolution effects created by the tip.[204,205] TEM micrographs were collected at 270,000-370,000 x magnification on a JEOL-100CX transmission electron microscope. TEM samples (typical concentration, 20-300 μg/mL) were dropped onto nickel grids pretreated with Formvar and allowed to settle for 2 min before removing the excess solution. The sample was negatively stained with either a 1 % phosphotungstic acid (PTA) stain or 2 % uranyl acetate (UA) stain prepared with deionized water.

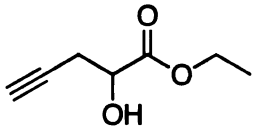

Synthesis of 2-hydroxy-4-pentynoic acid ethyl ester. Propargyl bromide (277 g, 2.35 mol) was added under a blanket of N_2 to a 3 L round bottom flask containing anhydrous THF (350 mL) and activated Zn (230 g, 3.5 mol). The mixture was stirred at room temperature for 30 min and then cooled in an ice bath. A toluene solution of ethyl glyoxalate (51 wt %, determined by NMR, 473 g, 2.36 mol) and a toluene solution of propargyl bromide (80 wt %, 352 g, 2.36 mol) were

combined with a mixture of 500 mL anhydrous THF and 700 mL anhydrous ether and added dropwise to the stirred slurry. After the addition was complete, the mixture was stirred at 0 °C overnight. The reaction mixture was then poured into a 4 L Erlenmeyer flask containing 1 L of ice-cold 3 M HCl. After separation of organic layer, the aqueous layer was extracted with ether (3 x 300 mL) and the combined organic layers were dried over $MgSO_4$. Filtration and removal of the solvents by rotary evaporation gave a dark blue oil, which was washed with EtOAc/hexanes (30/70, 3 x 200 mL) as the eluent. Vacuum distillation (50-55 °C/100 mTorr) gave 170 g of **1** as a colorless oil (1.20 mol, 51 %). ^{1}H NMR (500 MHz) δ 4.25 (m, 3H), 3.11 (d, 1H, J = 6.35 Hz), 2.65 (m, 2H), 2.03 (t, 1H, J = 2.68 Hz), 1.28 (t, 3H, J = 7.20 Hz). ^{13}C NMR (125 MHz) δ 172.99, 78.53, 71.25, 68.64, 62.11, 24.81, 14.13.

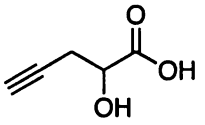

Synthesis of 2-hydroxy-4-pentynoic acid. The ethyl ester (170 g, 1.20 mol) was added to distilled water (800 mL) and heated to reflux for three days. After cooling to room temperature, the solution was acidified by the addition of concentrated HCl (100 mL) and continuously extracted with ether for two days. The ether solution was diluted to 1.5 L with additional ether and dried over $MgSO_4$ for two hours. After filtration, the solution was concentrated by rotary evaporation and dried under vacuum to give a light brown solid, which was purified by recrystallization from CH_2Cl_2 at 0 °C, followed by sublimation at 58 °C and a second recrystallization

from CH_2Cl_2 at 0 °C to give 115 g of 2-hydroxy-4-pentynoic acid as white crystals (1.01 mol, 84 %). ^1H NMR (500 MHz) δ 4.42 (t, 1H, *J*= 5.00 Hz), 2.75 (m, 2H), 2.10 (t, 1H, *J*= 2.56 Hz). ^{13}C NMR (125 MHz) δ 177.28, 77.97, 71.96, 68.51, 24.66. MS (m/z) 115.3 (M+1), mp 61-63 °C.

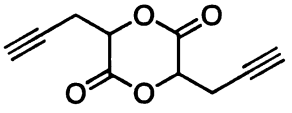

Synthesis of 3,6-di-2-propynyl-1,4-dioxane-2,5-dione. 2-Hydroxy-4-pentynoic acid (18 g, 173 mmol) and *p*-toluenesulfonic acid monohydrate (1.5 g) were added to a 2 L round bottom flask charged with 1.8 L of toluene. The flask was heated to reflux for 3 days, removing water azeotropically using a Dean-Stark trap. After cooling to room temperature, the toluene was removed by rotary evaporation, and the residue was dissolved in 500 mL CH_2Cl_2, washed with saturated aqueous $NaHCO_3$ (3 x 150 mL) and dried over $MgSO_4$. Filtration and removal of the CH_2Cl_2 gave the product as a light brown solid which was washed with diethyl ether (3 x 50 mL), recrystallized from toluene and sublimed at 75 °C to give 6.1 g propargylglycolide as white crystals (31.8 mmol, 34 %). ^1H NMR (300 MHz) δ 5.29 (t, *J* = 4.64 Hz), 5.05 (dd, *J* = 7.08 Hz, *J* = 4.39 Hz), (1H total for the signals at 5.29 and 5.05 ppm), 2.95 (m, 2H), 2.17 (t, *J* = 2.56 Hz), 2.11 (t, *J* = 2.69 Hz), (1H total for the signals at 2.17 and 2.11 ppm). ^{13}C NMR (75 MHz) δ 164.26, 163.44, 76.77, 76.67, 74.82, 74.15, 73.34, 72.02, 23.94, 21.24. Anal. Calcd. for $C_{10}H_8O_4$: C,

62.50; H, 4.17 Found: C, 62.80; H, 4.01. MS (CI, m/z) 193.2 (M+1), mp 103-106 °C.

General procedure for bulk polymerizations. Monomer(s) and a small magnetic stir bar were added to ampoules prepared from 3/8 in. diameter glass tubing. The ampoule was connected via a Cajon® fitting to a T-shaped vacuum adapter fitted with a stopcock and an air-free Teflon valve. The apparatus was attached to a vacuum line and evacuated through the Teflon valve. The ampoule was backfilled with argon, and a syringe was used to add predetermined amounts of the $SnOct_2$ and BBA solutions (both 38.1 mM in toluene) to the ampoule through the stopcock. After removing solvent *in vacuo*, the ampoule was flame-sealed and immersed in an oil bath at 130 °C for the desired polymerization time. The polymerization was quenched in ice and a portion of the polymer was analyzed ^1H NMR to evaluate conversion. The remaining polymer was dissolved in CH_2Cl_2, precipitated into cold methanol, and dried under vacuum (4 mTorr) at 40 °C for 24 h.

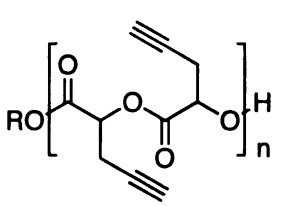

Representative polymerization of propargylglycolide. Propargylglycolide (0.65 g) was polymerized for 45 min of a [M]/[I] = 150. The conversion of monomer to polymer calculated from ^1H NMR was 97 %. Precipitation and drying under vacuum gave 0.64 g poly(propargylglycolide) as a light brown solid (98 %). ^1H NMR (300

MHz) δ 5.31-5.46 (br, 1H), 2.79-3.03 (br m, 2H), 2.01-2.18 (br, 1H). M_n, GPC-MALLS = 31.0 kg/mol, PDI = 1.28.

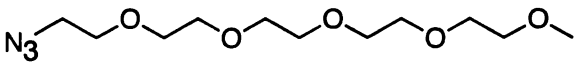

Synthesis of 16-azido-2,5,8,11,14-pentaoxahexadecane (mPEG-azide). Pentaethylene glycol (20.0 g, 80 mmol) in 60 mL THF was added dropwise to a solution of NaOH (10.0 g, 250 mol) in a water/THF mixture (3:2 vol %, 200 mL) at 0 °C. The mixture was stirred for 30 minutes and then *p*-toluenesulfonyl chloride (16 g, 170 mmol) in 100 mL THF was added dropwise. The mixture was stirred at 0 °C for 3 hours and then for 6 hours at room temperature. The mixture was poured into 30 mL ice water and the water layer was extracted with ether (3 x 250 mL). The combined organic layers were washed with a saturated aqueous NaCl solution and dried over $MgSO_4$. The ether was evaporated and the tosylate was used without further purification (29.5 g, 74.9 mmol, 94 %).

The tosyl PEG (29.0 g, 74 mmol) and sodium azide (9.6 g, 148 mmol) were dissolved in 200 mL DMF and the solution was heated at 60 °C for 15 hours. The solution was cooled and added to 100 mL water. The solution was extracted with ether (4 x 100 mL) and the combined organic layers washed with a saturated aqueous NaCl solution (2 x 100 mL) and dried over $MgSO_4$. The ether was evaporated and the residue was purified by vacuum distillation at 130 °C (50 mtorr) to give 16-azido-2,5,8,11,14-pentaoxahexadecane as a colorless liquid (15.4 g, 55.6 mmol, 77 %). ^{1}H NMR (500 MHz) δ 3.68-3.63 (m, 16H), 3.55-3.54 (m, 2H),

3.39-3.37 (m, 5H). ^{13}C NMR (125 MHz) δ 71.88, 70.65, 70.61, 70.58, 70.56, 70.54, 70.52, 70.46, 69.98, 58.96, 50.63.

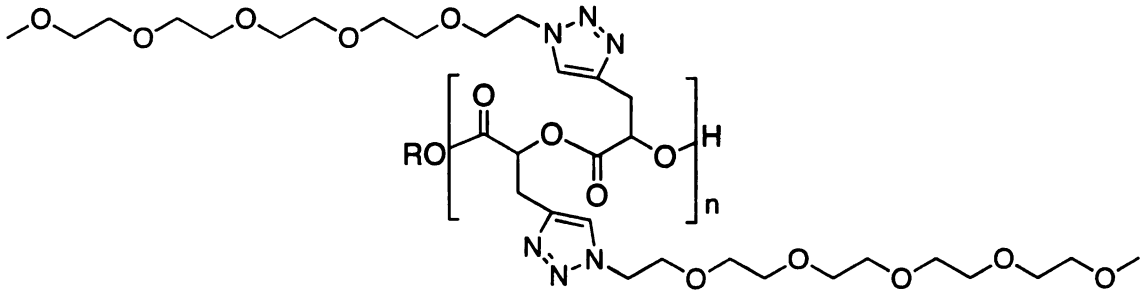

General procedure for "click" functionalization. The desired amount of acetylene functionalized polymer, 100 mol % of PEG-azide, and 12 mol % sodium ascorbate powder (all mole percent values are in reference to the mole percent of alkynyl groups on the polymer) were dissolved in 5 mL DMF in a Schlenk flask. The solution was deoxygenated by three freeze-pump-thaw cycles. After the solution warmed to room temperature a 0.1 M solution of $CuSO_4 \cdot 5H_2O$ in deoxygenated DMF (5 mol %) was added under nitrogen; the reaction mixture was stirred at room temperature for 3-16 hours. At the end of the reaction, the solids in the reaction mixture were removed by filtration and ion exchange resin beads (Amberlite® IRC-748 ion exchange resin) were added to the solution for 6-24 hours to remove residual copper. The beads were removed by filtration and the DMF removed *in vacuo*. The polymer was purified via dialysis (MWCO = 12-14 kD) in acetone/water (1:1) mixture overnight and then dried under vacuum.

PPGL-*g*-mPEG. PPGL (50 mg) (M_n, GPC-MALLS = 31.0 kg/mol, PDI = 1.28) and 140 mg PEG-azide (100 mol %) were dissolved in 5 mL DMF for the click reaction. Copper was removed from the polymer solution via ion exchange resin, the DMF

was evaporated and the polymer was purified via dialysis (MWCO 12-14 kD) (180 mg, 95 %). ^{1}H NMR (500 MHz) δ 7.8-7.4 (b, 1H), 5.6-5.2 (b, 1H), 4.5-4.4 (b, 2H), 3.9-3.7 (b, 2H), 3.6-3.4 (b, 16H), 3.3 (b, 3H), 3.3-3.2 (b, 2H). ^{13}C NMR (125 MHz) δ 167.37, 141.19, 123.87, 71.78, 70.37, 69.21, 58.86, 50.06, 27.31, 21.89.

Formation of unimolecular micelles (1 mg/mL solution). A solution of PPGL-*g*-mPEG (20 mg) in 0.5 mL acetone was slowly added dropwise to stirred ice-cold Milli-Q water (20 mL) in a Schlenk flask. The solution was allowed to stir for 30 minutes before the acetone was removed under a stream of nitrogen or *in vacuo*.

Azobenzene encapsulation and release from unimolecular micelles. Encapsulation: to encapsulate azobenzene or azobenzene-initiated PMMA, the polymer and azobenzene were dissolved in acetone (<1 mL) and the acetone solution was added dropwise to Milli-Q water. The acetone was removed and the solution was filtered to remove any unencapsulated azobenzene. We confirmed its encapsulation by it characteristic absorbance at 320 nm, seen in UV-vis spectroscopy. Release: azobenzene-loaded polymeric micelles were placed in dialysis membrane (MWCO 12-14 kD) and dialyzed with Milli-Q water. At allotted times, aliquots of the polymer solution was removed from the dialysis bag, filtered to remove any insoluble released azobenzene, and the azobenzene remaining was determined using UV-vis.

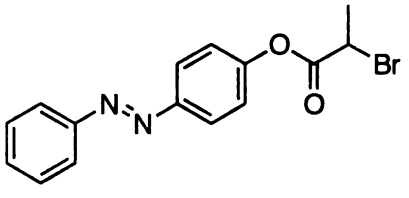

Synthesis of 2-bromopropionic acid-2-(4-phenylazophenyl)ethyl ester.[206] Triethylamine (7.6 mmol, 0.765 g) was added to a solution of 4-hydroxy azobenzene (3.8 mmol, 0.75 g) dissolved in 60 mL anhydrous CH_2Cl_2. The solution was stirred at 0 °C and 2-bromopropionyl bromide (7.6 mmol, 1.65 g) dissolved in 10 mL anhydrous CH_2Cl_2 was added dropwise over 30 min under a nitrogen atmosphere. The mixture was stirred at room temperature overnight, filtered and washed 3x with deionized water. The organic layer was dried over $MgSO_4$, and the methylene chloride evaporated. The crude product was recrystallized from ethanol 2x and dried under vacuum 4 hours to yield an orange solid (0.30 g, 0.95 mmol, 25 % after two recrystallizations). ^{1}H NMR (500 MHz, DMSO-d_6) δ 7.97-7.96 (dd, 2H, J = 6.84 and 2.07), 7.91-7.89 (dd, 2H, J = 6.84 and 1.53), 7.52-7.47 (m, 3H), 7.29-7.27 (dd, 2H, J = 6.84 and 2.20), 4.60 (q, 1H, J = 6.96), 1.97-1.95 (d, 3H, J = 6.84). ^{13}C NMR (125 MHz, DMSO-d_6) δ 201.87, 168.46, 152.31, 131.17, 129.11, 124.13, 122.89, 121.73, 39.45, 21.42.

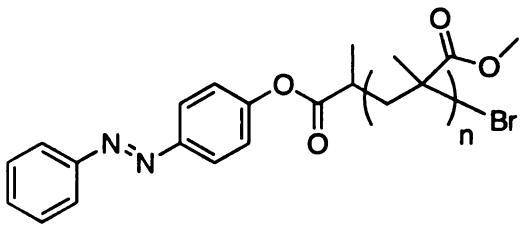

Synthesis of azobenzene-initiated PMMA.[206] A 3.5 M solution of methyl methacrylate (monomer, 106 mmol) in anisole, 2-bromopropionic acid-2-(4-phenylazophenyl)ethyl ester (initiator, 21.2 mmol, 70 mg) and 2,2'-bipyridine

(ligand, 21 mmol, 33.1 mg) (monomer: initiator: catalyst: ligand = 50:1:1:1) were added to a Schlenk flask and deoxygenated by three freeze-pump-cycles. The solution was refrozen and copper(I) bromide (catalyst, 21 mmol, 31 mg) was added under nitrogen. After an additional freeze-pump-thaw cycle, the polymerization was stirred at room temperature for 16 hr and then quenched. The polymer solution was purified by precipitation from cold methanol (yield = 0.124 g, 15 %, M_n, GPC-MALLS = 10.0 kg/mol, PDI = 1.12).

Synthesis of 3-azidopropan-1-ol.[207] 3-chloropropan-1-ol (17.3 g, 183 mmol) and sodium azide (366 mmol, 17.8 g) were dissolved in 200 mL deionized water and stirred at 70 °C overnight. The solution was cooled and extracted with ether (3 x 75 mL). The organic layers dried over $MgSO_4$, filtered and concentrated. The liquid was purified via vacuum distillation (25 °C at 10 mTorr) to give 14.0 g (139 mmol, 76 %) of 3-azidopropan-1-ol as a colorless liquid. ^{1}H NMR (500 MHz) δ 3.72-3.70 (t, 2H, J = 5.98), 3.43-3.40 (t, 2H, J = 6.59), 2.01 (b, 1H, OH), 1.82-1.77 (dt, 2H, J = 5.98 and 5.69). ^{13}C NMR (125 MHz) δ 59.7, 48.4, 31.4.

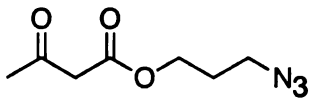

Synthesis of 3-azidopropyl-3-oxobutanoate.[208] A mixture of methyl acetoacetate (26 mmol, 3.0 g), 3-azidopropan-1-ol (28.4 mmol, 2.87 g), and DMAP (0.05 equiv., 1.3 mmol, 0.15 g) were dissolved in cyclohexanol (30 mL, 1 mL/mmol alcohol) and heated to reflux overnight. The water was removed azeotropically via a Dean-

Stark trap. The solution was concentrated, dissolved in ethyl acetate and washed with 1 M HCl (2 x 60 mL). The organic layer was dried over $MgSO_4$, filtered and concentrated. The 3-aziodpropyl-3-oxobutanoate was purified by vacuum distillation at 80 °C (5 mTorr) to give 3.6 g (19.5 mmol, 77 %) as a colorless liquid. ^{1}H NMR (500 MHz) δ 4.22-4.20 (t, 2H, J = 6.16), 3.45 (s, 2H), 3.39-3.37 (t, 2H, J = 6.65), 2.24 (s, 3H), 1.93-1.89 (m, 2H). ^{13}C NMR (125 MHz) δ 200.4, 166.9, 49.9, 48.0, 30.2, 28.0.

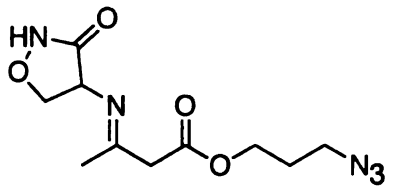

Synthesis of 3-azidopropyl 3-(3-oxoisoxazolidin-4-ylimino)butanoate.[187] *L*-cycloserine (50 mg, 0.49 mmol) and 3-azidopropyl 3-oxobutanoate (45 mg, 0.25 mmol) were placed in a 25 mL round bottom flask and stirred overnight. Methylene chloride (10 mL) was added and the solution filtered to remove any free and insoluble L-cycloserine. The methylene chloride solution was concentrated and dried under vacuum to give 69 mg (100 % recovery of 3-aziodpropyl-3-oxobutanoate, 72 % conversion to imine) of 3-azidopropyl 3-(3-oxoisoxazolidin-4-ylimino)butanoate as a colorless liquid. To determine the percent conversion to the imine, we compared the integration of the methyl protons from the acetoacetate derivative with and without LCS bound. For example, the methyl protons shift from 2.2 ppm (singlet) to 2.0 ppm (singlet) upon LCS attachment (see Appendix 43).

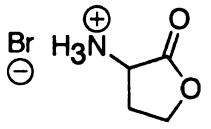

Synthesis of *L*-homoserine lactone hydrobromide.[209] A mixture of bromoacetic acid (1.54 g, 11.0 mmol) and *L*-methionine (1.52 g, 10 mmol) in 14.4 mL of H_2O/2-propanol/AcOH (5:5:2 v/v) was refluxed for 8 hours. The reaction was cooled and the solvents evaporated. The orange solid was dissolved in 6 mL dioxane/HCl (2:1), heated at 50 °C for 10 min and then stirred at room temperature for 5 hours. The mixture was placed on ice 1 hr to evoke precipitation. The colorless solid was isolated by filtration and washed with cold isopropanol to give 1.00 g (5.6 mmol, 56 %). ^{1}H NMR (500 MHz, DMSO-d_6) δ 4.46-4.42 (dt, 1H, J = 8.91 and 1.22), 4.35-4.24 (m, 2H), 2.58-2.52 (m, 1H), 2.34-2.26 (m, 1H). ^{13}C NMR (125 MHz, DMSO-d_6) δ 173.7, 66.6, 48.1, 27.4. mp = 230 °C (lit 233-236 °C)[210]

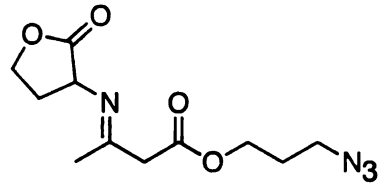

Synthesis of 3-azidopropyl 3-(2-oxo-tetrahydrofuran-3-ylimino)butanoate.[189] Homoserine lactone hydrobromide (0.55 mmol, 100 mg), triethylamine (0.66 mmol, 0.09 mL), and $MgSO_4$ (0.5 g) were stirred in 10 mL anhydrous CH_2Cl_2 at room temperature for 1.5 hours. 3-azidopropyl 3-oxobutanoate (0.86 mmol, 0.17 g) was then added and the heterogeneous mixture stirred overnight. The reaction was filtered to remove the $MgSO_4$ and concentrated. The white solid was triturated in

ether to precipitate the amine salt and filtered. The ether was evaporated giving 105 mg (72 % recovery of 3-azidopropyl-3-oxobutanoate, 100 % conversion to imine) of the imine as a colorless liquid. ^{1}H NMR (500 MHz) δ 4.6 (s, 3H), 4.4-4.3 (m, 1H), 4.3-4.3 (m, 1H), 4.2-4.1 (m, 1H), 4.1 (t, 2H, J = 6.10), 3.7-3.6 (t, 2H, J = 6.75), 2.7-2.6 (m, 1H), 2.4-2.3 (m, 1H), 2.02 (s, 3H), 1.9-1.8 (m, 2H). ^{13}C NMR (125 MHz) δ 175.6, 170.1, 160.6, 85.5, 65.0, 59.5, 51.5, 48.3, 30.7, 28.4, 19.6.

Experimental procedure for continuous release of *L*-cycloserine or *L*-homoserine lactone from PPGL-*g*-mPEG polymers. PPGL-*g*-(mPEG-*co*-LCS) (M_n = 90.0 kg/mol, 120 mg) containing LCS (0.12 mmol) was dissolved in 10 mL Milli-Q water or PBS solution and placed in a dialysis membrane (MWCO = 1,000 Da). The membrane was placed in 100 mL Milli-Q water (pH = 6.0) or 100 mL PBS solution (pH = 7.4) at 37 °C and kept in the dark. At predetermined times, a portion of the solution surrounding the dialysis bag was removed, placed in a 1.5 mL vial, and stored at –20 °C. The remaining solvent was discarded and replaced by fresh Milli-Q water or PBS solution (100mL). The thawed samples were analyzed using LC-MS to determine the concentration of released *L*-cycloserine in solution. The same procedure was used for determining the release kinetics of LHS.

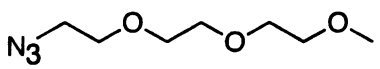

Synthesis of 1-azido-2-(2-(2-methoxyethoxy)ethoxy)ethane (mDEG-azide). Triethylene glycol (20.0 g, 122 mmol) in 60 mL THF was added dropwise to a solution of NaOH (14.6 g, 366 mmol) in a water/THF mixture (6:4 vol %, 200 mL) at

0 °C. The mixture was stirred for 30 minute and then *p*-toluenesulfonic chloride (23 g, 122 mmol) in 100 mL THF was added dropwise. The mixture was stirred at 0 °C for 3 hours and then for 6 hours at room temperature. The mixture was poured into 30 mL ice water and the water layer was extracted with ether (3 x 250 mL). The combined organic layers were washed with a saturated aqueous NaCl solution and dried over $MgSO_4$. The ether was evaporated and the tosylate was used without further purification (35.4 g, 111 mmol, 91 %).

The tosyl PEG (35.4 g, 111 mol) and sodium azide (14.4 g, 222 mmol) were dissolved in 200 mL DMF and the solution was heated at 60 °C for 15 hours. The solution was cooled and added to 100 mL water. The solution was extracted with ether (4 x 100 mL) and the combined organic layers washed with a saturated aqueous NaCl solution (2 x 100 mL) and dried over $MgSO_4$. The ether was evaporated and the product was purified via vacuum distillation at 130 °C (50 mtorr) to provide 16-azido-2,5,8,11,14-pentaoxahexadecane[211] as a colorless liquid (16.7 g, 88.3 mmol, 80 %). ^{1}H NMR (500 MHz) δ 3.65-3.62 (m, 8H), 3.53-3.51 (m, 2H), 3.36-3.34 (m, 5H). ^{13}C NMR (125 MHz) δ 71.88, 70.66, 70.61, 70.57, 69.98, 58.98, 50.63.

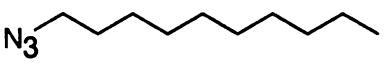

Synthesis of 1-azidodecane.[212] 1-Bromodecane (10.0 g, 45.2 mmol) and sodium azide (5.88 g, 90.4 mmol) were dissolved in 50 mL DMF and stirred at 60 °C for 16 hours and cooled. The mixture was added to 50 mL water and extracted with ether

(4 x 50 mL). The combined organic layers were dried over $MgSO_4$, filtered, and the ether evaporated. 1-Azidodecane was collected as a colorless liquid via bulb-to-bulb distillation (10 mtorr, 35 °C) (7.70 g, 42.1 mmol, 93 %). ^{1}H NMR (500 MHz) δ 3.25-3.22 (t, 2H, J = 6.96), 1.61-1.55 (m, 2H), 1.36-1.25 (m, 14H), 0.88-0.85 (dd, 2H, J = 6.84, 7.08). ^{13}C NMR (125 MHz) δ 51.49, 31.86, 29.49, 29.47, 29.27, 29.14, 28.82, 26.71, 22.66, 14.08.

LCST measurements. The side chain compositions of PPGL-*g*-(*n*-decyl-*co*-mDEG) were determined using ^{1}H NMR comparing the integration of the methylene protons adjacent to the triazole (DEG functionalized = 4.6-4.4 ppm and alkyl functionalized = 4.4-4.2 ppm, see Appendix 52). The polymers isolated and purified by dialysis (MWCO = 14-16 kD; Milli-Q water, 16 hr). LCST behavior was determined by dissolving polymer samples (10 mg/mL) in Milli-Q water and monitoring solution turbidity by measuring transmittance at 450 nm as a function of temperature.

PPGL-*g*-(decyl-*co*-mDEG). PPGL (122 mg, M_n, GPC = 35.5 kg/mol, PDI = 1.44), 1-azido-2-(2-(2-methoxyethoxy)ethoxy)ethane (480 mg, 2.6 mmol), and 1-azidodecane (240 mg, 1.3 mmol) were dissolved in 5 mL of DMF for the "click" reaction. The product was isolated via dialysis (320 mg, 88 %). ^{1}H NMR (500 MHz) (70:30 ratio of mDEG:*n*-decyl) δ 7.8-7.4 (b, 1H), 5.6-5.3 (b, 1H), 4.6-4.4 (b, 1.4H), 4.4-4.2 (b, 0.6H), 3.8 (b, 1.4H), 3.6-3.4 (b, 2.8H), 3.4-3.3 (b, 2.1H), 3.3-3.1 (b, 2H), 1.9-1.8 (b, 0.6H), 1.3-1.2 (b, 4.2H), 0.84-0.82 (b, 0.3H). ^{13}C NMR (125 MHz) δ

167, 141, 123, 122, 71.85, 70.41, 69.30, 59.92, 50.08, 31.84, 30.24, 29.50, 29.44, 29.26, 29.03, 26.51, 22.63, 14.09.

Degradation of PPGL-*g*-mPEG. 10 mg samples of PPGL-*g*-mPEG were placed in 20 mL culture tubes and 10 mL of Milli-Q water was added. The tubes were capped and placed in a degradation chamber at 36 °C. Samples were removed at predetermined times, dried, and the molecular weight was determined by GPC-MALLS. For comparison, the accelerated degradation of *rac*-LA was determined at 50 °C. The results are normalized to account for the degree of polymerization ($P_n(0)$) of each polymer.

Chapter 5 Biodegradable Cross-Linked Nanoparticles

Introduction

Inorganic nanoparticles have a long and rich history, having benefited from favorable physical properties such as mechanical, thermal, and chemical stability. While comparable developments in organic nanoparticles are more recent, the structural diversity of organic materials and their application to complex problems in medicine has made the synthesis and characterization of organic nanoparticles one of the most active topics in polymer science.[213]

Organic nanoparticles are important in many applications, but especially for the encapsulation of small molecules for the delivery of therapeutic agents, personal care products, and colorants.[214] Until recently, nearly all applications were based on nanoparticles prepared by spray drying or an oil-in-water emulsion approach, using homopolymers as the host. The need for "smart" particles in medical applications, to control release rates, target specific sites in the body, and to transport large biomolecules such as small double stranded RNA for gene therapy, instigated interest in more complicated polymer architectures and function.[121,215,216] A variety of architectural motifs were synthesized including many varieties of linear homopolymers and block copolymers, and branched polymers such as stars,[43-45] combs,[217-220] dendrimers, [46-48] and hyper-branched[40-42] structures that provide multiple sites (usually at chain ends) for tethering molecules.

Although many of these polymers assemble into traditional micelles in aqueous solution, their aggregation numbers vary and the critical micelle concentration defines their lower concentration limit. Many applications, however, require stable nanoparticles that maintain their shape and structure under a variety of conditions. Therefore significant progress has been made by cross-linking the core[221,222] or shell[223-229] domains of amphiphilic polymer micelles.

Cross-linking was first introduced in 1979 by Prochaska and Baloch who photochemically irradiated a polybutadiene micellar assembly, cross-linking its core.[230] Following this initial account, many others have utilized cross-linking strategies to stabilize polymeric micelles. For example, Ding and Liu exposed poly(styrene)-*block*-poly(2-cinnamoylethyl methacrylate) (PS-*b*-PCEMA) to UV light inducing the cycloaddition of the cinnamoyl groups.[224,231-236] Hawker[237] and Harth[238] provided a route to well defined nanoparticles by thermal cross-linking of well-defined styrene-vinylbenzocyclobutene copolymers. Using a dilute solution to promote intramolecular cross-linking, the well-dispersed benzocyclobutene units were activated in hot benzyl ether forming cycloaddition cross-links. The robust particles behaved similarly to polystyrene, however their T_g was approximately 20° higher than polystyrene, reflecting the nature of cross-linked materials.

Alternatively, cross-linking can be accomplished through a difunctional cross-linker. Wooley[227,239-241] and others used water-soluble diamines to cross-link the poly(carboxylic acid) shell of poly(styrene)-*block*-poly(acrylic acid) (PS-*b*-PAAc) micelles via DCC coupling. The cross-linked micelles were unaffected by solution

concentration. Armes and co-workers[242] reported the shell cross-linking of thermoresponsive poly[2-(dimethylamino) ethyl methacrylate-*block*-2-(*N*-(morpholino)ethyl methacrylate)] (PDMA-*b*-PMEMA) using 1,2-bis(2-iodoethoxy)-ethane (BIEE) as a cross-linking agent. The difunctional reagent selectively quarternized unreacted tertiary amines on the PDMA blocks, leaving the thermoresponsive PMEMA core unaffected. The cross-linked polymeric micelles showed a lower critical solution temperature of 25 °C. Armes also used divinyl sulfone (DVS) to covalently cross-link poly[ethylene oxide-*block*-glycerol monomethacrylate-*block*-2-(diethylamino) ethyl methacrylate] (PEO-*b*-PGMA-*b*-PDMA) and poly[ethylene oxide-*block*-2-hydroxylethyl methacrylate-*block*-2-(dimethylamino) ethyl methacrylate] (PEO-*b*-PHEMA-*b*-PDMA) pH responsive micelles.[243] Using DVS as the cross-linker provides a convenient method to determine the cross-linking efficiency by sulfur microanalysis.

More recently Wooley and co-workers reported "click cross-linking" within the shell and core of polymeric nanoparticles.[229] Azido-terminated dendrimers were used to cross-link the shell domain of acetylene-functionalized poly(acrylic acid)-*block*-poly(styrene) (PAAc-*b*-PS).[244] The alkyne groups, located at the corona reacted with a G(1.0) – G(3.0) azide-terminated dendrimer cross-linking the shell. Moving the alkynyl groups to the poly(styrene) block allowed core click cross-linked (CCL) nanoparticles to be synthesized.[222] The efficiency of click cross-linking was determined by ^{1}H NMR; upon cross-linking, new triazole proton signals appear at

7.6 ppm. Furthermore, it has been suggested that the triazole chromophore could be monitored by UV spectroscopy.[245]

Unfortunately many cross-linking reaction require high dilution to promote intramolecular cross-linking and avoid inter-micelle cross-linking, which leads to micelle agglomeration. Many shell cross-linking reactions are run below 0.5 % solids, presenting problems for scale-up and industrial use of these materials. To circumvent this problem, Armes and co-workers synthesized a triblock copolymer that could be cross-linked under higher polymer concentration.[246] Steric stabilization by the PEO cornea, allowed poly[ethylene oxide-*block*-2-(dimethylamino) ethyl methacrylate-*block*-2-(N-morpholino) ethyl methacrylate] (PEO-*b*-PDMA-*b*-PMEMA) to be cross-linked using BIEE, at 10 % solids.[247]

Cross-linked nanoparticles have many applications, one being the conjugation of biologically important molecules. For example, Wooley and co-workers conjugated fluorescently labeled shell cross-linked micelles with the protein transduction domain (PTD) peptide sequence derived from HIV.[241] The biologically active nanoparticle easily penetrated cell membranes. In addition, cancer cells have also been targeted by cross-linked nanoparticles bearing folate receptor ligands.[248] PAAc-*b*-PS cross-linked nanoparticles were also functionalized with tritrpticin, an antimicrobial agent.[249,250]

This chapter describes degradable comb polymers that individually self-assemble in aqueous solution and can be chemically cross-linked to from organic nanoparticles that retain their chemical functionality. Forming unimolecular

micelles from a single polymer chain is key to the formation of these nanoparticles. Analysis of these new materials revealed robust spherical nanoparticles with diameters ranging from 4-8 nm. The nanoparticles showed superior dimensional stability and were used for controlled release.

Results and Discussion

Synthesis of Cross-Linked Nanoparticles

The synthesis, characterization, and applications of the unimolecular micelles based on functionalized poly(propargylglycolide) were presented in chapter 4. To move from the amphiphilic comb polymers to cross-linked nanoparticles, we first appended short oligo(ethylene glycol) segments to ~75 % of available alkynes on the PPGL backbone (for example, poly(PGL[$EG_{75}X_{25}$] describes a poly(propargylglycolide) polymer functionalized such that 75 % of the pendent alkynes were reacted with the short oligo(ethylene glycol) segments and the other 25 % of alkynes are unreacted). The partially functionalized polymer was dissolved in a minimal amount of acetone followed by dropwise addition of the solution to stirred Milli-Q water (1 % solids) containing sodium ascorbate (1 equivalent with respect to the alkyne groups) and copper(II) sulfate (0.25 equivalents with respect to the alkyne groups). The acetone was removed by passing a stream of nitrogen through the solution and then 1,5-diazidopentane (1 mg/mL in acetone) was added dropwise. The reaction was stirred 2-3 days at room temperature, cross-linking the residual alkyne groups on the PPGL base polymer (poly(PGL[$EG_{75}CL_{25}$]) where CL_{25} denotes that the remaining 25 % of

the pendent alkynes were cross-linked) (**Scheme 40**). Initially we carried out the cross-linking reactions in dilute solution to prevent any intermolecular cross-linking reaction resulting in insoluble polymeric material; however, we determined that we could run the reaction at much higher polymer concentration (10 % solids) because of the steric stabilization of the PEG corona. We cross-linked 10-100 % of available alkynes within the preformed unimolecular micelles. The cross-linked nanoparticles were purified by dialysis to remove unreacted cross-linker and by Amberlite® beads to remove the residual copper. The progress of the cross-linking reaction was monitored by following the disappearance of the alkyne-stretching band in the IR spectrum (**Figure 55**).

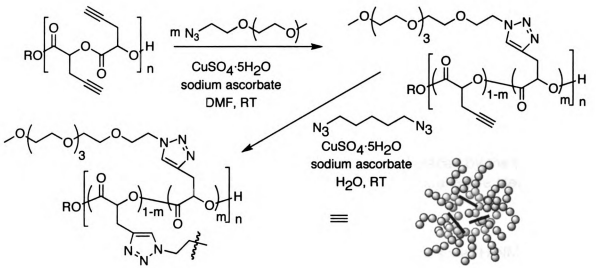

Scheme 40. Cross-linking of poly(PGL[$EG_{75}X_{25}$]) unimolecular micelles by 1,5-diazidopentane.

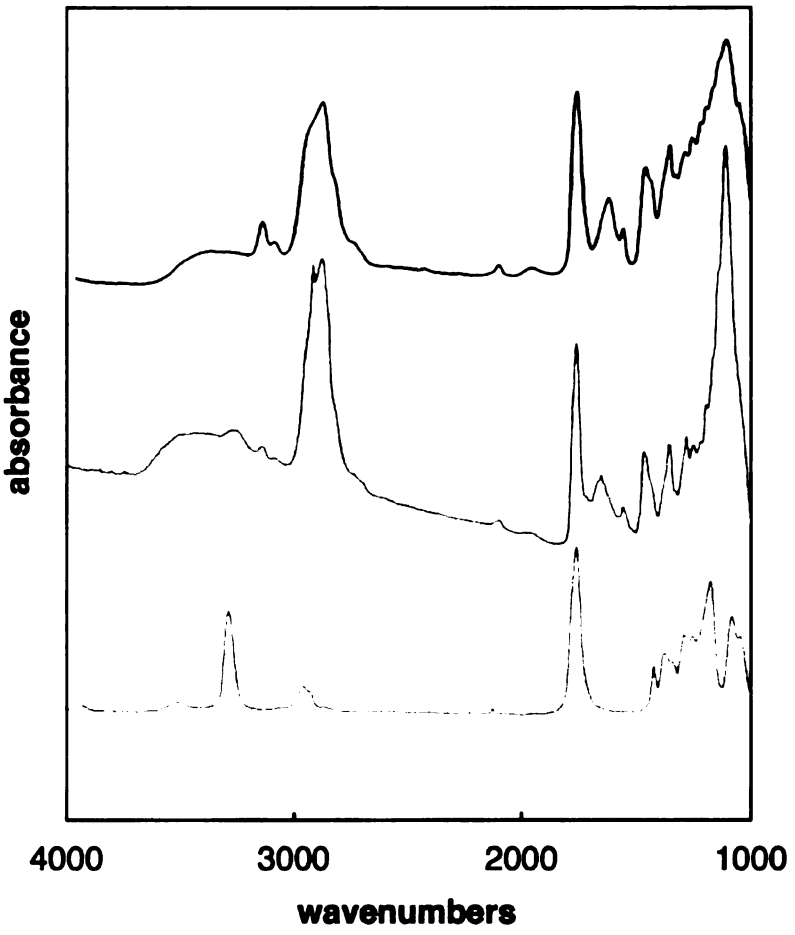

Figure 55. IR spectra of poly(PGL (bottom), poly(PGL[$EG_{75}X_{25}$] (middle), and cross-linked poly(PGL[$EG_{75}CL_{25}$] (top). Upon PEG functionalization and cross-linking, the alkyne stretching band (3340-3270 nm) was replaced by the triazole stretching band (N-H) (3300-2500 nm). In addition, no residual azide stetching bands were observed at 2100 nm.

We determined the number of remaining alkynyl groups via ^1H NMR comparing the integration of the methine protons on the polymer backbone (5.4 ppm) to the integration of the triazole protons (7.6 ppm) and the integration of the methylene protons adjacent to the triazole (4.5 ppm) provides the degree of click functionalization (**Figure 56**).

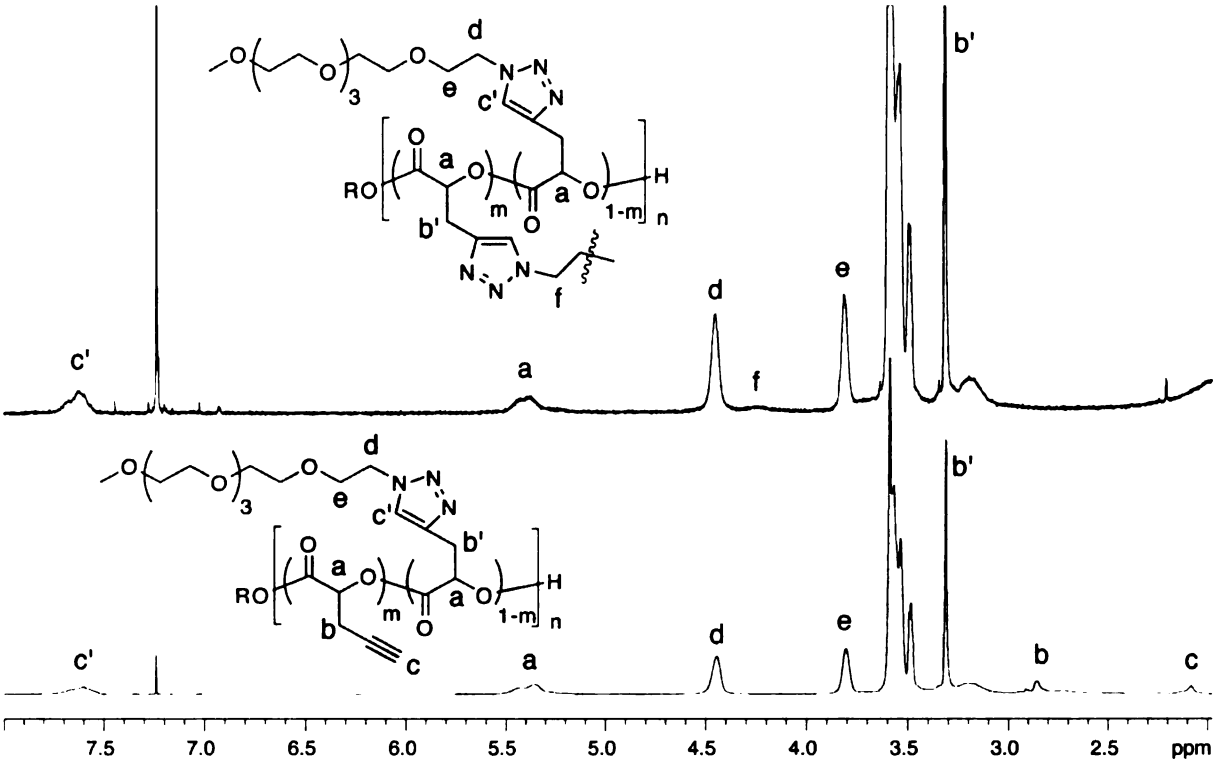

Figure 56. 500 MHz ^{1}H NMR of poly(PGL[$EG_{75}X_{25}$]) before (bottom) and after (top) cross-linking with 1,5-diazidopentane (integration of signal c:c' = 1:0.75 (bottom) and 1:1 (top).

Characterization of Cross-Linked Nanoparticles

Representative examples of unimolecular micelle solutions cross-linked at 10, 50, and 100 percent of available cross-linking sites are shown in **Table 14**. The percent cross-linking was determined using ^{1}H NMR because the number of triazole protons increases upon cross-linking. We also confirmed cross-linking within the nanoparticle cores using DLS, AFM, and TEM. Compared with noncross-linked material, cross-linked nanoparticles are more robust and dense as evidenced by their smaller hydrodynamic radius, measured by DLS, and increased height profile, measured by AFM, and smaller diameter, measured by TEM (**Table**

14). An example of the 50 % cross-linked nanoparticles as analyzed by AFM is shown in **Figure 57**.

Table 14. Characterization of cross-linked nanoparticles by DLS and AFM.

Polymer	M_n (poly(PGL$_a$[EG$_{75}$X$_{25}$]))	% cross-linked[b]	R_h (nm)[c]	H_{ave} (nm)[d]	D_{ave} (nm)[e]
1a	90,000	10	29 ±2	3.5 ± 0.8	7 ± 2
2a	69,000	50	18 ± 2	4.5 ± 0.3	6 ± 2
2b	69,000	100	12 ± 2	6.0 ± 1	4 ± 1

(a) determined by GPC-MALLS using THF as the eluting solvent at 35 °C. (b) percent cross-linking of available cross-linking sites; determined by ^{1}H NMR. (c) determined by dynamic light scattering at 25 °C. (d) determined by AFM; 200 μg/mL solution spin coated in Si wafer.

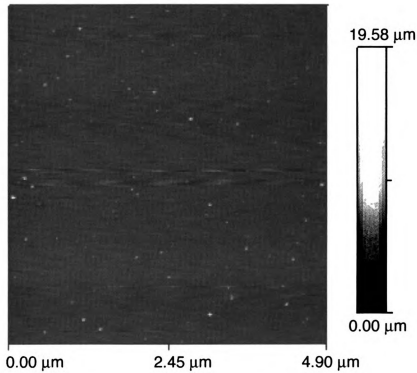

Figure 57. Representative AFM image of cross-linked nanoparticles (polymer 2a, Table 14, 200 μg/mL solution spin-coated on a Si wafer substrate).

TEM further confirmed cross-linking within the nanoparticle cores. A representative TEM image of 50 % cross-linked nanoparticles shows uniform spheres of 6 ± 1 nm (**Figure 58**). Depending on the cross-linking density, the nanoparticles had diameters of 4-8 nm. Samples were prepared for TEM by dropping an aqueous solution of the cross-linked nanoparticles on a Formvar-coated nickel grid. After two minutes, the excess water was removed and the sample was negatively stained with a 1 % phosphotungstic acid solution or 2 % uranyl acetate solution in deionized water.

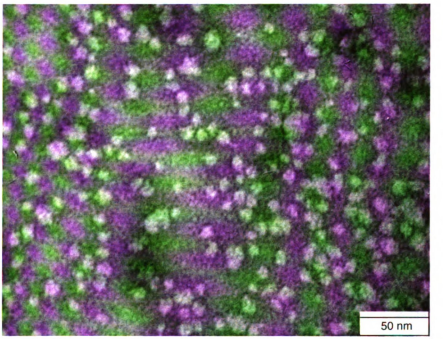

Figure 58. Representative TEM image of cross-linked nanoparticles (polymer 2a, Table 14, 100 μg/mL solution; 370,000x magnification; scale bar = 50 nm).

Estimation of Cross-linked Nanoparticle Size

We estimated the number of polymer chains in the cross-linked nanoparticles using basic algebra. For example, one polymer chain with M_n =

72,000 g/mol (from GPC) weighs approximately 1.19×10^{-19} g ($M_n \times 1$ mol/ 6.02 x 10^{23} chains). If we assume the polymer has a 3 nm radius (6 nm diameter measured by TEM) and that it can be approximated as a sphere of density (ρ) = 1 g/cm^3 then the mass of a dense particle would be 1.13×10^{-19} g ($m = V \times \rho = (4/3)\pi r^3 \times 1$ g/cm^3). Thus the mass of a 6 nm sphere (1.13×10^{-19} g) ≈ the mass of a single polymer chain (1.19×10^{-19} g).

Conjugation to Cross-linked Nanoparticles

To explore the possibility of loading cross-linked unimolecular micelles with covalently attached biologically relevant drugs and to confirm the core cross-linking, we used 3-azido-7-hydroxycoumarin (**Scheme 41**), which transforms into a fluorescent dye after undergoing a 1,3-dipolar cycloaddition reaction.[251]

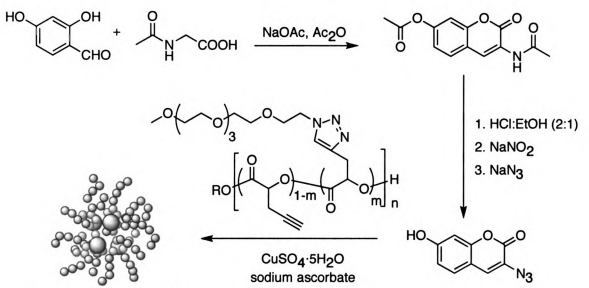

Scheme 41. Synthesis of 3-azido7-hydroxycoumarin and click attachment to poly(PGL[EG$_{75}$X$_{25}$).

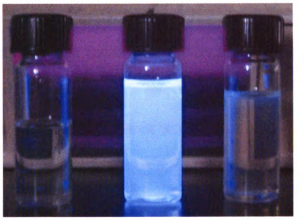

Figure 59. Reaction of 3-azido-7-hydroxycoumarin with polymer micelles. Vial 1: polymeric micelles and dye in the absence of "click" catalyst; Vial 2: polymer micelles and dye after the "click" reaction; Vial 3: dye and components for "click" reaction without polymer micelles.

Using poly(PGL[$EG_{75}X_{25}$]) as the substrate we carried out the click reaction with an equimolar mixture of the dye precursor and 1,5-diazidopentane. The resulting particles fluoresced brightly indicating successful reaction of the dye precursor. We monitored the reaction of nonfluorescent 3-azido-7-hydroxycoumarin with polymer micelles using a hand held UV lamp (**Figure 59**).

The ability to load previously characterized cross-linked particles may be advantageous, especially in standardizing drug delivery. Therefore, we investigated a 2-step process where we initially cross-linked 5, 10, or 100 % of the available alkynes on poly(PGL[$EG_{75}X_{25}$]) with 1,5-diazidopentane, and then carried out a second click reaction using an excess of the dye precursor. Reaction of the dye precursor with residual alkynes was evident from the luminescence of nanoparticles (**Figure 60**), providing proof of principle for loading cross-linked particles. We measured the fluorescence intensities of 1×10^{-6} M nanoparticle

solutions to assess the relative dye loadings, and as expected, particles prepared by the 2-step process had lower loadings. The dye precursor could also provide a method to count the number of available alkyne groups, which is important for drug delivery because each represents a site of drug attachment.

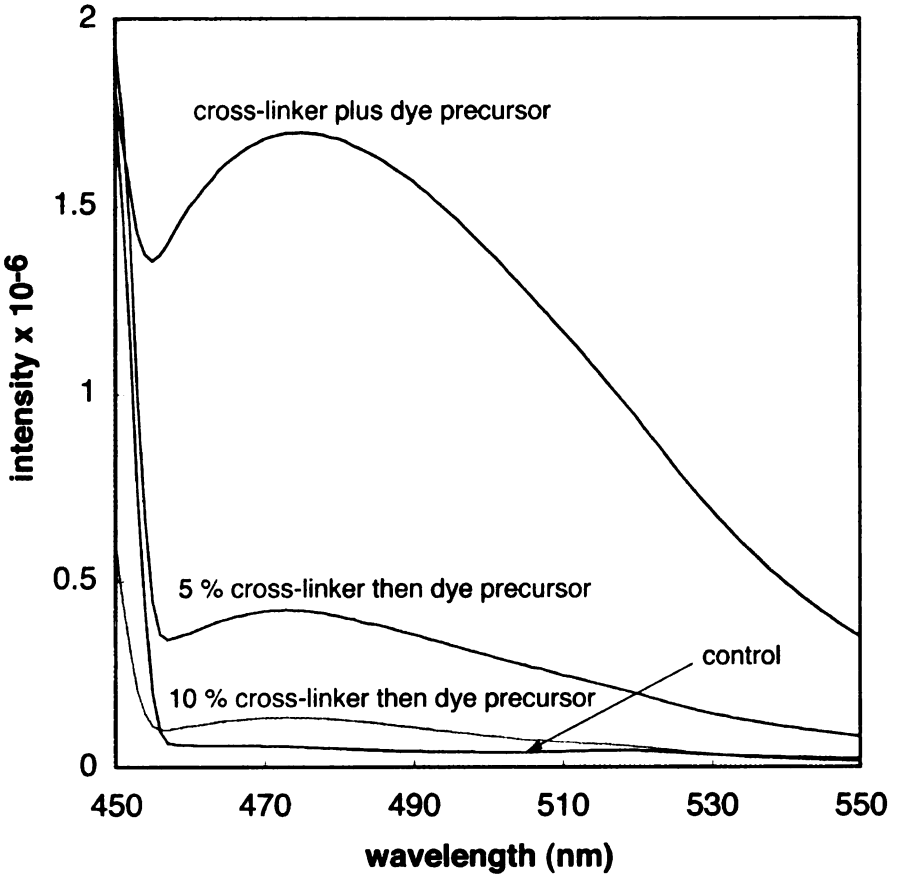

Figure 60. Fluorescence intensity of 1-step and 2-step click reactions on poly(PGL[$EG_{75}X_{25}$]) substrates. (From top to bottom): a single click step using an equimolar mixture of the dye precursor and 1,5-diazidopentane (blue), a two step process where 5 % of the remaining alkynes were cross-linked, followed by a second click reaction using an excess of the dye precursor (red); the same protocol, with 10 % cross-linking (orange), and the same protocol, with 100 % cross-linking (green).

Controlled Release from Cross-linked Nanoparticles

Controlled drug release improves drug efficacy, reduces toxicity and improves patient compliance and convenience.[123] Cross-linked nanoparticles are attractive for long-term controlled drug delivery since the release rate should be tunable by controlling the degree of cross-linking in the particles. We dissolved azobenzene, a surrogate for hydrophobic drugs, and poly(PGL[$EG_{75}X_{25}$]) in a minimal amount of acetone. After dispersing the solution in Milli-Q water, and removal of the acetone *in vacuo*, we confirmed encapsulation of azobenzene by its characteristic absorbance at 320 nm. We then repeated the experiment, using cross-linked poly(PGL[$EG_{75}CL_{25}$]). To track the release of azobenzene from the cross-linked and control nanoparticles, we placed the nanoparticle solutions in dialysis tubing (MWCO = 12-14 kD) and dialyzed with Milli-Q water. Removing aliquots of the nanoparticle solution from dialysis bag and measuring their UV-vis spectrum allowed us to monitor the continuous release of encapsulated azobenzene over 10 hours. As shown in **Figure 61**, the azobenzene release rate from the cross-linked nanoparticles was ~1/2 the rate measured for the noncross-linked control. These data are consistent with successful cross-linking, and proof of principle for long-term controlled drug delivery using a mixture of cross-linked nanoparticles with different release rates.

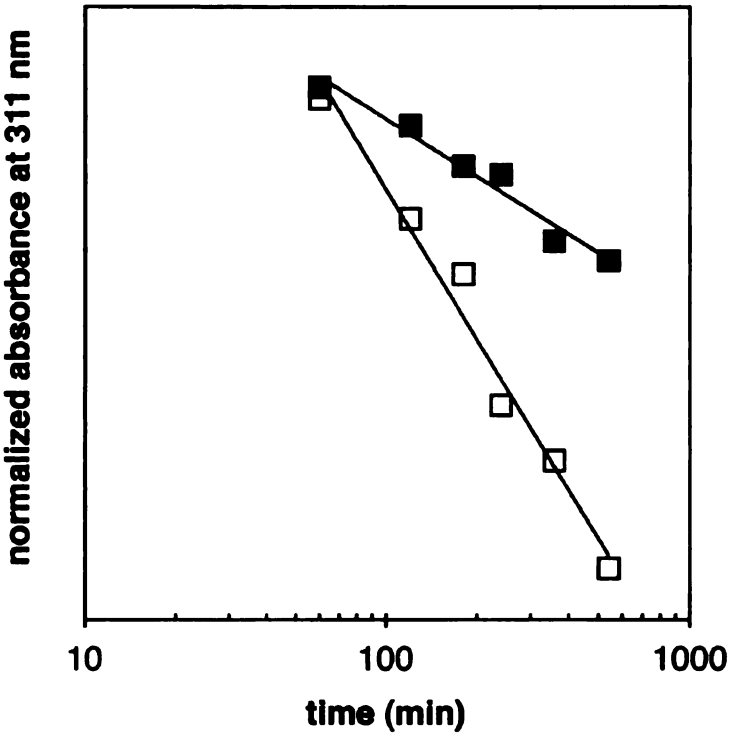

Figure 61. Release of azobenzene from nanoparticles suspended in Milli-Q water at room temperature (1 mg/mL). Cross-linked nanoparticles (■) show 2x slower release than noncross-linked nanoparticles (□). The loss of dye from the nanoparticles was monitored at 311 nm by UV spectroscopy.

Biocompatibility

For *in vivo* applications, nanoparticles must be biocompatible and degradable. In a single click reaction, we cross-linked the poly(PGL[$EG_{75}X_{25}$]) and appended a rhodamine dye to the nanoparticles. After dialysis to remove residual dye and click reagents, we cultured cortical astrocytes in a 10 μg/mL solution of dye-labeled nanoparticles. After 24 hours, the cells were washed to remove particles that had not entered the cells and then imaged by confocal microscopy. **Figure 62** shows that the nanoparticles readily entered the cells, probably due to their small size and their PEG exterior, which screens particle/protein interactions.

The cells remained healthy for more than 30 days and showed no signs of nanoparticle toxicity. These data are in agreement with the viability assays on various cross-linked nanoparticles, which show no detectable toxicity for nanoparticle concentrations as up to 3000 μg/mL (**Figure 63**).

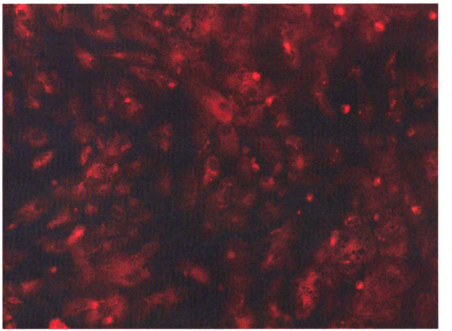

Figure 62. Cortical astrocytes cultured in media containing 10 μg/mL of cross-linked nanoparticles for 24 hours. The red color emanates from rhodamine dye covalently linked to the nanoparticles that have entered cells.

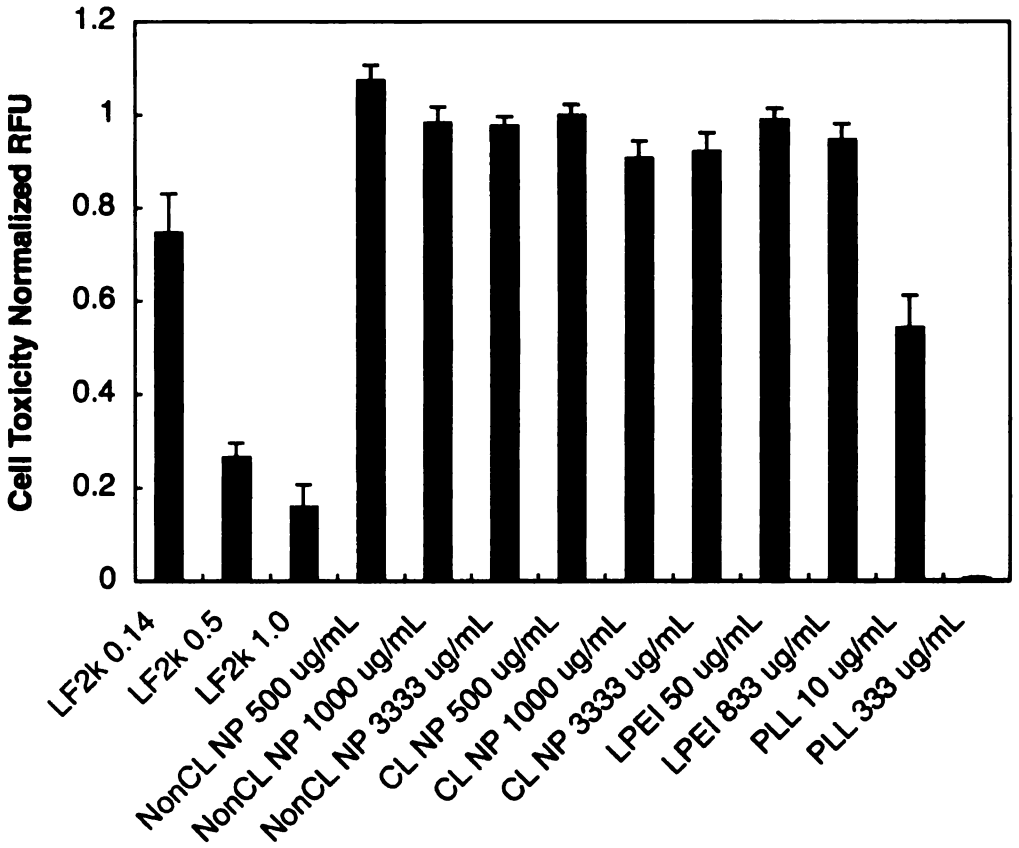

Figure 63. Evaluation of nanoparticle toxicity on cell viability reported in relative fluorescence units (RFU). Noncross-linked nanoparticles (poly(PGL[$EG_{75}X_{25}$]), NonCL NP) and cross-linked nanoparticles (poly(PGL[$EG_{75}CL_{25}$]), CL NP) correspond to polymers mentioned in the text. LipoFectamine (LF2k), linear poly(ethylene imine) (M_n = 25,000) (LPEI), and poly(*L*-lysine) (M_n = 150,000) (PLL) were used as controls. LF2k is reported as dilutions of the purchased solution.

Conclusion

Combining click chemistry and the unimolecular micelle approach provides a simple route to functional organic nanoparticles. The robust, stable particles encapsulate and release hydrophobic molecules and contain pendant reactive sites that can be used for cross-linking or covalent drug attachment. The nanoparticles are biodegradable and can be used in biomedical applications.

Experimental Section

General. Unless otherwise specified, ACS reagent grade starting materials and solvents were used as received from commercial suppliers without further purification. DMF was dried over activated 4Å molecular sieves. Ion exchange resin beads (Amberlite® IRC-748) were purchased from Aldrich and washed with DMF prior to use. ^{1}H NMR (300 or 500 MHz) and ^{13}C NMR (75 or 125 MHz) spectra were acquired using either a Varian Gemini 300 spectrometer or a Varian UnityPlus 500 spectrometer with the residual proton signal from the $CDCl_3$ solvent used as chemical shift standard. IR spectra were taken with Mattson Galaxy 3000 FT-IR.

Polymer Characterization. Polymer molecular weights were determined by using GPC-MALLS at 35 °C using two PLgel 10μ mixed-B columns in series (manufacturer-stated linear molecular weight range of 500-10×10^6 g/mol). The eluting solvent was THF at a flow rate of 1 mL/min, and the concentration of polymer solutions used for GPC was 1 mg/mL. An Optilab rEX (Wyatt Technology Co.) and a DAWN EOS 18-angle light scattering detector (Wyatt Technology Co.) with a laser wavelength of 684 nm were used to calculate absolute molecular weights. UV-Vis spectra were recorded with a Cary 300 Bio WinUV, Varian spectrophotometer. Fluorescence was recorded using a Fluorolog-3 (Instruments S.A., Inc.) fluorometer. All samples were diluted to 1 × 10^{-6} M using Milli-Q water, excited at λ_{ex} = 440 nm, and the fluorescence emission spectra were observed from 450-500 nm. Dynamic light scattering (DLS) data were obtained using a

temperature-controlled Protein Solutions Dyna Pro-MS/X system. All samples were filtered through a 0.2 μm Whatman PTFE syringe filter and allowed to equilibrate in the instrument for 15 minutes at 25 °C before measurements were taken. The uniformity of the particle sizes were determined by a monomodal curve fit, which assumes a single particle size with a Gaussian distribution. Surface profile measurements were performed with a Pacific Nanotechnology Nano-R atomic force microscope in close contact (oscillating) mode to generate height images that were not altered other than a simple leveling procedure. Silicon tips with a spring constant of 36 N/m, tip curvature of 10-20 nm, and a resonance frequency of 286-339 kHz were used for all experiments. The polymeric micelles were dispersed in Milli-Q water and the solutions (typical concentration, 20-300 μg/mL) were spin coated at 5000 rpm for 40 sec on freshly cut silicon substrates. Heights were determined using AFM by taking the average of 20 particle heights. The lateral size could not be determined due to convolution effects created by the tip.[204,205] TEM micrographs were collected at 270,000-370,000 x magnification on a JEOL-100CX transmission electron microscope. TEM samples (typical concentration, 20-300 μg/mL) were dropped onto nickel grids pretreated with Formvar and allowed to settle for 2 min before removing the excess solution. The sample was negatively stained with either a 1 % phosphotungstic acid (PTA) stain or 2 % uranyl acetate (UA) stain prepared with deionized water.

Synthesis of 1,5-diazidopentane. Sodium azide (1.65 mol, 107 g) was added to a solution of 1,5-dibromopentane (165 g, 720 mmol) in 600 mL DMF. The solution was stirred at 60 °C for 9 hours and cooled. The mixture was poured into 200 mL water and extracted with ether (3 x 75 mL). The combined organic layers were dried over $MgSO_4$ and the ether removed. The 1,5-diazidopentane[252] was purified by vacuum distillation (60 °C, 5 mtorr) to yield a colorless liquid (105 g, 680 mmol, 95 %). ^1H NMR (500 MHz) δ 3.29-3.26 (dd, 4H, J = 6.84, 6.71), 1.64-1.53 (m, 4H), 1.48-1.43 (m, 2H). ^{13}C NMR (125 MHz) δ 51.21, 28.42, 23.936.

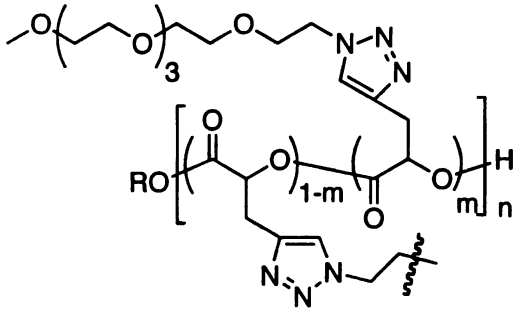

General procedure for cross-linking. The desired amount of PPGL-*g*-mPEG functionalized polymer dissolved in acetone (< 0.5 mL) was slowly added dropwise to stirred ice-cold Milli-Q water in a round bottom flask containing sodium ascorbate (1 eq with respect to the remaining acetylene groups) and $CuSO_4 \cdot 5H_2O$ (0.5 eq with respect to the remaining acetylene groups). The solution was stirred 5 min before a solution of 1,5-diazidopentane (10-100 mol% with respect to the remaining acetylene groups) dissolved in 1 mL acetone was added dropwise. The solution was allowed to stir under nitrogen 2 d and was then transferred to

presoaked dialysis tubing (MWCO = 12-14 kD), and dialyzed against a 4:1 solution of Milli-Q water and acetone overnight. To remove the copper, the nanoparticle solution was concentrated, redissolved in DMF and ion exchange resin was added (400 mg) for 24 hours. The nanoparticles were resuspended in Milli-Q water following DMF removal.

Cross-linked PPGL-*g*-mPEG nanoparticles (poly(PGL[$EG_{80}CL_{20}$])). ^{1}H NMR (500 MHz) δ 7.8-7.4 (b, 1H), 5.6-5.2 (b, 1H), 4.5-4.4 (b, 1.6H), 4.3 (b, 3.2H), 3.9-3.7 (b, 1.6H), 3.6-3.4 (b, 9.6H), 3.3 (b, 2.4H), 3.3-3.2 (b, 2H), 1.4-1.2 (b, 1.2H).

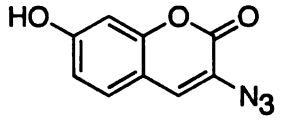

Synthesis of 3-azido-7-hydroxy-coumarin.[251] A mixture of 2,4-dihydroxybenzaldehyde (2.76 g, 20 mmol), N-acetyl glycine (2.34 g, 20 mmol), anhydrous sodium acetate (4.92 g, 60 mmol) in freshly distilled acetic anhydride (100 mL) was refluxed under nitrogen for 4 hours. The mixture was cooled and poured onto ice to provoke a yellow precipitate. After filtration, the yellow solid was washed with ice water and added to a solution of concentrated HCl and ethanol (2:1 vol %, 30 mL). The solution was refluxed for 1 hour, cooled to 0 ° C and ice (60 g) was added. After sodium nitrate (76 g, 40 mmol) was added in portions, the solution was stirred 10 minutes and sodium azide (3.91 g, 60 mmol) was added. The mixture was stirred an additional 30 minutes and filtered. The collected brown solid was washed with water and dried under vacuum to give 0.5 g (2.8 mmol, 14 %) of 3-azido-7-hydroxy coumarin. ^{1}H NMR (500 MHz) δ 7.57 (s, 1H), 7.46 (d, 1H,

J = 8.55), 6.81 (d, 1H, J = 8.55), 6.75 (s, 1H). ^{13}C NMR (125 MHz) δ 160.3, 157.3, 152.7, 129.1, 127.8, 121.1, 113.7, 111.3, 102.0.

Covalent attachment of 3-azido-7-hydroxycoumarin. Using PPGL-*g*-mPEG and the "click" conditions described earlier, we carried out two types of click reactions: (1) a single click step using an equimolar mixture of the dye precursor and 1,5-diazidopentane; and (2) a two step process where 5, 10, or 100 % of the remaining alkynes of PPGL-*g*-mPEG were first cross-linked with 1,5-diazidopentane, followed by a second click reaction using an excess of the dye precursor.

Azobenzene release from cross-linked nanoparticles. Encapsulation: to encapsulate azobenzene the polymer, azobenzene, 1,5-diazidopentane, sodium ascorbate, and copper(II) sulfate were dissolved in acetone (<1 mL) and the acetone solution was stirred for 2 days and then was added dropwise to Milli-Q water. The acetone was removed and the solution was filtered to remove any unencapsulated azobenzene. We confirmed its encapsulation by it characteristic absorbance at 320 nm using UV-vis spectroscopy. Release: azobenzene-loaded nanoparticles were placed in dialysis membrane (MWCO 12-14 kD) in stirred Milli-Q water. At allotted time intervals, the azobenzene solution was removed, filtered to remove any insoluble released azobenzene, and monitored using UV-Vis. The same procedure was followed for the noncross-linked micelles, except, 1,5-diazidopentane was not added to the reaction mixture.

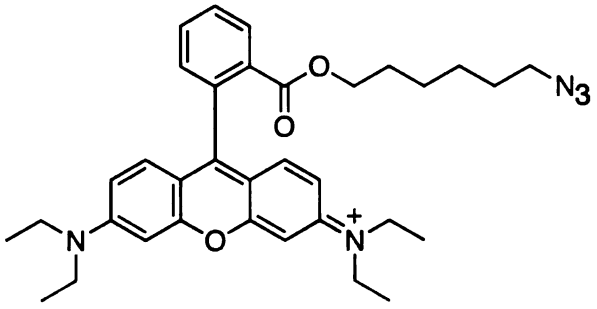

Synthesis of Rhodamine Derivative. DCC (459 μmol, 95 mg) in 2 mL anhydrous CH_2Cl_2 was added to a mixture of Rhodamine B (418 μmol, 0.20 g), 6-azidohexanol[253] (835 μmol, 0.20 g), and DMAP (84 μmol, 10 mg) in 10 mL anhydrous CH_2Cl_2. The mixture was stirred at room temperature for 8 hours under nitrogen and the insoluble urea was filtered from the solution. The CH_2Cl_2 was evaporated and the dye was triturated in hexanes to remove any unreacted alcohol and then dried under vacuum to give (0.231 g, 385 μmol, 92 %) of *N*-(9-(2-((6-azidohexyloxy)carbonyl)phenyl)-6-(diethylamino)-3*H*-xanthen-3-ylidene)-*N*-ethylethanaminium chloride. ^{1}H NMR (500 MHz) δ 8.28 (dd, 1H, *J* = 8.0 and 1.5), 7.82 (dt, 1H, *J* = 8.0 and 1.5), 7.75 (dt, 1H, *J* = 8.0 and 1.5), 7.31 (dd, 1H, *J* = 8.0 and 1.5), 7.10 (d, 2H, *J* = 9.5), 6.94 (dd, 2H, *J* = 9.5 and 2.5), 6.87 (d, 2H, *J* = 2.5), 3.62-3.60 (d, 2H, J = 6.7), 3.26-3.24 (t, 2H, J = 6.9), 1.32-1.30 (m, 8H). ^{13}C NMR (125 MHz) δ 165.2, 158.7, 157.7, 155.5, 133.3, 132.9, 131.9, 131.2, 131.2, 130.3, 130.2, 130.1, 114.2, 113.4, 96.3, 65.5, 51.4, 46.0, 32.5, 28,8, 26,5, 25.3, 12.5.

Toxicity Studies. HeLa cells were plated in 96-well black-clear bottom plates at 10,000 cells/well in 100 μL of culture medium lacking antibiotic and grown for 22 hr at 37 °C. Cells were ~70-80 % confluent based on microscopy. Nanoparticle

solutions (50 μl total volume, when required dilutions were prepared in OptiMEM, Invitrogen) were added to the 100 μL of culture medium. The cells were incubated for an additional 22 hr and then 20 μL Cell Titer Blue (CTB) reagent was added. Fluorescence was quantified in a fluorescence plate reader 2 hr after CTB reagent was added, according to the manufacturer's instructions. LipoFectamine (LF2k), linear poly(ethylene imine) (M_n = 25,000) (LPEI), and poly(*L*-lysine) (M_n = 150,000) (PLL) were used as controls. LF2k is reported as dilutions of the purchased solution.

Appendix

NMR SPECTRA

Appendix 1. ^1H NMR spectra for the determination of F_1 for the copolymerization of *rac*-lactide and *rac*-ethylglycolide.

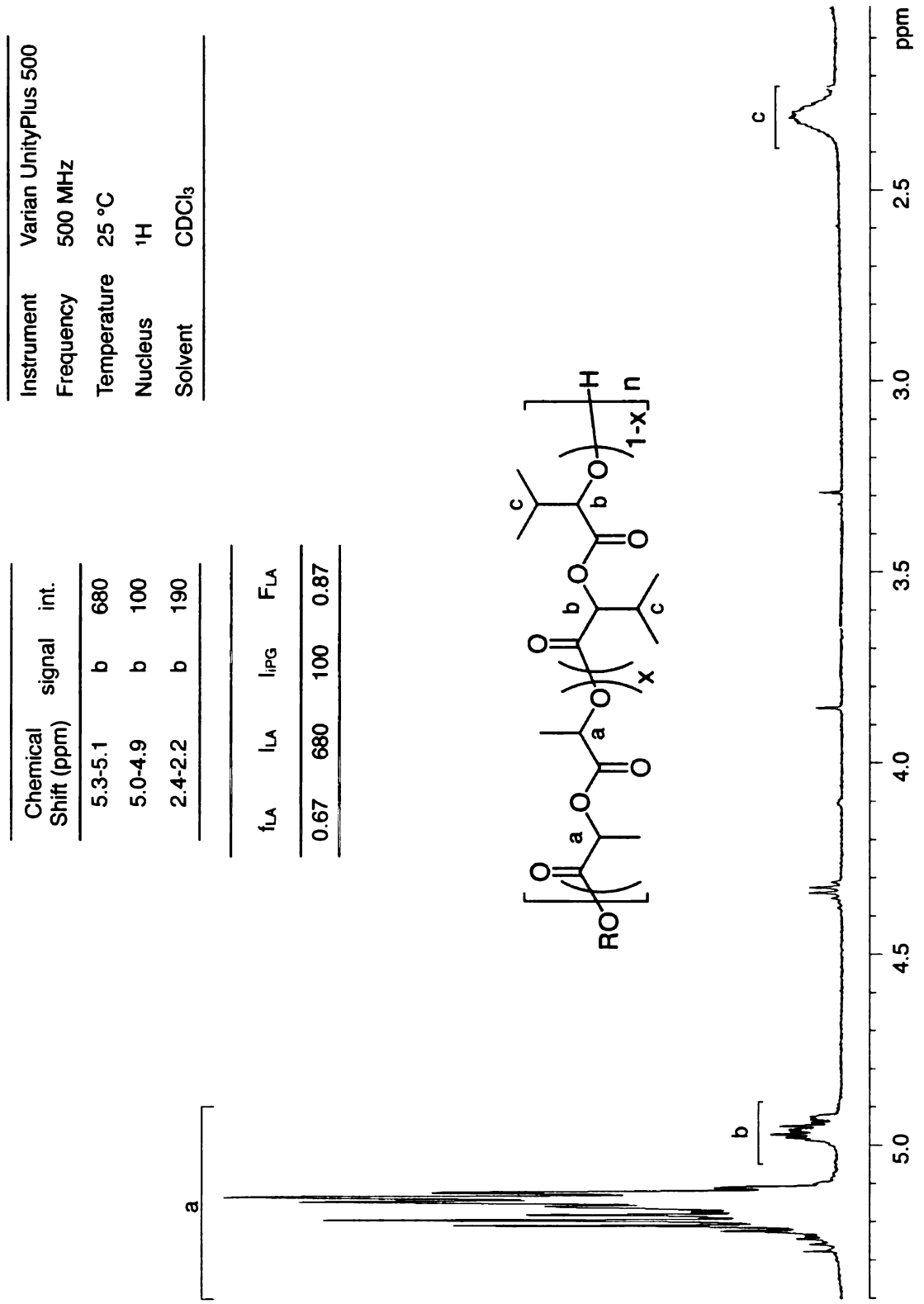

Appendix 2. ^{1}H NMR spectra for the determination of F_1 for the copolymerization of *rac*-lactide and *rac-iso*propylglycolide.

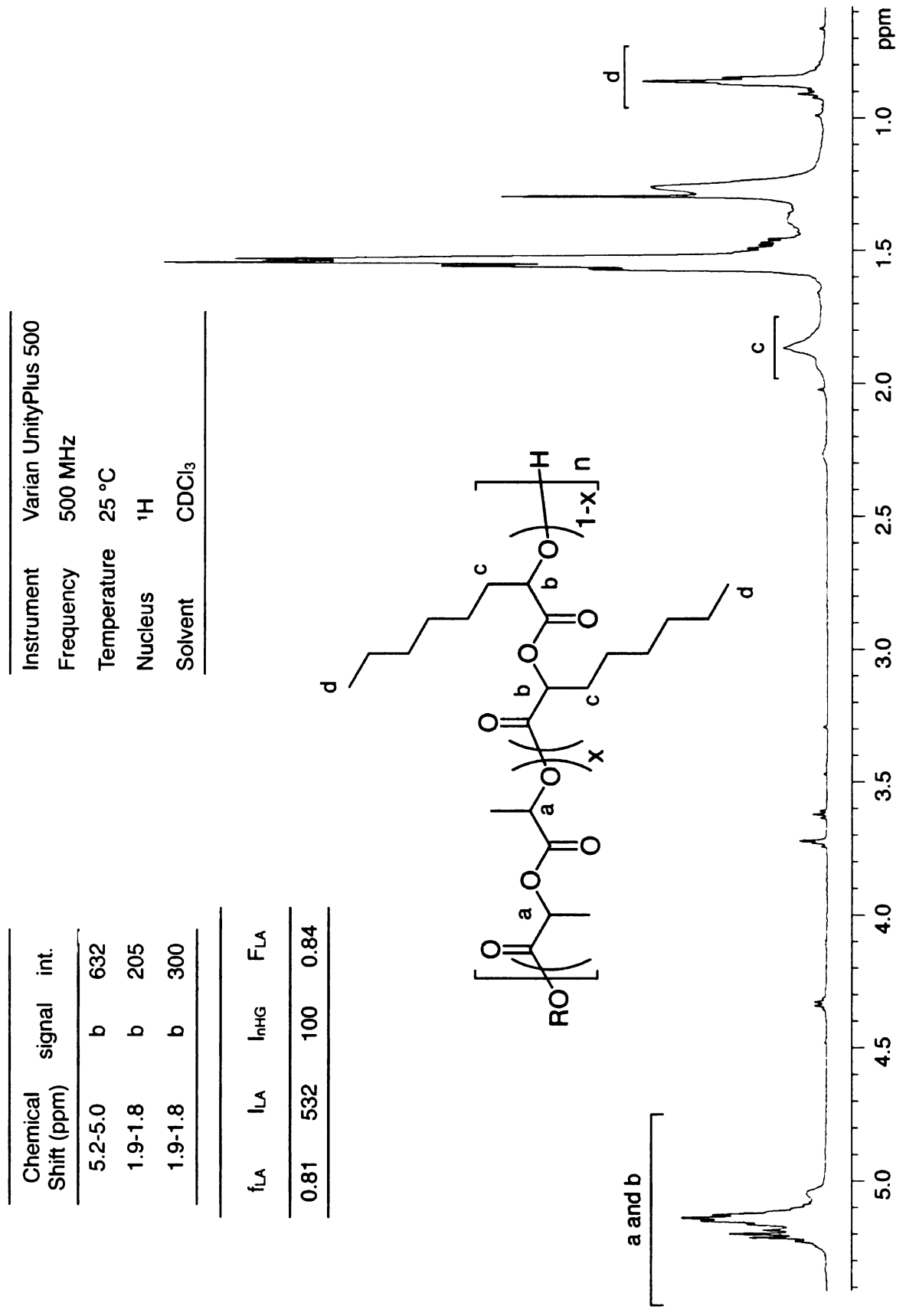

Appendix 3. ^{1}H NMR spectra for the determination of F_1 for the copolymerization of *rac*-lactide and *rac-n*-hexylglycolide.

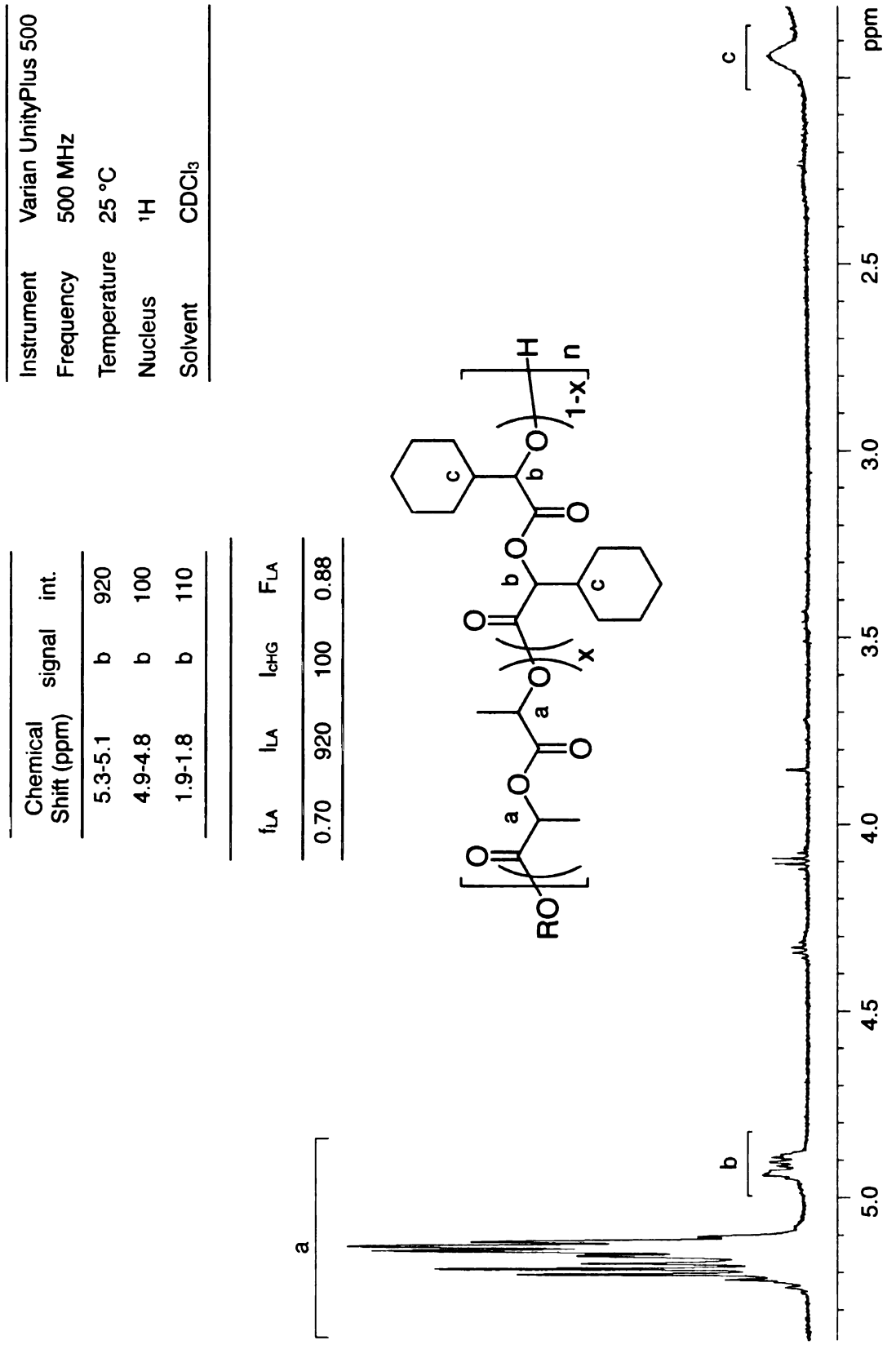

Appendix 4. ^{1}H NMR spectra for the determination of F_1 for the copolymerization of *rac*-lactide and *rac*-cyclohexylglycolide.

Appendix 5. ^{1}H NMR spectra for the determination of F_1 for the copolymerization of *rac*-lactide and *rac*-phenyllactide.

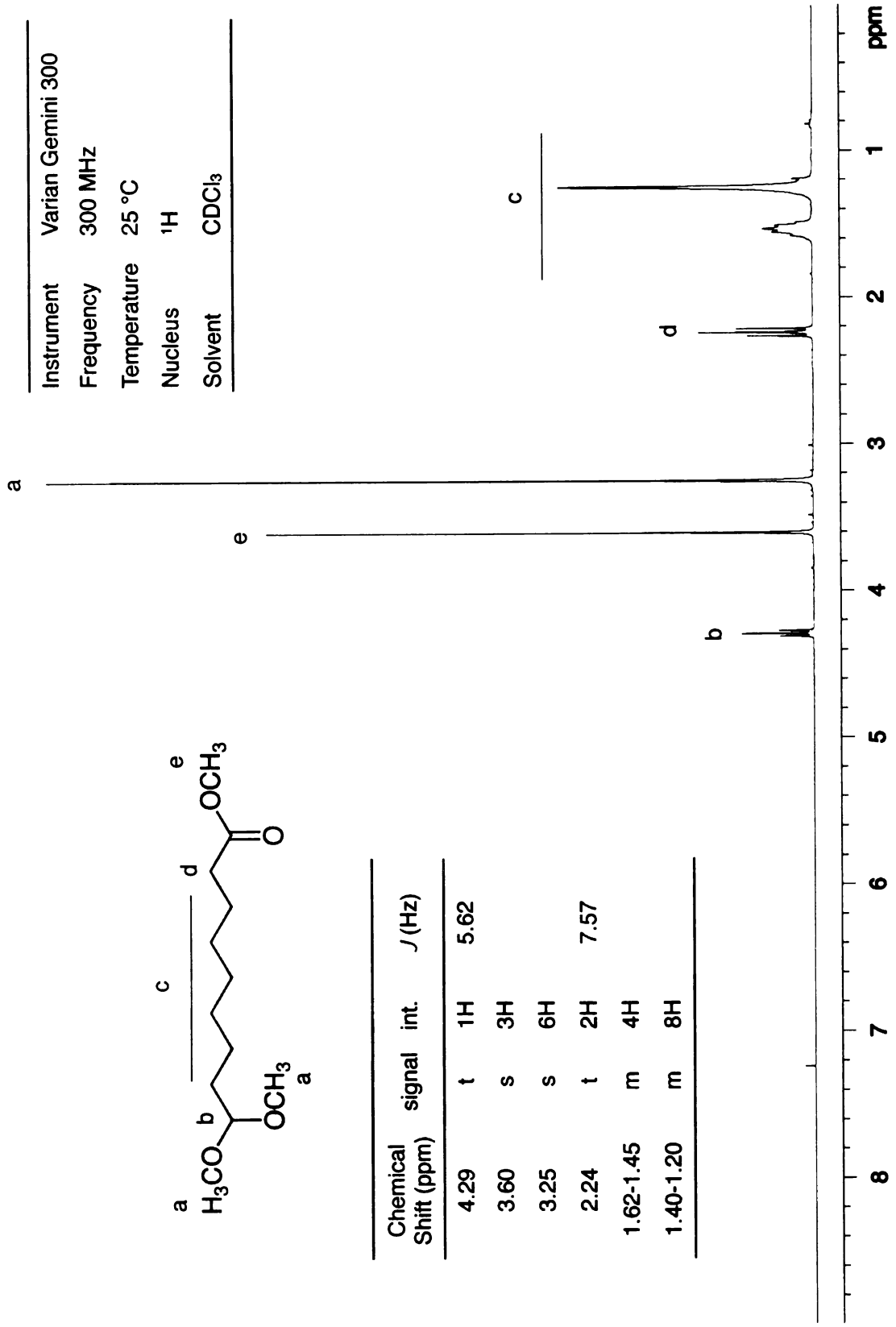

Chemical Shift (ppm)	signal	int.	*J* (Hz)
4.29	t	1H	5.62
3.60	s	3H	
3.25	s	6H	
2.24	t	2H	7.57
1.62-1.45	m	4H	
1.40-1.20	m	8H	

Appendix 6. ^{1}H NMR spectra of 9,9-dimethoxynonanoate.

Appendix 7. ^{13}C NMR spectra of 9,9-dimethoxynonanoate.

Instrument	Varian Gemini 300
Frequency	75 MHz
Temperature	25 °C
Nucleus	^{13}C
Solvent	$CDCl_3$

Chemical Shift (ppm)
174.2
104.4
52.5
51.3
34.0
32.3
29.2
29.1
28.9
24.8
24.2

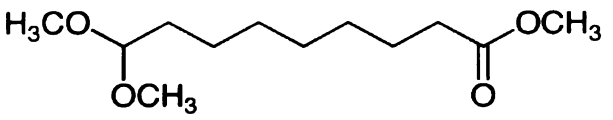

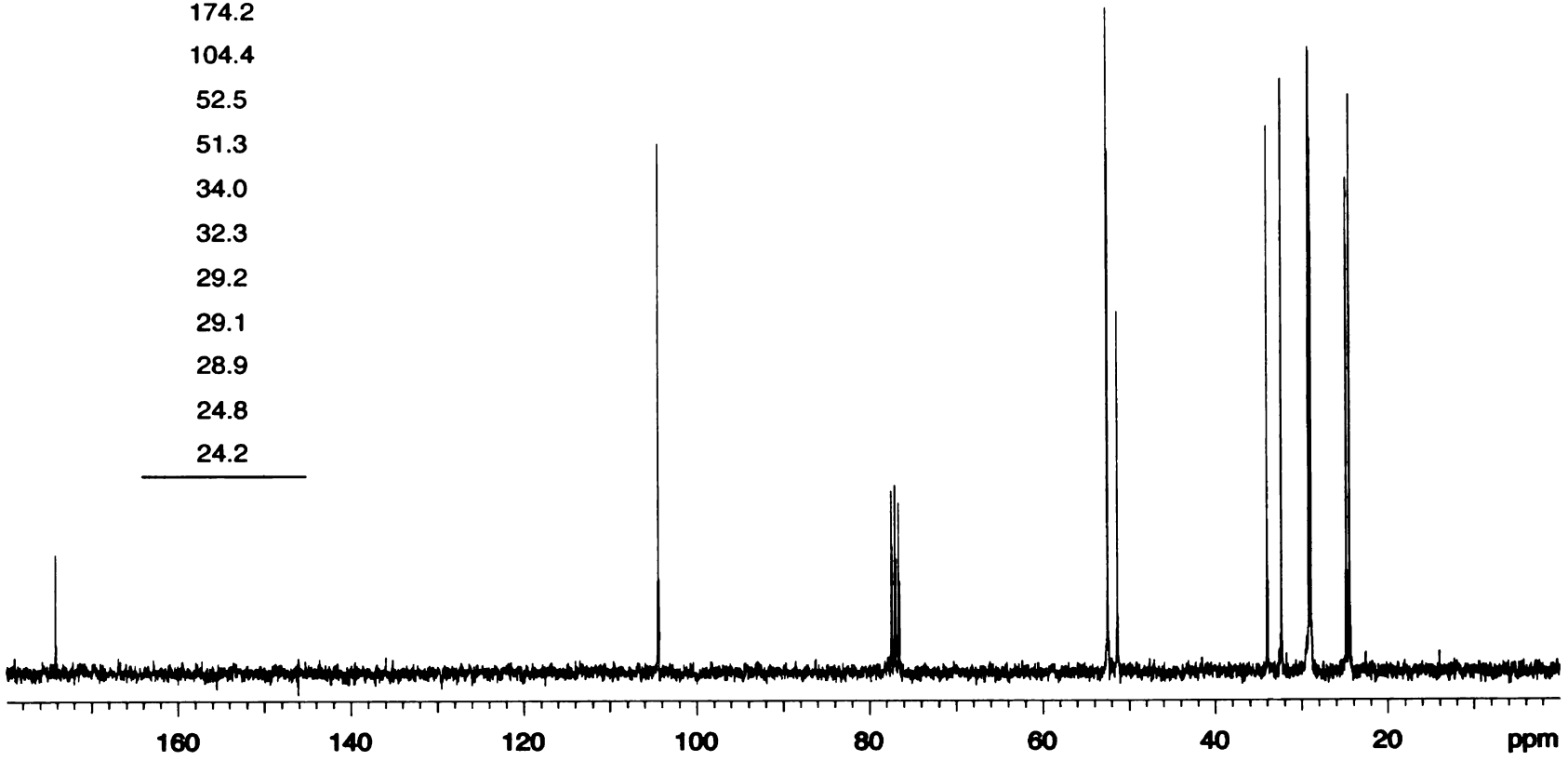

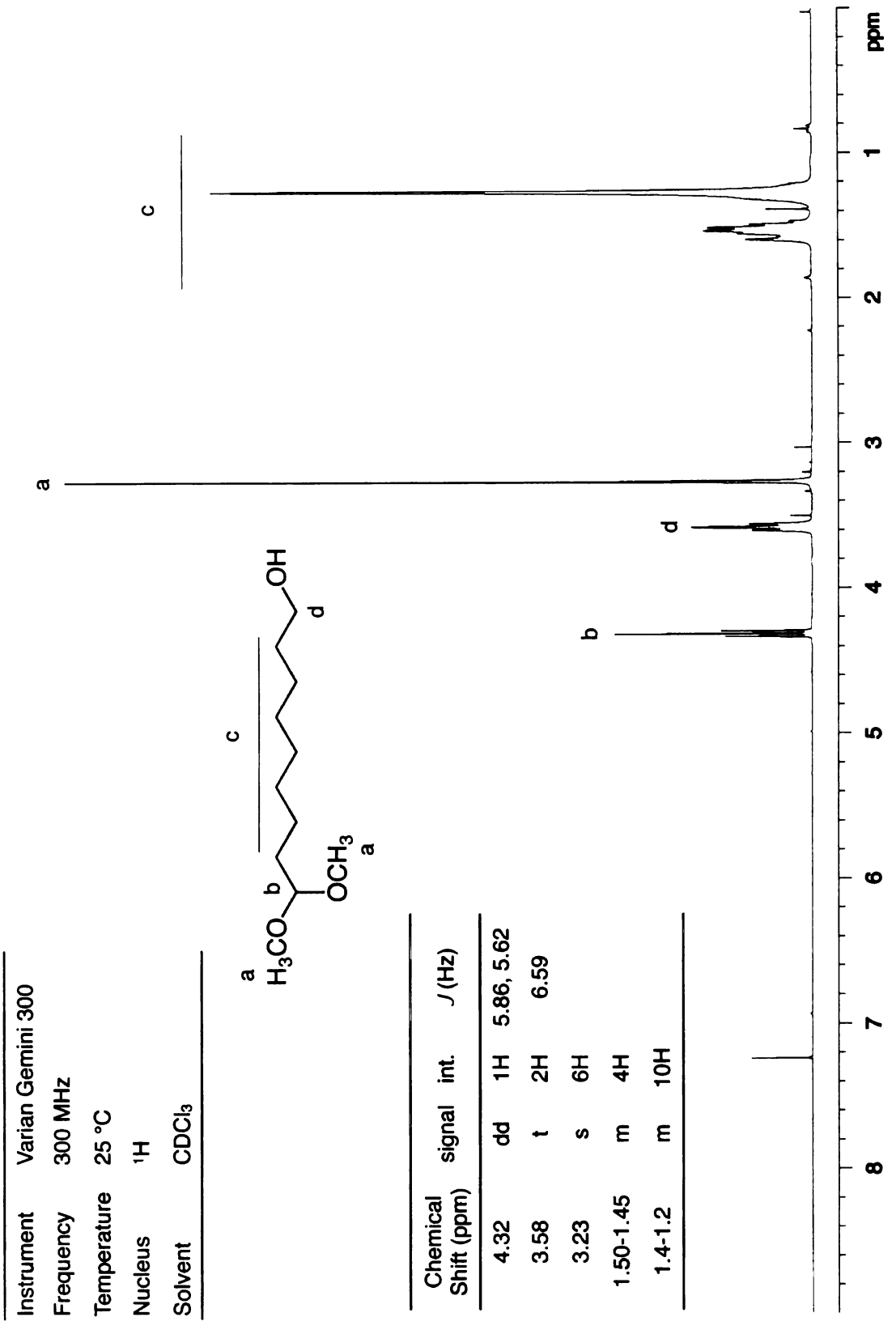

Appendix 8. ^1H NMR spectra of 9,9-dimethoxynonanol.

Appendix 9. ^{13}C NMR spectra of 9,9-dimethoxynonanol.

Appendix 10. ^{1}H NMR spectra of ((9,9-dimethoxynonyloxy)methyl)benzene.

Chemical Shift (ppm)	signal	int.	*J* (Hz)
7.33-7.20	m	5H	
4.5	s	2H	
4.38	t	1H	5.77
3.46	dd	2H	6.59, 6.87
3.1	s	9H	
1.65-1.55	m	4H	
1.41-1.2	m	10H	

Instrument	Varian Gemini 300
Frequency	300 MHz
Temperature	25 °C
Nucleus	^{1}H
Solvent	$CDCl_3$

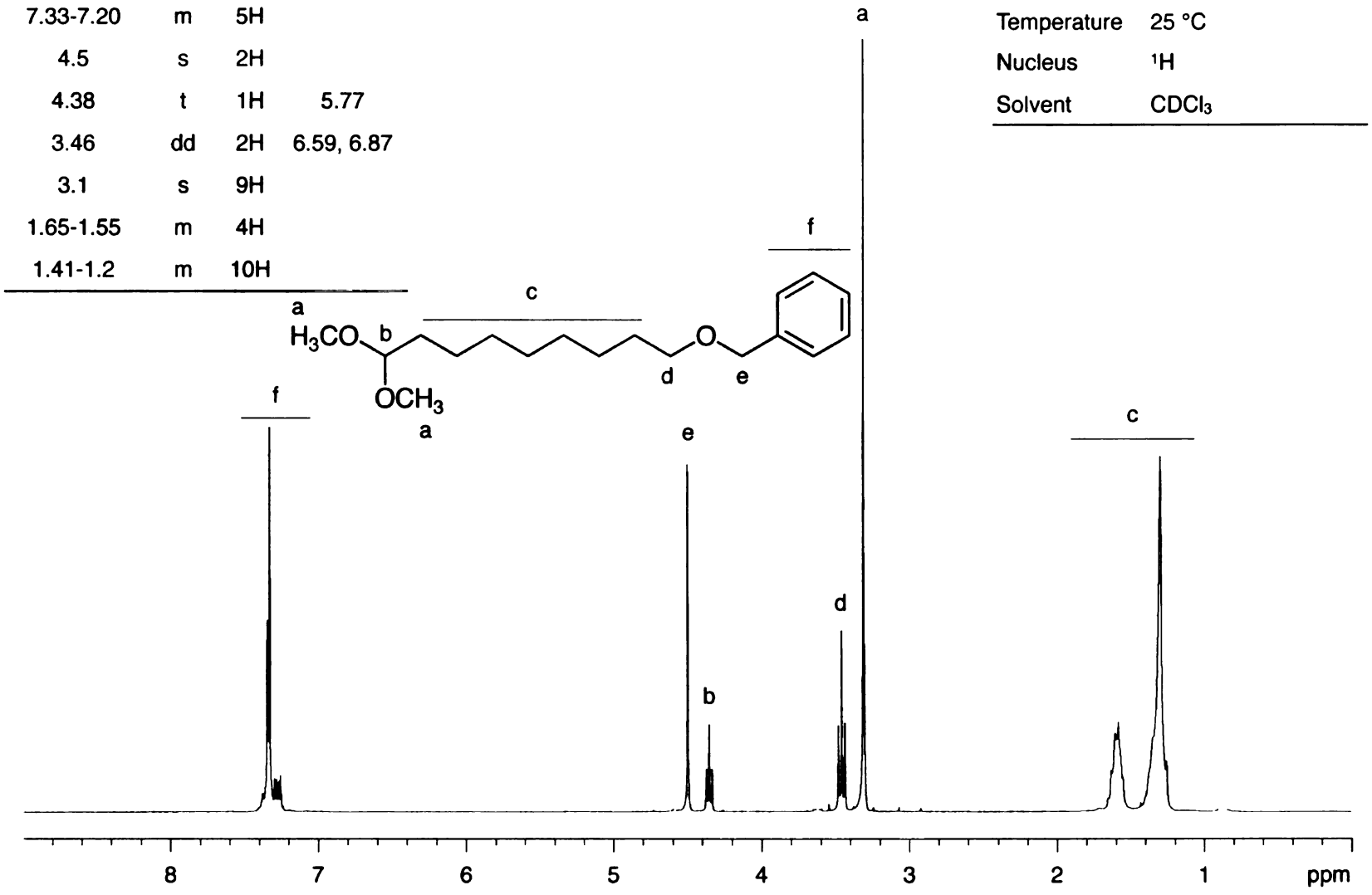

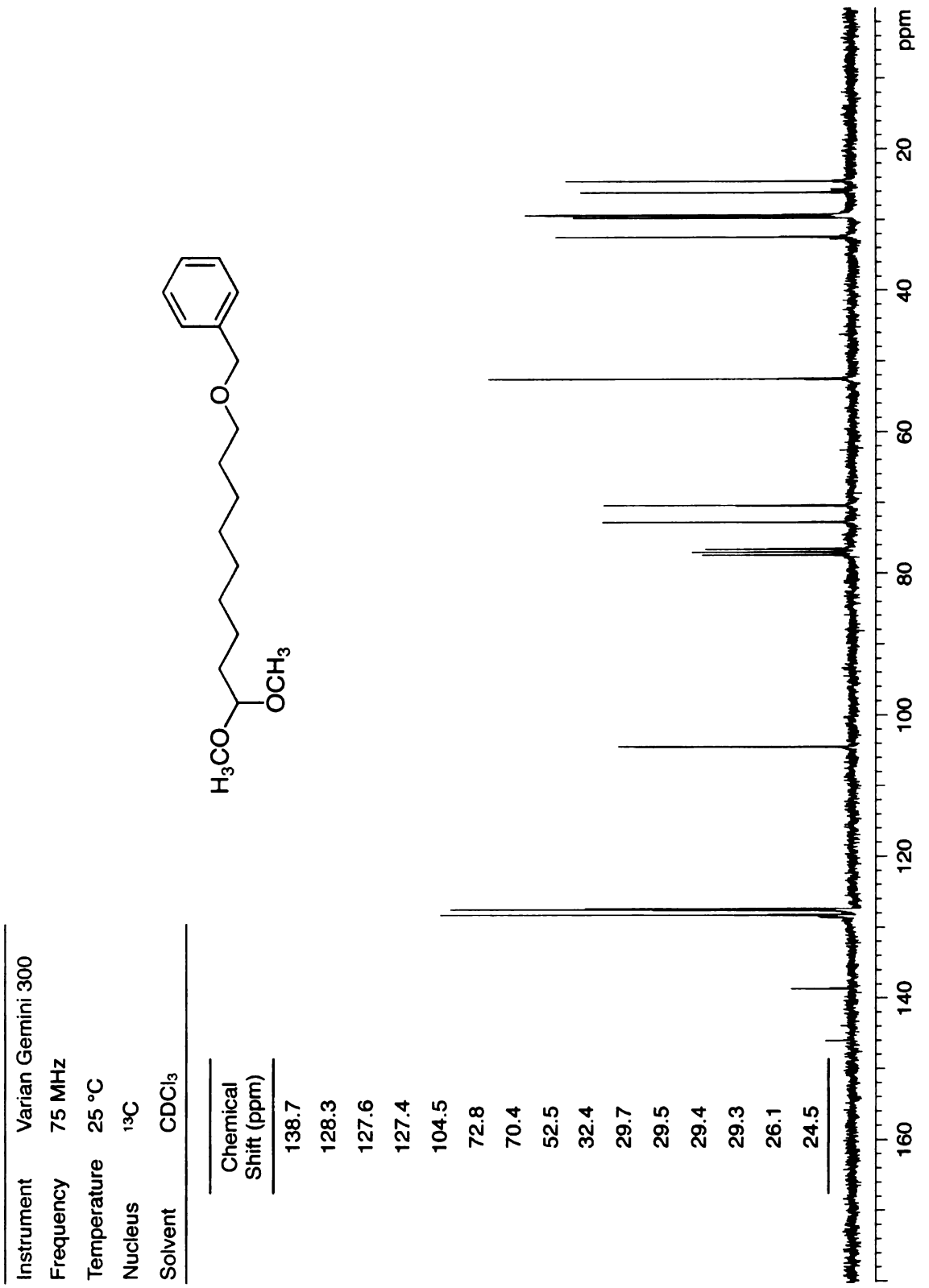

Appendix 11. ^{13}C NMR spectra of ((9,9-dimethoxynonyloxy)methyl)benzene.

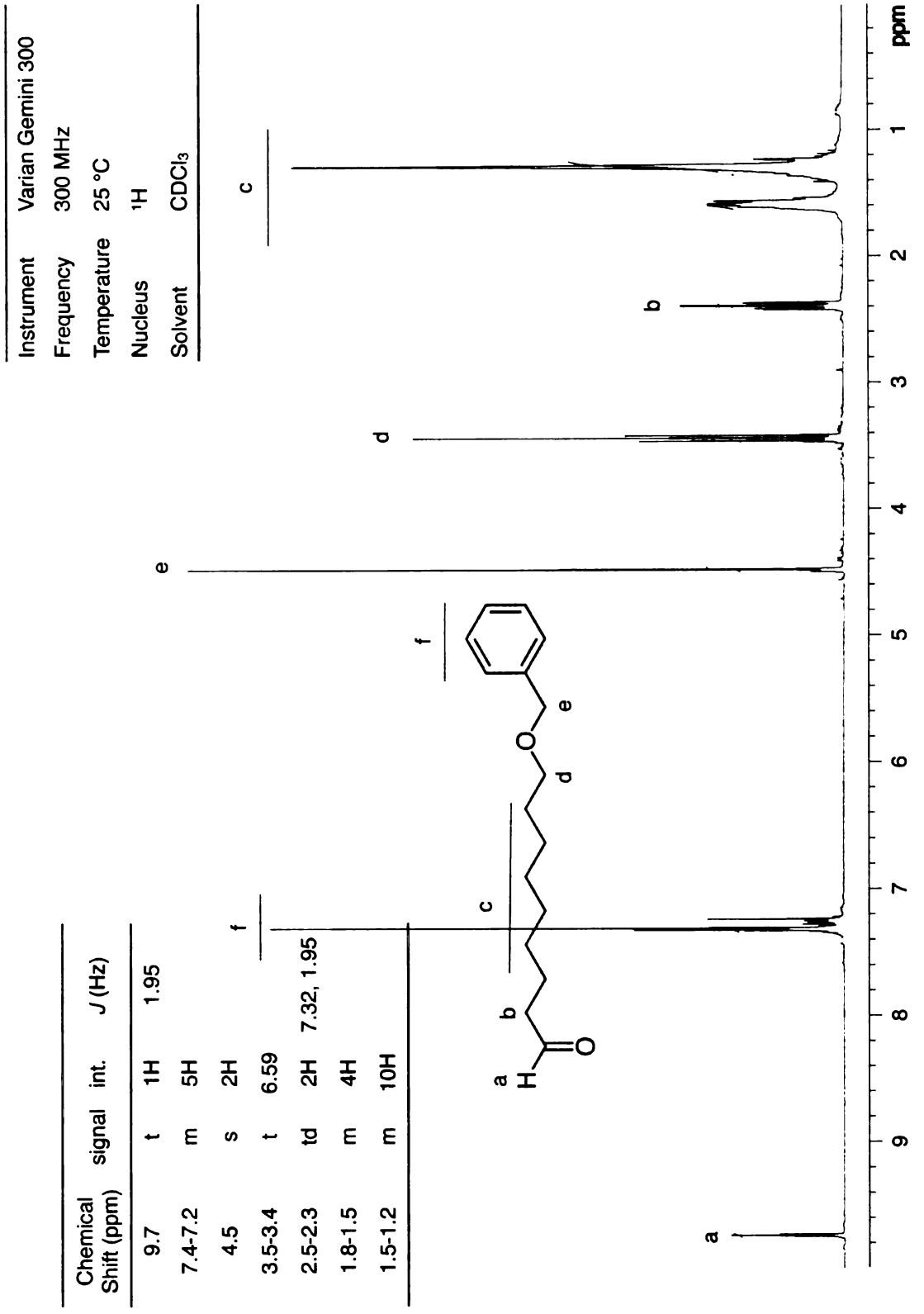

Appendix 12. ^{1}H NMR spectra of (9-benzyloxy)nonanal.

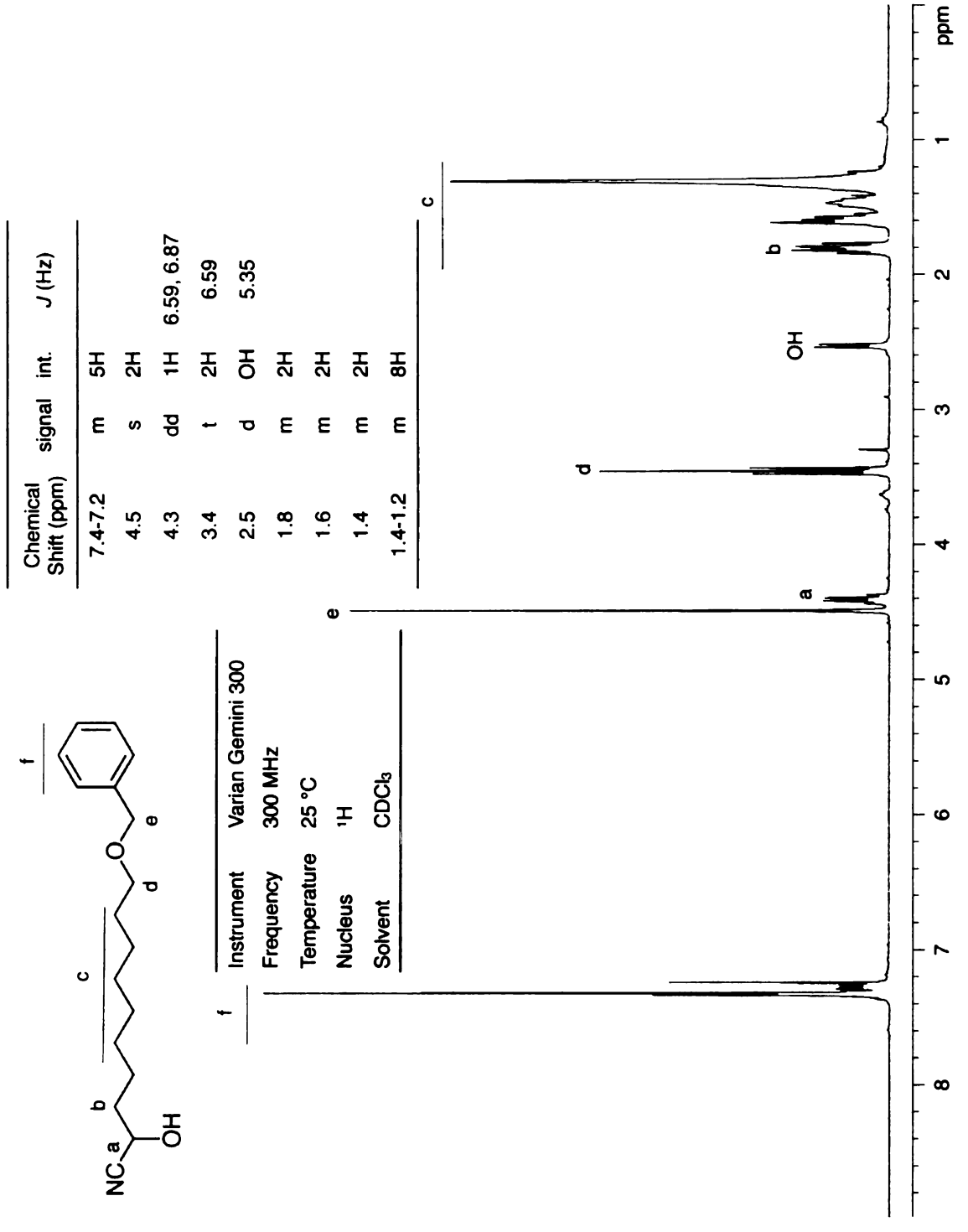

Appendix 13. ^{1}H NMR spectra of 10-(benzyloxy)-2-hydroxydecanenitrile.

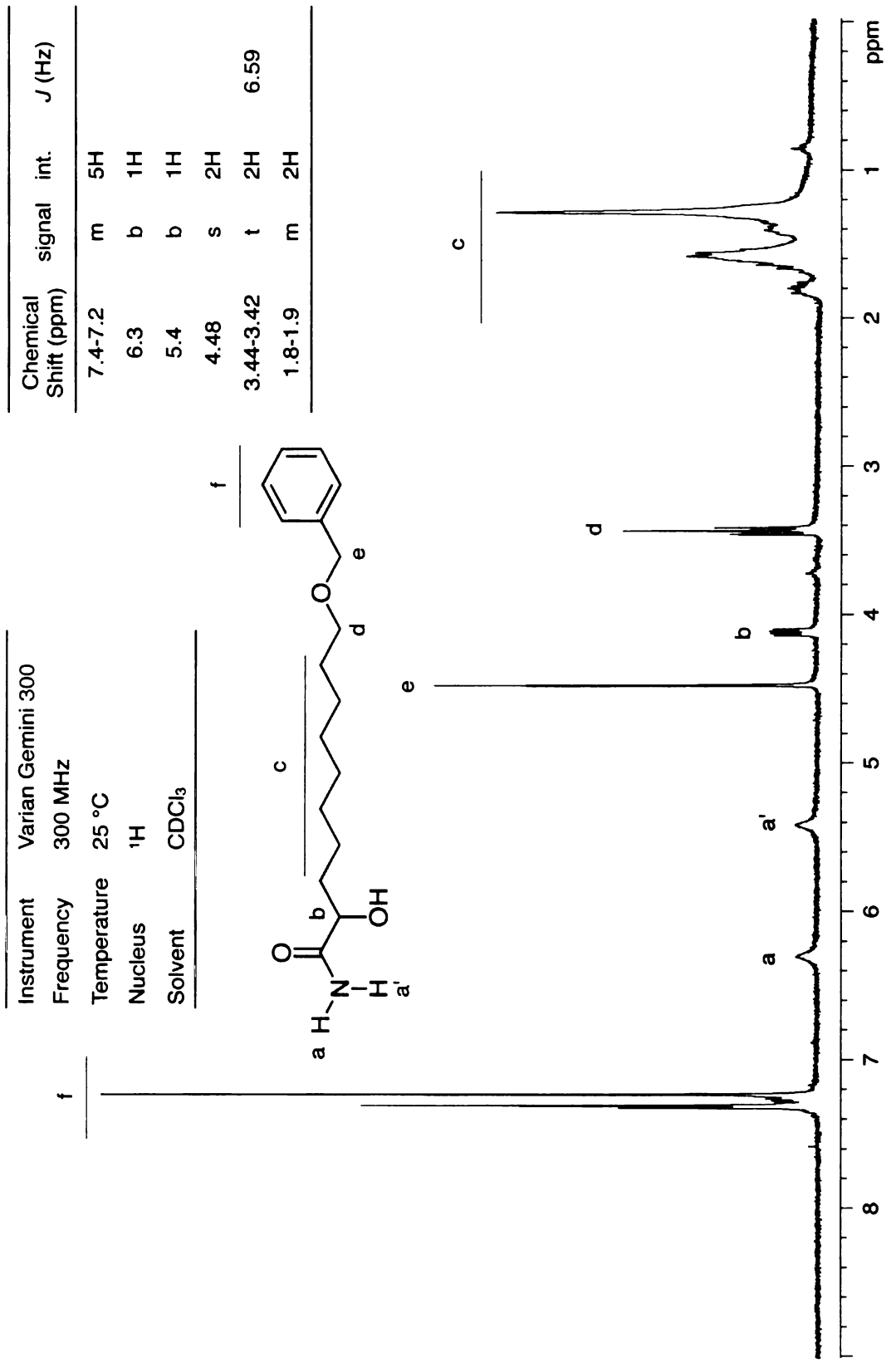

Appendix 14. ^{1}H NMR spectra of 10-(benzyloxy)-2-hydroxydecanamide.

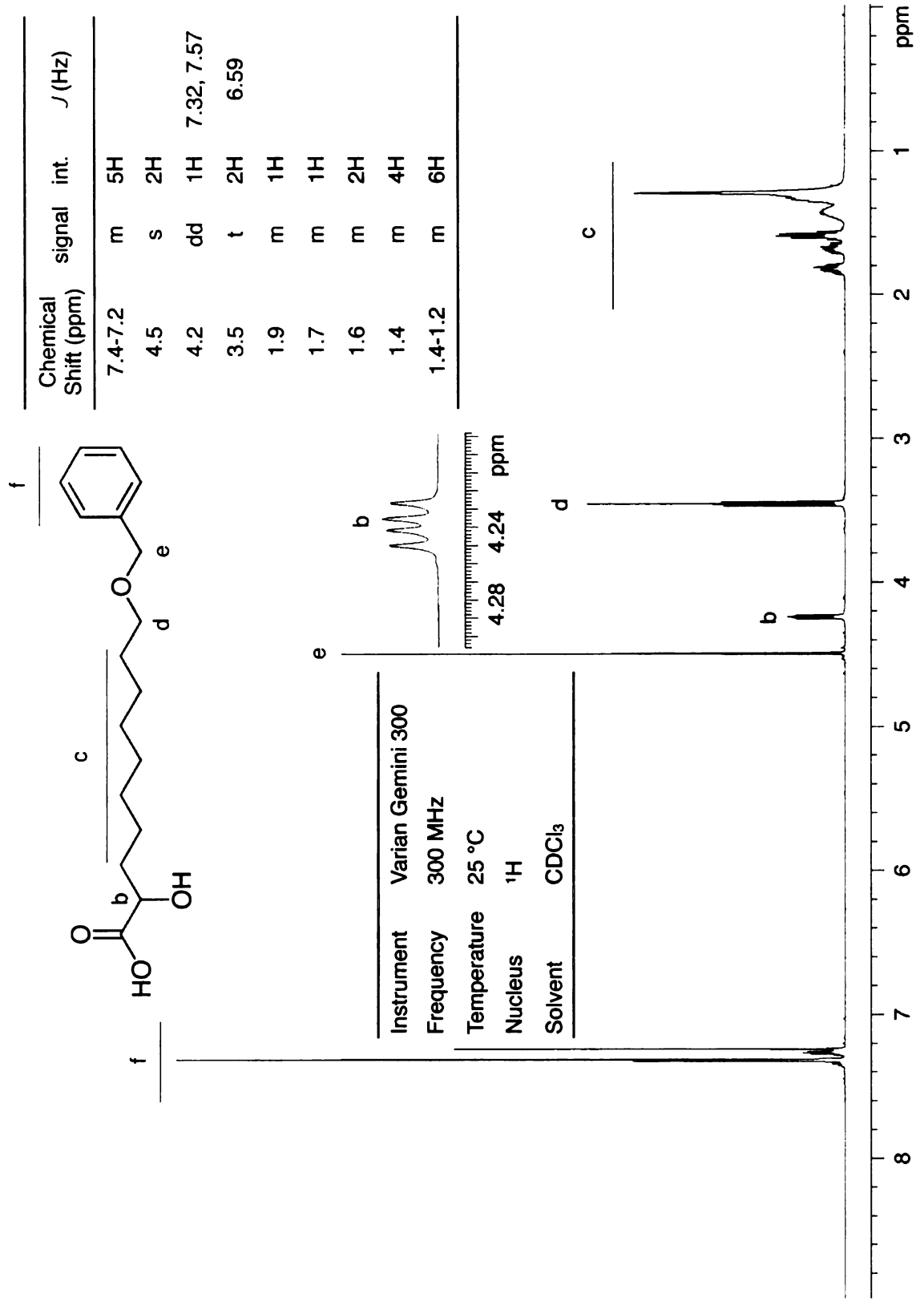

Appendix 15. ^{1}H NMR spectra of 10-(benzyloxy)-2-hydroxydecanoic acid.

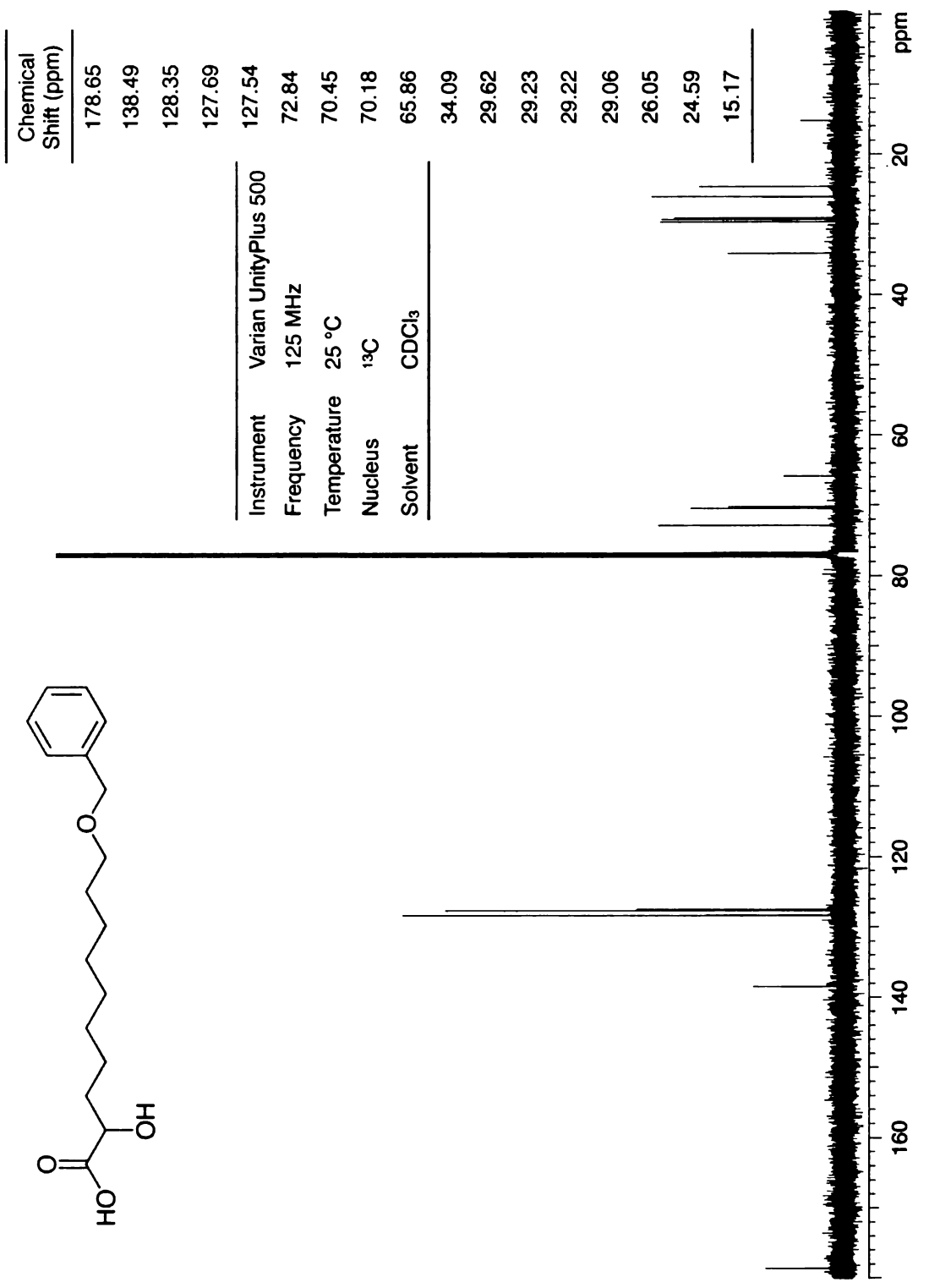

Appendix 16. ^{13}C NMR spectra of 10-(benzyloxy)-2-hydroxydecanoic acid.

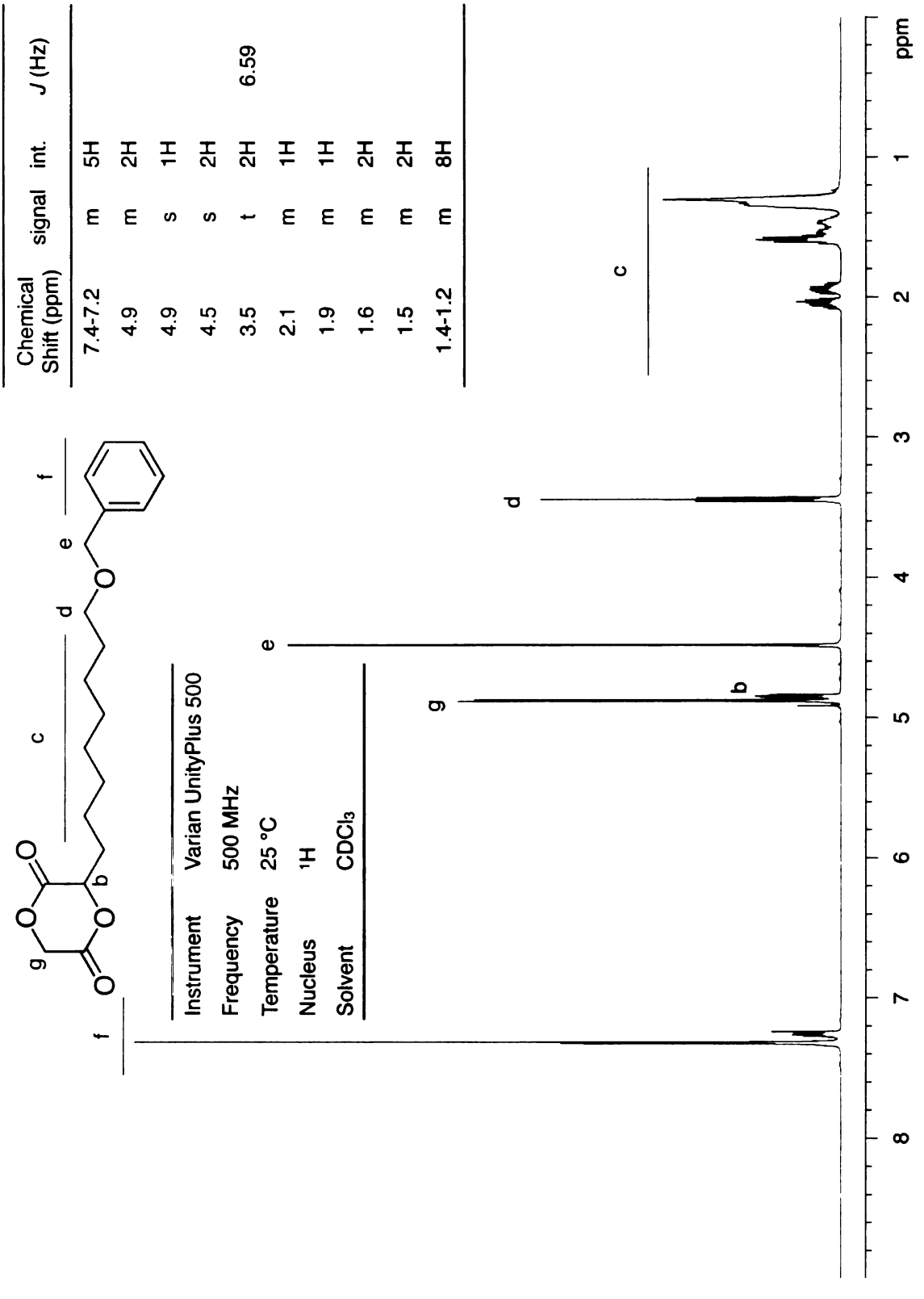

Appendix 17. ^{1}H NMR spectra 3-(8-(benzyloxy)octyl-1,4-dioxane-2,5-dione (BOG).

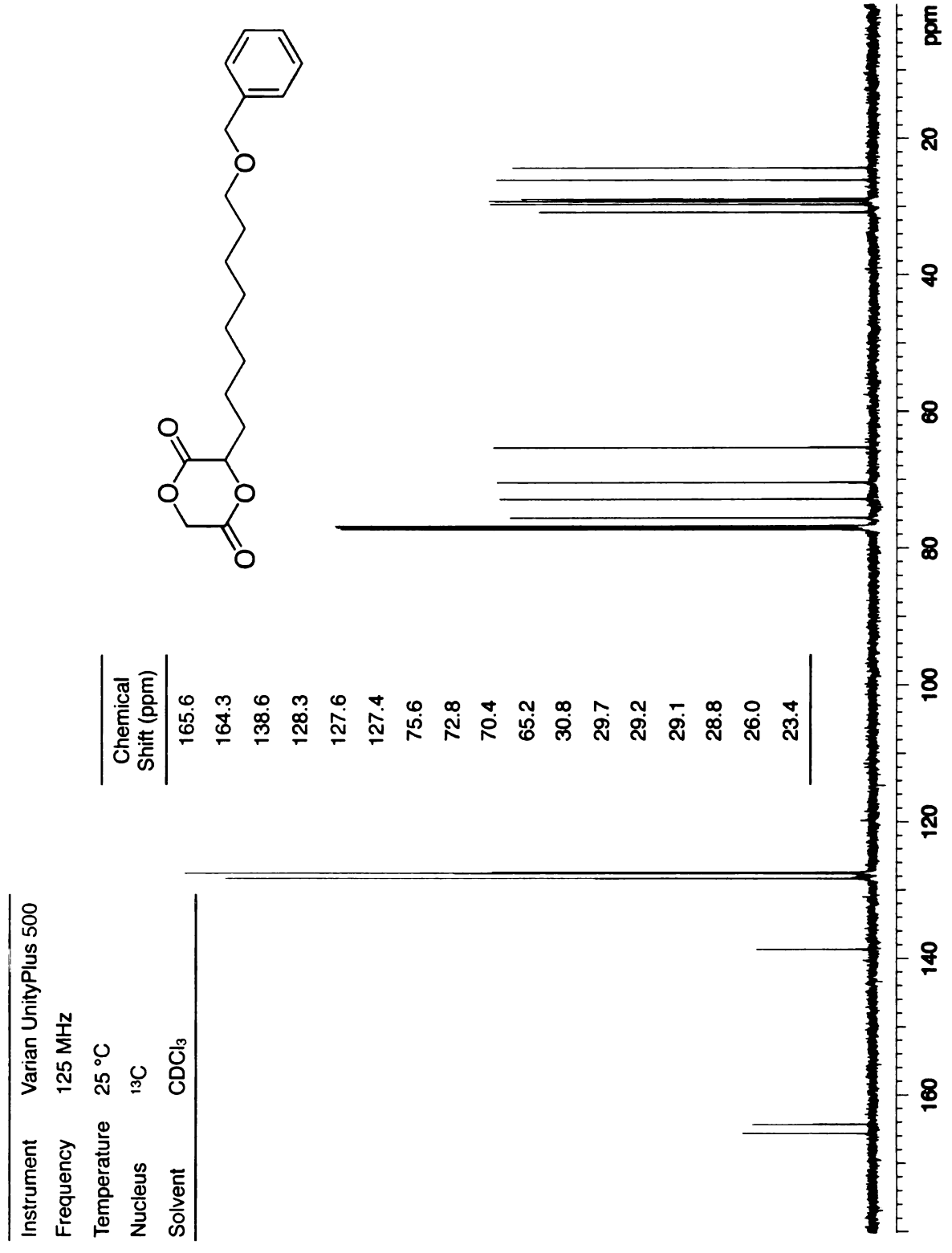

Appendix 18. ^{13}C NMR spectra 3-(8-(benzyloxy)octyl-1,4-dioxane-2,5-dione (BOG).

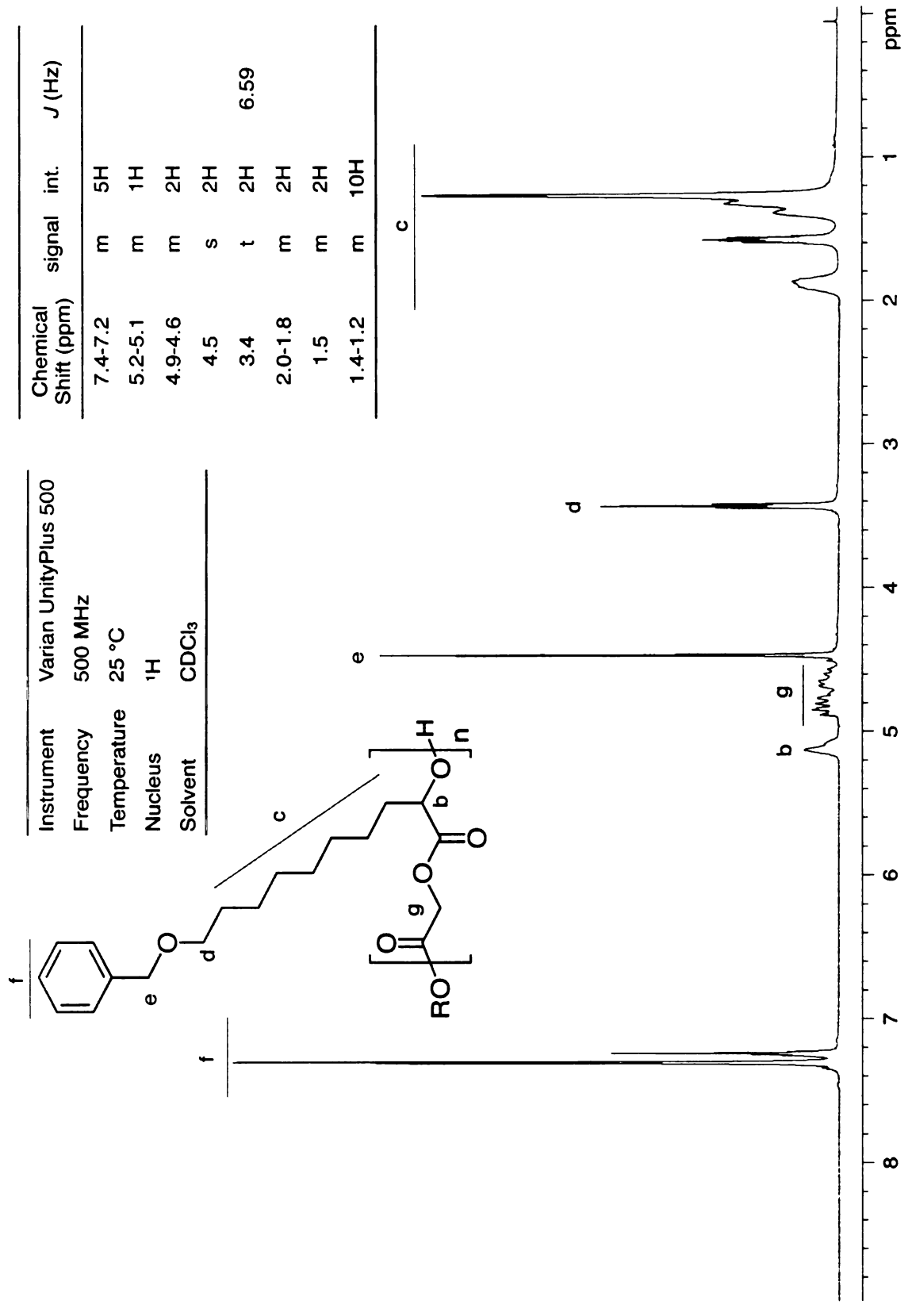

Appendix 19. ^1H NMR spectra of poly(BOG).

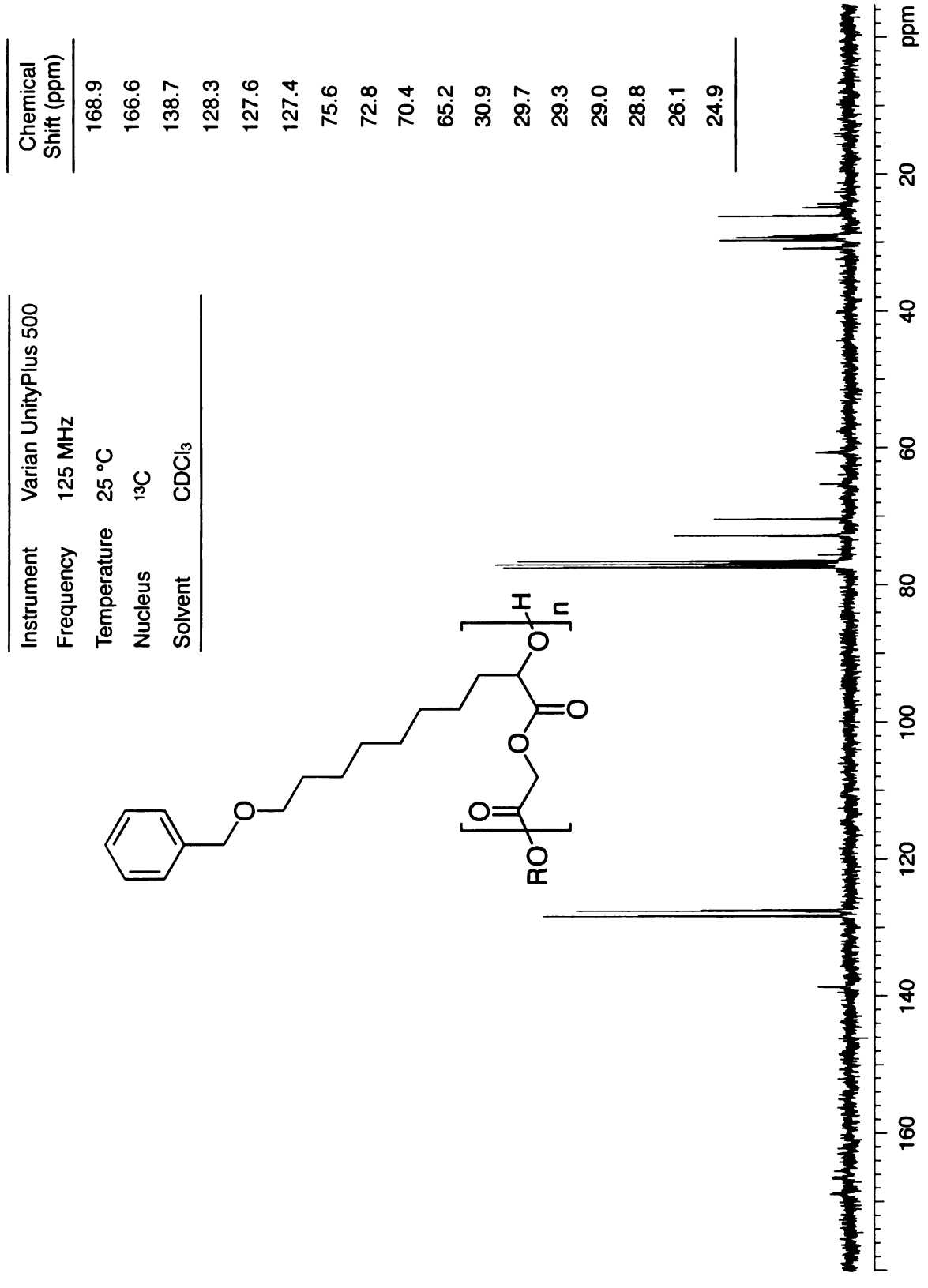

Appendix 20. ^{13}C NMR spectra of poly(BOG).

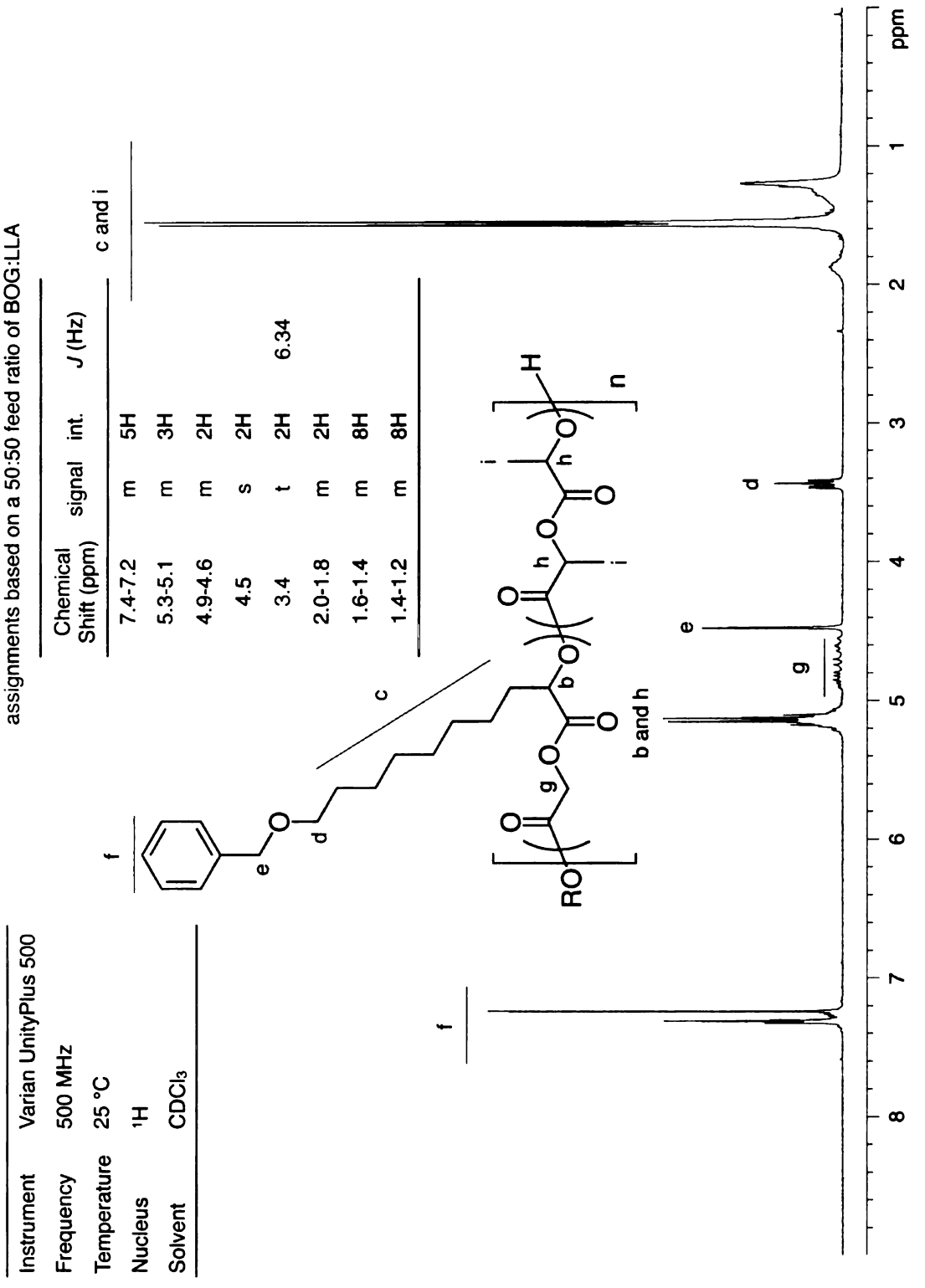

Appendix 21. ^{1}H NMR spectra of poly(BOG-*co*-LLA).

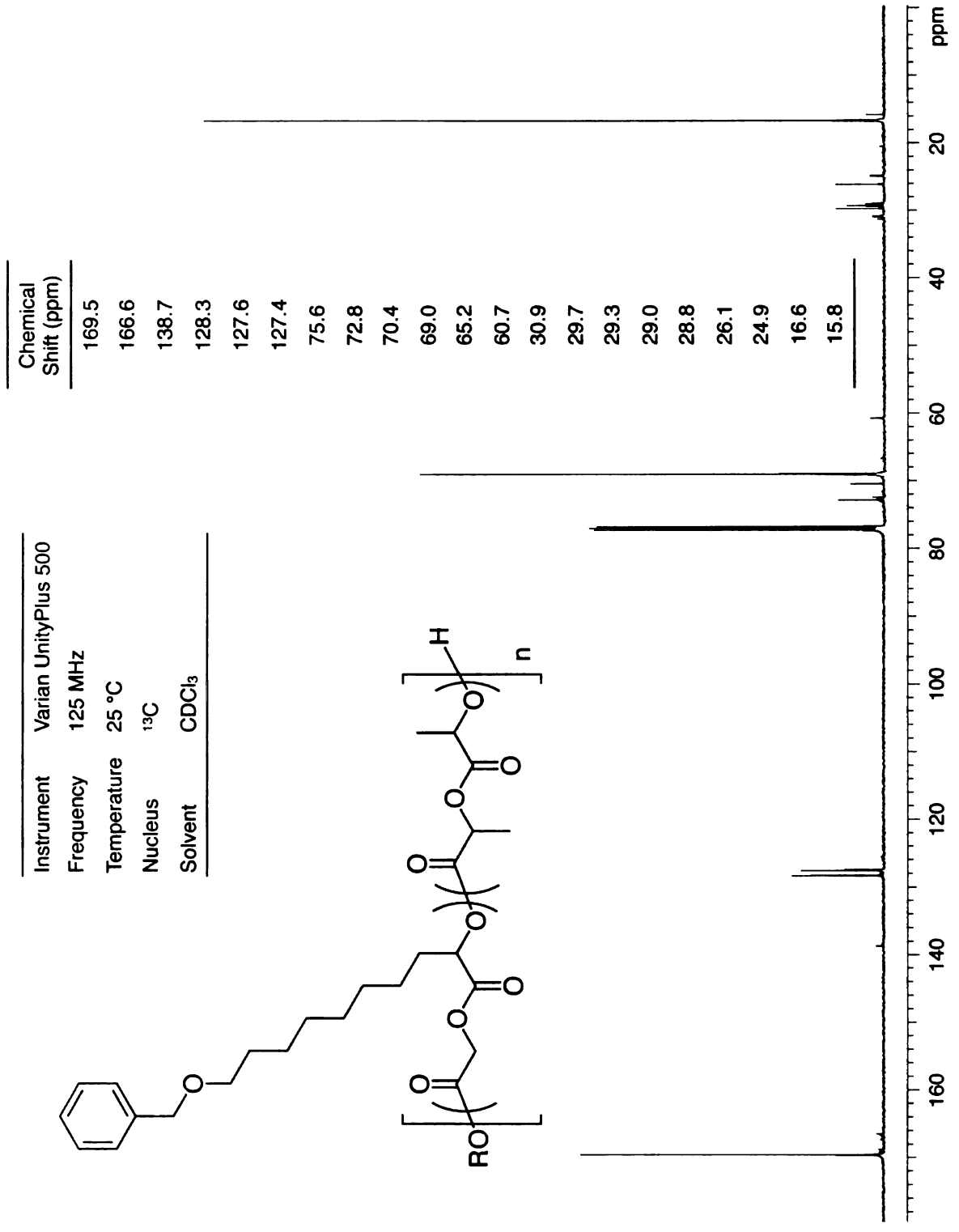

Appendix 22. ^{13}C NMR spectra of poly(BOG-*co*-LLA).

Appendix 23. ^{1}H NMR spectra of poly(HOG).

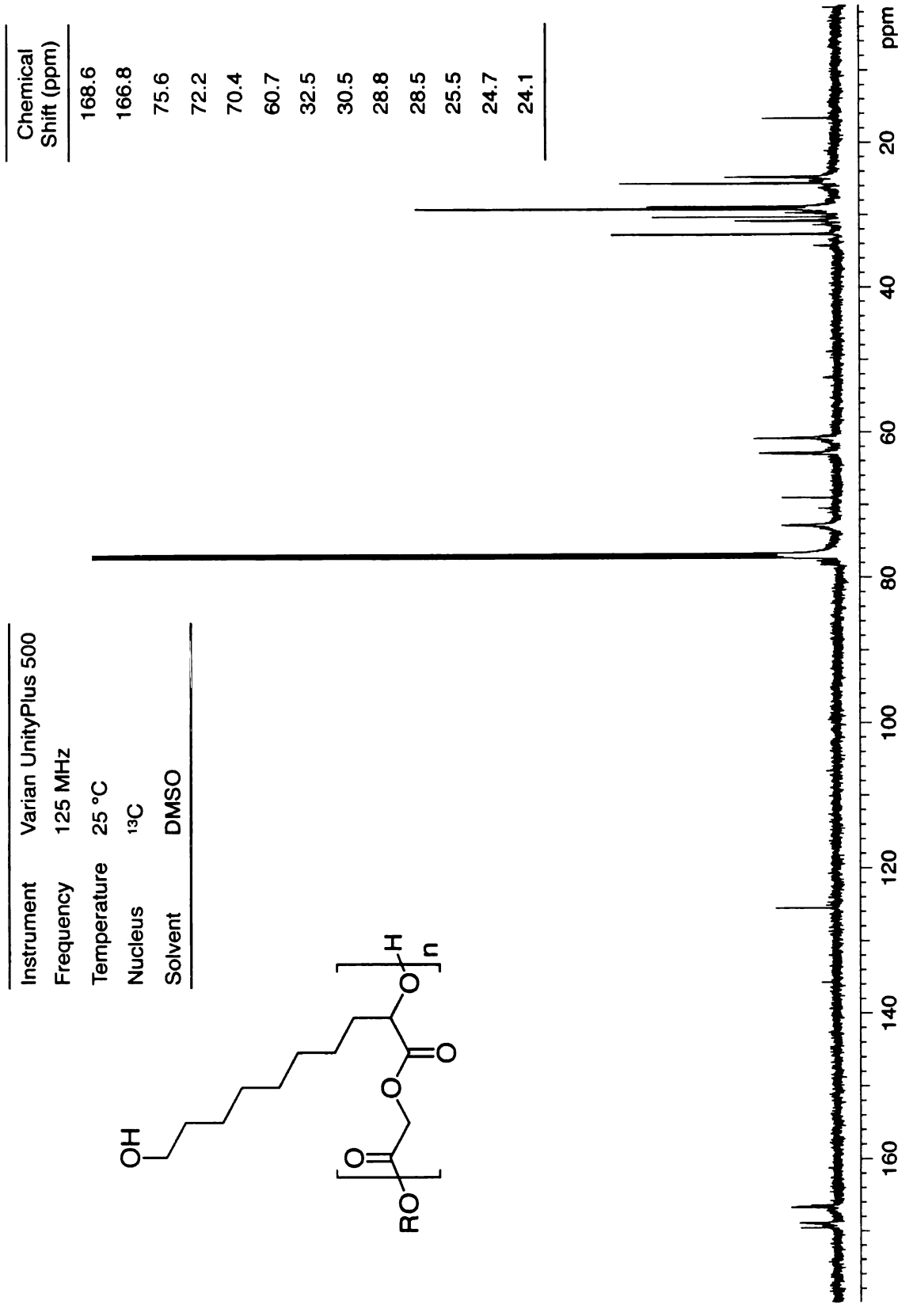

Appendix 24. ^{13}C NMR spectra of poly(HOG).

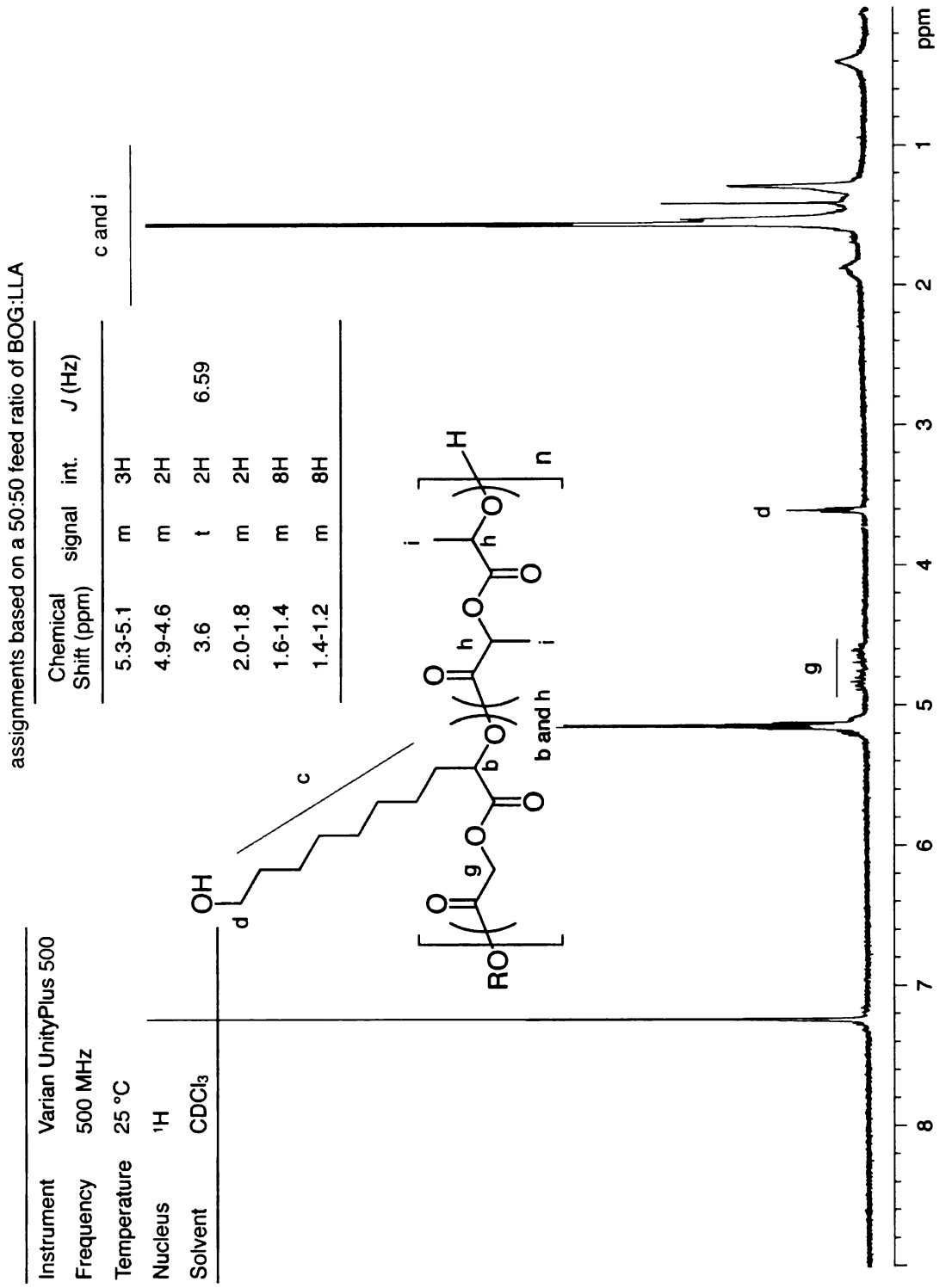

Appendix 25. ^{1}H NMR spectra of poly(HOG-*co*-LLA).

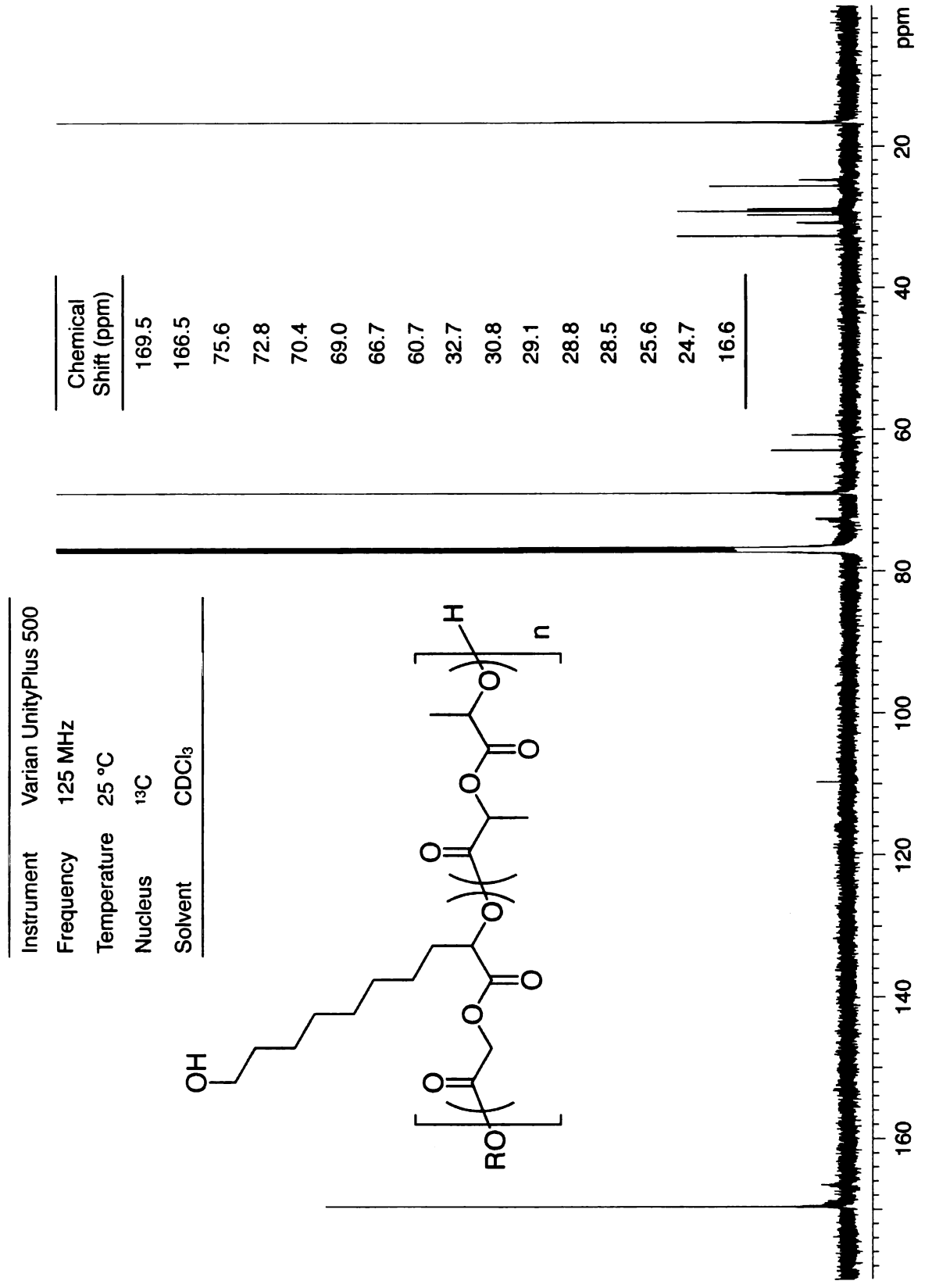

Appendix 26. ^{13}C NMR spectra of poly(HOG-*co*-LLA).

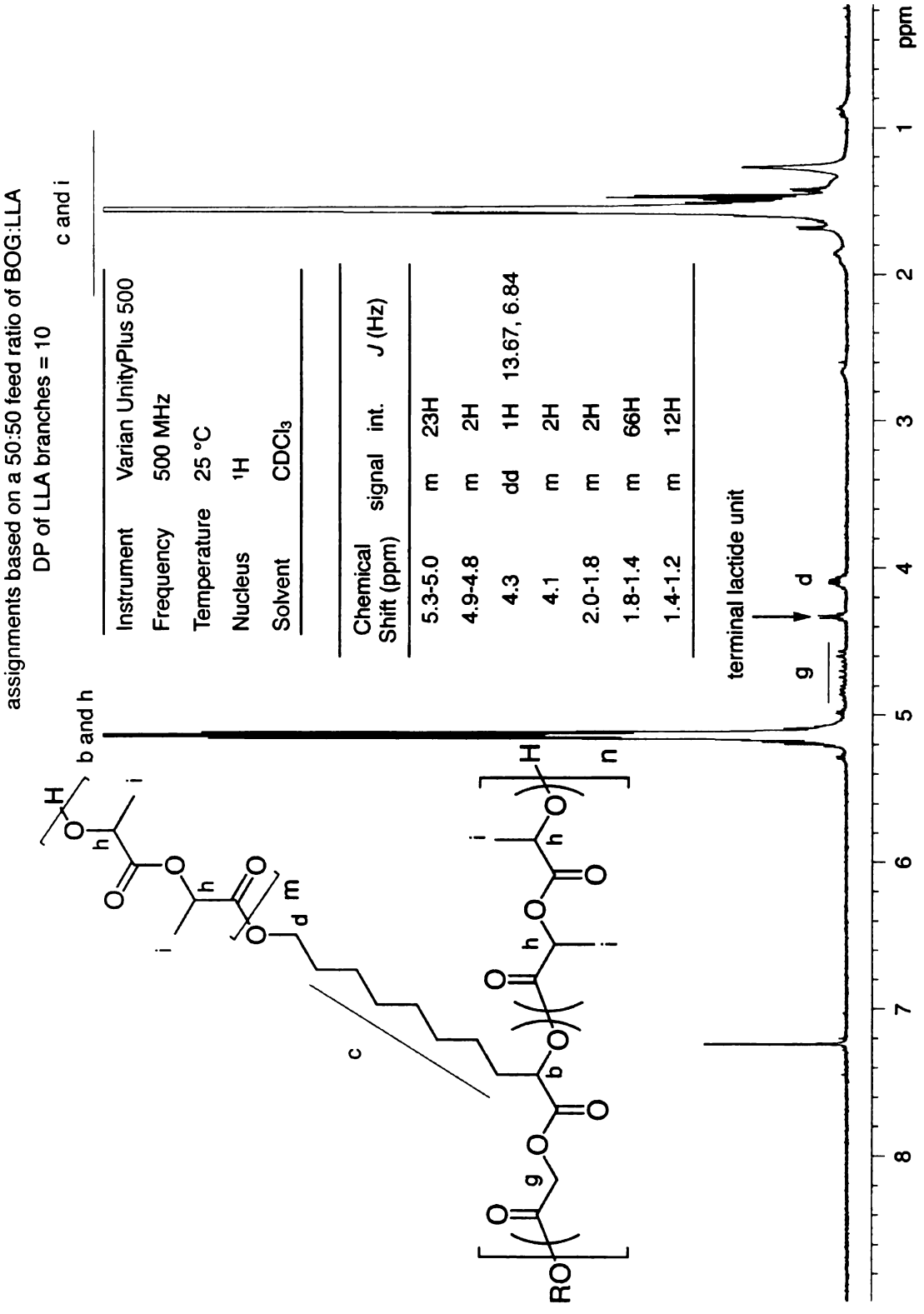

Appendix 27. ^{1}H NMR of poly((HOG-*co*-LLA)-*g*-LLA).

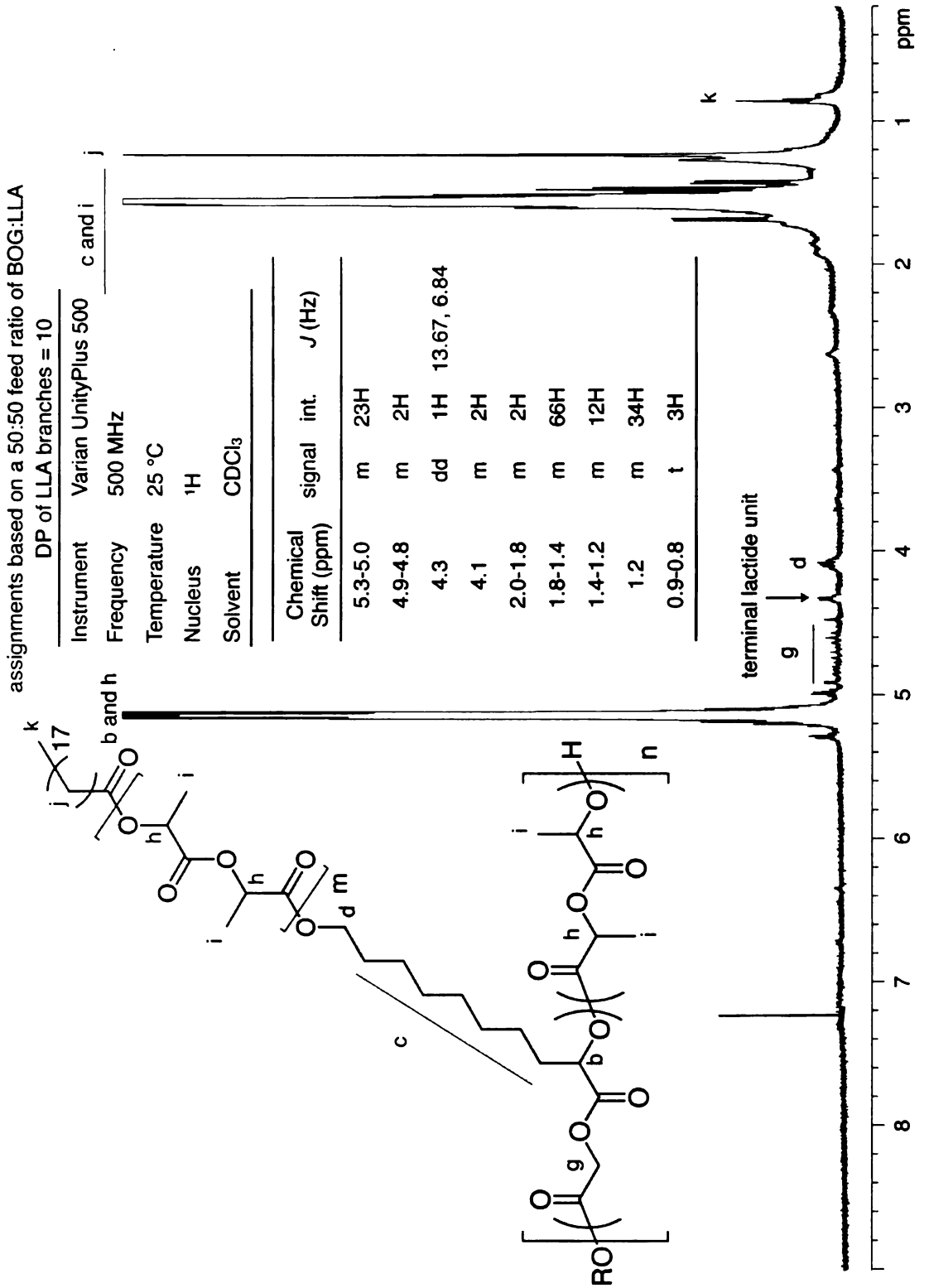

Appendix 28. ^{1}H NMR of poly((HOG-*co*-LLA)-*g*-LLA), stearic acid terminated.

Appendix 29. ^{1}H NMR spectra of propargylglycolide.

Appendix 30. ^{13}C NMR spectra of propargylglycolide.

Appendix 31. ^{1}H NMR spectra of poly(propargylglycolide).

Appendix 32. ^{13}C NMR spectra of poly(propargylglycolide).

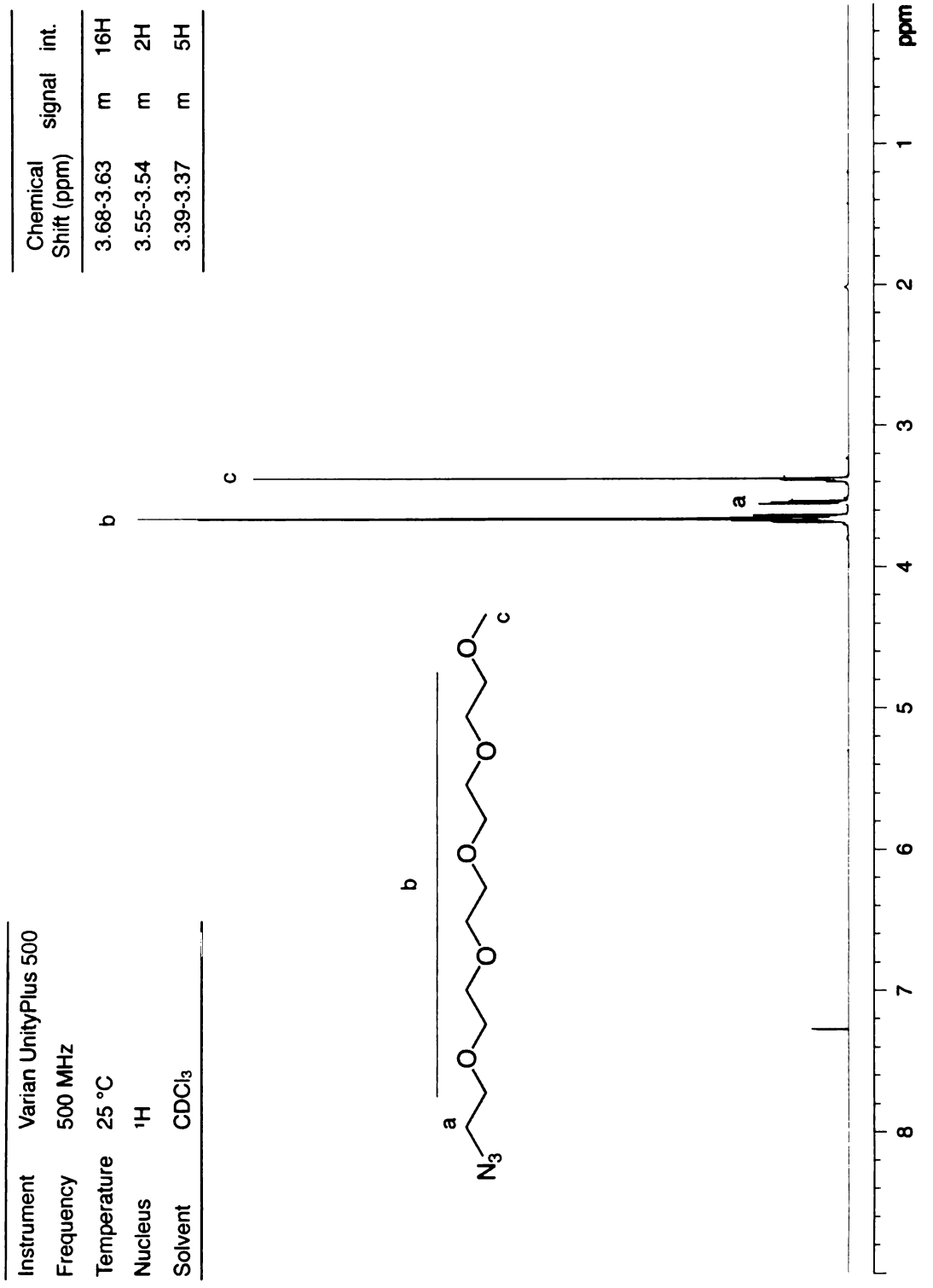

Appendix 33. ^{1}H NMR spectra of 16-azido-2,5,8,11,14-pentaoxahexadecane (mPEG).

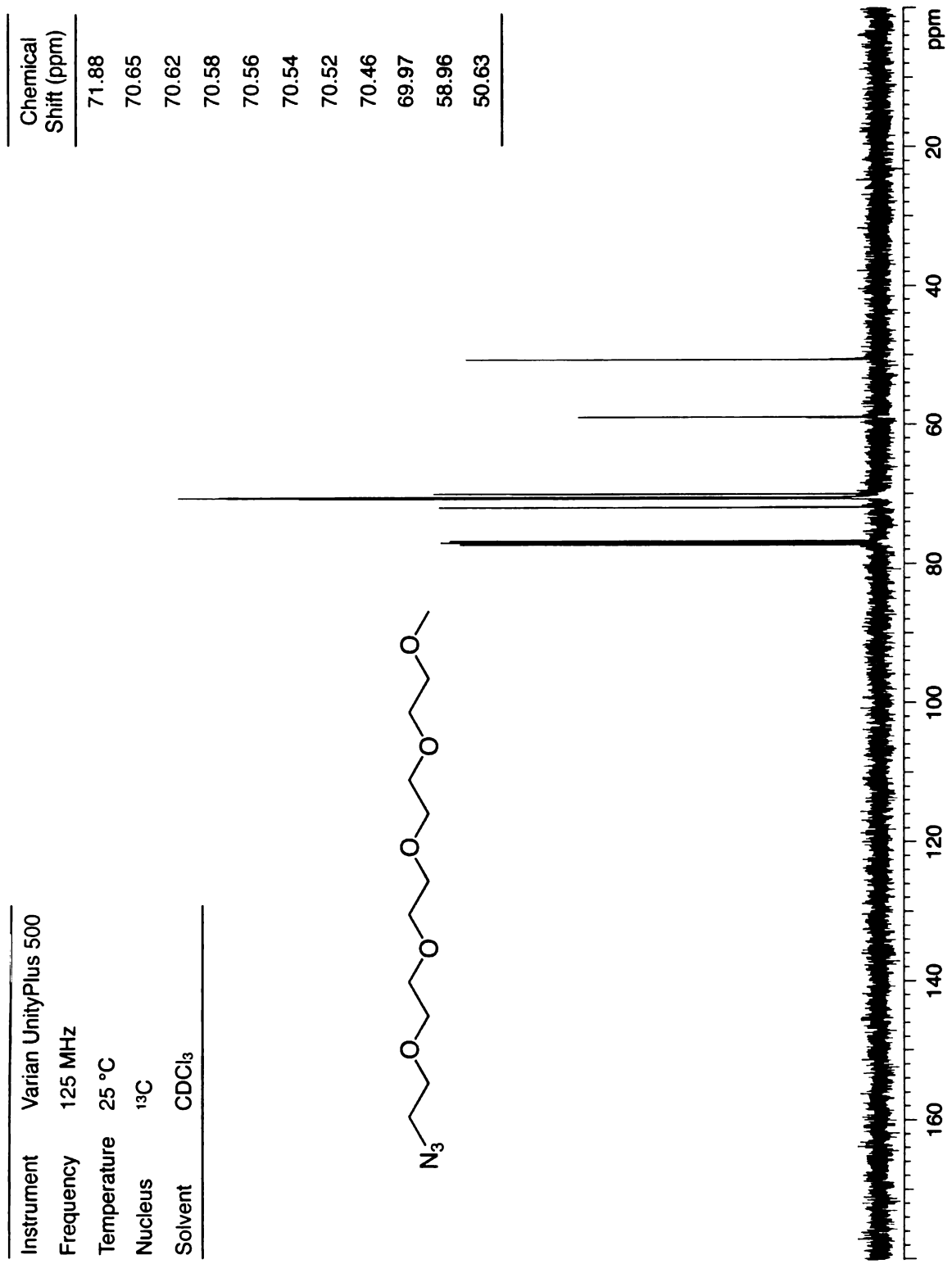

Appendix 34. ^{13}C NMR spectra of 16-azido-2,5,8,11,14-pentaoxahexadecane (mPEG).

Appendix 35. ^{1}H NMR spectra of PPGL-*g*-mPEG.

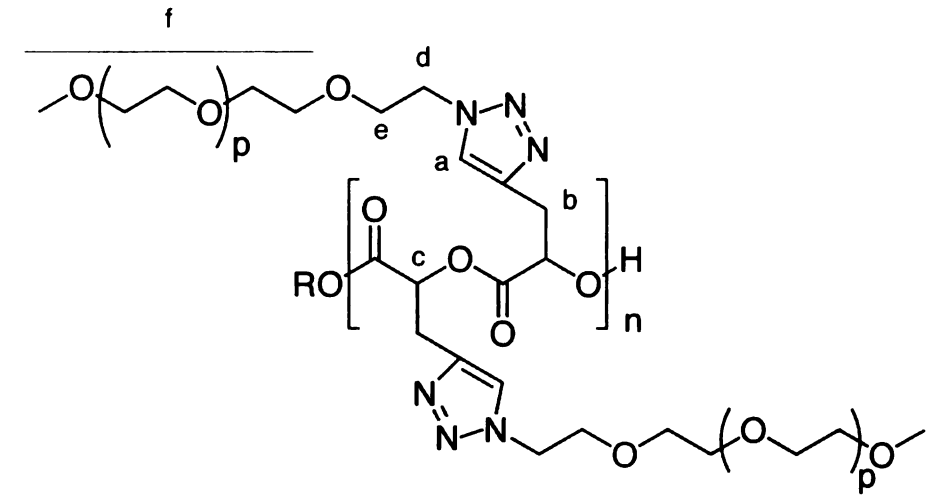

Instrument	Varian UnityPlus 500
Frequency	500 MHz
Temperature	25 °C
Nucleus	^{1}H
Solvent	$CDCl_3$

Chemical Shift (ppm)	signal	int.
7.8-7.4	b	1H
5.6-5.2	b	1H
4.5-4.4	b	2H
3.9-3.7	b	2H
3.6-3.4	b	16H
3.3	b	3H
3.3-3.2	b	2H

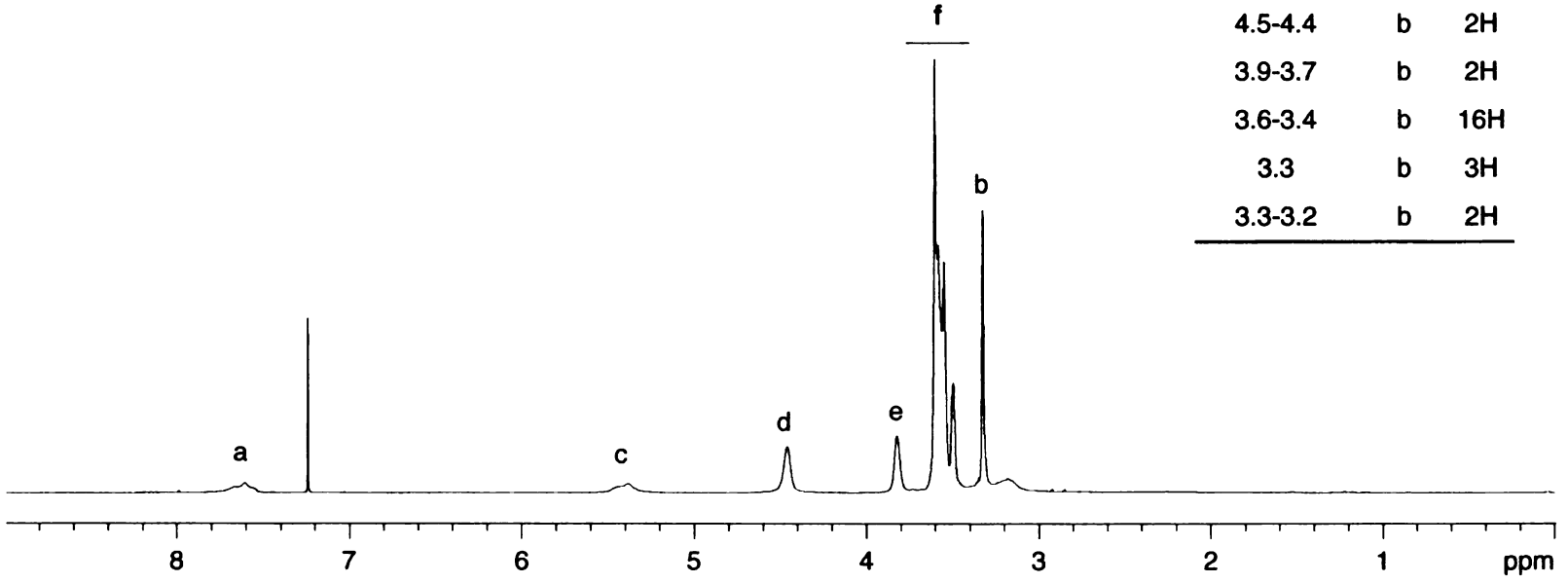

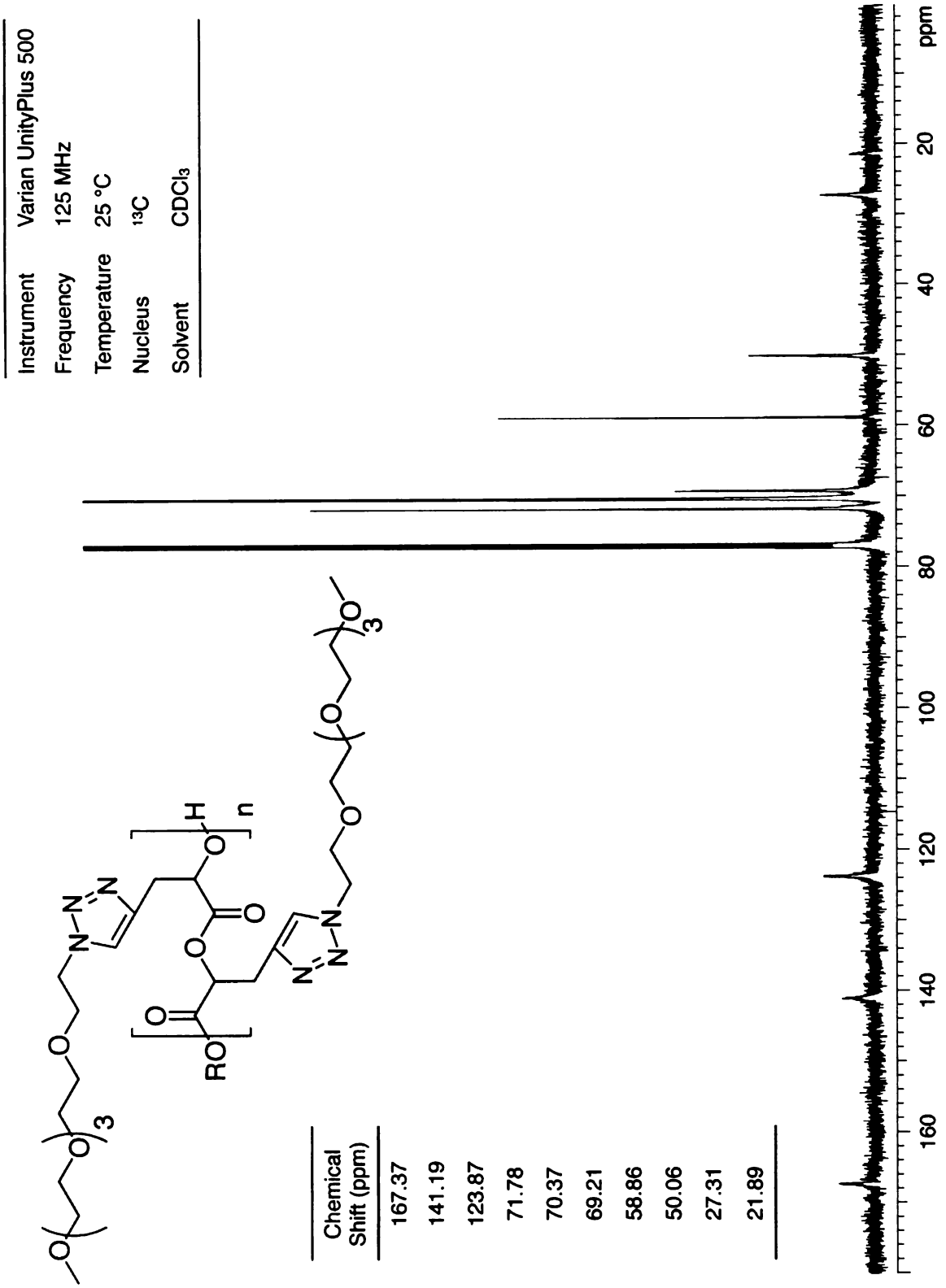

Appendix 36. ^{13}C NMR spectra of PPGL-*g*-mPEG.

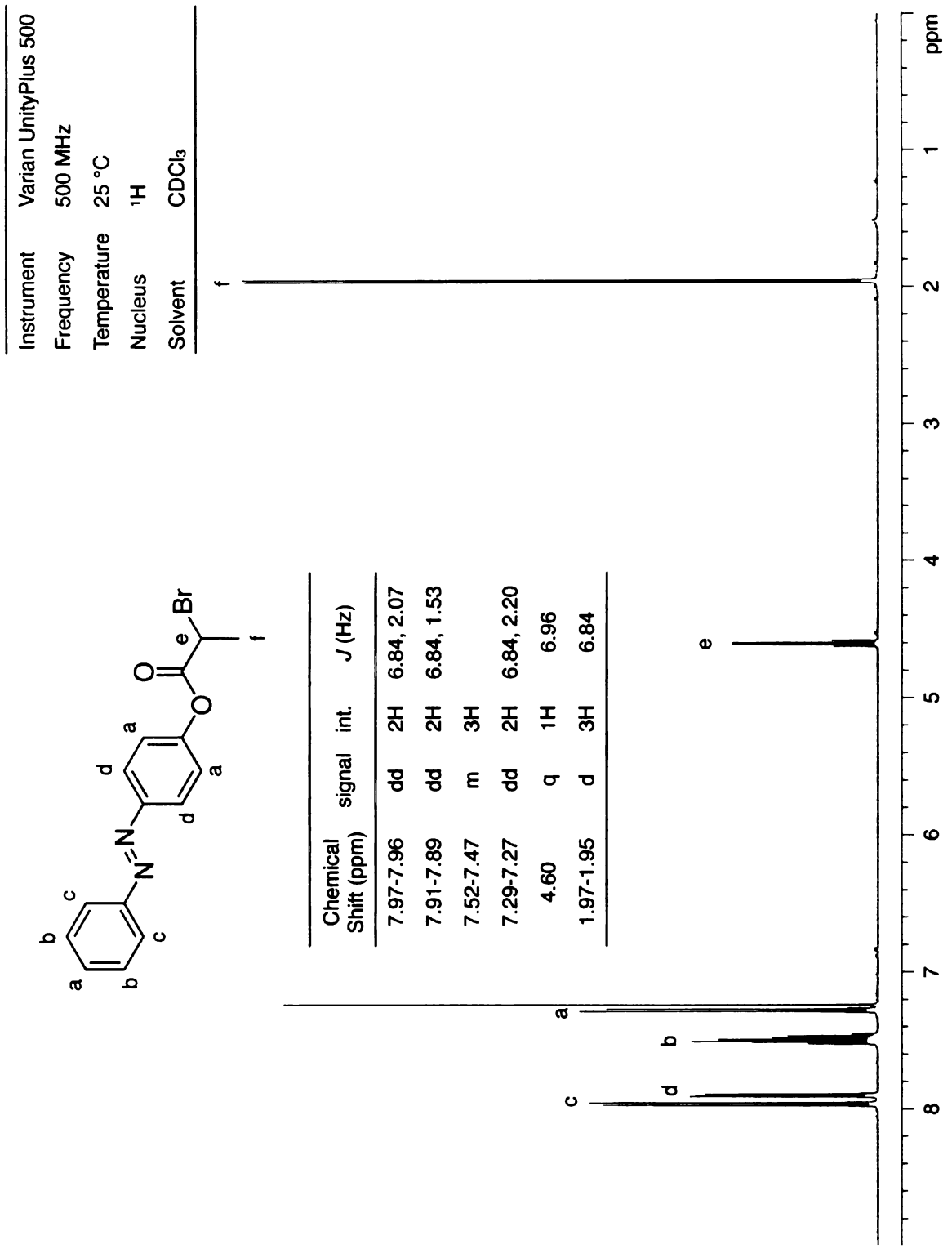

Appendix 37. ^{1}H NMR spectra of 2-bromopropionic acid-2-(4-phenylazophenyl)ethyl ester.

Appendix 38. ^{13}C NMR spectra of 2-bromopropionic acid-2-(4-phenylazophenyl)ethyl ester.

Appendix 39. ^{1}H NMR spectra of 3-azidopropanol.

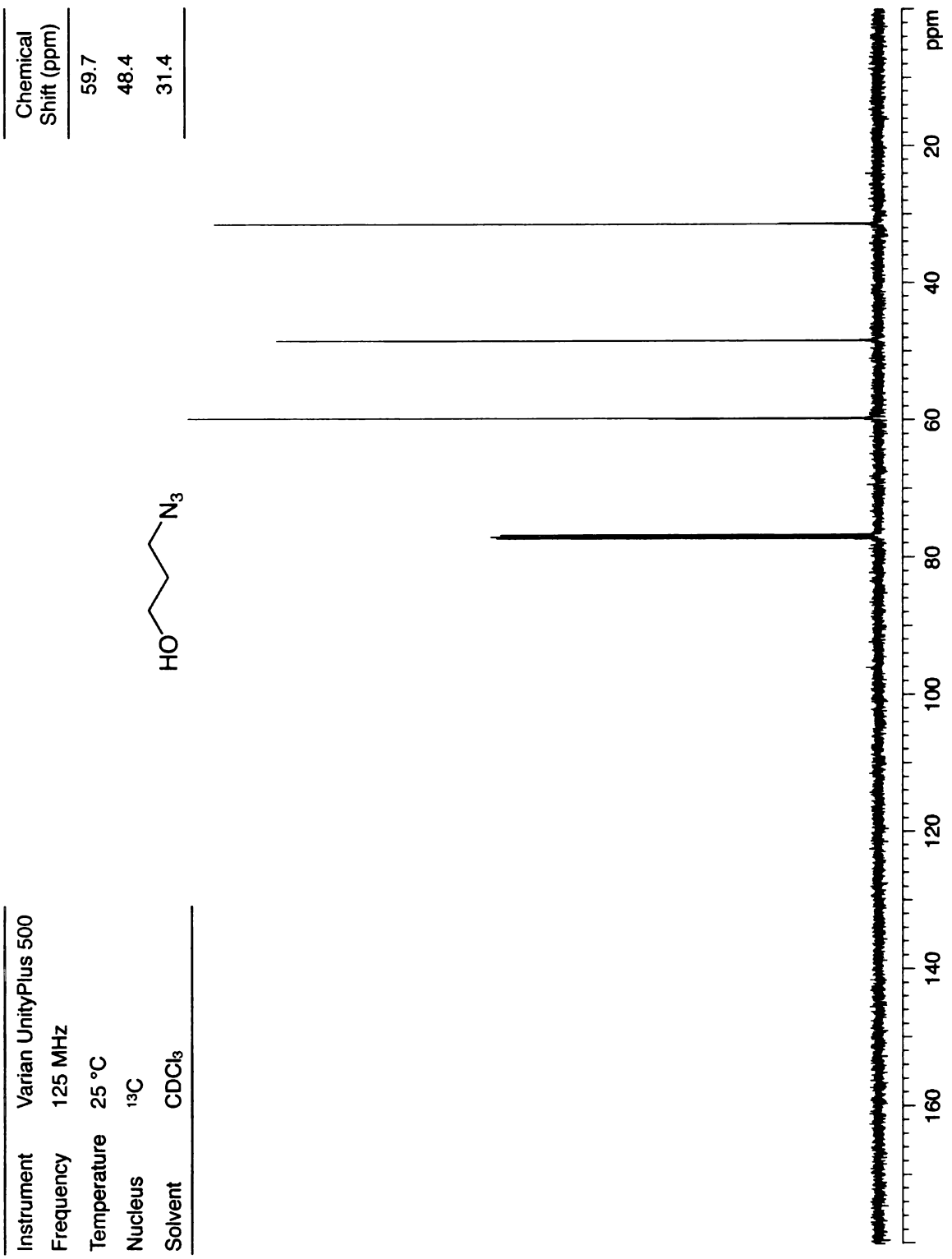

Appendix 40. ^{13}C NMR spectra of 3-azidopropanol.

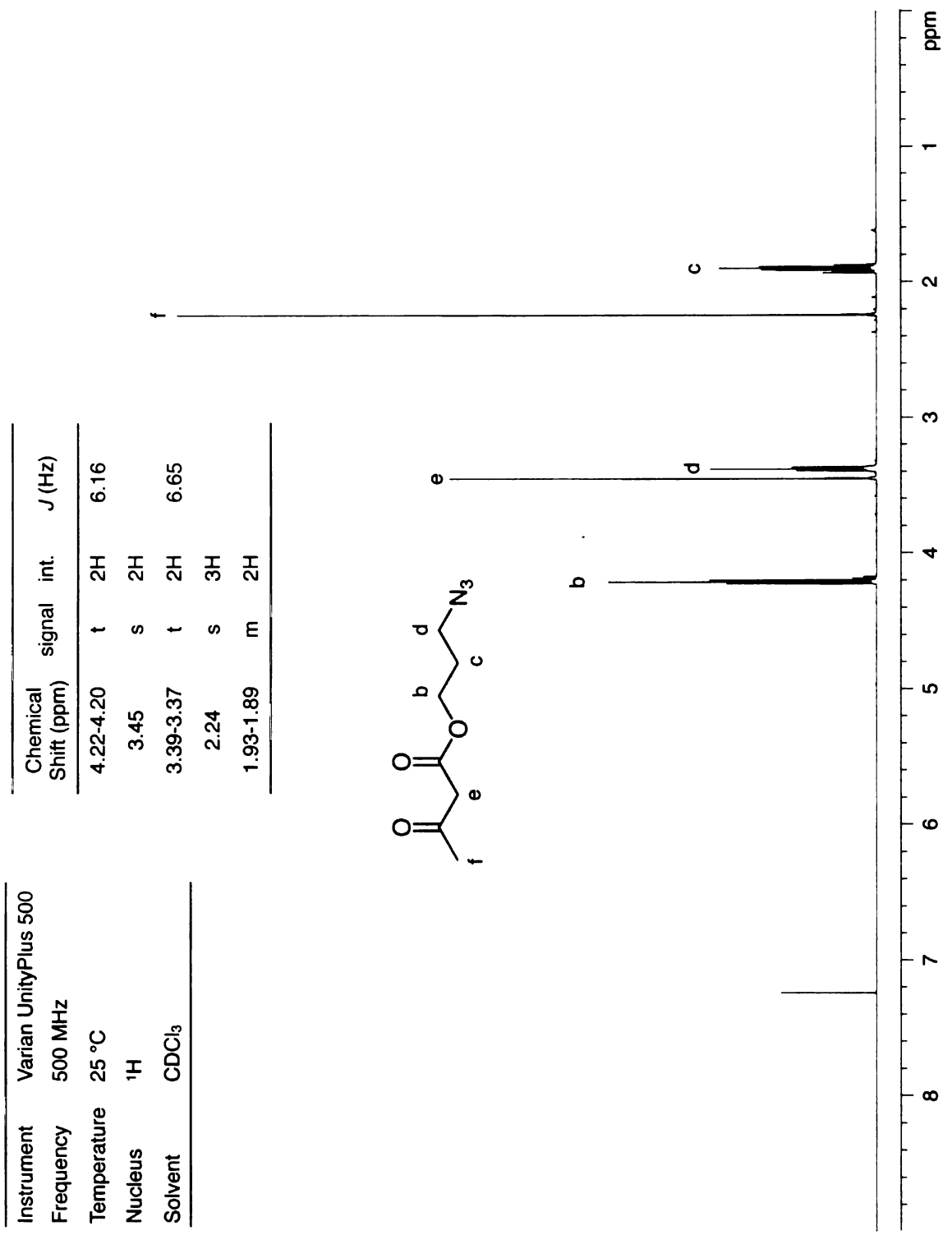

Appendix 41. ^{1}H NMR spectra of 3-azidopropyl-3-oxobutanoate.

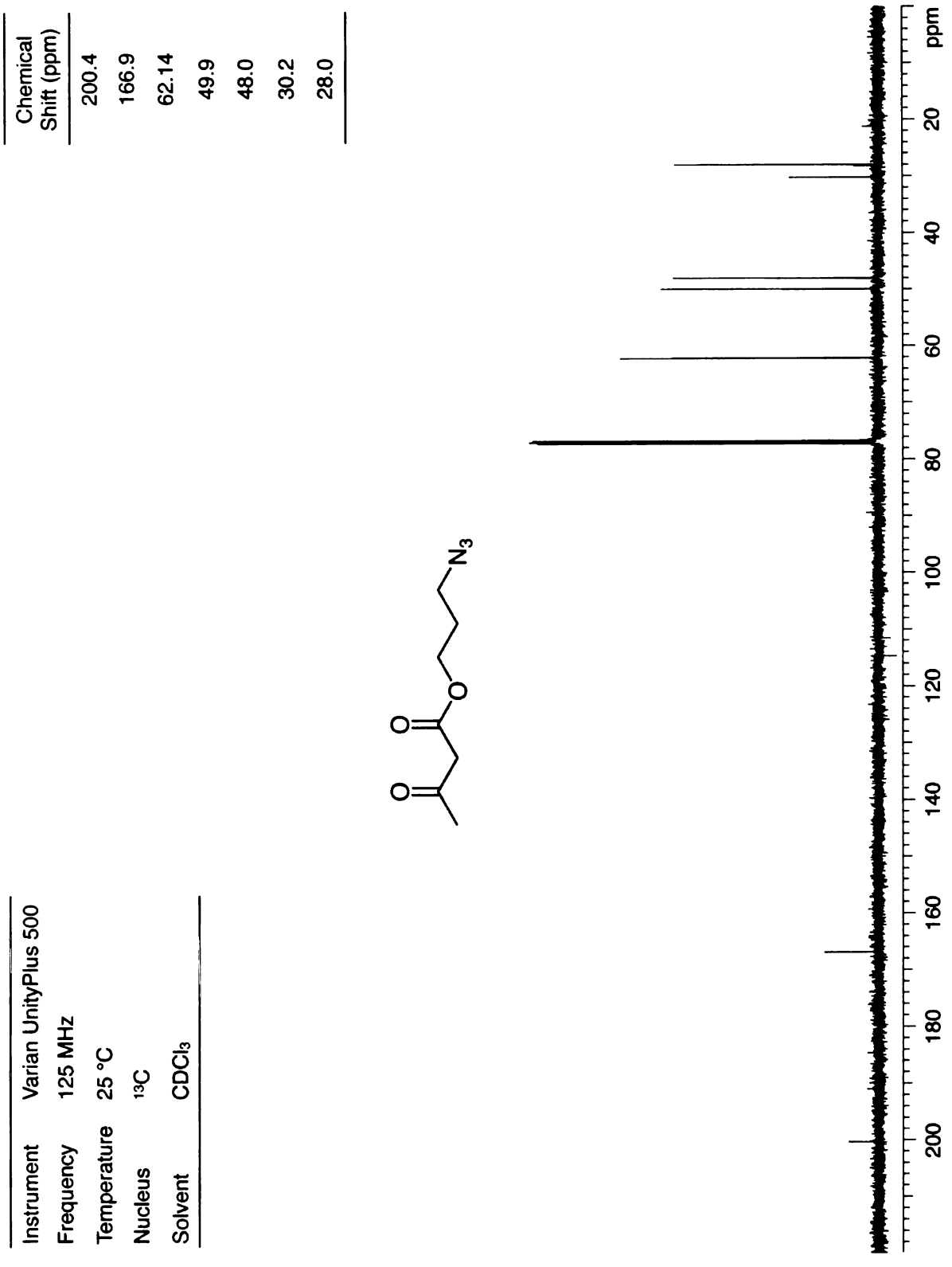

Appendix 42. ^{13}C NMR spectra of 3-azidopropyl 3-oxobutanoate.

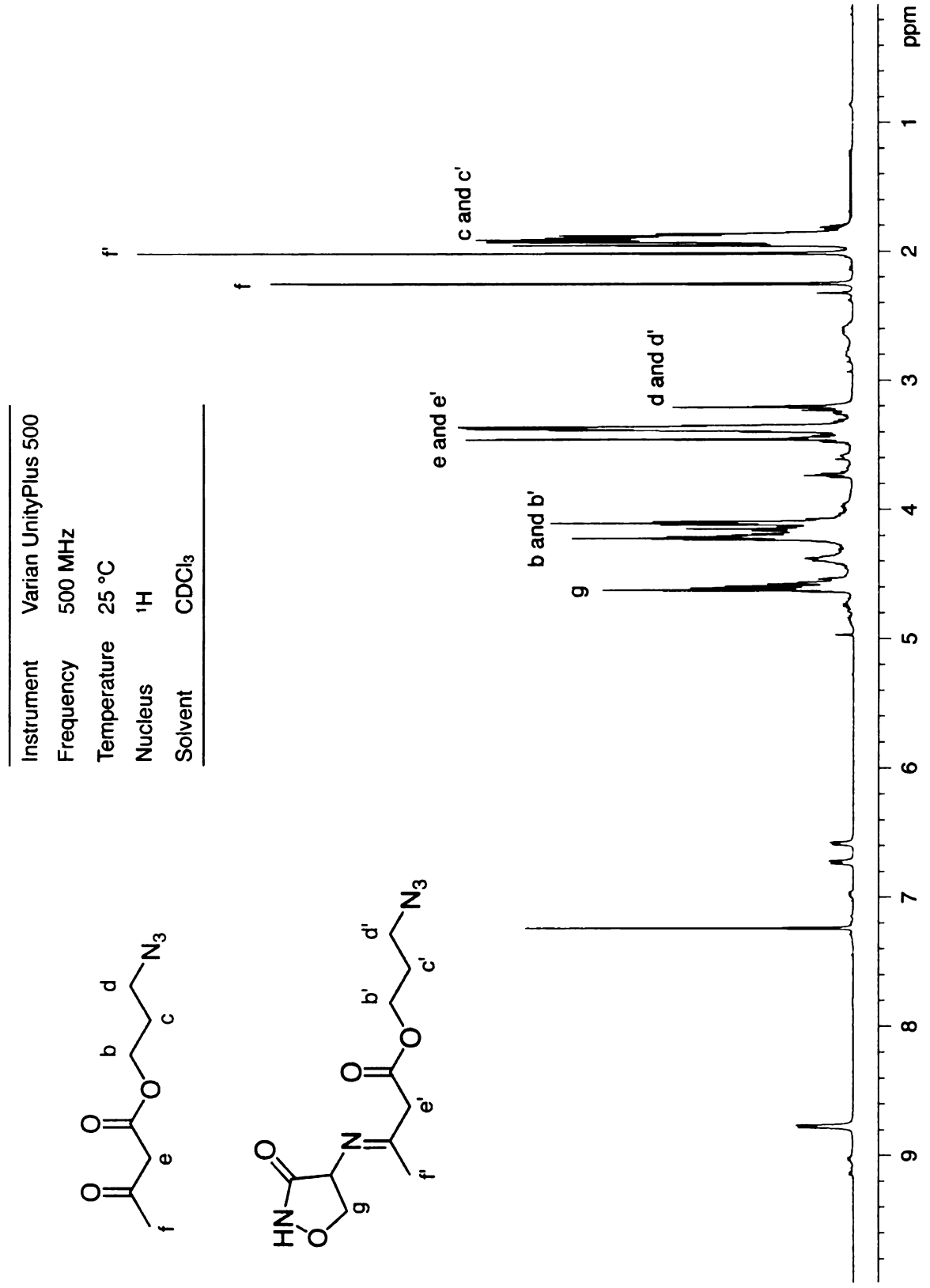

Appendix 43. ^{1}H NMR spectra of 3-azidopropyl 3-(2-oxo-tetrahydrofuran)-3-ylimino)butanoate.

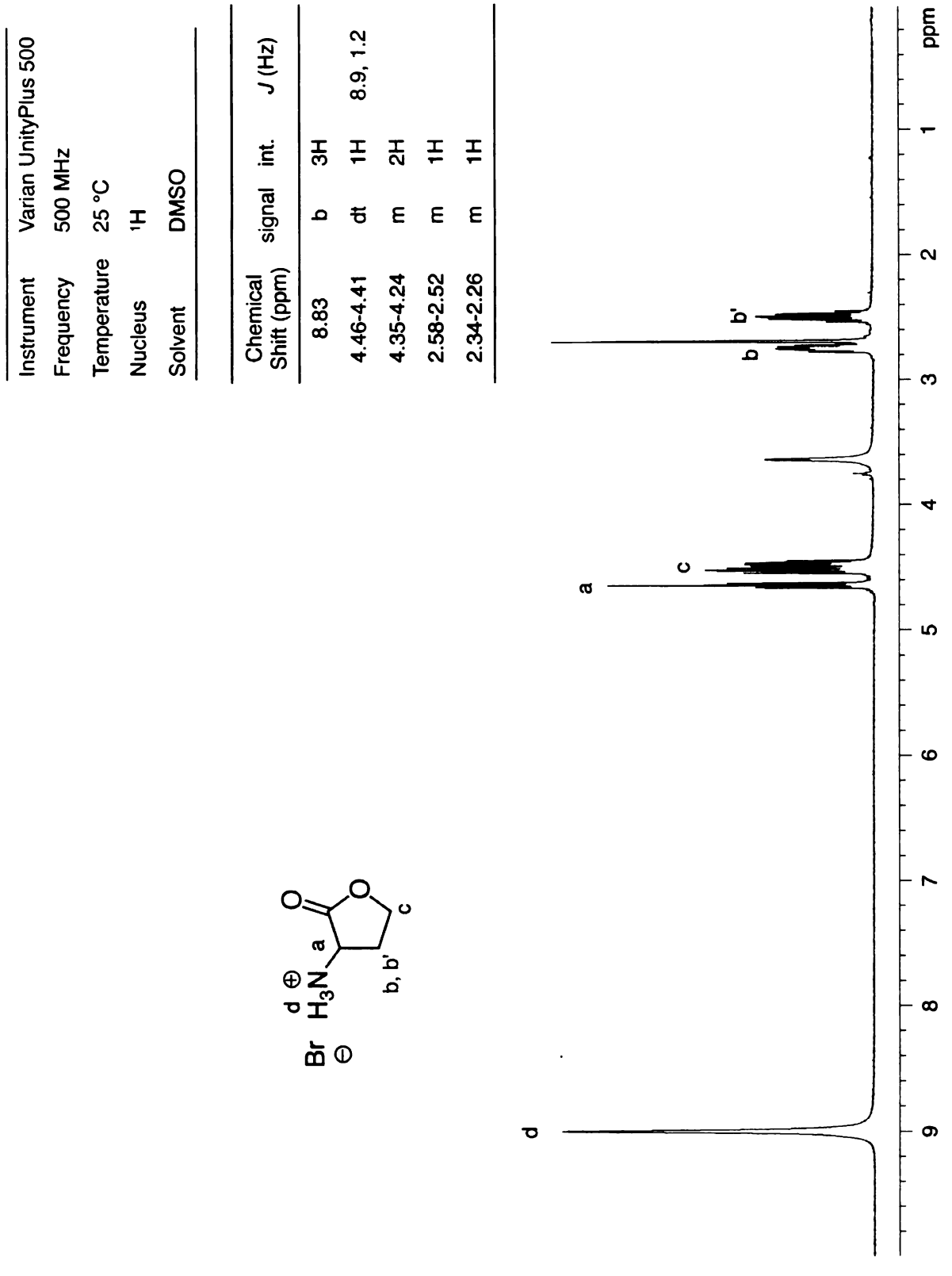

Appendix 44. ^{1}H NMR spectra of *L*-homoserine lactone hydrobromide.

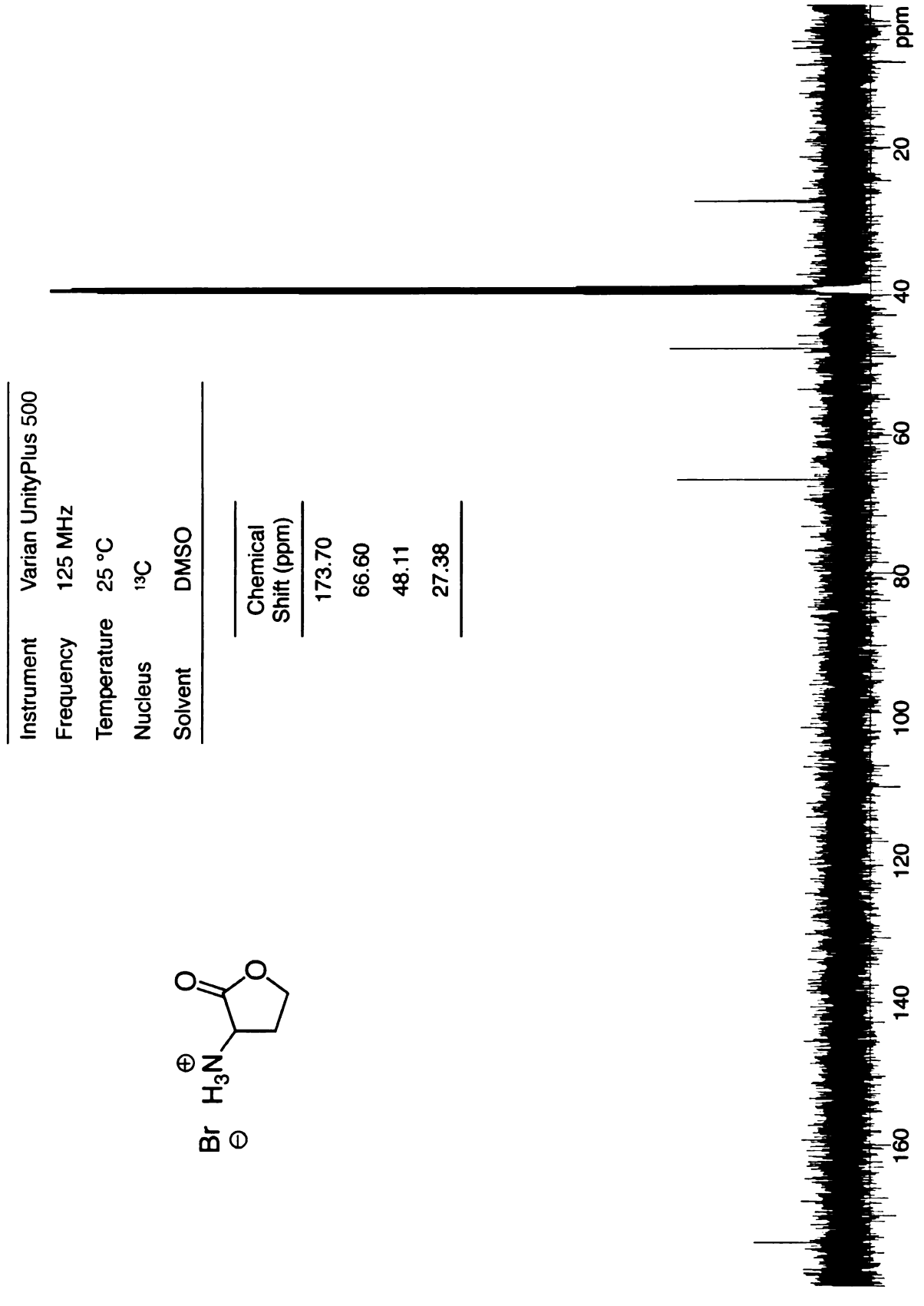

Appendix 45. ^{13}C NMR spectra of *L*-homoserine lactone hydrobromide.

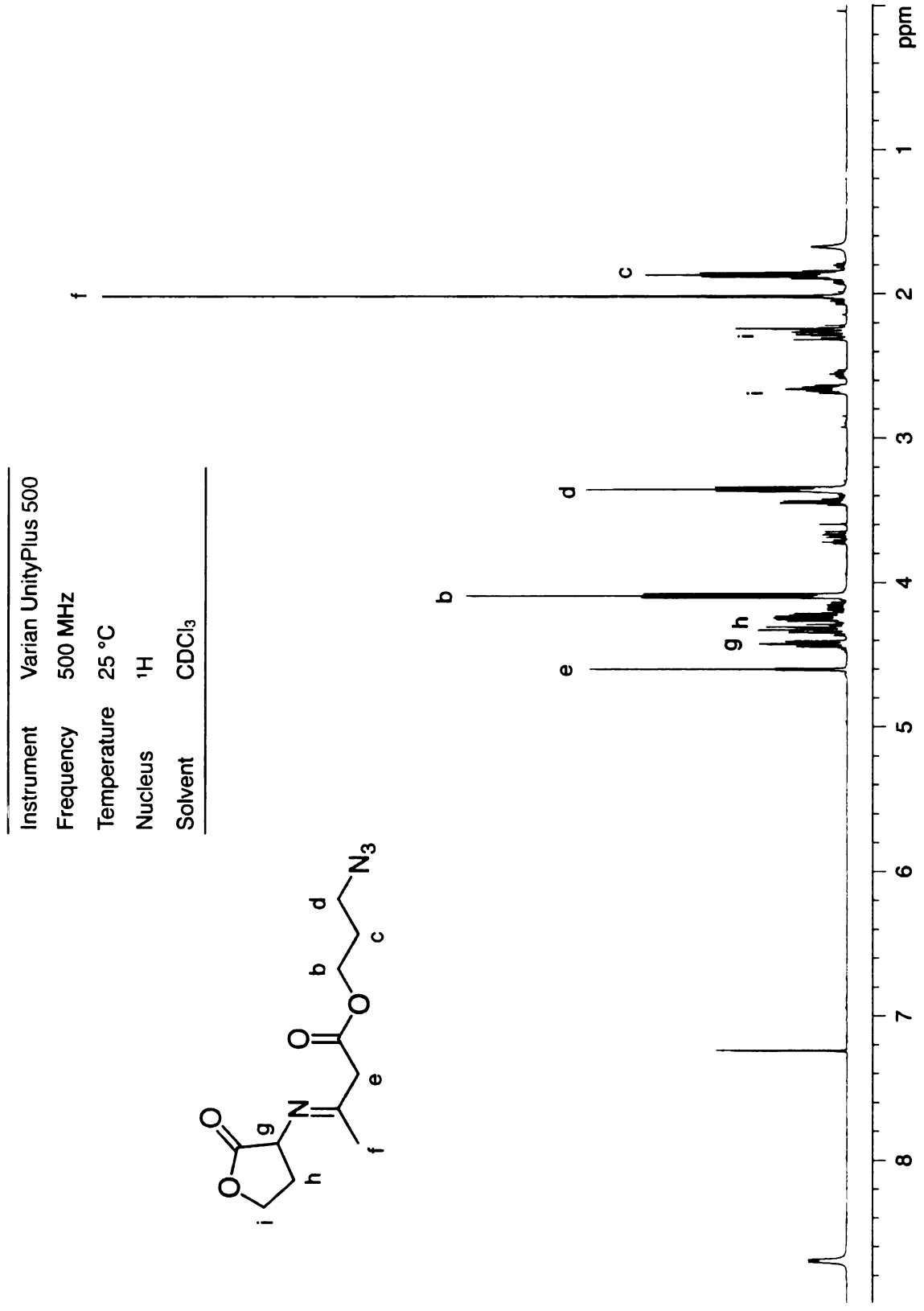

Appendix 46. ^{1}H NMR spectra of 3-azidopropyl-3-(3-oxoisoxazolidin-4-ylimino)butanoate.

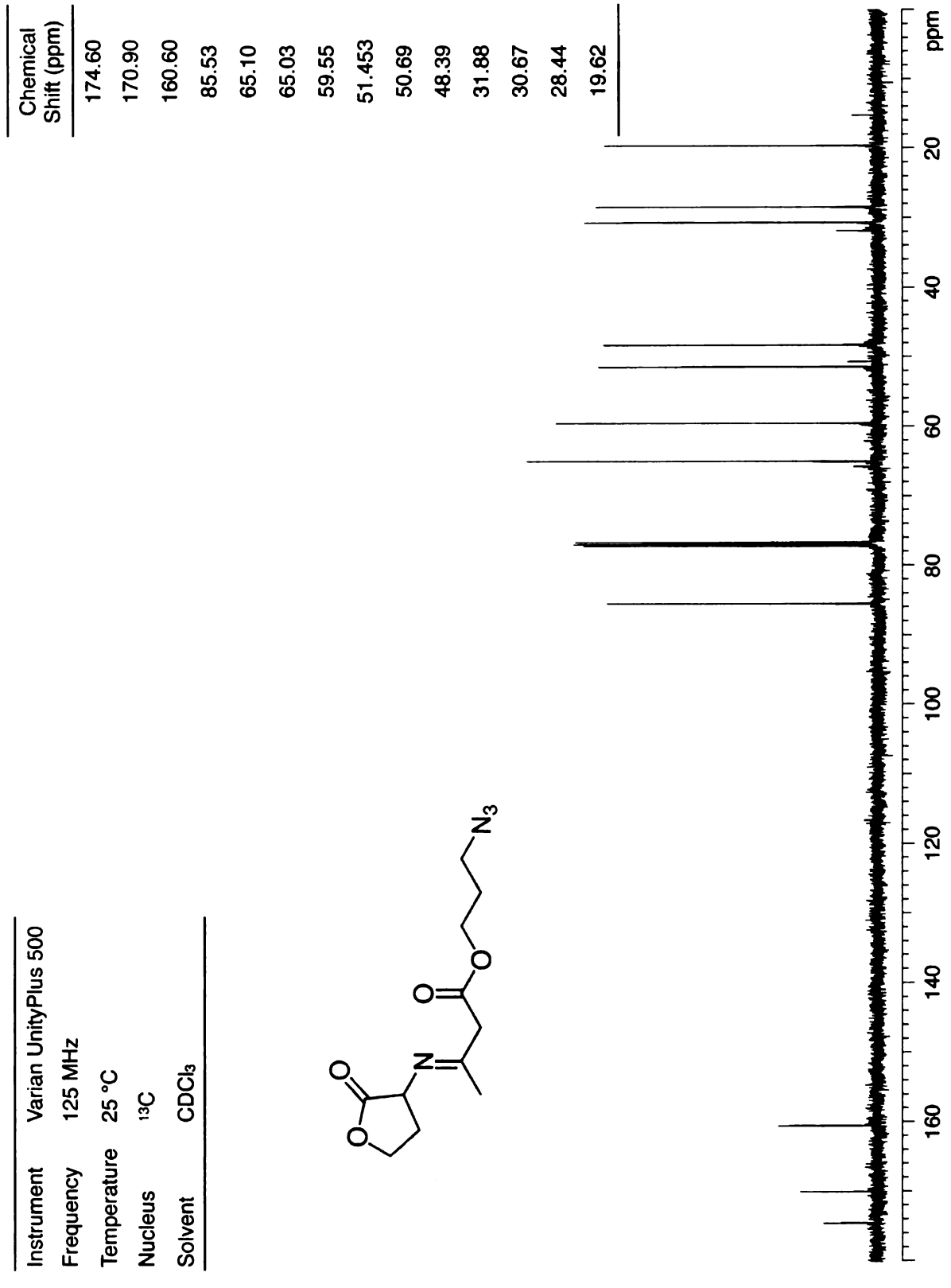

Appendix 47. ^{13}C NMR spectra of 3-azidopropyl-3-(3-oxoisoxazolidin-4-ylimino)butanoate.

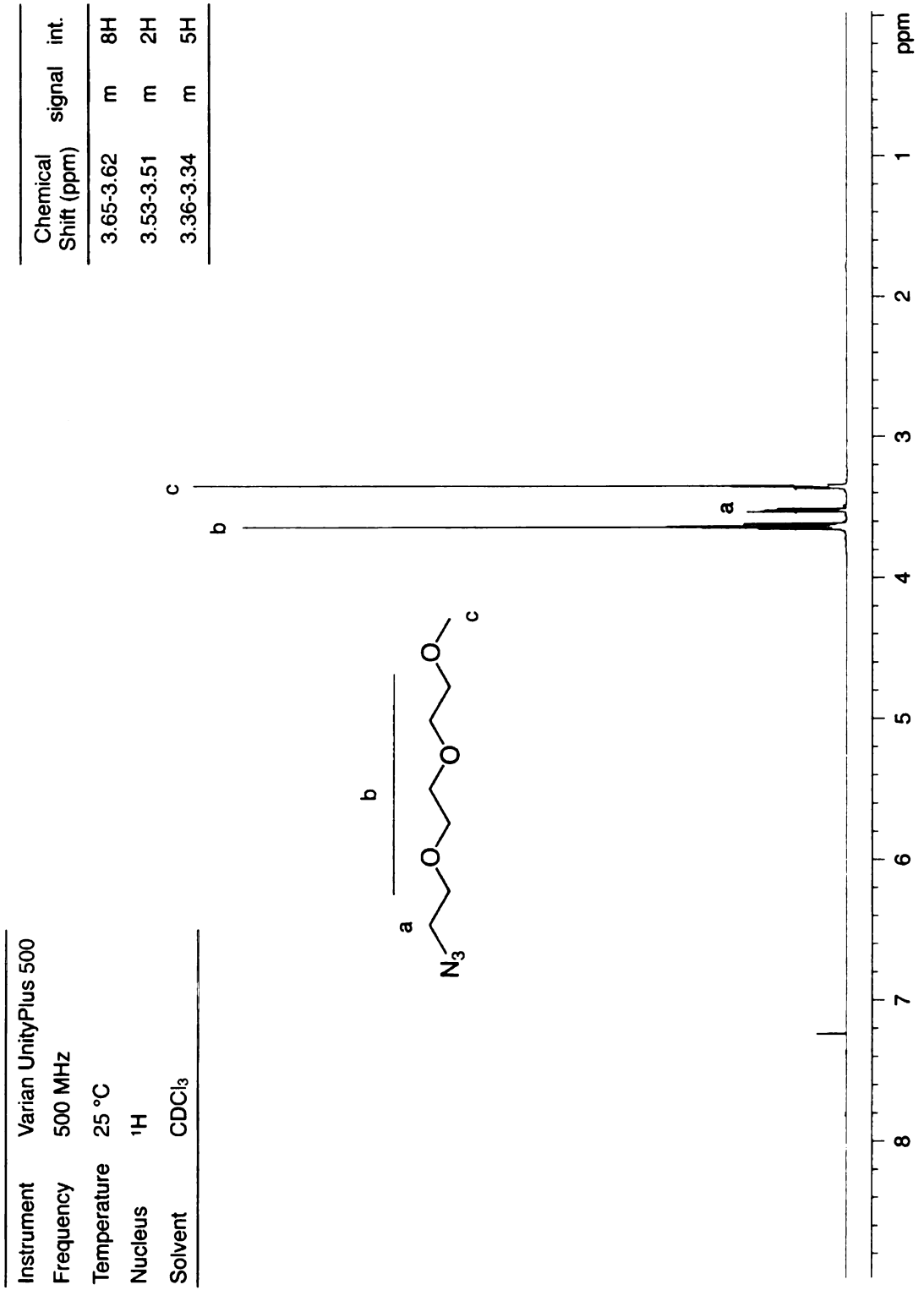

Appendix 48. ^{1}H NMR spectra of 1-azido-2-(2-(2-methoxyethoxy)ethoxy)ethane (mDEG).

Appendix 49. ^{13}C NMR spectra of 1-azido-2-(2-(2-methoxyethoxy)ethoxy)ethane (mDEG).

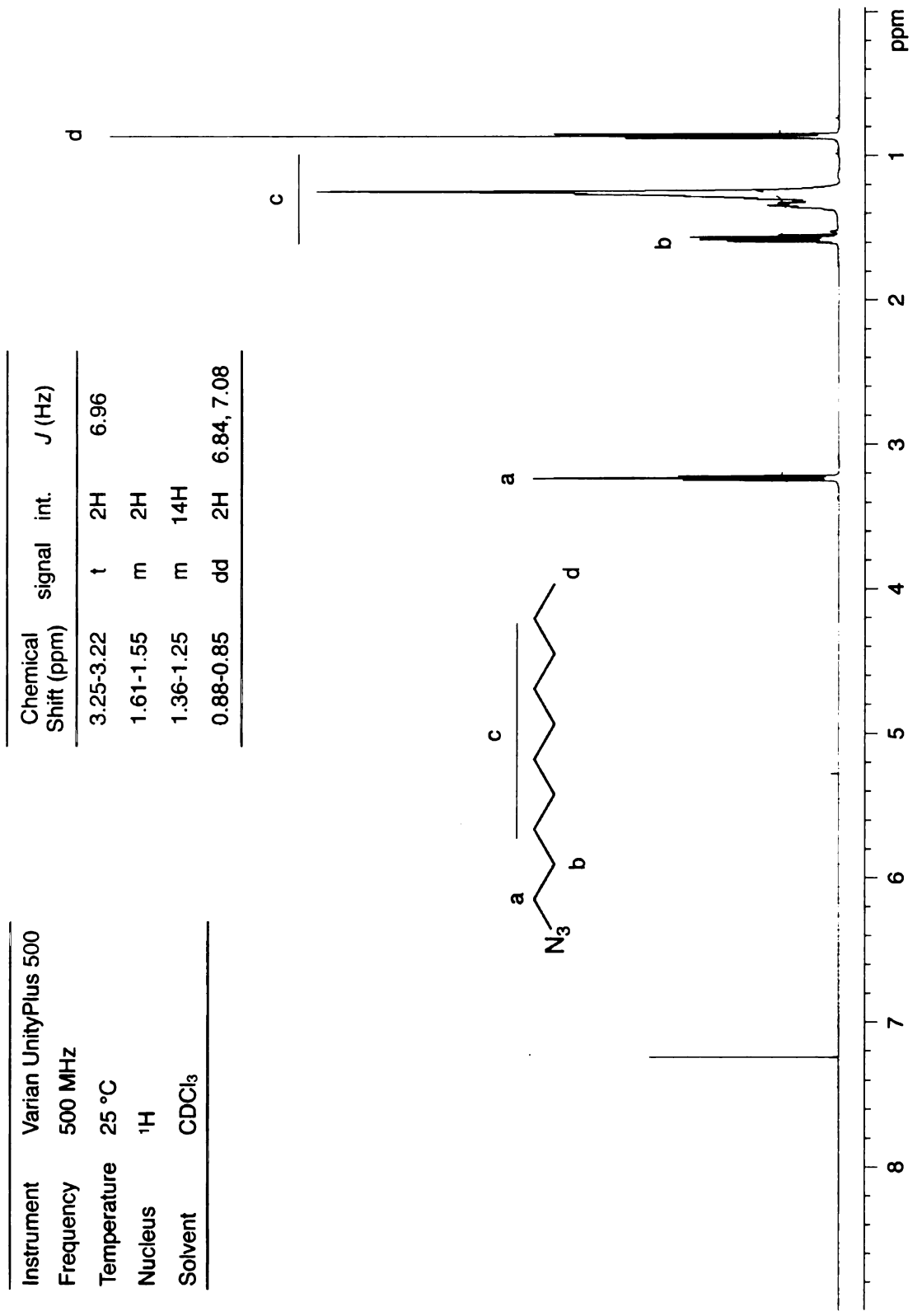

Appendix 50. ^1H NMR spectra of 1-azidodecane.

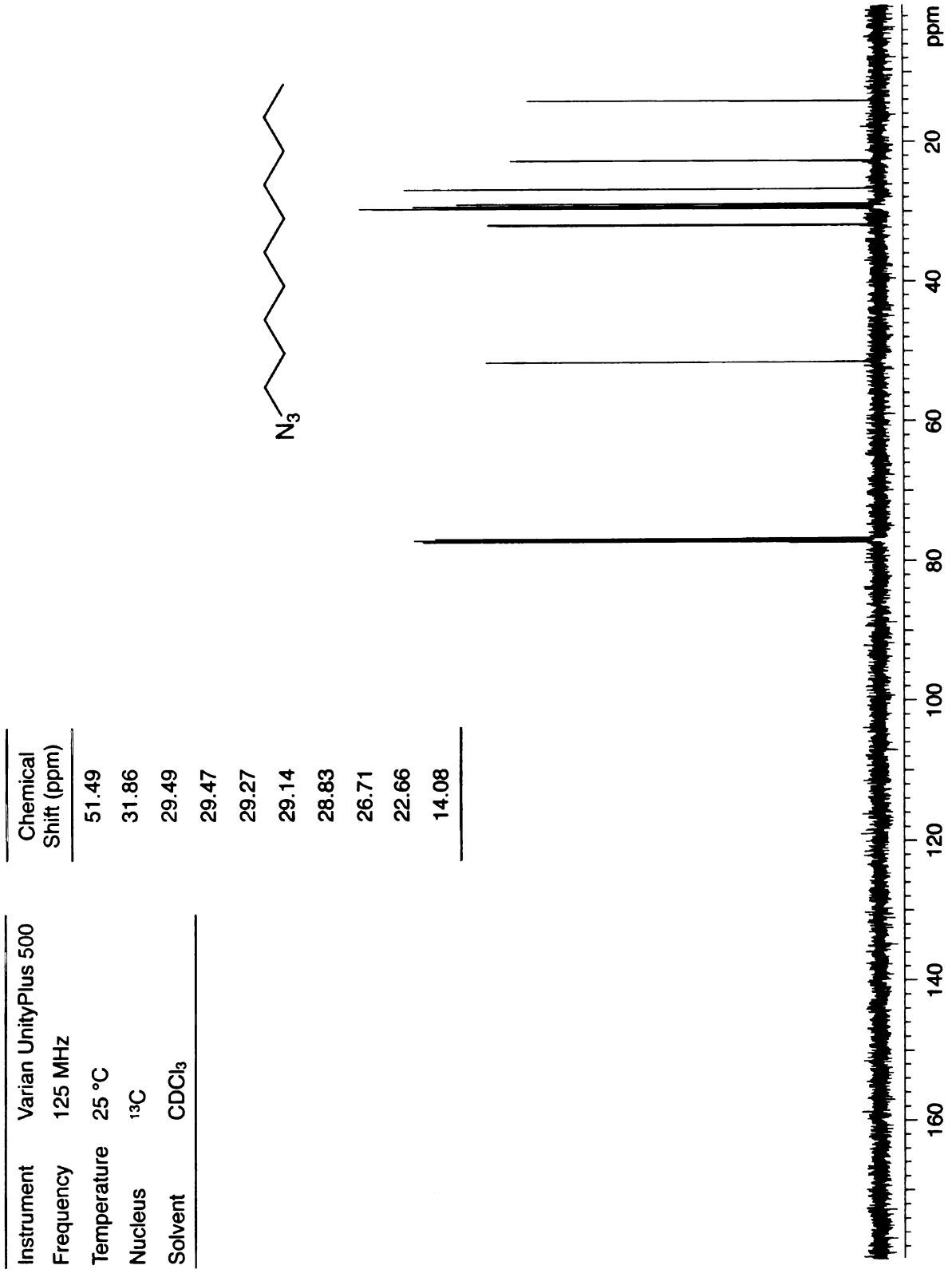

Appendix 51. ^{13}C NMR spectra of 1-azidodecane.

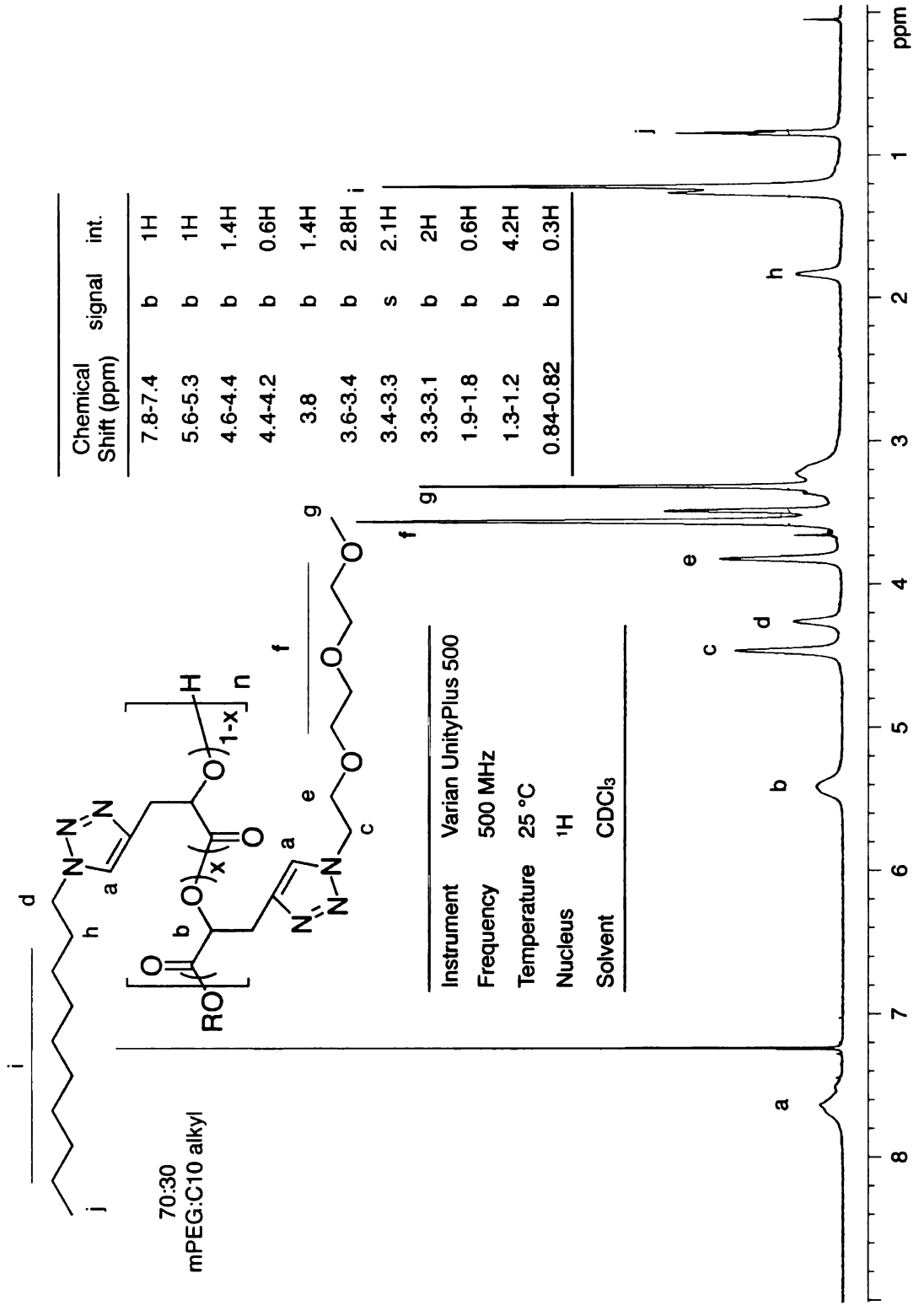

Appendix 52. ^{1}H NMR spectra of PPGL-*g*-*n*-decyl-*co*-mDEG.

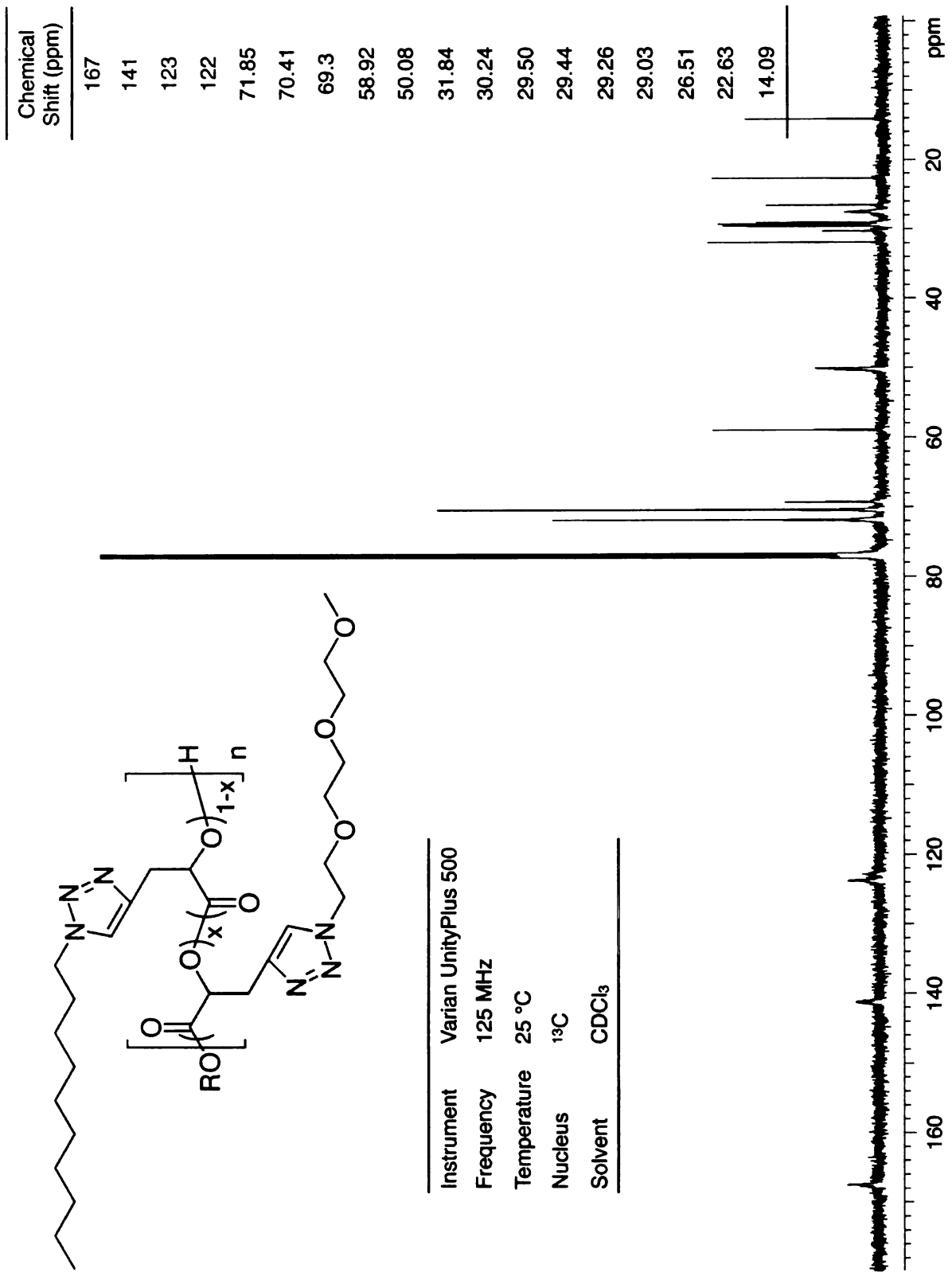

Appendix 53. ^{13}C NMR spectra of PPGL-*g*-*n*-decyl-*co*-mDEG.

Appendix 54. ^{1}H NMR spectra of 1,5-diazidopentane.

Instrument	Varian UnityPlus 500
Frequency	500 MHz
Temperature	25 °C
Nucleus	^{1}H
Solvent	$CDCl_3$

Chemical Shift (ppm)	signal	int.	*J* (Hz)
3.29-3.26	dd	4H	6.84, 6.71
1.64-1.53	m	4H	
1.48-1.43	m	2H	

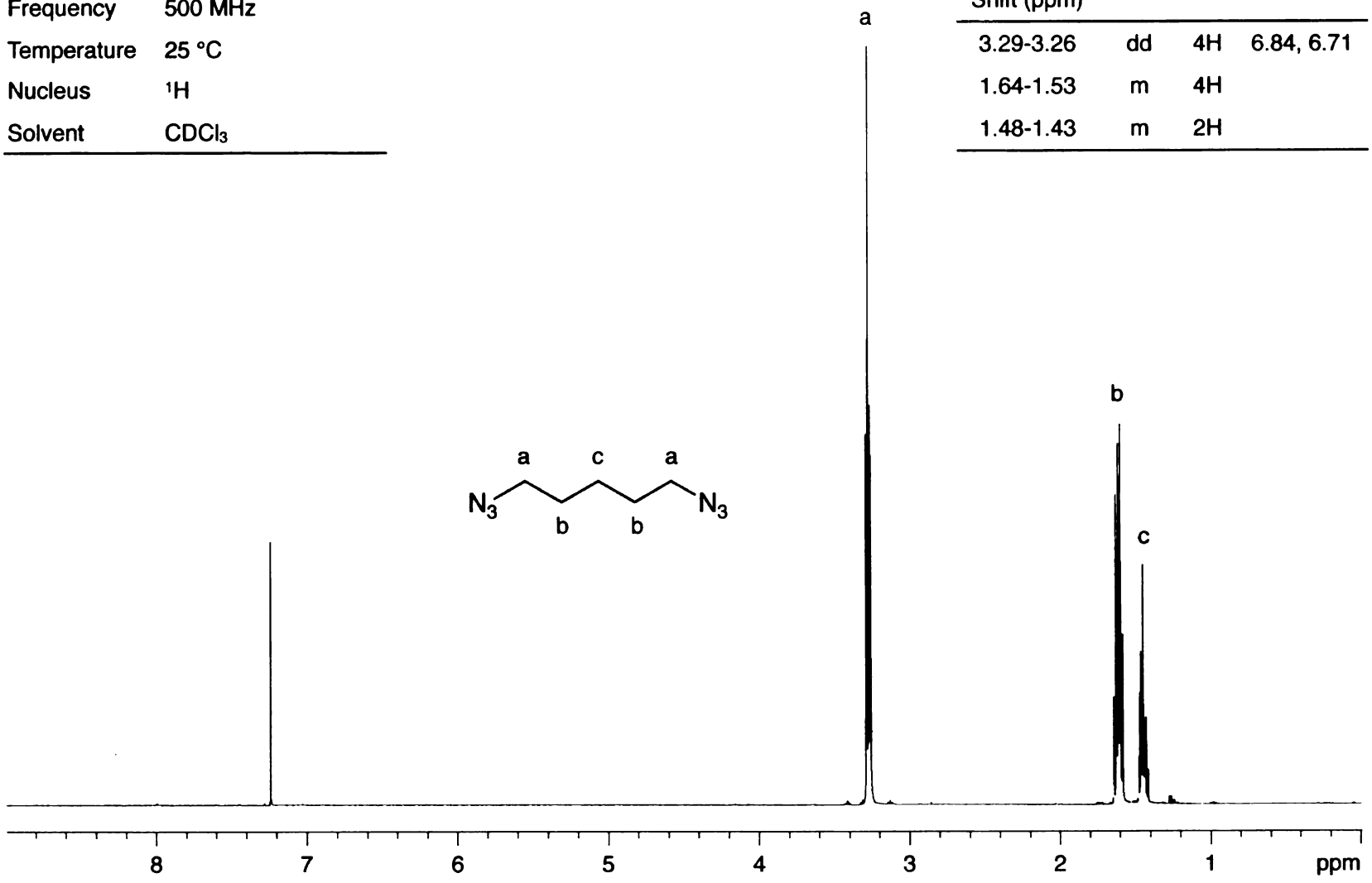

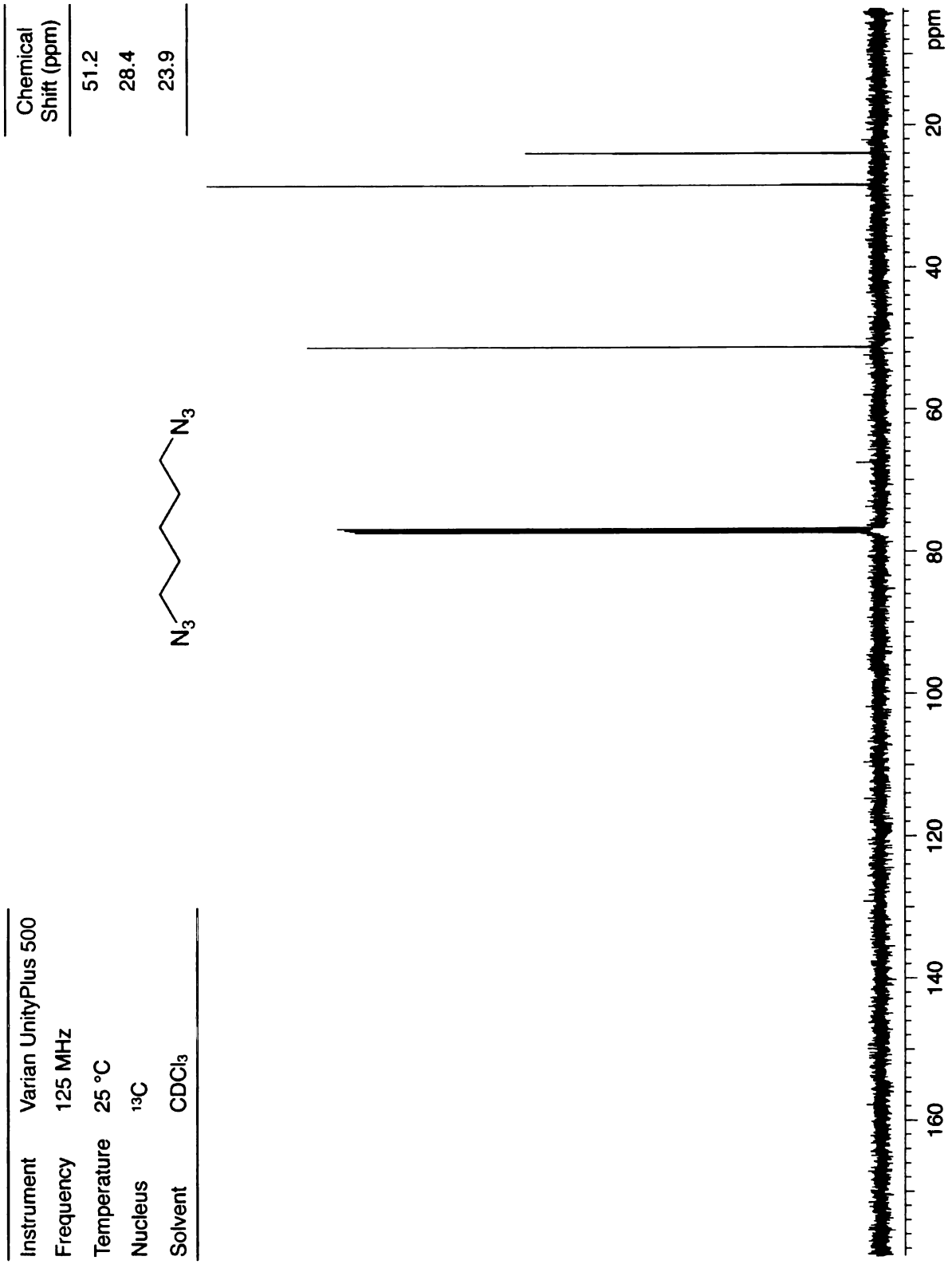

Appendix 55. ^{13}C NMR spectra of 1,5-diaziopentane.

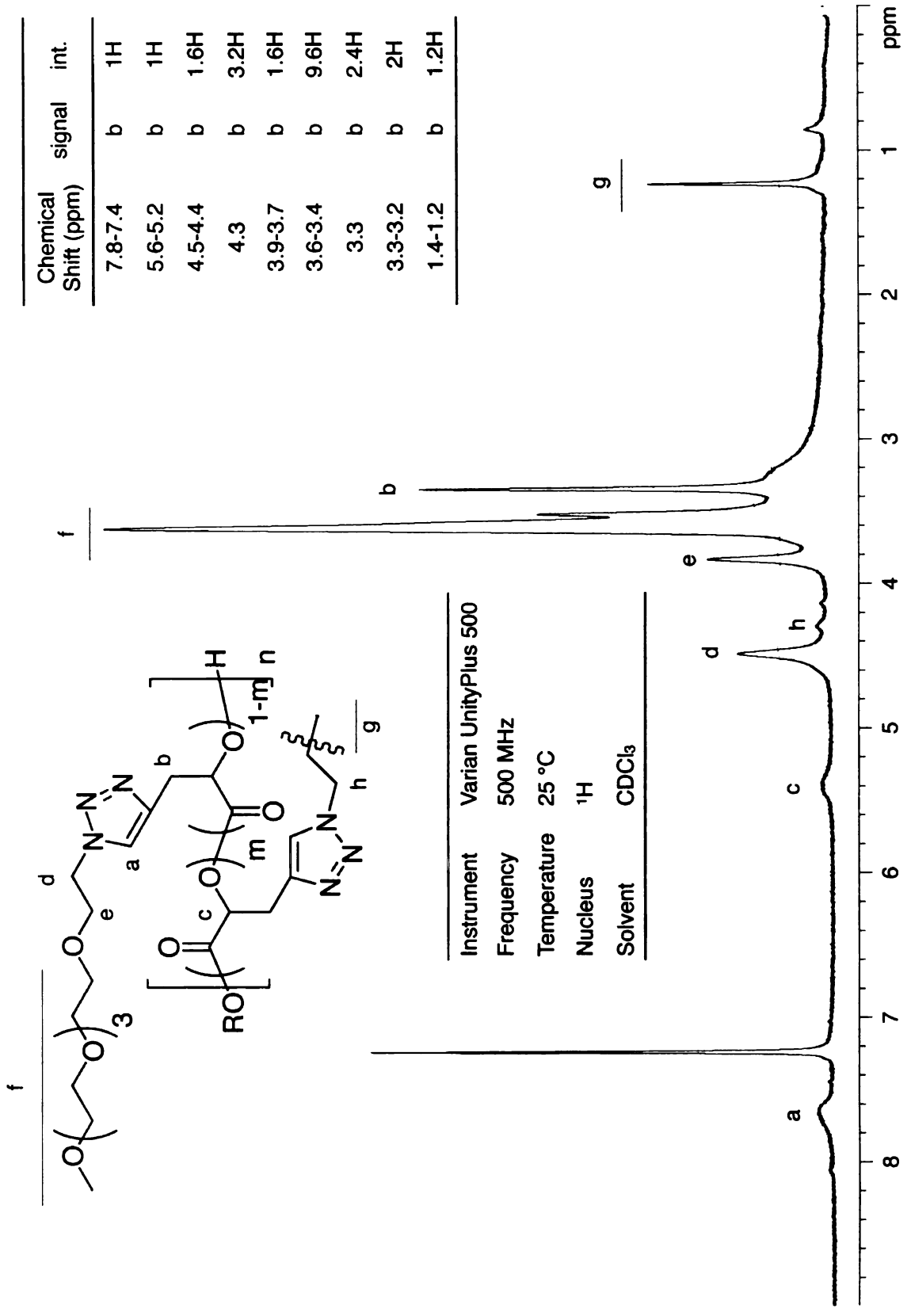

Appendix 56. ^{1}H NMR spectra of cross-linked PPGL nanoparticle by 1,5-diazidopentane.

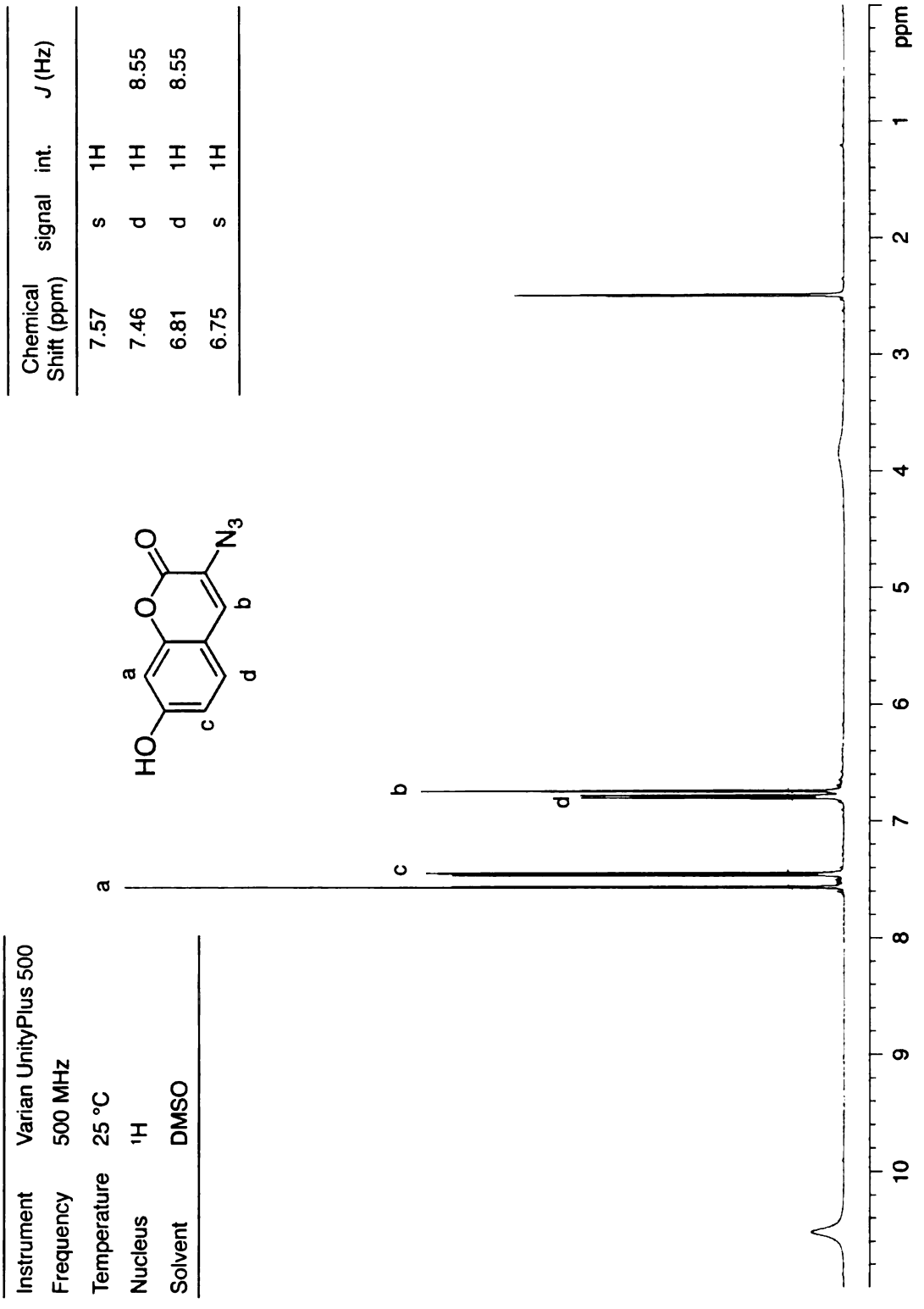

Appendix 57. ^{1}H NMR spectra of 3-azido-7-hydroxycoumarin.

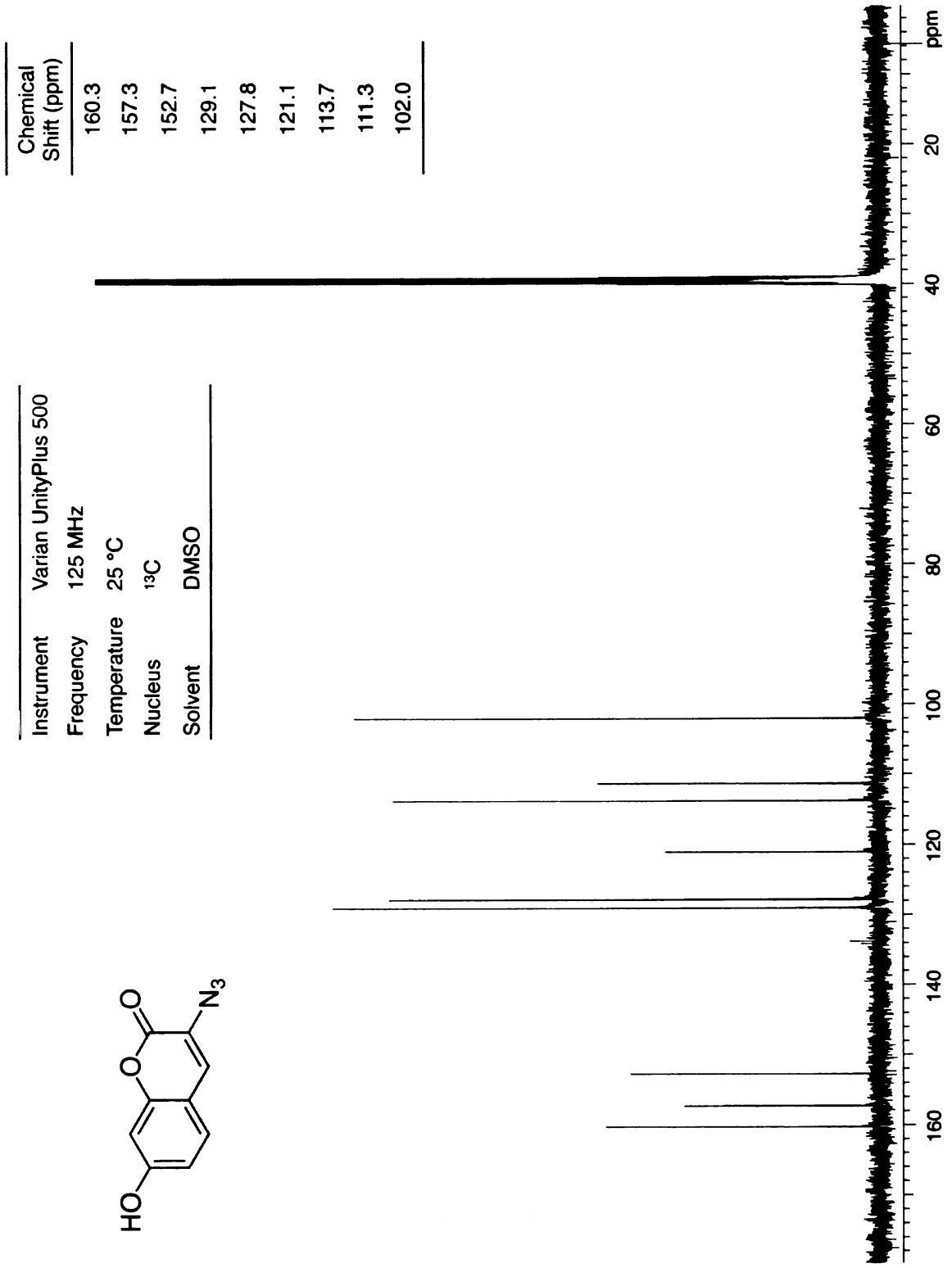

Appendix 58. ^{13}C NMR spectra of 3-azido-7-hydroxycoumarin.

References

(1) Baker, G. L.; Vogel, E. B.; Smith, M. R. *Polym. Rev.* **2008**, *48*, 64-84.

(2) Dechy-Cabaret, O.; Martin-Vaca, B.; Bourissou, D. *Chem. Rev.* **2004**, *104*, 6147-6176.

(3) Chiellini, E.; Solaro, R. *Adv. Mater.* **1996**, *8*, 305-313.

(4) Leenslag, J. W.; Pennings, A. J.; Bos, R. R. M.; Rozema, F. R.; Boering, G. *Biomaterials* **1987**, *8*, 70-73.

(5) Ashammakhi, N.; Rokkanen, P. *Biomaterials* **1997**, *18*, 3-9.

(6) Albertsson, A. C.; Varma, I. K. *Biomacromolecules* **2003**, *4*, 1466-1486.

(7) Agrawal, C. M.; Ray, R. B. *J. Biomed. Mater. Res.* **2001**, *55*, 141-150.

(8) Martin, W. R.; Jackson, M.; Wideburg, N. E.; Denison, F. W.; Coleman, W. H.; Cantrell, R. *Biochimica Et Biophysica Acta* **1962**, *62*, 165-&.

(9) Li, X. F.; Jiang, B.; Pan, B. L. *Biotech. Lett.* **2007**, *29*, 593-597.

(10) Yin, M.; Baker, G. L. *Macromolecules* **1999**, *32*, 7711-7718.

(11) Jing, F.; Smith, M. R.; Baker, G. L. *Abstr. Pap. Am. Chem. Soc.* **2005**, *230*, U4090-U4090.

(12) Liu, T. Q.; Simmons, T. L.; Bohnsack, D. A.; Mackay, M. E.; Smith, M. R.; Baker, G. L. *Macromolecules* **2007**, *40*, 6040-6047.

(13) Trimaille, T.; Gurny, R.; Moller, M. *Chimia* **2005**, *59*, 348-352.

(14) Snell, K. D.; Draths, K. M.; Frost, J. W. *J. Am. Chem. Soc.* **1996**, *118*, 5605-5614.

(15) Trimaille, T.; Moller, M.; Gurny, R. *J. Polym. Sci. Part A: Polym. Chem.* **2004**, *42*, 4379-4391.

(16) Simmons, T. L.; Baker, G. L. *Biomacromolecules* **2001**, *2*, 658-663.

(17) Yang, J. Y.; Yu, J.; Pan, H. Z.; Gu, Z. W.; Cao, W. X.; Feng, X. D. *Chin. J. Polym. Sci.* **2001**, *19*, 509-516.

(18) Gerhardt, W. W.; Noga, D. E.; Hardcastle, K. I.; Garcia, A. J.; Collard, D. M.; Weck, M. *Biomacromolecules* **2006**, *7*, 1735-1742.

(19) Leemhuis, M.; van Nostrum, C. F.; Kruijtzer, J. A. W.; Zhong, Z. Y.; ten Breteler, M. R.; Dijkstra, P. J.; Feijen, J.; Hennink, W. E. *Macromolecules* **2006**, *39*, 3500-3508.

(20) Marcincinova-Benabdillah, K.; Boustta, M.; Coudane, J.; Vert, M. *Biomacromolecules* **2001**, *2*, 1279-1284.

(21) Benabdillah, K. M.; Coudane, J.; Boustta, M.; Engel, R.; Vert, M. *Macromolecules* **1999**, *32*, 8774-8780.

(22) Taguchi, K. Y., S.; Hiratani, K.; Norikio, M.; Okahata, Y. *Macromolecules* **1988**, *21*, 3338-3340.

(23) Ouchi, T.; Fujino, A. *Makromol. Chem.* **1989**, *190*, 1523-1530.

(24) Barrera, D. A.; Zylstra, E.; Lansbury, P. T.; Langer, R. *J. Am. Chem. Soc.* **1993**, *115*, 11010-11011.

(25) Barrera, D. A.; Zylstra, E.; Lansbury, P. T.; Langer, R. *Macromolecules* **1995**, *28*, 425-432.

(26) Feng, Y.; Klee, D.; Hocker, H. *Macromol. Chem. Phys.* **2002**, *203*, 819-824.

(27) Veld, P.; Dijkstra, P. J.; Feijen, J. *Makromol. Chem.* **1992**, *193*, 2713-2730.

(28) Aoshima, S.; Oda, H.; Kobayashi, E. *Journal of Polymer Science Part a-Polymer Chemistry* **1992**, *30*, 2407-2413.

(29) Huh, K. M.; Bae, Y. H. *Polymer* **1999**, *40*, 6147-6155.

(30) Lutz, J. F.; Hoth, A. *Macromolecules* **2006**, *39*, 893-896.

(31) Zhong, Z. Y.; Dijkstra, P. J.; Jan, F. J.; Kwon, Y. M.; Bae, Y. H.; Kim, S. W. *Macromol. Chem. Phys.* **2002**, *203*, 1797-1803.

(32) Porjazoska, A.; Dimitrov, P.; Dimitrov, I.; Cvetkovska, M.; Tsvetanov, C. B. *Macromol. Symp.* **2004**, *210*, 427-436.

(33) Jiang, X., Michigan State University, 2006.

(34) Radano, C. P., Michigan State University, 2003.

(35) Ponsart, S.; Coudane, J.; Vert, M. *Biomacromolecules* **2000**, *1*, 275-281.

(36) Nottelet, B.; El Ghzaoui, A.; Coudane, J.; Vert, M. *Biomacromolecules* **2007**, *8*, 2594-2601.

(37) Huang, M. H.; Coudane, J.; Li, S. M.; Vert, M. *J. Poly. Chem. Part A-Poly. Chem.* **2005**, *43*, 4196-4205.

(38) Ponsart, S.; Coudane, J.; McGrath, J.; Vert, M. *J. Bioact. Compat. Polym.* **2002**, *17*, 417-432.

(39) Pan, J.; Wang, Y. L.; Qin, S. H.; Zhang, B. B.; Luo, Y. F. *J. Biomed. Mater. Res. Part B* **2005**, *74B*, 476-480.

(40) Tasaka, F.; Ohya, Y.; Ouchi, T. *Macromol. Rapid Comm.* **2001**, *22*, 820-824.

(41) Garlotta, D. *J. Polym. Environ.* **2001**, *9*, 63-84.

(42) Trollsas, M.; Atthoff, B.; Claesson, H.; Hedrick, J. L. *Macromolecules* **1998**, *31*, 3439-3445.

(43) Hao, Q. H.; Li, F. X.; Li, Q. B.; Li, Y.; Jia, L.; Yang, J.; Fang, Q.; Cao, A. M. *Biomacromolecules* **2005**, *6*, 2236-2247.

(44) Zhao, Y. L.; Qing, C.; Jing, J.; Shuai, X. T.; Bei, J. Z.; Chen, C. F.; Fu, X. *Polymer* **2002**, *43*, 5819-5825.

(45) Kricheldorf, H. R.; Ahrensdorf, K.; Rost, S. *Macromol. Chem. Phys.* **2004**, *205*, 1602-1610.

(46) Hay, G.; Mackay, M. E.; Hawker, C. J. *J. Polym. Sci. Pt. B-Polym. Phys.* **2001**, *39*, 1766-1777.

(47) Caminade, A. M.; Laurent, R.; Majoral, J. P. *Adv. Drug Deliv. Rev.* **2005**, *57*, 2130-2146.

(48) Zhao, Y. L.; Shuai, X. T.; Chen, C. F.; Xi, F. *Macromolecules* **2004**, *37*, 8854-8862.

(49) Tasaka, F.; Ohya, Y.; Ouchi, T. *Macromolecules* **2001**, *34*, 5494-5500.

(50) Tasaka, F.; Miyazaki, H.; Ohya, Y.; Ouchi, T. *Macromolecules* **1999**, *32*, 6386-6389.

(51) Wittmar, M.; Unger, F.; Kissel, T. *Macromolecules* **2006**, *39*, 1417-1424.

(52) Dailey, L. A.; Wittmar, M.; Kissel, T. *J. Control. Release* **2005**, *101*, 137-149.

(53) Pistel, K. F.; Breitenbach, A.; Zange-Volland, R.; Kissel, T. *J. Control. Release* **2001**, *73*, 7-20.

(54) Breitenbach, A.; Pistel, K. F.; Kissel, T. *Polymer* **2000**, *41*, 4781-4792.

(55) Breitenbach, A.; Li, Y. X.; Kissel, T. *J. Control. Release* **2000**, *64*, 167-178.

(56) Breitenbach, A.; Kissel, T. *Polymer* **1998**, *39*, 3261-3271.

(57) Parrish, B.; Emrick, T. *Macromolecules* **2004**, *37*, 5863-5865.

(58) Porter, K.; Hossain, M.; Wang, M.; Radano, C. P.; Baker, G.; Smith, M. R.; McCabe, L. R. *Mol. Biol. Rep.* **2006**, *33*, 1-12.

(59) Tian, D.; Dubois, P.; Jerome, R. *Macromolecules* **1997**, *30*, 2575-2581.

(60) Tian, D.; Dubois, P.; Jerome, R. *Macromolecules* **1997**, *30*, 1947-1954.

(61) Tian, D.; Dubois, P.; Grandfils, C.; Jerome, R. *Macromolecules* **1997**, *30*, 406-409.

(62) Taniguchi, I.; Mayes, A. M.; Chan, E. W. L.; Griffith, L. G. *Macromolecules* **2005**, *38*, 216-219.

(63) Lecomte, P.; Riva, R.; Schmeits, S.; Rieger, J.; Van Butsele, K.; Jerome, C.; Jerome, R. *Macromol. Symp.* **2006**, *240*, 157-165.

(64) Van Horn, B. A.; Wooley, K. L. *Soft Matter* **2007**, *3*, 1032-1040.

(65) Mecerreyes, D.; Humes, J.; Miller, R. D.; Hedrick, J. L.; Detrembleur, C.; Lecomte, P.; Jerome, R.; San Roman, J. *Macromol. Rapid Comm.* **2000**, *21*, 779-784.

(66) Rieger, J. V. B., K.; Lecomte, P.; Detrembleur, C.; Jerome, R.; Jerome, C. *Chem. Commun.* **2005**, *274*, 274-276.

(67) Lenoir, S.; Riva, R.; Lou, X.; Detrembleur, C.; Jerome, R.; Lecomte, P. *Macromolecules* **2004**, *37*, 4055-4061.

(68) Riva, R.; Lenoir, S.; Jerome, R.; Lecomte, P. *Polymer* **2005**, *46*, 8511-8518.

(69) Riva, R.; Rieger, J.; Jerome, R.; Lecomte, P. *J. Poly. Chem. Part A-Poly. Chem.* **2006**, *44*, 6015-6024.

(70) Parrish, B.; Breitenkamp, R. B.; Emrick, T. *J. Am. Chem. Soc.* **2005**, *127*, 7404-7410.

(71) Riva, R.; Schmeits, S.; Jerome, C.; Jerome, R.; Lecomte, P. *Macromolecules* **2007**, *40*, 796-803.

(72) Riva, R.; Schmeits, P.; Stoffelbach, F.; Jerome, C.; Jerome, R.; Lecomte, P. *Chem. Commun.* **2005**, 5334-5336.

(73) Jiang, X.; Vogel, E. B.; Smith, M. R.; Baker, G. L. *Macromolecules* **2008**, *41*, 1937-1944.

(74) Kimura, Y.; Shirotani, K.; Yamane, H.; Kitao, T. *Macromolecules* **1988**, *21*, 3338-3340.

(75) Kimura, Y.; Shirotani, K.; Yamane, H.; Kitao, T. *Polymer* **1993**, *34*, 1741-1748.

(76) Leemhuis, M.; van Steenis, J. H.; van Uxem, M. J.; van Nostrum, C. F.; Hennink, W. E. *Eur. J. Org. Chem.* **2003**, 3344-3349.

(77) MacDonald, R. T.; McCarthy, S. P.; Gross, R. A. *Macromolecules* **1996**, *29*, 7356-7361.

(78) Ovitt, T. M.; Coates, G. W. *J. Am. Chem. Soc.* **1999**, *121*, 4072-4073.

(79) Thakur, K. A. M.; Kean, R. T.; Hall, E. S.; Kolstad, J. J.; Munson, E. J. *Macromolecules* **1998**, *31*, 1487-1494.

(80) Jacobs, C.; Dubois, P.; Jerome, R.; Teyssie, P. *Macromolecules* **1991**, *24*, 3027-3034.

(81) Kumar, N.; Ravikumar, M. N. V.; Domb, A. J. *Adv. Drug Deliv. Rev.* **2001**, *53*, 23-44.

(82) Ouchi, T.; Miyazaki, H.; Arimura, H.; Tasaka, F.; Hamada, A.; Ohya, Y. *J. Polym. Sci. Part A: Polym. Chem.* **2002**, *40*, 1218-1225.

(83) Veld, P.; Velner, E. M.; VanDeWitte, P.; Hamhuis, J.; Dijkstra, P. J.; Feijen, J. *J. Polym. Sci. Part A: Polym. Chem.* **1997**, *35*, 219-226.

(84) Ouchi, T.; Ohya, Y. *J. Polym. Sci. Part A: Polym. Chem.* **2004**, *42*, 453-462.

(85) Shen, Y. Q.; Zhu, K. J.; Shen, Z. Q.; Yao, K. M. *J. Polym. Sci. Part A: Polym. Chem.* **1996**, *34*, 1799-1805.

(86) Vanhoorne, P.; Dubois, P.; Jerome, R.; Teyssie, P. *Macromolecules* **1992**, *25*, 37-44.

(87) Li, X. R.; Yuan, X. Y. *Prog. Chem.* **2007**, *19*, 973-981.

(88) Tu, C. F.; Cai, Q.; Yang, J.; Wan, Y. Q.; Bei, J. Z.; Wang, S. *Polym. Adv. Technol.* **2003**, *14*, 565-573.

(89) Li, S. M.; Garreau, H.; Vert, M. *J. Mater. Sci.-Mater. Med.* **1990**, *1*, 131-139.

(90) Grijpma, D. W.; Pennings, A. J. *Macromol. Chem. Phys.* **1994**, *195*, 1633-1647.

(91) Liu, G.; Fang, Y. E.; Shi, T. Y. *Chem. J. Chin. Univ.-Chin.* **1997**, *18*, 486-488.

(92) Fineman, M.; Ross, S. D. *J. Polym. Sci.* **1950**, *5*, 259-262.

(93) Tudos, F.; Kelen, T. *J. Macromol. Sci.: Chem.* **1981**, *A16*, 1283-1297.

(94) Tidwell, P. W.; Mortimer, G. A. *J. Polym. Sci. Pt A-Gen. Pap.* **1965**, *3*, 369-387.

(95) Dong, C. M.; Qiu, K. Y.; Gu, Z. W.; Feng, X. D. *Chin. Chem. Lett.* **2000**, *11*, 815-818.

(96) Saulnier, B.; Coudane, J.; Garreau, H.; Vert, M. *Polymer* **2006**, *47*, 1921-1929.

(97) Yang, J. Y.; Yu, J.; Li, M.; Gu, Z. W.; Feng, X. D. *Chin. J. Polym. Sci.* **2002**, *20*, 413-417.

(98) Jiang, X.; Vogel, E. B.; Smith III, M. R.; Baker, G. L. *J. Poly. Chem. Part A-Poly. Chem.* **2007**, *45*, 5227-5236.

(99) Jiang, X. W.; Smith, M. R.; Baker, G. L. *Macromolecules* **2008**, *41*, 318-324.

(100) Jing, F.; Smith, M. R.; Baker, G. L. *Macromolecules* **2007**, *40*, 9304-9312.

(101) Mori, K.; Takaishi, H. *Tetrahedron* **1989**, *45*, 1639-1646.

(102) Odian, G. *Principles of Polymerization*; 4th ed.; John Wiley & Sons: New York, 2004.

(103) Yin, M., Michigan State University, 2000.

(104) Wang, C., Michigan State University, 2001.

(105) Jing, F., Michigan State University, 2006.

(106) Liu, T., Michigan State, 2002.

(107) Rozen, S.; Ben-David, I. *J. Org. Chem.* **2001**, *66*, 496-500.

(108) Guest, H. H. *J. Am. Chem. Soc.* **1947**, *69*, 300-302.

(109) Soppimath, K. S.; Aminabhavi, T. M.; Kulkarni, A. R.; Rudzinski, W. E. *J. Control. Release* **2001**, *70*, 1-20.

(110) Bourissou, D.; Moebs-Sanchez, S.; Martin-Vaca, B. *C. R. Chim.* **2007**, *10*, 775-794.

(111) Williams, C. K. *Chem. Soc. Rev.* **2007**, *36*, 1573-1580.

(112) Yang, J. Y.; Yu, J.; Li, M.; Pan, H. Z.; Gu, Z. W.; Cao, W. X.; Feng, X. D. *Acta Chimica Sinica* **2001**, *59*, 1809-1812.

(113) Parrish, B.; Emrick, T. *Bioconjugate Chem.* **2007**, *18*, 263-267.

(114) Lee, R. S.; Yang, J. M. *J. Appl. Polym. Sci.* **2001**, *81*, 1581-1587.

(115) Lee, R. S.; Yang, J. M. *J. Poly. Chem. Part A-Poly. Chem.* **2001**, *39*, 724-731.

(116) Nijenhuis, A. J.; Grijpma, D. W.; Pennings, A. J. *Macromolecules* **1992**, *25*, 6419-6424.

(117) Witzke, D. R.; Narayan, R.; Kolstad, J. J. *Macromolecules* **1997**, *30*, 7075-7085.

(118) Du, Y. J.; Lemstra, P. J.; Nijenhuis, A. J.; Vanaert, H. A. M.; Bastiaansen, C. *Macromolecules* **1995**, *28*, 2124-2132.

(119) Sperling, L. H. *Introduction to Physical Polymer Science*; 3rd ed.; Wiley-Interscience, 2001.

(120) Jiang, X. V., E. B; Smith III, M. R.; Baker, G. L. *Journal of Polymer Science Part a-Polymer Chemistry* **2007**, *45*, 5227-5236.

(121) Duncan, R. *Nat. Rev. Drug Discov.* **2003**, *2*, 347-360.

(122) Uhrich, K. E.; Anastasiou, T. J.; Beaton, M. L. *Abstr. Pap. Am. Chem. Soc.* **2001**, *222*, U317-U317.

(123) Uhrich, K. E.; Cannizzaro, S. M.; Langer, R. S.; Shakesheff, K. M. *Chem. Rev.* **1999**, *99*, 3181-3198.

(124) Vert, M. *Prog. Polym. Sci.* **2007**, *32*, 755-761.

(125) Nair, L. S.; Laurencin, C. T. *Prog. Polym. Sci.* **2007**, *32*, 762-798.

(126) Khandare, J.; Minko, T. *Prog. Polym. Sci.* **2006**, *31*, 359-397.

(127) Duncan, R.; Ringsdorf, H.; Satchi-Fainaro, R. In *Polymer Therapeutics I: Polymers as Drugs, Conjugates and Gene Delivery Systems* 2006; Vol. 192, p 1-8.

(128) Yokoyama, M.; Miyauchi, M.; Yamada, N.; Okano, T.; Sakurai, Y.; Kataoka, K.; Inoue, S. *J. Control. Release* **1990**, *11*, 269-278.

(129) Jeong, J. H.; Kim, S. W.; Park, T. G. *Prog. Polym. Sci.* **2007**, *32*, 1239-1274.

(130) Wong, S. Y.; Pelet, J. M.; Putnam, D. *Prog. Polym. Sci.* **2007**, *32*, 799-837.

(131) Zhu, S. G.; Li, G. Y. *Prog. Biochem. Biophys.* **2002**, *29*, 868-871.

(132) Rieger, J.; Bernaerts, K. V.; Du Prez, F. E.; Jerome, R.; Jerome, C. *Macromolecules* **2004**, *37*, 9738-9745.

(133) Adams, M. L.; Lavasanifar, A.; Kwon, G. S. *J. Pharm. Sci.* **2003**, *92*, 1343-1355.

(134) Mecerreyes, D.; Miller, R. D.; Hedrick, J. L.; Detrembleur, C.; Jerome, R. *J. Poly. Chem. Part A-Poly. Chem.* **2000**, *38*, 870-875.

(135) Kolb, H. C.; Finn, M. G.; Sharpless, K. B. *Angew. Chem.-Int. Edit.* **2001**, *40*, 2004-+.

(136) Rostovtsev, V. V.; Green, L. G.; Fokin, V. V.; Sharpless, K. B. *Angew. Chem.-Int. Edit.* **2002**, *41*, 2596-+.

(137) Wu, P.; Feldman, A. K.; Nugent, A. K.; Hawker, C. J.; Scheel, A.; Voit, B.; Pyun, J.; Frechet, J. M. J.; Sharpless, K. B.; Fokin, V. V. *Angew. Chem.-Int. Edit.* **2004**, *43*, 3928-3932.

(138) Wu, P.; Malkoch, M.; Hunt, J. N.; Vestberg, R.; Kaltgrad, E.; Finn, M. G.; Fokin, V. V.; Sharpless, K. B.; Hawker, C. J. *Chem. Commun.* **2005**, 5775-5777.

(139) Joralemon, M. J.; O'Reilly, R. K.; Matson, J. B.; Nugent, A. K.; Hawker, C. J.; Wooley, K. L. *Macromolecules* **2005**, *38*, 5436-5443.

(140) Fernandez-Megia, E.; Correa, J.; Rodriguez-Meizoso, I.; Riguera, R. *Macromolecules* **2006**, *39*, 2113-2120.

(141) Tsarevsky, N. V.; Sumerlin, B. S.; Matyjaszewski, K. *Macromolecules* **2005**, *38*, 3558-3561.

(142) Opsteen, J. A.; van Hest, J. C. M. *Chem. Commun.* **2005**, 57-59.

(143) Sumerlin, B. S.; Tsarevsky, N. V.; Louche, G.; Lee, R. Y.; Matyjaszewski, K. *Macromolecules* **2005**, *38*, 7540-7545.

(144) Helms, B.; Mynar, J. L.; Hawker, C. J.; Frechet, J. M. J. *J. Am. Chem. Soc.* **2004**, *126*, 15020-15021.

(145) Mynar, J. L.; Choi, T. L.; Yoshida, M.; Kim, V.; Hawker, C. J.; Frechet, J. M. J. *Chem. Commun.* **2005**, 5169-5171.

(146) Malkoch, M.; Thibault, R. J.; Drockenmuller, E.; Messerschmidt, M.; Voit, B.; Russell, T. P.; Hawker, C. J. *J. Am. Chem. Soc.* **2005**, *127*, 14942-14949.

(147) Newkome, G. R.; Moorefield, C. N.; Baker, G. R.; Saunders, M. J.; Grossman, S. H. *Angew. Chem.-Int. Edit. Engl.* **1991**, *30*, 1178-1180.

(148) Lawrence, M. J. *Chemical Society Reviews* **1994**, *23*, 417-424.

(149) Kakizawa, Y.; Kataoka, K. *Advanced Drug Delivery Reviews* **2002**, *54*, 203-222.

(150) Kataoka, K.; Harada, A.; Nagasaki, Y. *Advanced Drug Delivery Reviews* **2001**, *47*, 113-131.

(151) Becker, M. L.; Remsen, E. E.; Wooley, K. L. *Journal of Polymer Science Part a-Polymer Chemistry* **2001**, *39*, 4152-4166.

(152) Bhattarai, N.; Bhattarai, S. R.; Yi, H. K.; Lee, J. C.; Khil, M. S.; Hwang, P. H.; Kim, H. Y. *Pharmaceutical Research* **2003**, *20*, 2021-2027.

(153) Tomalia, D. A.; Berry, V.; Hall, M.; Hedstrand, D. M. *Macromolecules* **1987**, *20*, 1164-1167.

(154) Vanhest, J. C. M.; Delnoye, D. A. P.; Baars, M.; Vangenderen, M. H. P.; Meijer, E. W. *Science* **1995**, *268*, 1592-1595.

(155) vanHest, J. C. M.; Delnoye, D. A. P.; Baars, M.; ElissenRoman, C.; vanGenderen, M. H. P.; Meijer, E. W. *Chemistry-a European Journal* **1996**, *2*, 1616-1626.

(156) Chapman, T. M.; Hillyer, G. L.; Mahan, E. J.; Shaffer, K. A. *Journal of the American Chemical Society* **1994**, *116*, 11195-11196.

(157) Frey, H.; Lorenz, K.; Mulhaupt, R.; Rapp, U.; MayerPosner, F. J. *Macromolecular Symposia* **1996**, *102*, 19-26.

(158) Liu, H. B.; Jiang, A.; Guo, J. A.; Uhrich, K. E. *Journal of Polymer Science Part a-Polymer Chemistry* **1999**, *37*, 703-711.

(159) Jiang, X. V., E. B; Smith III, M. R.; Baker, G. L. *Macromolecules* **2008**, *41*, 1937-1944.

(160) Chan, T. R.; Fokin, V. V. *QSAR Comb. Sci.* **2007**, *26*, 1274-1279.

(161) Skwarczynski, M.; Hayashi, Y.; Kiso, Y. *J. Med. Chem.* **2006**, *49*, 7253-7269.

(162) Gref, R.; Minamitake, Y.; Peracchia, M. T.; Trubetskoy, V.; Torchilin, V.; Langer, R. *Science* **1994**, *263*, 1600-1603.

(163) Osada, K.; Kataoka, K. In *Peptide Hybrid Polymers* 2006; Vol. 202, p 113-153.

(164) Jette, K. K.; Law, D.; Schmitt, E. A.; Kwon, G. S. *Pharm. Res.* **2004**, *21*, 1184-1191.

(165) Otsuka, H.; Nagasaki, Y.; Kataoka, K. *Adv. Drug Deliv. Rev.* **2003**, *55*, 403-419.

(166) Yasugi, K.; Nagasaki, Y.; Kato, M.; Kataoka, K. *J. Control. Release* **1999**, *62*, 89-100.

(167) Hagan, S. A.; Coombes, A. G. A.; Garnett, M. C.; Dunn, S. E.; Davis, M. C.; Illum, L.; Davis, S. S.; Harding, S. E.; Purkiss, S.; Gellert, P. R. *Langmuir* **1996**, *12*, 2153-2161.

(168) Hussain, H.; Busse, K.; Kressler, J. *Macromol. Chem. Phys.* **2003**, *204*, 936-946.

(169) Wilhelm, M.; Zhao, C. L.; Wang, Y. C.; Xu, R. L.; Winnik, M. A.; Mura, J. L.; Riess, G.; Croucher, M. D. *Macromolecules* **1991**, *24*, 1033-1040.

(170) Castro, E.; Taboada, P.; Barbosa, S.; Mosquera, V. *Biomacromolecules* **2005**, *6*, 1438-1447.

(171) Astafieva, I.; Zhong, X. F.; Eisenberg, A. *Macromolecules* **1993**, *26*, 7339-7352.

(172) Liu, J.; Lee, H.; Allen, C. *Curr. Pharm. Design* **2006**, *12*, 4685-4701.

(173) Panyam, J.; Williams, D.; Dash, A.; Leslie-Pelecky, D.; Labhasetwar, V. *J. Pharm. Sci.* **2004**, *93*, 1804-1814.

(174) Xu, J. P.; Ji, J.; Chen, W. D.; Shen, J. C. *J. Control. Release* **2005**, *107*, 502-512.

(175) Kondo, S.; Hosaka, S.; Sasai, Y.; Kuzuya, M. *Chem. Pharm. Bull.* **2004**, *52*, 1302-1306.

(176) Wang, L. F.; Chiang, H. N.; Chen, W. B. *J. Pharm. Pharmacol.* **2002**, *54*, 1129-1135.

(177) Cho, S. H.; Kim, K. S. *Macromol. Res.* **2003**, *11*, 317-321.

(178) Erdmann, L.; Uhrich, K. E. *Biomaterials* **2000**, *21*, 1941-1946.

(179) Schmeltzer, R. C.; Anastasiou, T. J.; Uhrich, K. E. *Polym. Bull.* **2003**, *49*, 441-448.

(180) Schmeltzer, R. C.; Uhrich, K. E. *J. Bioact. Compat. Polym.* **2006**, *21*, 123-133.

(181) Anastasiou, T. J.; Uhrich, K. E. *J. Poly. Chem. Part A-Poly. Chem.* **2003**, *41*, 3667-3679.

(182) Prudencio, A.; Schmeltzer, R. C.; Uhrich, K. E. *Macromolecules* **2005**, *38*, 6895-6901.

(183) Patil, S.; Chan, C. *Neurosci. Lett.* **2005**, *384*, 288-293.

(184) Patil, S.; Sheng, L. F.; Masserang, A.; Chan, C. *Neurosci. Lett.* **2006**, *406*, 55-59.

(185) Patil, S. P.; Chan, C. *Faseb J.* **2006**, *20*, A1420-A1421.

(186) Patil, S.; Melrose, J.; Chan, C. *Eur. J. Neurosci.* **2007**, *26*, 2131-2141.

(187) Jensen, N. P.; Friedman, J. J.; Kropp, H.; Kahan, F. M. *J. Med. Chem.* **1980**, *23*, 6-8.

(188) Lassen, F. O.; Stammer, C. H. *J. Org. Chem.* **1971**, *36*, 2631-&.

(189) Grigg, R.; Sarker, M. A. B. *Tetrahedron* **2006**, *62*, 10332-10343.

(190) Yamamoto, K.; Serizawa, T.; Muraoka, Y.; Akashi, M. *Macromolecules* **2001**, *34*, 8014-8020.

(191) Schilli, C. M.; Zhang, M. F.; Rizzardo, E.; Thang, S. H.; Chong, Y. K.; Edwards, K.; Karlsson, G.; Muller, A. H. E. *Macromolecules* **2004**, *37*, 7861-7866.

(192) Jeong, B.; Gutowska, A. *Trends Biotechnol.* **2002**, *20*, 305-311.

(193) Gil, E. S.; Hudson, S. A. *Prog. Polym. Sci.* **2004**, *29*, 1173-1222.

(194) Yoo, M. K.; Seok, W. K.; Sung, Y. K. *Macromol. Symp.* **2004**, *207*, 173-186.

(195) Iijima, M.; Nagasaki, Y. *J. Poly. Chem. Part A-Poly. Chem.* **2006**, *44*, 1457-1469.

(196) Tsuda, Y.; Kikuchi, A.; Yamato, M.; Nakao, A.; Sakurai, Y.; Umezu, M.; Okano, T. *Biomaterials* **2005**, *26*, 1885-1893.

(197) Yang, J.; Yamato, M.; Kohno, C.; Nishimoto, A.; Sekine, H.; Fukai, F.; Okano, T. *Biomaterials* **2005**, *26*, 6415-6422.

(198) Nakayama, M.; Okano, T.; Miyazaki, T.; Kohori, F.; Sakai, K.; Yokoyama, M. *J. Control. Release* **2006**, *115*, 46-56.

(199) Yang, H.; Kao, W. Y. J. *Pharmaceutical Research* **2006**, *23*, 205-214.

(200) Lutz, J. F.; Akdemir, O.; Hoth, A. *J. Am. Chem. Soc.* **2006**, *128*, 13046-13047.

(201) Zhao, B.; Li, D. J.; Hua, F. J.; Green, D. R. *Macromolecules* **2005**, *38*, 9509-9517.

(202) Han, S.; Hagiwara, M.; Ishizone, T. *Macromolecules* **2003**, *36*, 8312-8319.

(203) Shih, C. *Pharm. Res.* **1995**, *12*, 2036-2040.

(204) Markiewicz, P.; Goh, M. C. *Langmuir* **1994**, *10*, 5-7.

(205) Ebenstein, Y.; Nahum, E.; Banin, U. *Nano Lett.* **2002**, *2*, 945-950.

(206) Wang, G.; Zhu, X. L.; Cheng, Z. P.; Zhu, J. *J. Poly. Chem. Part A-Poly. Chem.* **2005**, *43*, 2358-2367.

(207) Boyer, J. H.; Hamer, J. *J. Am. Chem. Soc.* **1955**, *77*, 951-954.

(208) Christoffers, J.; Onal, N. *Eur. J. Org. Chem.* **2000**, 1633-1635.

(209) Angle, S. R.; Henry, R. M. *Journal of Organic Chemistry* **1998**, *63*, 7490-7497.

(210) Natelson, S.; Natelson, E. A. *Microchem J.* **1989**, *40*, 226-232.

(211) Schmidt, M.; Amstutz, R.; Crass, G.; Seebach, D. *Chemische Berichte-Recueil* **1980**, *113*, 1691-1707.

(212) Lieber, E.; Chao, T. S.; Rao, C. N. R. *J. Org. Chem.* **1957**, *22*, 238-240.

(213) Liu, Y. Y.; Miyoshi, H.; Nakamura, M. *Int. J. Cancer* **2007**, *120*, 2527-2537.

(214) Couvreur, P.; Puisieux, F. *Adv. Drug Deliv. Rev.* **1993**, *10*, 141-162.

(215) Jin, S.; Ye, K. M. *Biotechnol. Prog.* **2007**, *23*, 32-41.

(216) Hawker, C. J.; Wooley, K. L. *Science* **2005**, *309*, 1200-1205.

(217) Westedt, U.; Kalinowski, M.; Wittmar, M.; Merdan, T.; Unger, F.; Fuchs, J.; Schaller, S.; Bakowsky, U.; Kissel, T. *J. Control. Release* **2007**, *119*, 41-51.

(218) Liu, P.; Liu, W. M.; Xue, Q. J. *J. Macromol. Sci.-Pure Appl. Chem.* **2004**, *A41*, 1001-1010.

(219) Dailey, L. A.; Kleemann, E.; Wittmar, M.; Gessler, T.; Schmehl, T.; Roberts, C.; Seeger, W.; Kissel, T. *Pharm. Res.* **2003**, *20*, 2011-2020.

(220) Breitenbach, A.; Jung, T.; Kamm, W.; Kissel, T. *Polym. Adv. Technol.* **2002**, *13*, 938-950.

(221) Kakizawa, Y.; Harada, A.; Kataoka, K. *J. Am. Chem. Soc.* **1999**, *121*, 11247-11248.

(222) O'Reilly, R. K.; Joralemon, M. J.; Hawker, C. J.; Wooley, K. L. *New J. Chem.* **2007**, *31*, 718-724.

(223) Butun, V.; Lowe, A. B.; Billingham, N. C.; Armes, S. P. *J. Am. Chem. Soc.* **1999**, *121*, 4288-4289.

(224) Ding, J. F.; Liu, G. J. *Macromolecules* **1998**, *31*, 6554-6558.

(225) Hales, M.; Barner-Kowollik, C.; Davis, T. P.; Stenzel, M. H. *Langmuir* **2004**, *20*, 10809-10817.

(226) Sanji, T.; Nakatsuka, Y.; Kitayama, F.; Sakurai, H. *Chem. Commun.* **1999**, 2201-2202.

(227) Huang, H. Y.; Remsen, E. E.; Wooley, K. L. *Chem. Commun.* **1998**, 1415-1416.

(228) Joralemon, M. J.; Murthy, K. S.; Remsen, E. E.; Becker, M. L.; Wooley, K. L. *Biomacromolecules* **2004**, *5*, 903-913.

(229) Joralemon, M. J.; O'Reilly, R. K.; Hawker, C. J.; Wooley, K. L. *J. Am. Chem. Soc.* **2005**, *127*, 16892-16899.

(230) Prochazka, K.; Baloch, M. K.; Tuzar, Z. *Makromol. Chem.* **1979**, *180*, 2521-2523.

(231) Ding, J. F.; Liu, G. J. *J. Phys. Chem. B* **1998**, *102*, 6107-6113.

(232) Henselwood, F.; Liu, G. J. *Macromolecules* **1997**, *30*, 488-493.

(233) Henselwood, F.; Wang, G. C.; Liu, G. J. *J. Appl. Polym. Sci.* **1998**, *70*, 397-408.

(234) Liu, G. J. *Curr. Opin. Colloid Interface Sci.* **1998**, *3*, 200-208.

(235) Wang, G. C.; Henselwood, F.; Liu, G. J. *Langmuir* **1998**, *14*, 1554-1559.

(236) Stewart, S.; Liu, G. J. *Chem. Mater.* **1999**, *11*, 1048-1054.

(237) Harth, E.; Van Horn, B.; Lee, V. Y.; Germack, D. S.; Gonzales, C. P.; Miller, R. D.; Hawker, C. J. *J. Am. Chem. Soc.* **2002**, *124*, 8653-8660.

(238) Croce, T. A.; Hamilton, S. K.; Chen, M. L.; Muchalski, H.; Harth, E. *Macromolecules* **2007**, *40*, 6028-6031.

(239) Huang, H. Y.; Kowalewski, T.; Remsen, E. E.; Gertzmann, R.; Wooley, K. L. *J. Am. Chem. Soc.* **1997**, *119*, 11653-11659.

(240) Remsen, E. E.; Thurmond, K. B.; Wooley, K. L. *Macromolecules* **1999**, *32*, 3685-3689.

(241) Wooley, K. L. *J. Poly. Chem. Part A-Poly. Chem.* **2000**, *38*, 1397-1407.

(242) Butun, V.; Billingham, N. C.; Armes, S. P. *J. Am. Chem. Soc.* **1998**, *120*, 12135-12136.

(243) Liu, S. Y.; Weaver, J. V. M.; Save, M.; Armes, S. P. *Langmuir* **2002**, *18*, 8350-8357.

(244) O'Reilly, R. K.; Joralemon, M. J.; Hawker, C. J.; Wooley, K. L. *Chem.-Eur. J.* **2006**, *12*, 6776-6786.

(245) Read, E. S.; Armes, S. P. *Chem. Commun.* **2007**, 3021-3035.

(246) Butun, V.; Wang, X. S.; Banez, M. V. D.; Robinson, K. L.; Billingham, N. C.; Armes, S. P.; Tuzar, Z. *Macromolecules* **2000**, *33*, 1-3.

(247) Napper, D. H. *Polymeric Stabilization of Colloidal Dispersions*; Acadmic Press: London, 1983.

(248) Pan, D.; Turner, J. L.; Wooley, K. L. *Chem. Commun.* **2003**, 2400-2401.

(249) Becker, M. L.; Liu, J. Q.; Wooley, K. L. *Biomacromolecules* **2005**, *6*, 220-228.

(250) Angot, S.; Ayres, N.; Bon, S. A. F.; Haddleton, D. M. *Macromolecules* **2001**, *34*, 768-774.

(251) Sivakumar, K.; Xie, F.; Cash, B. M.; Long, S.; Barnhill, H. N.; Wang, Q. *Organic Letters* **2004**, *6*, 4603-4606.

(252) Thomas, J. R.; Liu, X. J.; Hergenrother, P. J. *J. Am. Chem. Soc.* **2005**, *127*, 12434-12435.

(253) Mantovani, G.; Ladmiral, V.; Tao, L.; Haddleton, D. M. *Chem. Commun.* **2005**, 2089-2091.